The analysis of Cav1α function in *Xenopus* motoneuron outgrowth and neuromuscular integrity

Dissertation

zur Erlangung des Doktorgrades
der Naturwissenschaften
(Dr. rer. nat.)

dem Fachbereichs Biologie
der Philipps-Universität Marburg
Vorgelegt von

Marlen Breuer

geboren in Chemnitz

Marburg an der Lahn, Juli 2020

Die Untersuchungen zur vorliegenden Arbeit wurden von Oktober 2016 bis Juli 2020 unter der Leitung von Prof. Dr. Annette Borchers im Fachbereich der Biologie sowie im Rahmen des Graduiertenkollegs GRK2213 „Membrane Plasticity in Tissue Development and Remodeling“ an der Philipps-Universität Marburg durchgeführt.

Vom Fachbereich Biologie der Philipps-Universität Marburg als Dissertation angenommen am:

Erstgutachterin: Prof. Dr. Annette Borchers, Molekulare Embryologie, Philipps-Universität Marburg

Zweitgutachter: Prof. Dr. Christian Helker, Entwicklungsgenetik und Zellbiologie der Tiere, Philipps-Universität Marburg

Weitere Mitglieder der Prüfungskommission:

Prof. Dr. Ralf Jacob, Institut für Zytobiologie und Zytopathologie, Philipps-Universität Marburg

Prof. Dr. Uwe Homberg, Tierphysiologie, Philipps-Universität Marburg

Tag der Disputation: 29.09.2020

Teile dieser Arbeit wurden in dem folgenden Artikel veröffentlicht:

Breuer, M., Berger, H., Borchers, A., 2020. Caveolin 1 is required for axonal outgrowth of motor neurons and affects Xenopus neuromuscular development. Scientific reports 10 (1), 16446. https://doi.org/10.1038/s41598-020-73429-x.

Folgende Publikation wurde im Rahmen dieser Promotion veröffentlicht:

Berger, H., **Breuer, M.**, Peradziryi, H., Podleschny, M., Jacob, R., Borchers, A., 2017. PTK7 localization and protein stability is affected by canonical Wnt ligands. Journal of Cell Science 130 (11), 1890–1903. https://doi.org/10.1242/jcs.198580.

Table of content

Abstract

Caveolin 1 (Cav1) is a versatile membrane protein that plays a role in the pathogenesis of hereditary lipodystrophy and neurodegenerative diseases such as Alzheimer. As an essential structural component of caveolae, specialized membrane invaginations, it participates in a broad spectrum of cellular processes, including the regulation of lipid homeostasis, endocytosis as well as cell signaling by acting as adapter molecule for a diverse number of signaling molecules, including small RhoGTPases. The loss of Cav1 function in mice causes distinct neurological abnormalities, including deficits in motor coordination and strength, behavioural changes as well as progressive neurodegeneration. However, the contribution of Cav1 to this phenotype is currently under investigation. Here, *Xenopus laevis* was used as model organism to study the developmental relevance of Cav1α with the main focus on the neuromuscular system. Morpholino oligonucleotide (MO) mediated knockdown of Cav1α results in a striking swimming defect, which is characterized by the paralysis of the injected side in combination with a severely disrupted sarcomeric organization of the somitic muscle cells. Expression analysis of Cav1 revealed a prominent expression in motoneurons, but not in the musculature indicating that Cav1 functions in the neuromuscular system. This could be confirmed by targeted injection of the Cav1α MO into neural tissue, which disrupted swimming behaviour as well as axonal growth of motoneuron. In contrast, targeted injection of Cav1 into muscular tissue had no effect on the swimming behaviour. In addition, neuronal explants revealed a striking increase in both lamellipodia as well as filopodia formation in the Cav1α morphant axons. By performing rescue experiments, it could be demonstrated that Cav1 regulates the activity of the small RhoGTPases Cdc42, Rac1 as well as RhoA during axonal growth. Further, phosphorylation on tyrosine 14 of the Cav1α protein likely modulates this process, as a phosphorylation-null mutant was not able to rescue the morphant swimming phenotype. Taken together, this thesis demonstrated a previously unrecognized function of Cav1α in the neuromuscular system, by regulating the activity of the small RhoGTPases RhoA, Rac1 and Cdc42, thereby affecting the dynamic of the actin cytoskeleton.

Zusammenfassung

Caveolin 1 (Cav1) ist ein vielseitiges Membranprotein, das eine Rolle bei der Pathogenese der erblichen Lipodystrophie sowie neurodegenerativen Erkrankungen wie Alzheimer spielt. Als wesentlicher struktureller Bestandteil von caveolae sowie der caveolae-vermittelten Endozytose, ist es an einem breiten Spektrum zellulärer Prozesse, einschließlich der Regulation der Lipidhomöostase, der Endozytose sowie diversen Signalwegen beteiligt, indem es als Adaptermolekül für eine große Anzahl von Signalmolekülen fungiert. In Mäusen konnte bereits gezeigt werden, dass der Verlust der Cav1-Funktion zu deutlichen neurologischen Anomalien, einschließlich Defiziten in der motorischen Koordination und Muskelkraft, Verhaltensänderungen sowie einer fortschreitenden Neurodegeneration führt. Der exakte molekulare Hintergrund dieser Phänotypen, sowie die genaue Funktion von Cav1 in der Entstehung neurodegenerativer Krankheiten ist noch relativ unbekannt und ist derzeit Gegenstand vieler wissenschaftlicher Studien. In dieser Arbeit wurde deshalb *Xenopus laevis* als Modellorganismus verwendet, um die entwicklungsbiologische Relevanz von Cav1α, mit Schwerpunkt auf dem neuromuskulären System, zu untersuchen. Hierbei konnte gezeigt werden, dass der Morpholino Oligonukleotid (MO) -vermittelte Funktionsverlust von Cav1α zu charakteristischen Schwimmdefekten, sowie dem Verlust der muskulären Integrität führt. Expressionsanalysen zeigten eine Expression von Cav1 in Motoneuronen, jedoch nicht in der Muskulatur, was auf eine Funktion von Cav1α in der neuromuskulären Entwicklung hinweist. Dies konnte durch gezielte Injektion von Cav1α MO bestätigt werden, da der spezifische Verlust der Cav1α Expression in neuralen-, jedoch nicht in muskulären Geweben, die charakteristischen Schwimmdefekten reproduzierte. Des Weiteren zeigte sich, dass der Funktionsverlust von Cav1α ein fehlerhaftes Auswachsen der Motorneurone *in vivo*, sowie morphologische Veränderungen in kultivierten Neuronen *in vitro* verursacht. Diese Neurone zeigen einen starken Anstieg der Lamellipodien- sowie Filopodienbildung in den Cav1α-Morphant-Axonen. Durch Durchführung von Rettungsexperimenten konnte gezeigt werden, dass Cav1α die Aktivität der kleinen RhoGTPasen Cdc42, Rac1 sowie RhoA während des axonalen Wachstums reguliert. Darüber hinaus wurde gezeigt, dass die posttranslationale Phosphorylierung des Tyrosin-Rest 14 eine wichtige Funktion in der Modulation der RhoGTPasen spielt, da die phosphorylierungs Mutante Cav1α-A14Y nicht in der Lage war die oben genannten Phänotypen zu retten.

Zusammenfassend wurde in dieser Arbeit eine bisher nicht bekannte Funktion von Cav1α in der Entwicklung des neuromuskulären Systems, sowie in der Modulation der Aktivität der kleinen RhoGTPasen RhoA, Rac1 und Cdc42 im Wachstum von Motoneuronen in *Xenopus* Embryonen beschrieben.

List of Figures

List of Tables

Abbreviations

°C	Degrees Celsius	**csk**	C-terminal Src kinase
aa	aortic arches	**CTD**	C-terminal domain
Abl	Abelson murine leukemia viral oncogene homolog 1	**C-terminus**	Carboxy-terminus
aIN	inhibitory ascending interneurons	**DAPI**	4′,6-Diamidin-2-phenylindol
ALS	amyotrophic lateral sclerosis	**Dbx**	Developing brain homeobox protein
ANOVA	analysis of variance	**dH2O**	distilled water
AP	alkaline phosphatase	**Dig**	digoxigenin
APS	Ammonium Persulfate	**dIN**	descending interneurons
Aβ	amyloid-β	**dIa**	dorsolateral commissural interneuron
B3GNT5	Beta-1,3-N-Acetylglucosaminyltransferase 5	**Dlav**	dorsal longitudinal anastomosis vessel
BBB	blood brain barrier	**dIc**	dorsolateral ascending interneuron
BCIP	5-bromo-4-chloro-3-indolyl-phosphate	**DNA**	deoxyribonucleic acid
BCNE	blastula Chordin- and Noggin expressing	**DNase**	deoxyribonuclease
bHLH	basic helix-loop-helix	**dNTP**	Deoxynucleotide triphosphate
BMB	Boehringer Mannheim blocking reagent	**DR**	disordered regions
BMP	Bone Morphogenic Protein	**DTT**	Dithiothreitol
Bp	base pairs	**E(spl)**	Enhancer of split
BSA	Bovine serum albumin	***E. coli***	*Escherichia coli*
Cav	Caveolin	**ECM**	extracellular matrix
Cdc42	Cell division control protein 42	**EDTA**	Ethylendiamin-tetra-acetic acid
CE	convergent extension	**Egr-1**	Early growth response protein 1
cg	cement gland	**EHD2**	EHD2 (Eps-15-homology domain-containing protein 2
cIN	commissural interneurons	**engr**	engrailed
CNS	central nervous system	**eNOS**	endothelial-Nitric oxide synthases
COPII	coat protein complex II	**ER**	endoplasmic reticulum
CSD	Caveolin scaffolding domain	**ERK**	extracellular signal-regulated kinases

et al.	*et alii*	**kDa**	kilo-Dalton
EtOH	ethanol	**L**	liter
FAK	focal adhesion kinase	**LB**	Luria-Bertani
FGF	fibroblast growth factor	**lg**	lung
for	forward	**lh**	lymph heart
FoxD	Forkhead-Box D	**M**	Molar
GAP	GTPase-activating proteins	**MAB**	maleic acid buffer
GD3	Ganglioside 3	**MAP**	Mitogen activated Protein
GFP	green fluorescent protein	**Math**	atonal family
Gli	glioma-associated oncogene transcription factors	**MDCK**	Madin-Darby Canine Kidney
GM1	monosialotetrahexosylganglioside	**mDia**	Diaphanous-related formin-1
GSK3β	glycogen synthase kinase β	**MEK**	MAPK/ERK kinases
h	hour	**mg**	Milligram
HA	hemagglutinin-tag	**MgCl2**	Magnesium chloride
HCG	human chorionic gonadotropin	**min**	Minute
Her	Hairy	**ml**	Millilitre
HR	helical regions	**mm**	Millimeter
Hyb-mix	Hybridization mix	**mM**	Millimolar
Ig	Immunoglobulin	**mn**	motoneuron
IGF	insulin-like growth factors	**MO**	Morpholino
ILK	integrin-linked kinase	**MRL**	membrane lipid rafts
IMD	intramembran domain	**mRNA**	messenger RNA
Irx	Iroquois-class homeodomain protein	**Murc**	muscle-restricted coiled-coil protein
Isv/Isa	intersomitic vessels/artery	**nAChR**	nicotinic Acetylcholine Receptor
IX	glossopharyngeal nerve	**NBT**	nitro-blue-tetrazolium
k	kilo	**nc**	notochord
KA	Kolmer-Adghur cells	**N-cadherin**	neural-calcium-dependent adhesion
kb	kilo base	**NCAM**	neural cell adhesion molecule

Ngnr1-3	neurogenin-related 1-3
NICD	notch intracellular Domain
nm	Nanometer
nM	Nanomolar
np	neural plate
nt	neural tube
NTD	N-terminal domain
N-terminus	Amino-terminus
OD	oligomerization domain
Olig	oligo family
PAGE	polyacrylamid gel elektrophoresisXIII
Pascin 3	PKC and casein kinase substrate in neurons 2
Pax6	paired box *gene* 3
PBS	Phosphate buffered saline
PCR	Polymerase chain reaction
pH	*potentium hydrogenium*
PKC	protein kinase C
PMCA	Plasma membrane Ca^{2+} ATPase
PNS	peripheral nervous system
Pol	Polymerase
Ppap	phosphatidic acid phosphatase
PSD-95	postsynaptic density protein 95
PSM	Presomitic mesoderm
Psm	paraxial mesoderm
PtdIns (4,5) P2	phosphatidylinositol (4,5) bisphosphate
PtdSer	phosphatidylserine
PTK7	protein tyrosine kinase 7
PTRF	Polymerase I and transcript release factor
Rac1	Ras-related C3 botulinum toxin substrate 1
Ras	Rat sarcoma
RB	Rohon-Beard neuron
rev	reverse
RhoA	Ras homolog family member A
RNA	Ribonucleic acid
rpm	Rounds per minute
RT	Room temperature
RT-PCR	reverse transcription-polymerase chain reaction
SDRP	serum deprivation response protein
SDS	sodium dodecyl sulfate
Sec	Second
Siat9	Sialyltransferase 9
sl	sensory layer
SoxB	sex determining region Y (SRY)- box
Spl	Splice
SRBC	sdr-related gene product that binds to c-kinase
Src	sarcoma
SSC	Standard sodium citrate
st	stage
SU(H)	Suppressor of hairless
TAE	Tris-Acetate-EDTA
Taq	*Thermus aquaticus*
TBS(T)	Tris-buffered saline (with Tween)
TCPTPT	Cell protein-tyrosine phosphatase
TEM	transmission electron microscopy

PTP1B	protein tyrosine phosphatase 1b	**Temp.**	Temperature
tg	trigeminal ganglion		
Tris	Tris-hydroxymethyl-aminomethane		
TRK	tyrosine kinase		
U	Units		
UV	Ultra violet light		
V	Volt		
v/v	Volume to volume		
VEGF	vascular endothelial growth factor		
VII	Facial nerve		
VmD	mandibular trigeminal ganglion		
Vop	ophthalmic trigeminal ganglion		
w/v	Weight to volume		
wt	wild type		
X	vagus nerve		
Xebf3	*Xenopus* early B-cell factor		
X-Gal	5-Bromo-4-chloro-3-indoxyl-D-galactopyranoside		
Xiro	*Xenopus* Iroquois gene family		
X-MyT1	Myelin Transcription Factor 1		
X-nr3	*Xenopus* Nodal-related 3		
Zic	Zinc finger of the cerebellum		
µg	Microgram		
µl	Microlitre		
µm	Micrometer		
µM	Micromolar		

1 Introduction

1.1 Caveolae-versatile membrane invaginations

The interests in caveolae-mediated endocytosis arose almost 70 years ago with the morphological discovery of the 50- to 100 nm plasma membrane invaginations and is now, along with clathrin-mediated endocytosis, one of the best studied endocytic mechanisms (Palade, 1953; Yamada, 1955). Caveolae, also “little-caves” are named after their characteristic flask-shaped or cave-like morphology and were first discovered in blood capillaries and mouse gall bladder epithelium by George E. Palade and Eichi Yamada (Figure 1) (Palade, 1953; Yamada, 1955). They most likely represent specialized lipid domains in the plasma membrane as caveolae, similar to lipid rafts, are highly enriched in cholesterol and sphingolipids such as glycosphingolipids and sphingomyelin (Liu et al., 1997; Ortegren et al., 2004; Rajendran and Simons, 2005; Simons and Toomre, 2000). Caveolae exist mostly as single membrane pits either fused or detached from the plasma membrane, but can also assemble to clusters of multiple caveolae. Thereby, they organize to tubular structures as well as rosettes dependent on the cell type they are expressed in (Figure 1) (Parton et al., 1997; Scherer et al., 1994; Simionescu et al., 1975).

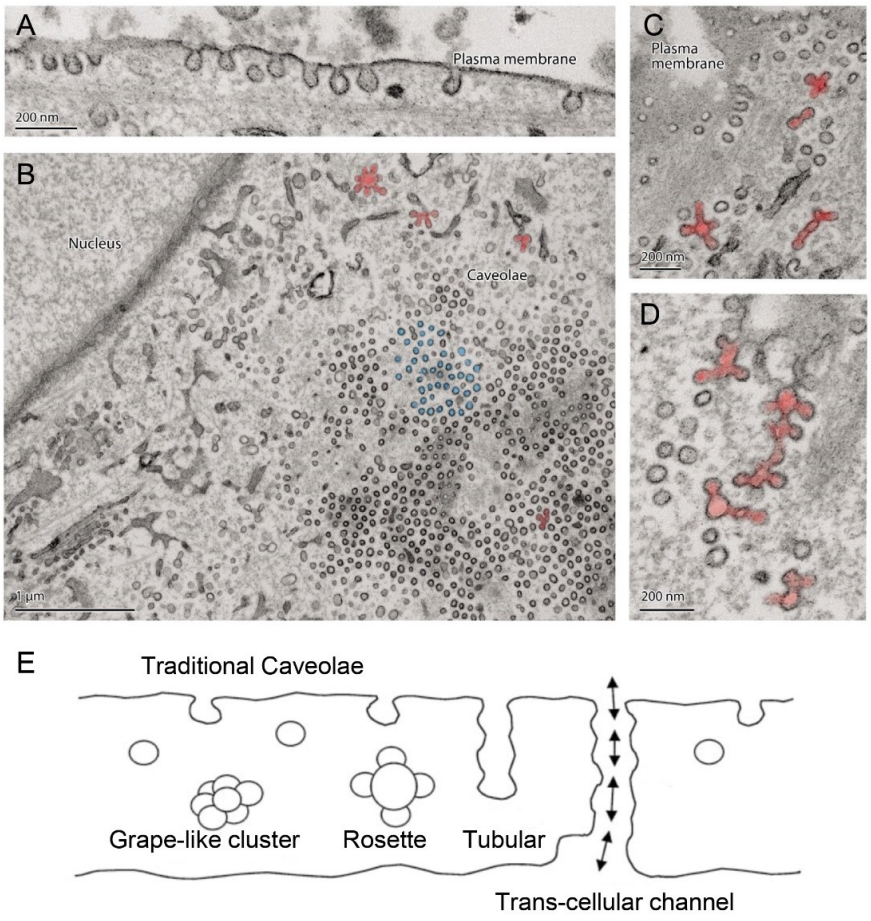

Figure 1: The morphology of caveolae.
A Transmission electron micrograph of an 3T3-L1 adipocyte. Caveolae are visible as single pits at the plasma membrane. **B-D** High density of caveolae structures at the cell surface. High ordered caveolae structures, called rosettes are highlighted in red. **E** Scheme of the caveolae morphology. They can exist as single membrane or vesicular-like pits, but also organized to grape-like clusters, rosette structures or elongated tubules (Modified after Parton, 2018; Razani et al., 2002c)

However, they can also bud from the plasma membrane in response to several signaling events and fuse with other cellular components, such as the early endosome, in a Rab5-dependent manner (Cheng and Nichols, 2016; Mayor et al., 2014; Pelkmans et al., 2004). Morphological detectable caveolae are heterogeneously distributed in a variety of cell types, with high abundance in adipocytes, epithelial cells, fibroblast and endothelial cells, where they can cover up to 70 % of the plasma membrane (Gabella, 1976; Gil, 1983; Mobley and Eisenberg, 1975; Palade, 1953; Scherer et al., 1994). Caveolae have been associated with a broad range of cellular processes due to their involvement in endocytosis, transcytosis, lipid homeostasis as well as cell signalling (Gupta et al., 2014; Navarro et al., 2004; Parton and del Pozo, 2013; Parton and Simons, 2007). In particular, as subdomains of lipid rafts they are acting as signalling centers and platforms for a diverse number of signalling molecules. Among these are the EGFR family of protein kinases, MAP kinases, Src-kinases, small RhoGTPases and endothelial nitric oxide synthase (eNOS) (Couet et al., 1997b; Engelman et al., 1998a; Feron et al., 1996; Gingras et al., 1998; Oka et al., 1997; Razani and Lisanti, 2001). Further, they also play a remarkable role during mechanoprotection by acting as stretch-sensors and by serving as membrane reservoirs during mechanical stress (Dulhunty and Franzini-Armstrong, 1975; Joshi et al., 2008; Parton and del Pozo, 2013; Sinha et al., 2011).
In the following sections, the cellular function of caveolae are discussed in more detail.

1.2 Structural components and biogenesis of caveolae

Although caveolae were initially described as uncoated vesicles, high resolution scanning electron microscopy and tomography revealed that they possess a characteristic striated coat that wraps in spirals around this pits (Figure 2) (Lebbink et al., 2010; Palade, 1953; Peters et al., 1985; Richter et al., 2008; Yamada, 1955). This coat is formed by high molecular weight complexes of approximately 160 Caveolin (Cav) and 60-80 Cavin monomers (Hayer et al., 2010).

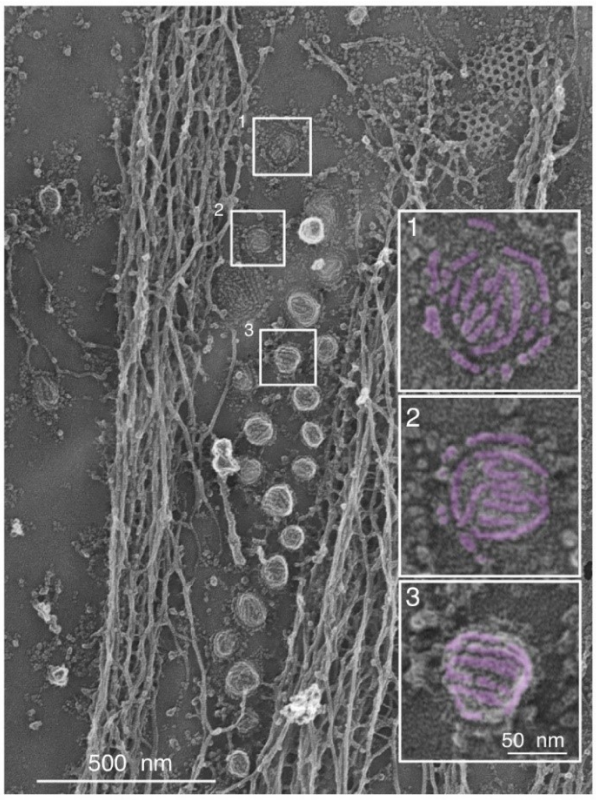

Figure 2: Caveolae possess a characteristic striated coat.
Figure shows different budding stages of caveolae at the plasma membrane of myotubes; (1) flat, unbudded caveolae. A characteristic striated coat is visible, highlighted in purple. (2) circular caveolae. (3) fully budded caveolae. (Lamaze et al., 2017)

1.2.1 Caveolin protein family- key regulators for caveolae formation

It took almost 40 year after the initial discovery of caveolae to identify the first core structural components of this membrane vesicles: the Cav protein family (Glenney, 1989; Kurzchalia et al., 1992; Scherer et al., 1996b; Way and Parton, 1996). Similar to caveolae, they are associated with a broad spectrum of signaling events by regulating the activity, compartmentalization as well as internalization of signaling molecules in the context of cell proliferation, survival as well as cellular integrity (Cohen et al., 2004).

The first Cav protein discovered was Cav1, which was originally described as a phosphorylation substrate of the Rous sarcoma virus protein V-src (Glenney, J R Jr, 1989; Kurzchalia et al., 1992). Following this, a few years later, two additional members of the Cav protein family were discovered in a search for homologous Cav proteins: Cav2 and Cav3 (Scherer et al., 1996b; Way and Parton, 1996). Cav proteins are highly conserved among vertebrate and even some invertebrate species, including *Caenorhabditis elegans* and the honey bee (*Apis mellifera*), but are absent in fungi and plants (Field et al., 2007; Kirkham et al., 2008). Cav1 and 3 are the key structural components of caveolae, as they facilitate the formation of caveolae in a broad spectrum of cells (Drab et al., 2001; Galbiati et al., 2001a; Kirkham et al., 2008; Lipardi et al., 1998). While Cav1 is expressed almost ubiquitously in most cell types, except muscle cells, Cav3 is the Cav homologue driving the formation of caveolae in smooth and striated muscle cells (Carpentier et al., 1977; Kurzchalia et al., 1992;

Liu et al., 1999; Newman et al., 1999; Scherer et al., 1997; Scherer, 1996a; Way and Parton, 1996). Cav2, which is co-expressed with Cav1 and is also a component of the caveolae coat, lacks the ability to form caveolae (Scherer et al., 1997; Scherer et al., 1996b). Interestingly, while Cav proteins facilitates the formation of caveolae in all vertebrates and most invertebrate species, *C.elegans* expresses two caveolin genes (cav1 and 2), however, lacks identifiable caveolae structures (Kirkham et al., 2008). This implies, that the function of Cav proteins is not limited to caveolae formation.

Cav proteins are small ~20-24 kDA integral membrane proteins, which are highly associated with cholesterol and sphingolipids within the plasma membrane (Figure 3), but also exist as cytosolic or secreted proteins (Liu et al., 1999; Uittenbogaard and Smart, 2000). The protein structure of the three Cav proteins is evolutionary conserved among different species and can be subdivided into five functional domains: the N-terminal domain (NTD), the oligomerization domain (OD), the scaffolding domain (CSD), the intramembrane domain (IMD) and the C-terminal domain (CTD) (Figure 3). Cav proteins are inserted into the plasma membrane through a hairpin-like structure formed by the hydrophobic IMD (Figure 3). Thereby, both the hydrophilic N-terminal domain as well as the C-terminal domains face the cytoplasm, whereby the NTD protrudes into the cytoplasm and the CTD is associated with lipids of the membrane via palmitoylation sites (Dietzen et al., 1995; Monier et al., 1995; reviewed in Root et al., 2019; Scherer et al., 1995; Uittenbogaard and Smart, 2000). The NTD of Cav1 and 2 contains several phosphorylation sites, which are important not only for the trafficking of Cav but also for signal transduction and protein-protein interaction, for example with ERKs (extracellular signal-regulated kinases) and IGFs (insulin-like growth factors) (Glenney, 1989; Kwon et al., 2009; Li et al., 1996a; Schlegel et al., 2001; Sowa et al., 2008; Wang et al., 2004). Similarly, the Cav scaffolding domain facilitates the interaction and regulation of numerous signaling proteins, including eNOS, Src-tyrosine family kinases, small GTPases as well as G-protein coupled receptors (Couet et al., 1997a; Couet et al., 1997c; Grande-García et al., 2007; Ju et al., 1997; Li et al., 1996a; Nethe et al., 2010; Ostrom and Insel, 2004). In addition, the scaffolding domain plays an important role for the association of Cav with the membrane by regulating the interaction of Cav proteins with cholesterol and other lipids (Arbuzova et al., 2000; Carozzi et al., 2002; Fielding et al., 2004; Schlegel and Lisanti, 2000; Wanaski et al., 2003).

Cav proteins are inserted into the plasma membrane as high molecular mass homo-oligomers as well as hetero-oligomers (Li et al., 1998; Monier et al., 1995). The process of oligomerization is mediated by the Cav oligomerization domain, which facilitates the interaction of Cav monomers with other Cav proteins (Li et al., 1998; Sargiacomo et al., 1995). Interestingly, while both Cav1 and 3 can form homo-oligomeric structures, Cav2 requires

Cav1 for hetero-oligomerization and membrane localization (Li et al., 1998; Scherer et al., 1996b). Similar to the oligomerization domain, the C-terminal domain also appears to be required for Cav oligomerization. In contrast to the oligomerization domain, the CTD only mediates homotypic interactions by associating with both the N-terminal and the C-terminal domains of neighboring Cav monomers (Schlegel and Lisanti, 2000; Song et al., 1997). Further, a specialized region within the CTD, also known as the C-terminal membrane attachment domain (C-MAD), is required for the exit of newly synthesized Cav proteins from the Golgi apparatus and for membrane localization. Deletion of this domains leads to the accumulation of newly synthetized Cav in the Golgi (Machleidt et al., 2000; Schlegel and Lisanti, 2000). Further, Cav1 can be palmitoylated on three cysteine residues located in the CTD (Figure 3) (Dietzen et al., 1995). Although this posttranslational modification is not required for the membrane localization of Cav1 per se, it has been shown to be necessary for cholesterol binding (Dietzen et al., 1995; Uittenbogaard and Smart, 2000).

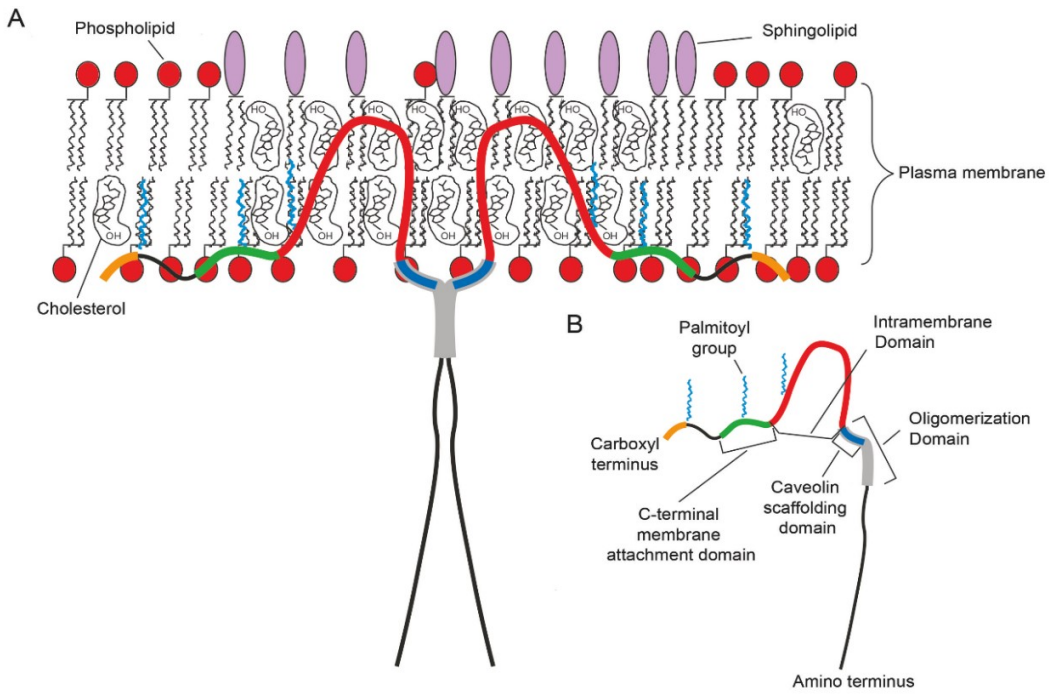

Figure 3: Membrane topology and structure of Cav1.
A Two Cav proteins forming a dimer within the plasma membrane are shown. Cav proteins are inserted into the membrane via a hairpin like structure, with both the amino and carboxy terminus facing the cytoplasm. Cav proteins are associated with lipids within the plasma membrane. **B** Scheme of a Cav1 monomer and its functional domains. (Modified after Williams and Lisanti, 2004).

1.2.2 Cavin protein family-structural coat proteins driving the formation of caveolae

It was originally suggested that the characteristic striated coat of caveolae is formed by oligomers of Cav proteins (Fernandez et al., 2002; Peters et al., 1985; Rothberg et al., 1992). However, when Cav1 is over expressed in bacterial cells, which do not express Cav proteins themselves, the induced caveolae lacks the characteristic striated coat observed in vertebrate cells (Walser et al., 2012). In the past decade, the Cavin protein family was identified as another structural component that regulate both the formation as well as stabilization of caveolae. This family, originally described in a caveolae-independent context, comprises four isoforms: Cavin 1 (Polymerase I and transcript release factor; PTRF), which is involved in transcription termination, Cavin 2 (serum deprivation response protein; SDRP) and Cavin 3 (sdr-related gene product that binds to c-kinase; SRBC) both associated with cell survival after serum starvation and the muscle specific Cavin 4 (muscle-restricted coiled-coil protein; MURC) (Burgener et al., 1990; Gustincich and Schneider, 1993; Izumi et al., 1997; Jansa, 1998; Mason et al., 1997; Ogata et al., 2008). Cavin proteins show a expression pattern similar to Cav proteins, with Cavin 4 being mainly expressed in skeletal muscle cells and Cavin 1 being rather ubiquitously expressed (Bastiani et al., 2009; Hansen et al., 2013; Hill et al., 2008; Liu et al., 2008; McMahon et al., 2009). Similar to Cav1 and 3, Cavin 1 is essential to drive the formation of caveolae and is also associated with the regulation of Caveolin protein levels (Figure 4). The loss of Cavin 1 decreases or completely abolishes caveolae formation in both non-muscle and muscle cells and additionally reduces Cav1 expression levels (Hansen et al., 2013; Hill et al., 2008; Liu et al., 2008). Cavin 2 is also required to some extent for caveolae formation in a tissue-specific manner. In contrast to the loss of Cavin 1 expression, however, which abolishes the formation of caveolae in all tissues, the loss of Cavin 2 expression only leads to a depletion of caveolae in the lungs and in the fat endothelium (Hansen et al., 2013). Moreover, Cavin 2 both controls caveolae morphology as well as the size of the Cavin complexes incorporated into the caveolae membrane (Figure 4) (Hansen et al., 2013). Although Cavin 3 and 4 are not essential for caveolae formation per se, they are important regulators for caveolae dynamics (reviewed in Briand et al., 2011; Hansen et al., 2013). It has been shown that Cavin 3 coordinates the intracellular trafficking of caveolae and functions as adaptor molecule that links caveolae to microtubules (Figure 4) (McMahon et al., 2009). Cavin 4 expression is restricted to muscle cells, and its function is required for the proper localization of Cav3 to the plasma membrane (Bastiani et al., 2009; Faggi et al., 2015; Naito et al., 2015).

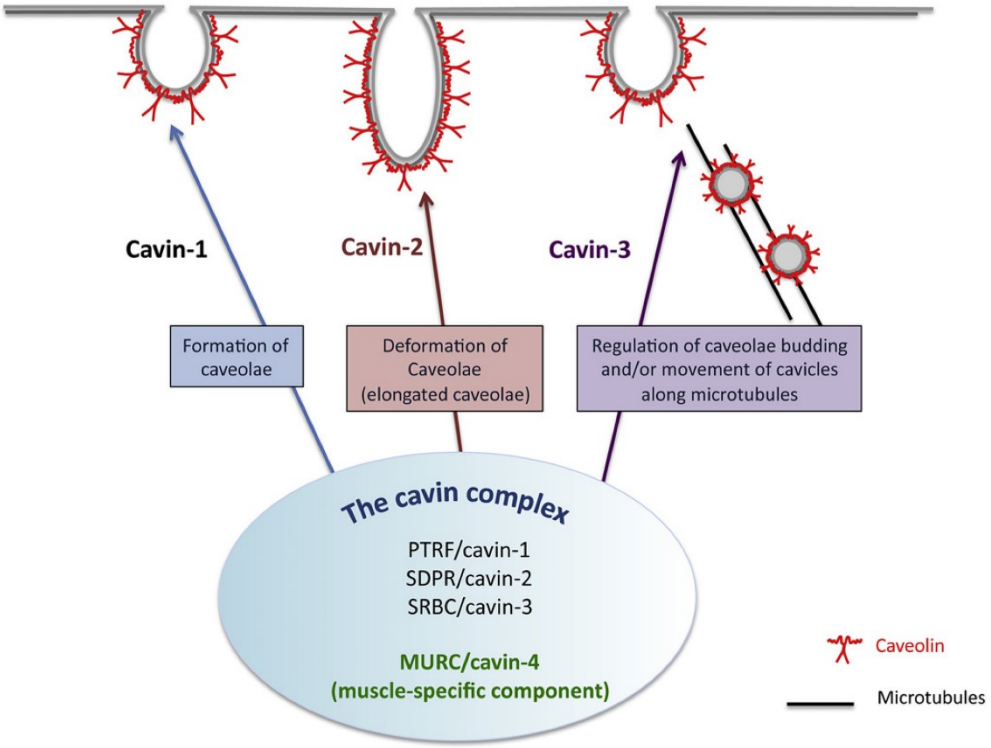

Figure 4: Cavin protein function in the biogenesis of caveolae.
Scheme showing the different function of Cavin proteins in the biogenesis as well as trafficking of caveolae. Cavin 1 is essential for caveolae formation and its loss-of-function results in the depletion of these membrane structures. Cavin 2 is required for the caveolae morphology as well as the size of the Cavin complexes incorporated into the caveolae membrane. Cavin 3 regulates caveolae trafficking along microtubules (Briand et al., 2011).

Cavin proteins are highly conserved with a characteristic domain arrangement. They possess two conserved, positively charged helical regions, HR1 and HR2, which are each flanked and separated by the poorly conserved, acidic disordered regions DR1, 2 and 3 (Figure 6A) (Kovtun et al., 2014). While both the HR1 and 2 domain are required for the association of the Cavin proteins with lipids of the plasma membrane, including phosphatidylinositol (4,5) bisphosphate (PtdIns (4,5)P2) and phosphatidylserine (PtdSer), the HR1 domain also mediates the Cavin oligomerization (Hansen et al., 2009; Kovtun et al., 2014; McMahon et al., 2009). Cavin proteins can form homo- and hetero-oligomeric complexes, independently of Cav proteins (Gambin et al., 2013; Hayer et al., 2010; Kovtun et al., 2014; Ludwig et al., 2013). Further, while Cavin 1 can induce caveolae formation even in the absence of other Cavin proteins, Cavin 2 and 3 require Cavin 1 to form hetero-oligomeric complexes and to be incorporated into the plasma membrane (Bastiani et al., 2009; Gambin et al., 2013; Ludwig et al., 2013).

1.2.3 Caveolae accessory proteins-additional regulators controlling caveolae endocytosis

In addition to Caveolin and Cavin proteins several accessory proteins, which are required for caveolae internalization, have been identified: The Dynamin-2 GTPase and the Dynamin-like ATPase EHD2 (Eps-15-homology domain-containing protein 2) have been found to be associated with the caveolae neck and are required for caveolae stabilization and dynamics (Ludwig et al., 2013; Oh et al., 1998; Stoeber et al., 2012). While EHD2 acts as negative regulator for caveolae endocytosis, dynamin positively affects caveolae internalization by mediating caveolae scission (Henley et al., 1998; Morén et al., 2012; Oh et al., 1998; Stoeber et al., 2012). Further, Pascin 3 (PKC and casein kinase substrate in neurons 2), another caveolae associated protein, has been linked to caveolae formation and endocytosis (Hansen et al., 2011; Seemann et al., 2017).

1.3 Caveolae biogenesis-the assembly of Caveolin and Cavin proteins

Caveolin as well as Cavin proteins assemble in two separate steps to form the caveolae coat. Caveolins are synthesized in the endoplasmic reticulum (ER) as integral membrane proteins, where they adapt their characteristic hairpin-like conformation and oligomerize to low molecular weight 8S complexes (Figure 5). These consist either of approximately 14-25 Cav1-Cav2 heteromers or, in muscle cells, of Cav3 homomers (Hayer et al., 2010; Monier et al., 1995; Scheiffele et al., 1998). If the appropriate oligomeric size is reached, these 8S complexes travel in a COPII (coat protein complex II) dependent manner to the Golgi apparatus, where they undergo a second round of oligomerization to form large 70S complexes containing approximately 160 Cav molecules (Figure 5) (Hayer et al., 2010; Scherer et al., 1997; Tang et al., 1996). Both the assembly of these complexes as well as the following transport to the plasma membrane is tightly associated with and dependent on cholesterol (Pol et al., 2005). Once these 70S complexes are introduced into the plasma membrane, they facilitate the assembly of lipids including sphingomyelin, GD3 and GM1 gangliosides, PtdIns (4,5)P2 and PtdSer (Figure 5) (reviewed in Sonnino and Prinetti, 2009). This creates specialized lipid nanodomains, which in turn initiate the recruitment of other caveolae accessory proteins including EHD2, dynamin-2 and cavin proteins (reviewed in Kovtun et al., 2015; Morén et al., 2012; Senju et al., 2011; Simone et al., 2013; Wanaski et al., 2003; Yao et al., 2005).

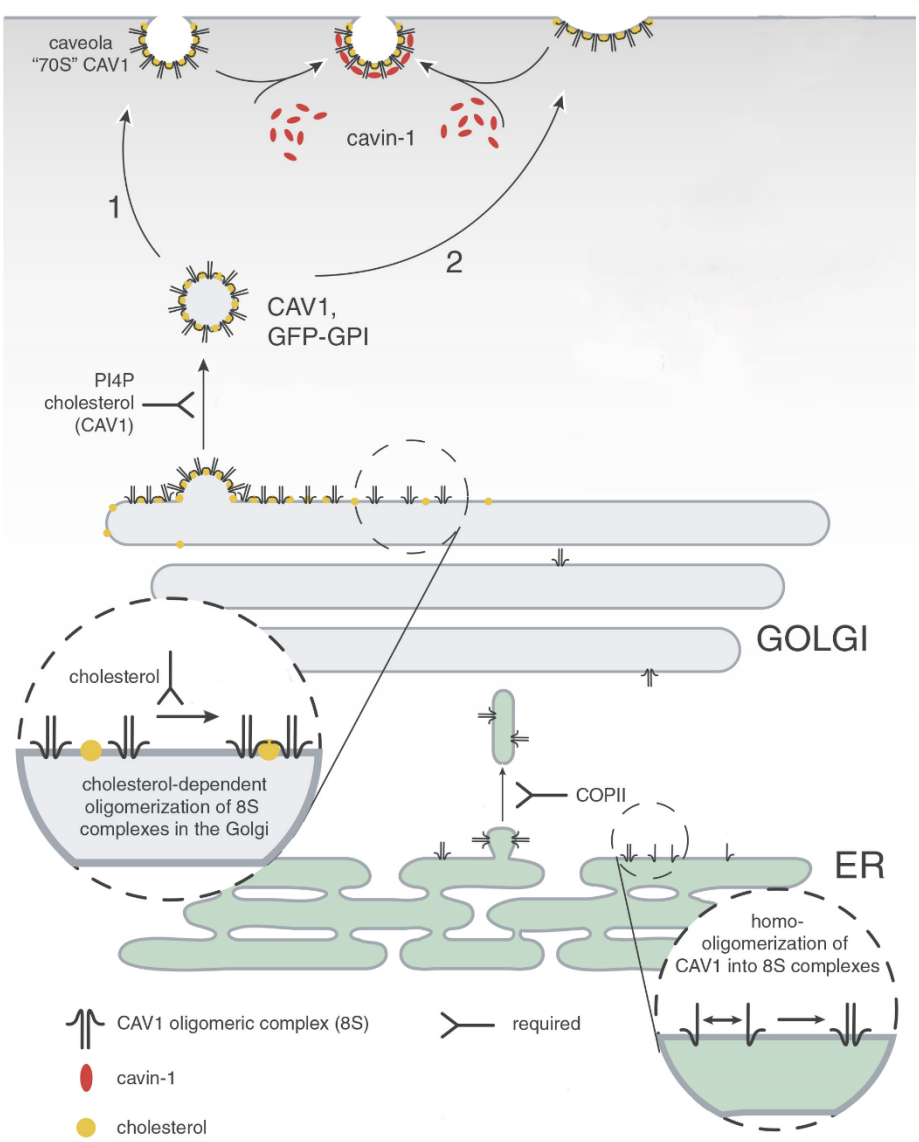

Figure 5: Biogenesis of Cav proteins.
Scheme of the biogenesis of Cav proteins. Cav proteins are expressed within the endoplasmic reticulum and are assembled as low weight 8S complexes to homo-oligomers. These complexes exit the ER in a COPII-dependent manner and travel to the Golgi apparatus. Cav oligomers undergo a second cholesterol-depended oligomerization process to form large 70S complexes, which are then inserted into the plasma membrane. Caveolae structures are stabilized by Cavin proteins. (Modified after Hayer et al., 2010).

Cavin proteins are synthesized into the cytoplasm and form, independently of Cav expression, heterotrimers consisting of either three Cavin 1 monomers or two Cavin 1 and one Cavin 2 or Cavin 3 monomer (Figure 6B) (Gambin et al., 2013; Hansen et al., 2013; Hansen et al., 2011; Hayer et al., 2010; Kovtun et al., 2014). This is mediated by the HR1 domain of the Cavin 1 protein, which determines the Cavin-Cavin specificity (Kovtun et al., 2014). Once trimerized, the HR2 domain of the Cavin proteins folds into a helical structure, facilitating the assembly of higher Cavin multimers of approximately 60-80 monomers (Gambin et al., 2013; Hayer et al., 2010; Kovtun et al., 2014). It has been shown that the composition of these complexes can differ between tissues (Hansen et al., 2013; Hayer et

al., 2010). These high-order Cavin oligomers then get stably inserted into the plasma membrane and induce the stabilization and invagination of caveolae membrane curvatures (Figure 6B) (Hansen et al., 2009; Kovtun et al., 2014). This process strongly depends on the high affinity of Cavin proteins to specific lipids found in these Cav-rich microdomains (Kovtun et al., 2014). The exact mechanism how Cavin proteins interact with the Cav proteins to form the characteristic striped coat is still a subject of ongoing research (Kovtun et al., 2015). However, cholesterol is known to play an essential role in this process, since cholesterol depletion leads to the flattening of this membrane curvatures, Cav1-Cavin 1 dissociation as well as degradation of Cavin 2 (Breen et al., 2012; Hailstones et al., 1998; Hill et al., 2008).

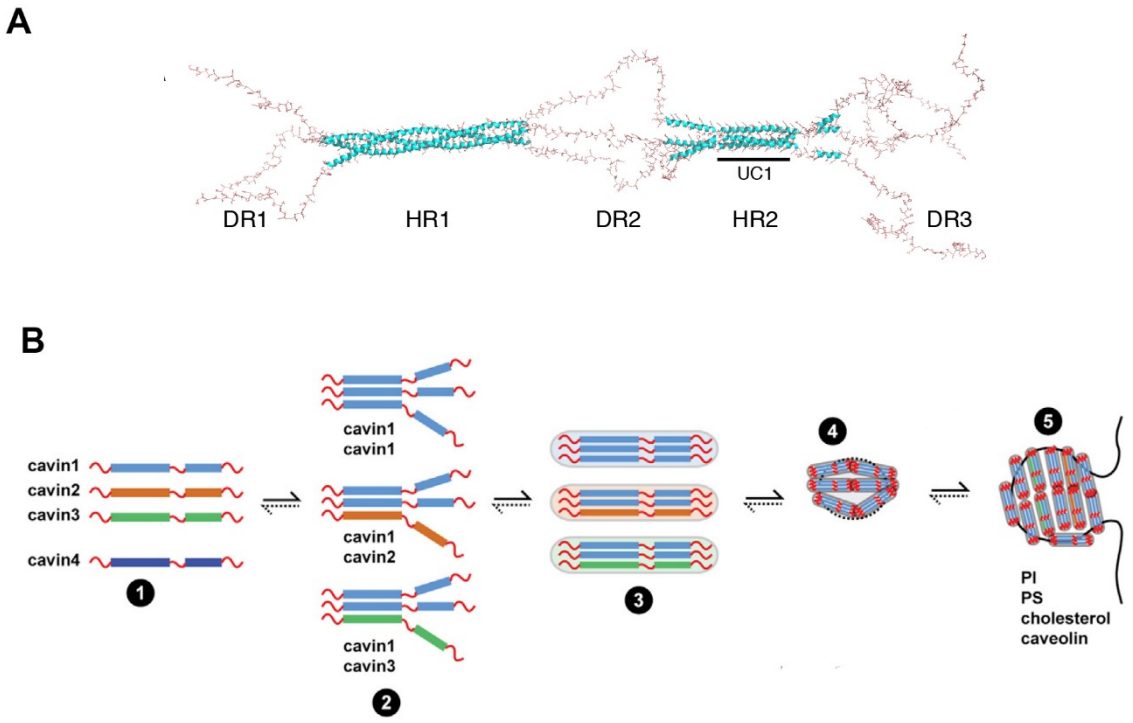

Figure 6: Ultrastructure and stepwise assembly of Cavin proteins
A Heterotrimeric structure of three Cavin proteins. **B** Scheme of the assembly of cavin hetero-oligomer complexes and insertion into the plasma membrane. 1) Single Cavin proteins are shown. 2) Cavin 1 proteins either form homo-oligomeric structures containing three Cavin 1 proteins, or oligomerize with either one Cavin 2 or one Cavin 3 protein to form hetero-oligomeric trimers. 3) The HR2 domain of the Cavin proteins folds into a helical structure, facilitating the assembly of higher Cavin multimers (4). 5) At the plasma membrane, Cavin multimers associated with specific lipids found in Caveolin-rich microdomains (Modified after Kovtun et al., 2014; Tillu et al., 2019).

1.4 Caveolae are stable membrane structures linked to the actin cytoskeleton

Caveolin as well as Cavin proteins are not only required for the formation of caveolae, but also connect this membrane structures to the actin cytoskeleton and microtubules. While Cavin 1 is directly associated with the actin cytoskeleton, Cav1 facilitates this interaction via the actin binding protein filamin A (for more details see Echarri and del Pozo, 2015; Liu and

Pilch, 2008; Muriel et al., 2011; Richter et al., 2008; Stahlhut and van Deurs, 2000; Sverdlov et al., 2009). The caveolae dynamic is highly dependent on the actin cytoskeleton. In contrast to clathrin-coated pits, caveolae are relatively immobile and only 5-20% of the caveolae exist as mobile vesicles (Hommelgaard et al., 2005; Stahlhut and van Deurs, 2000; van Deurs et al., 2003). It has been shown that caveolae are immobilized by the actin cytoskeleton at the plasma membrane. The remodelling of the actin cytoskeleton, by for example through okadaic acid, leads to a rapid reorganization and internalization of caveolae from the plasma membrane (Parton et al., 1994; Thomsen et al., 2002). Interestingly, activated Abl tyrosine kinases and formin mDIA1, which play a role in the formation of stress fibers, affect the dynamics of caveolae (Echarri et al., 2012). Silencing of one of these proteins leads to the clustering of Cav1 and inhibition of caveolae endocytosis. Likewise, actin depolarization by cytochalasin D blocks the internalization of caveolae (Parton et al., 1994; Thomsen et al., 2002), highlighting the importance of the actin cytoskeleton and stress fibers for caveolar dynamics.

Similarly, microtubules are also required for caveolae dynamics. For example, microtubules regulate the trafficking of caveolae back to the plasma membrane in an β-Integrin and Integrin-linked kinase (ILK) mediated manner. The loss of one of these two proteins depletes caveolae from the membrane and leads to the accumulation of caveolae vesicles in intracellular structures (Singh et al., 2010; Wickström et al., 2010). It is proposed, that β-Integrin and Integrin-linked kinases promote local microtubule stabilization by recruiting the F-actin binding protein IOGAP1 as well as mDIA1 to the cell cortex and promoting the trafficking of caveolae to the membrane (Wickström et al., 2010).

1.5 Caveolae are important regulators for mechanoprotection and -sensing

Caveolae have been ascribed to a diverse number of cellular processes, including endocytosis, lipid regulation and signal transduction (for more details see Cheng and Nichols, 2016; Harvey and Calaghan, 2012; van Deurs et al., 2003). However, the most remarkable function of caveolae, which has attracted the interest of many scientists in recent years, is its role in mechanosensing and mechanoprotection (reviewed in Parton and del Pozo, 2013). Caveolae are particularly abundant in cells that are exposed to high mechanical stress, such as fibroblast, endothelial cells and in particular in muscle cells (Gabella, 1976; Gil, 1983; Mobley and Eisenberg, 1975; Palade, 1953; Scherer et al., 1994). Early studies in muscle cells demonstrated that these specialized membrane invaginations are sensitive to mechanical strain: increased membrane tension results in the flattening of caveolae, which

in turn increases the surface area of the plasma membrane (Dulhunty and Franzini-Armstrong, 1975; Sinha et al., 2011). This mechanism has been shown to protect cells against membrane damage in response to extensive mechanical strain and increased cell tension (Lo et al., 2016; Sinha et al., 2011). Loss-of-function studies resulting in the depletion of caveolae emphasized the importance of these membrane structures for the protection against mechanical-induced damage. In mice, the loss of either Cavin 1 or Cav3 expression in the musculature, results in an increased sensitivity of the muscle cells to membrane tension, disorganization of the sarcolemmal organization as well as aberrant T-tubule structures (Galbiati et al., 2001a; Galbiati et al., 2000b; Hagiwara et al., 2000; Lo et al., 2015). Similarly in zebrafish, the muscle-specific depletion of either Cavin 1 or the expression of a Cav3 mutant, which is associated with human limp-girdle muscular dystrophy, leads to mechanical induced damage of the muscles in response to excessive muscle activity (Lo et al., 2016; Lo et al., 2015; Nixon et al., 2005). Likewise, the loss of caveolae in the zebrafish notochord through Cavin 1 depletion caused severe cellular damage upon mechanical stress induced by swimming (Figure 7) (Garcia et al., 2017; Lim et al., 2017).

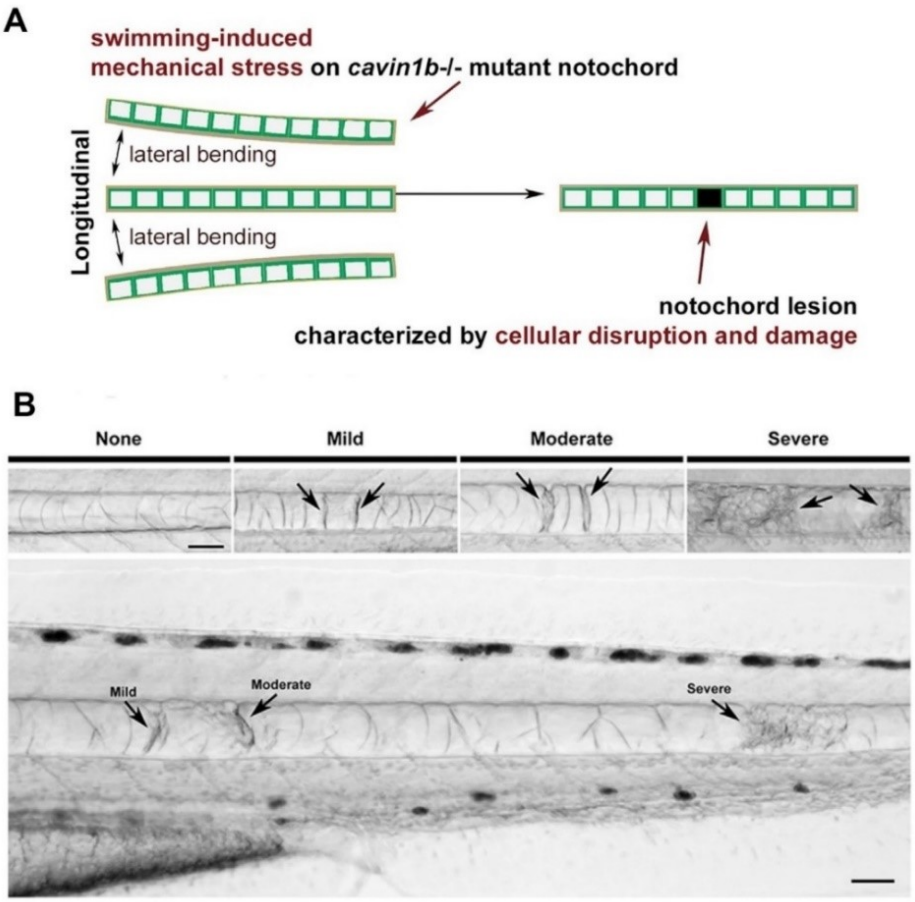

Figure 7: Caveolae protect the notochord against mechanical stress.
A Cavin 1 knockout leads to the global loss of caveolae structures. Swimming induced bending of the notochord results in cellular lesions of the notochord. **B** Cavin 1 KO zebrafish showing various degrees of cellular damage within the notochord, ranging from mild to severe (Modified after Lim et al., 2017).

In the recent years it has been shown that caveolae not only play a role in mechanoprotection through physical enlargement of the membrane surface, but also contribute to mechanosensitive signaling in response to membrane stretching, shear stress as well as cell detachment during migration (Figure 8) (Boyd et al., 2003; Grande-García et al., 2007; Muriel et al., 2011; Radel and Rizzo, 2005). Mechanosensing plays an important role in many cellular processes that involve morphological changes, including cell migration and differentiation, as it converts mechanical forces into biochemical signals (mechanotransduction). This leads for example to the rearrangement of the actin cytoskeleton allowing cells to respond to mechanical stimuli (for more detail see: Jaalouk and Lammerding, 2009; Ohashi et al., 2017; Orr et al., 2006; Vogel and Sheetz, 2006). It has been demonstrated that Cav as well as Cavin proteins contribute to mechanotransductive pathways by indirectly regulating the reorganization of the actin cytoskeleton and focal adhesion stability as well as the positive regulation of caveolae formation (del Pozo et al., 2005; Dewulf et al., 2019; reviewed in Echarri and del Pozo, 2015; Grande-García et al., 2007; Nethe et al., 2010; and Parton and del Pozo, 2013). The phosphorylation of Cav1α on tyrosine 14 plays a crucial role in these processes: Cav1α can be phosphorylated on tyrosine 14 (pY14) in a Src-, Fyn- or Abl-dependent manner in response to mechanical force or oxidative stress (Cao et al., 2004; Glenney, 1989; Joshi et al., 2012; Li et al., 1996b; Radel and Rizzo, 2005; Sanguinetti et al., 2003; Sanguinetti and Mastick, 2003; Wary et al., 1998; Zhang et al., 2007). This phosphorylation has been associated with Integrin-dependent focal adhesion dynamics and the modulation of RhoGTPase activity during cell migration (Figure 8) (del Pozo et al., 2005; Goetz et al., 2008a; Grande-García et al., 2007). In endothelial cells, shear stress mediates the recruitment of mechanical sensitive Integrins to Integrin adhesion sites located in caveolae-signaling domains (Radel and Rizzo, 2005; Yang et al., 2011). The interaction of these Integrins with Cav1α initiates the inhibition of the Src/p190RhoGAP pathway and consequently the positive regulation of RhoA activity, inducing the remodeling of the actin cytoskeleton as well as stabilization of focal adhesion sites (Figure 8) (del Pozo et al., 2005; Goetz et al., 2008a; Grande-García et al., 2007; Yang et al., 2011). Tyrosine phosphorylated Cav1α also regulates the expression of core caveolae components in a positive feedback loop in response to mechanical force: pT14Cav1 inhibits the transcription factor Egr-1, which normally represses the expression of both caveolin 1 and cavin 1, in a PKC- and RhoA-dependent manner (Figure 8). This leads to the positive regulation of caveolae formation to buffer the increased membrane tension (Joshi et al., 2012). In view of the important function of Cav and Cavin proteins in mechanosensing and -protection, it is not surprising that dysfunction of these proteins contributes to the pathogenesis of many diseases, such as muscular dystrophy, cardiomyopathy, lipodystrophy and cancer (reviewed in Razani et al., 2002c; Sohn et al., 2016).

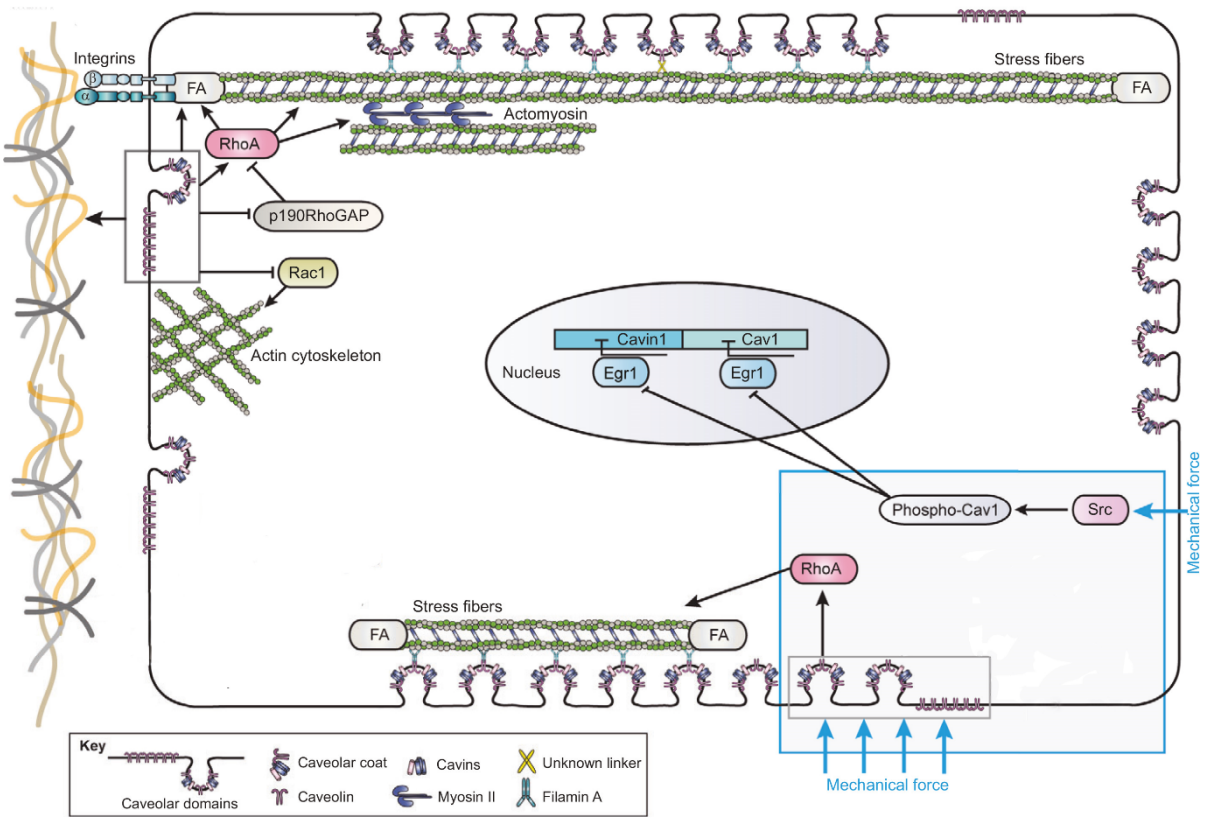

Figure 8: Caveolin proteins participate in a diverse number of mechanotransduction pathways.
Overview of the signaling pathways regulated by Caveolin proteins. In response to mechanical force, caveolae membrane domains regulate the actin cytoskeleton dynamic and stress fiber formation by the modulation of the small RhoGTPases RhoA and Rac1 at focal adhesion sites (FA). Cav1 expression positively regulates RhoA activity by inhibiting the p190RhoGAP pathway and inhibiting Rac1 activity. Src-mediated Cav1 phosphorylation inhibits the Erg1-dependent transcriptional repression of caveolae protein components, which leads to the positive regulation of caveolae formation (modified after Echarri and del Pozo, 2015).

1.6 Caveolin 1- functional role in cellular processes

Cav1 was the first caveolae component to be discovered and is considered as the key structural component of caveolae. Cav1 is involved in a variety of physiological and pathophysiological processes as it regulates many cellular processes that play an essential role in maintaining the general health of the organism. These include endocytosis, cell signaling, lipid and cholesterol homeostasis (Razani et al., 2002c).

The cav1 gene is highly conserved among different species and contains three exons. The encoded protein of approximately 178 amino acids in length is expressed as an α - and β-isoform. These isoforms differ in their size due to alternative splicing and alternative translating start sides: While the Cav1α isoform is considered to be the full length protein, the β-isoform lacks the first 32 N-terminal amino acids of the α-isoform (Kogo and Fujimoto, 2000; Scherer et al., 1995). Both isoforms are capable to induce caveolae formation and show overlapping expression profiles (Fujimoto et al., 2000; Li et al., 1996c; Scherer et al., 1995).

Although detailed studies analyzing the isolated function of these two isoforms have not yet been performed in higher vertebrate, loss-of-function studies in zebrafish suggest that Cav1α and β have distinct but overlapping functions during development (Fang et al., 2006). While the Morpholino-mediated knockdown of both Cav1α and Cav1β in zebrafish resulted in defects in neuronal and notochord structures as well as in disorganized actin structures of the somites, only Cav1α loss-of-function caused impaired formation of vascular-endothelial tissue (Fang et al., 2006).

The main difference between these two isoforms is the tyrosine phosphorylation site at position 14 (Y14) of the Cav1α-isoform, which is associated with caveolae internalization, focal adhesion dynamics, cell motility and polarization (Beardsley et al., 2005; del Pozo et al., 2005; Goetz et al., 2008a; Grande-García et al., 2007; Radel and Rizzo, 2005; Wary et al., 1998; Zimnicka et al., 2016).

1.6.1 Cav1α is a modulator for RhoGTPase activity

The small RhoGTPases Cdc42 (cell division cycle 42), Rac1 (Ras-related C3 botulinum toxin substrate 1) and RhoA (Ras homologous member A) act as molecular switches controlling a variety of cellular processes, including actin remodeling during cell polarity and cell migration (reviewed in Etienne-Manneville and Hall, 2002). They are constantly cycling between an “active” and an “inactive” state by the hydrolysis of GTP to GDP and vice versa. In general, Rac1 regulates lamellipodia formation and Cdc42 filopodia extension by promoting actin polymerization (Kozma et al., 1995; Nobes and Hall, 1995; Ridley et al., 1992). In contrast, RhoA functions in microtubule stabilization and stress fiber formation by counteracting Rac1 and Cdc42 activity (Nobes and Hall, 1995; Ridley and Hall, 1992).

The Src-dependent phosphorylation of Cav1α on tyrosine 14 (pY14Cav1α) has been associated with focal adhesion maturation and dynamics by modulating the activity of these small RhoGTPases in the process of cell migration and polarization (Grande-García et al., 2007; Nethe et al., 2010; Wei et al., 1999). Activated Rac1 at nascent focal adhesion contacts mediates the recruitment as well as the Src-dependent phosphorylation of Cav1α at Integrin adhesion sites located at the leading edge of migrating cells (Nethe et al., 2010; Radel and Rizzo, 2005). This re-localization both promotes the clustering and stabilization of Integrins and subsequently focal adhesion assembly by the inhibition of Rac1 and the activation of RhoA (Figure 8, Figure 9) (Gaus et al., 2006; Goetz et al., 2008a; Grande-García et al., 2007; Joshi et al., 2008; Nethe et al., 2010). Nethe and colleagues were able to demonstrate, that focal-adhesion-localized pY14Cav1α negatively modulates the activity of Rac1 by regulating the ubiquitylation and consequently the degradation of active Rac1 (Figure 9) (Nethe et al., 2010). Further, in a negative feedback loop, pY14Cav1α mediates the recruitment of the Src

inhibitor csk (C-terminal Src kinase), which phosphorylates and inhibits Src-kinases localized at focal adhesion sites. This results in the inhibition of p190RhoGAP and activation of RhoA, which in turn stabilizes newly formed focal adhesion sites (Cao et al., 2004; Grande-García et al., 2007; Radel and Rizzo, 2005). Consistently, mouse embryonic fibroblasts from cav1 knockout mice display impaired focal adhesion maturation and stabilization as well as loss of cell polarity and migration due to elevated Rac1 and decreased RhoA activity (Grande-García et al., 2007; Nethe et al., 2010). In addition, pY14Cav1α not only modulates the stabilization of focal adhesion sites, but also regulates the turnover of focal adhesions complexes through endocytosis. It is proposed, that de-phosphorylation of Cav1α by focal adhesion resident phosphatases, such as protein tyrosine phosphatase 1b (PTP1B) and its homologue activating T cell protein-tyrosine phosphatase (TCPTP), results in its destabilization and subsequent internalization (Borza et al., 2010; Lee et al., 2006). This in turn leads to the turnover of FA components together with Cav1α by caveolae-mediated endocytosis (Figure 9) (del Pozo et al., 2005; Nethe and Hordijk, 2011).

The role of Cav1 in the regulation of Cdc42 activity is still a subject of ongoing research. Nevis and Thurmond proposed a model where Cav1 functions as Cdc42 guanine nucleotide dissociation inhibitor in pancreatic β-cells, as Cav1 maintains Cdc42 in its inactive state under basal condition in these cells (Nevins and Thurmond, 2006). Thus, although Cav1 may not be a major factor for the direct regulation of RhoGTPase activity, it seems to be required for the fine-tuning of their spatial-temporal activity during cell migration.

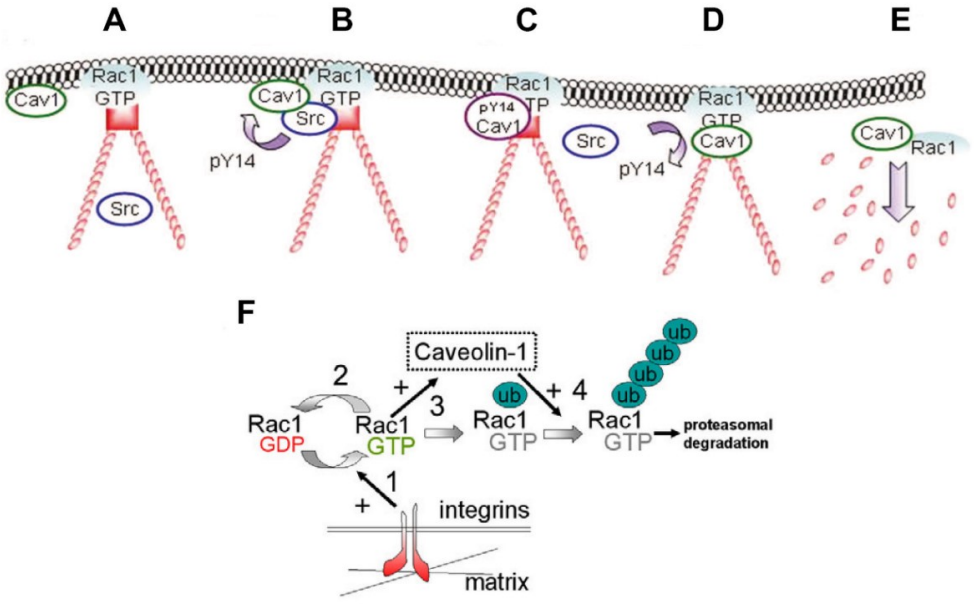

Figure 9: Model for Caveolin 1 dependent Rac1 regulation.
A Activated Rac1 recruits Src-kinases as well as Cav1 to focal adhesion sites (FA). **B-C** The association of Cav1 with Src-kinases drives the phosphorylation of Cav1Y14 and the accumulation of phosphorylated Cav1 at focal adhesion sites. **D-E** FA-associated tyrosine phosphatases dephosphorylate Cav1, which causes the internalization of Cav1 together with FA components. **F** Localization of Rac1 at Integrin attachment domains (1) is either regulated by the cycling GTP hydrolysis (2) but also by the Cav1-mediated polyubiquitylation pathway (3-4) (Modified after Nethe et al., 2010; Nethe and Hordijk, 2011).

1.6.2 The role of Cav proteins in health and disease

The misexpression of Cav1 in humans is associated with the pathogenesis of various diseases, including Berardinelli-Seip congenital lipodystrophy, cardiac diseases and cancer but also with age-related diseases such as vascular and pulmonary dysfunction, impaired wound healing and fibrosis as well as Alzheimer disease (Cao et al., 2008; Gaudreault et al., 2004; Parton and del Pozo, 2013; Rhim et al., 2010; Volonte et al., 2009)
A better understanding of the pathophysiological function of Cav proteins in human diseases has been gained through the establishment of several animal models; Cav1 null mice, which show a complete loss of caveolae formation in all non-muscle cells, are surprisingly viable and fertile. However, they display a broad spectrum of abnormalities such as a reduced live span (Park et al., 2003), cardiac hypertrophy, and pulmonary defects (Razani et al., 2001) as well as abnormal lipid homeostasis (Razani et al., 2002a). Cav1 KO mice are lean with an abnormal adipocyte's physiology including a reduced diameter of adipocytes, resistance for diet-induced obesity and insulin resistance (Le Lay and Kurzchalia, 2005; Razani et al., 2002a). One of the highest expression level of Cav1 can be detected in adipocytes, suggesting that Cav1 functions in lipid metabolism (Scherer et al., 1997; Scherer et al., 1994). And indeed, while cholesterol is essential for Cav trafficking and caveolae formation, Cav1 has been shown to regulate cholesterol homeostasis by modulation its trafficking to the plasma membrane or other cellular compartments (Bist et al., 1997; Fielding et al., 1997; Le Lay et al., 2006; Murata et al., 1995).

The function of Cav1 is also associated with cell proliferation, differentiation and survival (reviewed in Goetz et al., 2008b). In mouse embryonic fibroblasts, Cav1 negatively regulates cell proliferation by mediating the p53/p21-dependent G0/G1 cell cycle arrest (Galbiati et al., 2001b; Razani et al., 2001). Furthermore, it has been shown that Cav1 regulates cell cycle progression via the Ras-p42/44 MAP kinase pathway (Galbiati et al., 2001b; Sanna et al., 2007; Williams and Lisanti, 2005). The loss of Cav1 expression in *C. elegans* results in a burst of egg laying, due to an elevated activation of the Ras/MAP-kinase pathway and consequently an increased cell division (Scheel et al., 1999). Cav1 also negatively regulates the Wnt/β-Catenin-dependent Cyclin D1 transcription by inhibiting the translocation of β-catenin in the nucleus and the Lef1-mediated transcription of Cyclin1D (Galbiati et al., 2000a). Consistently, cav1 KO mice display pulmonary defects characterized by a thickening of the alveolar septa due to increased cell proliferation (Razani et al., 2001). Further, mice deficient for Cav1 expression exhibit deficits in wound healing and also show a higher susceptibility to carcinogens (Capozza et al., 2003; Razani et al., 2001), suggesting that Cav1 might be involved in tumorigenesis. Indeed, Cav1 has been found to be mis-regulated in many tumors: it is downregulated in breast, gastrointestinal and multidrug resistant cancers and

upregulated in lung, brain and prostate cancer (Barresi et al., 2006; Bryant et al., 2011; Goetz et al., 2008b; Ho et al., 2002). For this reason, Cav1 is believed to function both as tumor suppressor as well as tumor promoter, depending on the type of cancer in which Cav1 is expressed.

Similar to the observed phenotype in mice, the loss-of-function of cav1 also leads to cardiac dysfunctions in zebrafish (Fang et al., 2006; Grivas et al., 2020). Morpholino-mediated knockdown of Cav1 results in a disruption of vascular endothelial tissue, including enlarged pericardial heart sacs and abnormal heart chambers formation (Fang et al., 2006). In contrast, while the knockout of cav1 does not cause developmental defects of the zebrafish heart, heart regeneration was affected due to decreased cardio-myocyte proliferation and reduced cardiac elasticity in the adult zebrafish (Grivas et al., 2020). In addition, Cav1 is required for notochord, lateral line, neural as well as vascular development in this model organism. Morpholino-mediated knockout of Cav1α results in a deformed notochord, abnormal development of both eye and neural tissue, disrupted patterning of the vascular endothelium (Fang et al., 2006) as well as impaired maturation of the neuromasts (Fang et al., 2006; Nixon et al., 2007).
Taken together, although Cav1 may not be essential for survival, there is a growing body of evidence that Cav1 is required for cell and tissue integrity and health.

1.6.3 Functions of Cav1 in the nervous system

The function of Cav1 is not only associated with metabolic diseases. Increasing evidence shows that dysfunctions of this protein is also linked to the progression of a variety of neurodegenerative diseases, including Alzheimer disease, schizophrenia and Huntington (Allen et al., 2011; Eser Ocak et al., 2019; Gaudreault et al., 2004; Kassan et al., 2017; Trushina et al., 2006a). Further, progressive neurodegenerative spinal cord and cerebellar dysfunctions were found in patients with atypical partial lipodystrophy caused by a Cav1 frame shift mutation (Berger et al., 2002; Cao et al., 2008). These neurological conditions were characterized by severely reduced lower extremity weakness, spastic-ataxia gait, an inability to perform rapid, alternating movements (dysdiadochokinesis) and bilateral Babinski signs, indicating dysfunctions of the corticospinal tract (Berger et al., 2002; Cao et al., 2008). Similarly, by analyzing the brain of Cav1 KO mice, it has been shown that the loss of Cav1 expression leads to an age-dependent decrease in both brain size and weight due to accelerated neuronal aging and degeneration (Head et al., 2010; Trushina et al., 2006a). They also display distinct neurological abnormalities, which include deficits in motor coordination, gait abnormalities and muscle weakness (Figure 10) (Gioiosa et al., 2008; Head

et al., 2010; Trushina et al., 2006a). Additionally, Cav1 KO mice show behavioral changes associated with cholinergic dysfunction, characterized by impaired spatial memory, increased anxiety and reduced exploratory behavior in a new environment (Gioiosa et al., 2008). Interestingly, the most striking phenotype of Cav1 KO mice was observed during a tail-suspension test; when suspended on their tail, these mice exhibit a phenotype referred as “clasping”, where the mice press all their four paws against the body, or a unique spinning phenotype, in which the mice spin in horizontal plane upon tail suspension (Figure 10) (Trushina et al., 2006a). Interestingly, the clasping phenotype is associated with transgenic mice models for neurodegenerative diseases, including Huntington and Alzheimer disease (Lalonde and Strazielle, 2011). Similarly the spinning behavior has been previously observed in mice with vestibular dysfunction (Gnedeva and Hudspeth, 2015; GORRILL, 1956) or cerebellar deficits (Cemal et al., 2002).

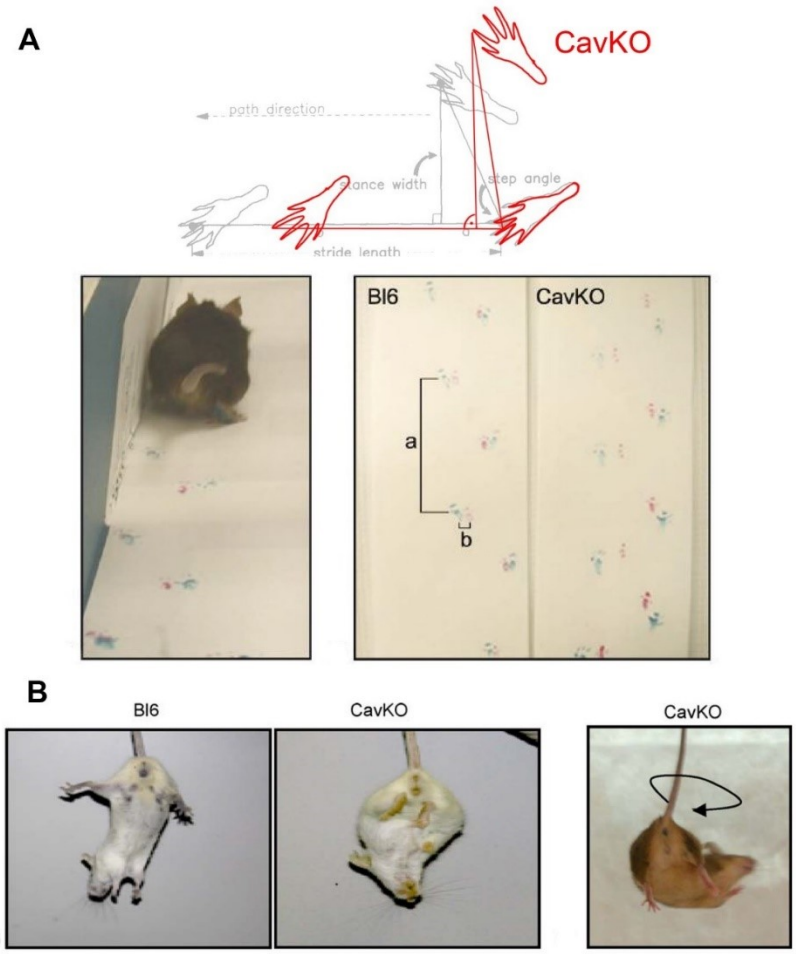

Figure 10: Cav1 loss-of-function in mice causes impaired motor control and behavioral abnormalities.
A Gait abnormalities in Cav1 KO mice in comparison to wild type littermates (Bl6). Gait behavior of wild type mice is shown in grey and those of Cav1 KO mice in red. Cav1 KO mice display a shorter stride length (a) as well as a wider overlap between paws (b). **B** Representative behavior of wild type (Bl6) or Cav1 KO mice during a tail suspension test. Wild type mice display normal behavior upon tail suspension. Cav1 KO mice shows an age-dependent clasping and spinning phenotype (Modified after Trushina et al., 2006a).

Caveolin proteins are expressed in various areas and cell types of the brain such as astrocytes, Schwann cells, dorsal root ganglia cells and microvessels (Cameron et al., 1997; Galbiati et al., 1998; MacDonald et al., 2018; Mikol et al., 1999; Virgintino et al., 2002). It has been shown that Cav1 is important for the blood brain barrier integrity and physiology by negatively regulating the degradation of tight junction proteins through the inhibition of Metalloproteases during ischemic stroke (Choi et al., 2016; Gu et al., 2012; Li et al., 2015). In contrast, Cav1 also increases the blood brain barrier permeability by regulating the caveolae-dependent trafficking of tight junction proteins (Liu et al., 2016; Stamatovic et al., 2009). Further, Cav1 appears to have a function in glia cells, as it is upregulated during myelination of Schwann cells (glia cell of the PNS) and oligodendrocytes (glia cell of the CNS).

Expression studies of the murine brain have also shown that Cav1 is expressed in neurons of the cerebral cortex, hippocampus, cerebellum and the midbrain (Kang et al., 2006). Thereby, protein expression seems to be age-dependent, as Cav1 expression levels are the lowest in the brain of young and the highest in aged rats (Kang et al., 2006). Similarly, Shikanai and colleagues demonstrated that Cav1 shows a spatial and temporal expression in hippocampal neurons, with high expression in the neurites and somas of immature neurons and a decreased or non-detectable expression in mature hippocampal neurons of young mice (Shikanai et al., 2018). Further, they also reported that Cav1 regulates early pruning processes and leading process elongation of hippocampal neurons during neuronal maturation and migration *in vivo* (Figure 11) (Shikanai et al., 2018). Loss-of-function of Cav 1 in these neurons resulted in an increased number of immature neurites as well as a shorter leading process compared to wild type neurons, due to the impaired trafficking and recycling of N-cadherin from immature neurites to the leading process (Figure 11) (Shikanai et al., 2018).

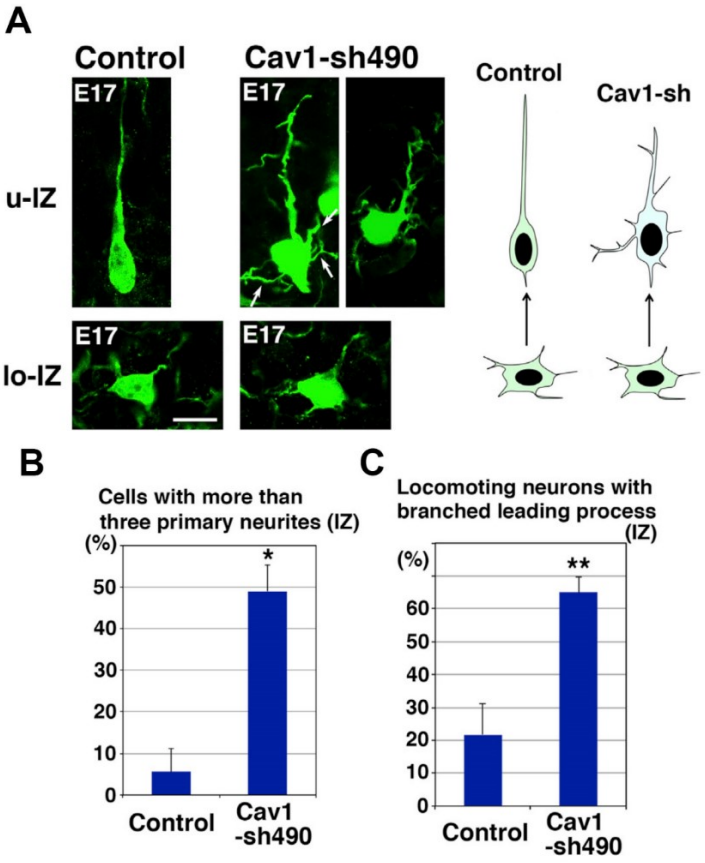

Figure 11: Cav1 regulates neuronal maturation.
A Neural specific loss-of-function of Cav1 (Cav-sh490) impairs neurite pruning and leading process elongation during early neuronal maturation. Neurons from the upper intermediate zone (u-IZ), which are depleted of Cav1 expression, show an increased number of primary neurites (B) as well as an increased number of branched leading processes (C) in comparison to control neurons (Modified after Shikanai et al., 2018).

Cav1 is a negative regulator for cell proliferation. Up-regulation of this protein has been associated with cellular senescence (Galbiati et al., 2001b; Park et al., 2005; Park et al., 2000). Interestingly, the loss of Cav1 expression in the brain leads to an increased VEGF (vascular endothelial growth factor)-dependent proliferation of neural stem cells in the subventricular zone and the hippocampal dentate gyrus of adult mice (Jasmin et al., 2009; Li et al., 2011). Further, Cav1 has been found to be upregulated in the brain of aged murine models and rats as well as in patients with Alzheimer diseases (Gaudreault et al., 2004; Kang et al., 2006) indicating a function for Cav1 in neuronal senescence. Interestingly, findings of age-related expression and function of Cav1 in the brain are inconclusive. While some studies showed an age-dependent increase of Cav1 in the hippocampus (Gaudreault et al., 2004; Kang et al., 2006) others reported the opposite (Head et al., 2010; Liu et al., 2013). Similarly, both the knockout (Eisinger et al., 2020; Li et al., 2011) as well as overexpression (Head et al., 2011; Mandyam et al., 2017) of Cav1 are reported to enhance dendritic number, length and arborization of neurons *in vivo* and *in vitro*.

Interestingly, while increased expression of Cav1 has been associated with elevated amyloid-β (Aβ) secretion and the pathogenesis of Alzheimer and Huntington disease (Kang et al., 2006; Trushina et al., 2014; Trushina et al., 2006b), the loss of Cav1 in the brain is also linked with neuronal degradation, loss of synaptic plasticity, increased astrogliosis and increased amyloid-β (Aβ) and P-Tau expression (Head et al., 2010). The amyloid-β (Aβ) peptides, proteolytic byproducts of the amyloid precursor protein (APP), are the major components of the senile plaques found in brains of Alzheimer's patient and are associated with neurodegeneration and cognitive regression in Alzheimer's disease (Knowles et al., 1999; Malek-Ahmadi et al., 2016).

In addition, Cav1 misregulation has been associated with dysregulated cholesterol homeostasis in the brain (Gaudreault et al., 2004). It has been shown that mutant huntingtin protein, the key-role player in the pathogenesis of Huntington's disease, interacts with Cav1 and inhibits Caveolin-mediated endocytosis in neurons, which leads to abnormal accumulation of cholesterol (Trushina et al., 2006b). Interestingly, depletion of Cav1 in a mouse model for Huntington's disease rescues the abnormal cholesterol accumulation and also delays Huntington-related phenotypes (Trushina et al., 2014).

While the overexpression of Cav1 is associated with the pathogenesis of neurodegenerative disease, Sawada *et al*. were able to show that neuronal targeted overexpression of Cav1 improves the overall pathophysiology of amyotrophic lateral sclerosis (ALS) mice (Sawada et al., 2019). Moreover, several studies demonstrated that neuronal targeted Cav1 positively modulates intracellular signaling including Trk tyrosine kinase receptor family- as well as Rac1/cdc42 signaling in membrane lipid rafts, thereby improving both synaptic plasticity and neuronal survival (Wang et al. 2019; Bilderback et al. 1999; Stern und Mermelstein 2010).

Given the similarities between loss-of-function and overexpression phenotypes, it seems likely that a balanced expression of Cav1 is required for a healthy development and aging of the brain.

1.7 The development of the *Xenopus* neuromuscular system

1.7.1 The organization of the spinal cord circuit

Due to the well-characterized and low complexity of its nervous system, the model organism *Xenopus laevis* provides a useful system to study the early development of the central nervous system (CNS). The spinal cord of *Xenopus* tadpoles contains eight easy distinguishable types of neurons: Rohon-Beard neurons (RB), motoneurons (mn), Kolmer-Adghur cells (KA) and five types of interneurons (Figure 12) (Hartenstein, 1989b; Roberts, 2000b; Roberts and Clarke, 1982). Rohon-Beard neurons are touch-sensitive sensory neurons that innervate the skin. The soma of these neurons is located dorsally of the neural

tube and extents three axons: a peripheral axon, which innervates the skin and two central axons that are located within the neural tube. These transmit excitations via interneurons to the ventrally located motoneurons to generate coordinated motor responses (Clarke et al., 1984; Li et al., 2003; Roberts et al., 2010; Roberts, 2000b). Another class of sensory neurons found in the *Xenopus* spinal cord are the so called Kolmer-Agduhr cells (Dale et al., 1987). These cells are cerebrospinal fluid-contacting neurons which contain multiple cilia and microvilli reaching into the neurocoele of the spinal cord (Dale et al., 1987). The cholinergic primary motoneurons are located in the ventral portion of the spinal cord. The soma of these neurons is multipolar with an ipsilateral descending axon that innervates the axial musculature (Roberts et al., 1999; Soffe and Roberts, 1982). *Xenopus* interneurons can be divided into three classes depending on their axonal projection: ascending interneurons, commissural interneuron and descending interneurons (Li et al., 2001). There are overall five types of interneurons described in the *Xenopus* spinal cord: excitatory dorsolateral commissural (dla) and inhibitory commissural interneurons (cIN), excitatory dorsolateral ascending (dlc) and inhibitory ascending interneurons (aIN) as well as excitatory descending interneurons (dIN) (Li et al., 2001; Roberts et al., 1981).

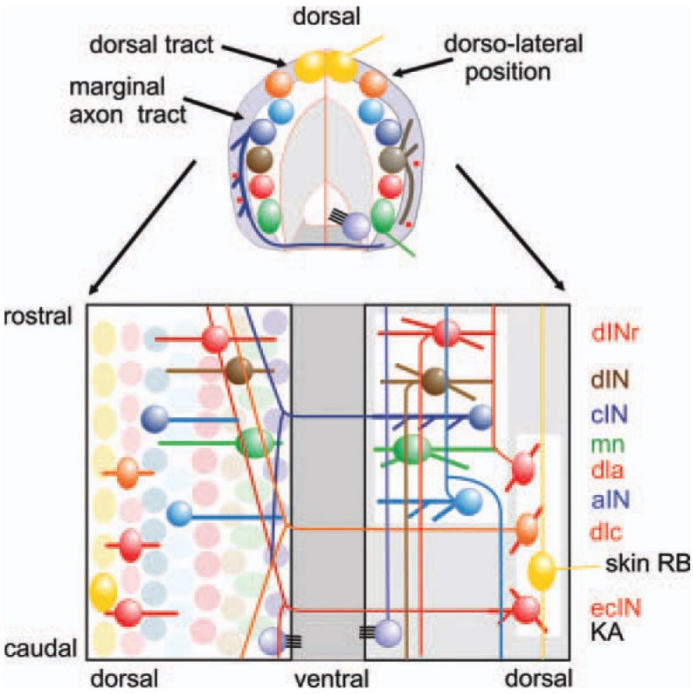

Figure 12: Neuron types in the *Xenopus laevis* embryo.
Schema of the neuronal types as well as axonal tracts in the spinal cord of *Xenopus* embryos in a transverse section (top) as well as horizontal cross-section (bottom). Rohon-Beard neurons (RB) are shown in yellow, motoneurons (mn) in green, excitatory dorsolateral commissural interneurons (dlc) in orange, excitatory descending interneurons (dIN) in brown, inhibitory commissural interneurons (cIN) in dark purple, inhibitory ascending interneurons (aIN) in blue and excitatory dorsolateral interneurons (dla) in red. Kolmer-Agdhur (KA) neurons are shown in purple (Roberts, 2000a).

1.7.2 Early neurogenesis in *Xenopus laevis*

Similar to other anamniote species, *Xenopus* neurogenesis occurs in two distinct stages, including the primary neurogenesis, which provides the rudimentary nervous system controlling early embryonic behaviour and the secondary neurogenesis forming the adult central nervous system (CNS) (Hartenstein, 1989b; Thuret et al., 2015; Wullimann et al., 2005). The establishment of the primary neural circuit starts with neural induction, in which the neural plate is formed by a fate change of epidermal cells to neural precursors during gastrulation (Harland, 2000). This process is mediated by secreted factors produced by the adjacent mesoderm, which inhibit the Bone Morphogenetic Protein (BMP) signaling in the prospective neural plate and prime the epidermal cells to adopt a neural fate. Among these factors are the BMP antagonists Chordin and Noggin as well as *Xenopus* Nodal-related 3 (Xnr3), which are secreted from the blastula Chordin- and Noggin expressing (BCNE) centre (Fainsod et al., 1997; Kuroda et al., 2004; Piccolo et al., 1996; Smith et al., 1995; Zimmerman et al., 1996). Similarly, the fibroblast growth factor (FGF) as well as canonical Wnt signalling promote neural fate by acting antagonistically to BMP signaling (Baker et al., 1999; Delaune et al., 2005; Pera et al., 2003; Wilson et al., 2000) and further modulate the posteriorization of the neuroectoderm together with retinoic acid (Blumberg et al., 1997; McGrew et al., 1997). Following the establishment of the presumptive neural ectoderm, the inhibition of BMP signaling induces the expression of a set of pan-neural markers in broad overlapping regions (reviewed in Moody and Je, 2002). These factors regulate the stabilization and maintenance of the neural fate as well as the following initiation of neuronal differentiation (Mizuseki et al., 1998a; Rogers et al., 2008). While members of the SoxB (sex determining region Y (SRY)-box, Sox 1-3) as well as the Zic (Zinc finger of the *c*erebellum; Zic1 and Zic3) protein-family modulate the sensitivity of the neuroectoderm in respond to neural inductive signals such as Noggin and FGF (Brewster et al., 1998; Kishi et al., 2000; Kuo et al., 1998; Mizuseki et al., 1998a; Nakata et al., 1997), the coiled-coil protein Geminin as well as FoxD (Forkhead-Box D), a member of the *forkhead/winged helix* family of transcription factors, maintains the immature state of the neural progenitors by inhibiting their differentiation (Seo and Kroll, 2006; Sullivan et al., 2001). Downstream of the early neural stabilizing genes, SoxD as well as the Iroquois gene family (Xiro 1-3) promote the initiation of neuronal differentiation by the regulation of the basic helix-loop-helix (bHLH) proneural genes (Bellefroid, 1998; Gomez-Skarmeta, 1998; Gómez-Skarmeta et al., 2001; Mizuseki et al., 1998b).

The newly formed neuroectoderm is comprised of undifferentiated neuronal progenitor cells, from which only a restricted number will differentiate into primary neurons (Hartenstein, 1989b). The open neural plate of the *Xenopus* embryo consists of a bi-layered epithelium, a

so called deep and a sensorial layer, which later intercalates during neural tube closure to form the neural tube (Figure 13) (Davidson and Keller, 1999). While the progenitors of the primary neurons are located within the deep layer of the neural tube, secondary neurons arise both equally from the deep as well as the superficial layer, but stay differentially inactive until the onset of metamorphosis (Hartenstein, 1989b; Thuret et al., 2015; Wullimann et al., 2005).

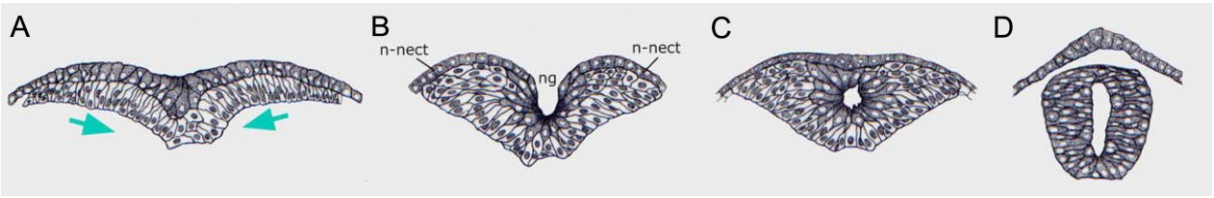

Figure 13: Formation of the neural tube in *Xenopus* embryos
A The neural plate of Xenopus embryos is a bi-layered epithelium, containing a deep/inner layer and a superficial or sensorial layer. **B-D** Upon neural tube closure, involving the invagination (B) of the neural plate, the two layer intercalates (C) to form a neural tube (D). ng = neural groove, n-nect = non-neural ectoderm (Modified after Werner et al., 2019).

The exact molecular mechanism of how the spatial-temporal expression of these distinct neuronal populations is regulated is still not well understood. However, it is proposed that Geminin, which is both expressed in the deep as well as superficial layer, modulates the spatiotemporal regulation of neuronal differentiation (Seo et al., 2005). With the onset of primary neurogenesis Geminin expression is eliminated in the primary neuronal progenitor cells, while it remains expressed in progenitors for secondary neurons (Seo et al., 2005).

The neuronal differentiation of primary neurons takes place in so called neurogenic regions, which are determined by secreting factors from the midline. Among these, shh as well as retinoic acid regulate the expression of Gli and Zic2 genes, which are required to restrict the expression of proneural genes within the three longitudinal neurogenic domains on each side of the embryonic midline (Figure 14) (Brewster et al., 1998; Franco et al., 1999). Proneural genes are transcription factors belonging to the bHLH gene class and are subdivided into distinct protein families such as the atonal family (Math1 and 2), olig family (Olig 1-3), neuroD family (NeuroD), neurogenin family (Ngnr1-3) as well as the achaete-scute family (ash) (Bertrand et al., 2002). These proneural genes function as positive regulators for neurogenesis by providing initial positional information for the prospective neuronal identity and regulating the expression of genes, which are required for neuronal differentiation (Bertrand et al., 2002).

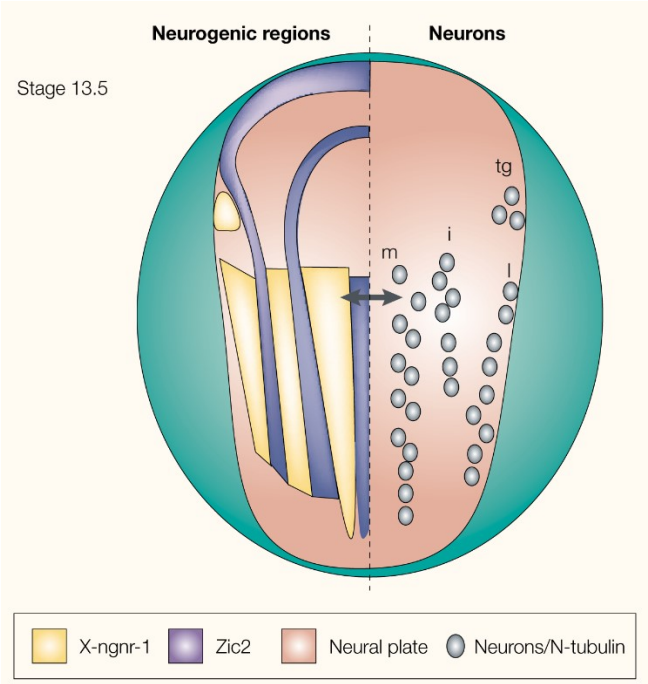

Figure 14: Primary neurogenesis in *Xenopus laevis.*
Schematic scheme of the neural plate (red) and the neurogenic regions (yellow) is shown. The expression of Zic 2 restricts the expression of proneural genes, including x-ngnr 1, within the three longitudinal neurogenic domains on each side of the embryonic midline. These domains represent the future position of primary neurons. The medial (m) domain gives rise to motoneurons, interneurons are derived from the intermediate (I) domain and sensory Rohon-Beard neurons from the lateral (l) domain. An additional domain (trigeminal ganglion (tg) is shown. X-ngnr 1 functions as positive regulator for neurogenesis by providing initial positional information for the prospective neuronal identity (Corral and Storey, 2001).

Despite the potential of the neuronal precursors to differentiate into mature neuronal cells, only a subset of cells undergo differentiation. In a process called lateral inhibition, mediated by the Delta-Notch pathway, the number of neuronal precursor cells, that are committed to a neuronal fate, gets restricted (Figure 15). The expression of the bHLH proneural gene neurogenin-related 1 (ngnr-1) promotes the expression of the membrane bound Notch ligand X-Delta within a nascent neuroblast (Chitnis et al., 1995; Haenlin et al., 1994; Kunisch et al., 1994). The binding of X-Delta to its receptor Notch, which is presented on neighboring cells, induces the proteolytic cleavage and release of the intracellular domain (NICD) of Notch and its subsequent translocation into the nucleus (Figure 15) (Brou et al., 2000; Mumm et al., 2000; Schroeter et al., 1998; Strooper et al., 1999). Within the nucleus, the NICD facilitates as transcriptional co-activator together with the transcription factor Suppressor of hairless (SU(H)) the expression of genes, such as the transcriptional repressors Enhancer of split E(spl) and Hairy (Her), which inhibit neuronal differentiation (Figure 15) (Dawson et al., 1995; Jennings et al., 1994; Lecourtois and Schweisguth, 1995; Wettstein et al., 1997). Consequently, while cells expressing the X-Delta1 protein undergo neuronal differentiation, the expression of E(spl) and Her in the neighboring cells antagonize neuronal differentiation by repressing the transcription of proneural genes such as ngnr-1, but also the ligand X-Delta1 (Dawson et al., 1995; Oellers et al., 1994). Besides the transcription of X-Delta, ngnr-

1 also facilitates the expression of regulators for terminal differentiation, such as X-NeuroD, X-MyT1 and Xebf3 (Bellefroid et al., 1996; Chitnis and Kintner, 1996; Lee et al., 1995; Pozzoli et al., 2001).

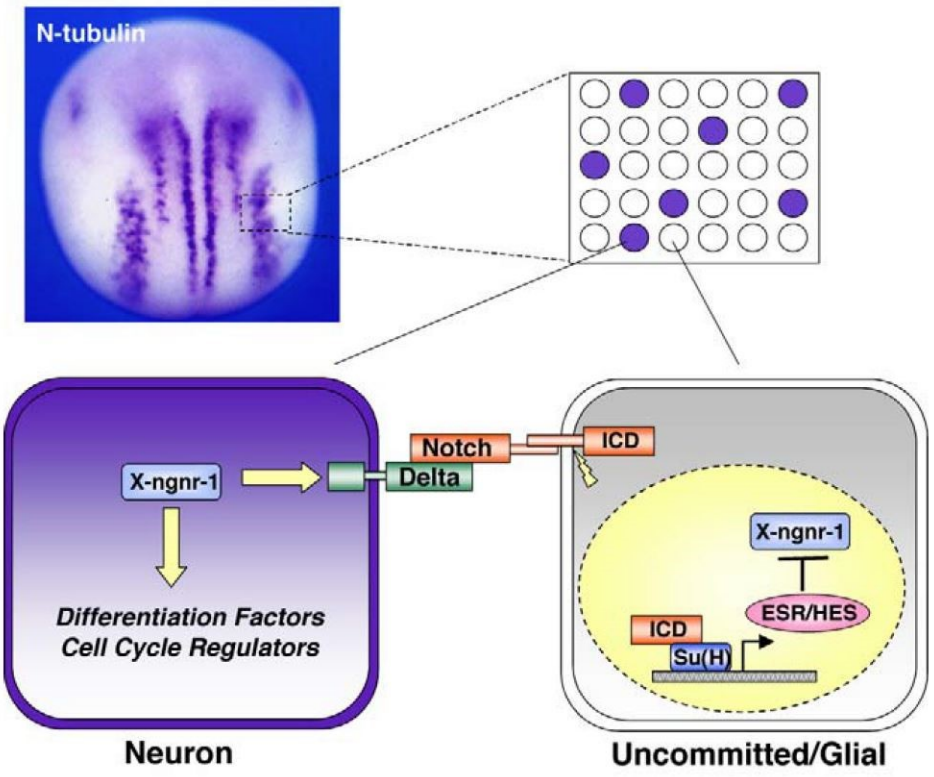

Figure 15: The Delta-Notch pathway mediates lateral inhibition during early neurogenesis. N-tubulin shows the localization of neuronal progenitors in three longitudinal domains on both sites of the midline. Lateral inhibition, mediated by the Delta-Notch pathway restricts the number of neuronal progenitors that are subjected to neuronal differentiation (purple). The proneural protein X-ngnr-1 induces the expression of the Notch ligand Delta. Binding of Delta to its receptor Notch presented on the neighboring cell, leads to proteolytic cleavage of the intracellular domain of Notch (ICD) and its translocation into the nucleus. Together with Su(H), the ICD mediates the expression of genes required for the transcriptional repression of proneural genes and the subsequent inhibition of neuronal differentiation (Henningfeld *et al*. 2007).

Differentiated neurons are positive for the neural-specific marker neuron specific class II β tubulin (n-tubulin), which is expressed in a punctuated pattern within three longitudinal stripes on each side of the embryonic midline (Oschwald et al., 1991). The position of these expression domains represents the identity of the neuronal subtypes that are found in the closed embryonic neural tube. Thereby, neuroblasts located in the lateral stripe give rise to the Rohon-Beard neurons, the interneurons derive from the intermediate stripe and the primary motoneurons from the medial stripe (Oschwald et al., 1991; Roberts, 2000b). During the process of neurogenesis, the neural plate begins to fold to form a closed spinal cord, involving the apical constriction and elongation as well as the convergent extension of the neuroepithelium (Figure 13) (Davidson and Keller, 1999; reviewed in Sokol, 2016). In *Xenopus*, the neural plate is formed by two layers, the superficial sensory layer as well as the deep layer. While the deep layer primarily gives rise to primary neurons, the superficial

layer contains neural precursors of both primary and secondary neurons (Hartenstein, 1989b; Roberts, 2000b; Thuret et al., 2015). These neurons remain in an undifferentiated state until the onset of metamorphosis (St.54 onwards), where they begin to differentiate to form the adult central nervous system (Chalmers et al., 2002; Thuret et al., 2015). During the process of neural tube closure, the deep as well as the superficial layer undergo radial intercalation to form a single-layered neural tube (Edlund et al., 2013). Within the closed neural tube three distinct regions can be identified: the ventricular layer in which neural stem cells as well as neural precursors reside, the intermediate layer, consisting out of proliferating postmitotic cells as well as the mantel layer, where the neuronal differentiation takes place and mature primary neurons locate (Figure 16) (Corral and Storey, 2001).

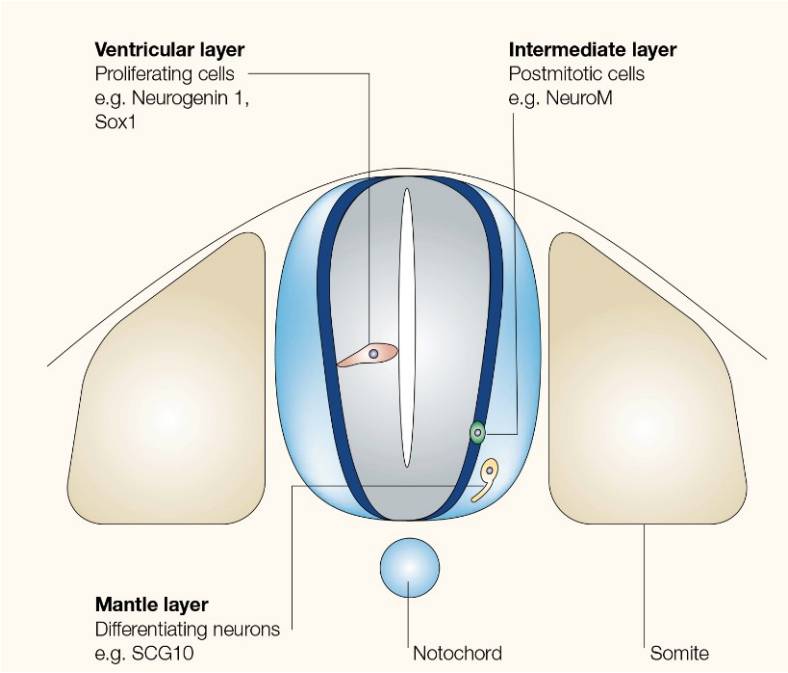

Figure 16: Domains of the closed spinal cord.
Schematic of a cross-section of the closed spinal cord. Proliferating cells are located in the ventricular layer. Postmitotic neuronal cells are present in the intermediate layer, while differentiating and mature neurons are found in the mantle layer (Corral and Storey, 2001).

Thereby, the positional identity of primary neurons is determined by their position within the neural tube and is specified by secreted morphogens from the floorplate as well as the roof plate of the spinal cord (Briscoe and Ericson, 1999). Each progenitor domain or neuronal subtype is characterized by the expression of a distinct subset of homeodomain transcription factors, including Pax6 and 7, Nkx 6.1, Nkx 2.2, Irx3 as well as Dbx 1 and 2, whose expression is determined by a gradient of sonic hedgehog (Shh), Bone morphogenic protein (BMP) as well as Wnt (Briscoe et al., 2000; Briscoe and Ericson, 1999; Briscoe and Novitch, 2008; Ulloa and Martí, 2010). Shh is secreted from the floor plate, resulting in a ventral to dorsal gradient. In turn, BMP and Wnt are expressed in the roof plate, which create a dorsal to ventral gradient within the neural tube and function antagonistically to the Shh morphogen (Megason and McMahon, 2002; Timmer et al., 2002). While, high levels of Shh and the lack

of BMP/Wnt in the most ventral region of the spinal cord induces the differentiation of motoneurons (Ericson et al., 1997; Ericson et al., 1996; Yu et al., 2008), high levels of BMP/Wnt and no expression of Shh in the most dorsal part of the neural tube gives rise to sensory neurons (Timmer et al., 2002).

1.7.3 The establishment of the early neuromuscular system

The first neuronal differentiation can be observed in the anterior region of the embryonic spinal cord between developmental stage 22-25 (NF), starting with Rohon-Beard neurons followed closely by motoneurons and interneurons (Hartenstein, 1993; Hartenstein, 1989a). Differentiation of primary neurons precedes in an anterior to posterior direction until stage 37/38 to form the embryonic CNS (Hartenstein, 1993).

The development of the musculature and the establishment of early neuromuscular circuits are temporally coupled. In *Xenopus*, myotomal segmentation starts at stage 17 and precedes until stage 40, with 45 somite-pairs forming in an average rate of 0.9 somite pairs per hour in an anterior to posterior direction (Chanoine and Hardy, 2003; Gurdon et al., 1997). This if followed by the growth of the first motoneuron axons into the intermyotomal clefts at a rate of 0.7 clefts per hour. At stage 25/26, which is referred as “early swimming stage”, the first involuntary movements can be observed. At this stage, 15 somite pairs have been formed with the first three myotomal segments being innervated and showing synaptic activity (Blackshaw and Warner, 1976; van Mier et al., 1989). The first rhythmic swimming behaviour can be observed between stage 27 and 30, in which at least 6 to 10 somites are functionally innervated (van Mier et al., 1989). Around stage 37, in the so called “free swimming stage”, a neural connectivity required for rhythmic swimming movements has been established in the spinal cord and primary motoneurons innervate a large number of somitic segments (Roberts, 2000b; van Mier et al., 1989).

1.8 Aim of this study

Caveolin 1 is an essential component of caveolae membrane domains and participates in a vast amount of cellular processes, including endocytosis, lipid homeostasis as well as signal transduction. During recent years, the participation of Cav1 in the pathogenesis of age-related neurodegenerative diseases, such as Alzheimer's, has sparked interest in the neuronal function of Cav1. However, the exact mechanism of how misexpression of Cav1 might contribute to neurodegeneration is still not well understood. Thus, the aim of this thesis is to add to the understanding of the neuronal function of Cav1, by using the model organism *Xenopus laevis*. Previous loss-of-function studies have shown that the injection of a translation blocking Morpholino of Cav1α (Cav1α MO) causes severe swimming defects in *Xenopus* embryos (Berger, 2016), suggesting that Cav1 might function in the neuronal circuits controlling swimming behavior. In this thesis the exact role of Cav1α in the development of *Xenopus* embryos as well as its function in the locomotor system will be examined in more detail by performing loss-of-function studies by using a Splice-blocking Morpholino (Cav1α-Spl MO) in addition to the Cav1α MO. Profound expression analysis of Cav1 during embryonic development will be performed by *in situ* hybridization as well as immunofluorescence staining. In addition, to characterize the mechanism causing the swimming defects, targeted injections will be performed. Therefore, the Morpholinos will be injected either into neural or muscular tissue, to distinguish between a neural or muscular function of Cav1α. If it is confirmed, that Cav1α functions in neuronal tissue, the nervous system of these embryos will be examined by immunofluorescence staining. Moreover, spinal cord explantation assays will be performed to gain insights into potential consequences of Cav1α loss-of-function on neuronal morphology.

As it is well known that Cav proteins also have a mechano-protective function within the notochord, the notochord of the morphant embryos will be analyzed by electron microscopy. In addition to that, Morpholino-mediated loss-of-function of Cavin 1 will be performed, to address how impaired notochord integrity contributes to the aberrant swimming behavior.

2 Material and Methods

2.1 Chemicals

The chemicals used in this work were purchased from the following companies: Carl Roth (Karlsruhe), Thermo Fisher Scientific (Waltham, MA, USA), Sigma -Aldrich (Munich), Roche (Mannheim), Applichem (Darmstadt), Merck (Darmstadt),

2.2 Buffers and Media

Table 1: Buffers and Media

Buffers and Media	
APB (alkaline phosphatase-buffer):	100 mM Tris (pH 9.5) 50 mM $MgCl_2$ 100 mM NaCl 0.1 % Tween20 (Roth)
APB/NBT/BCIP:	NBT/ BCIP stock-solution (Roche) diluted 1:50 in APB
BA/BB:	1:2 Benzylalcohol/ Benzylbezoate (Sigma-Aldrich)
Bleaching solution (whole mount *in situ* hybridization):	1 % H_2O_2 5 % Formamide (Sigma) 0.5 % SSC
Blocking reagent (BR):	10 % BSA (Roth) in MAB heat to dissolve
Blockingsolution (Western blot):	1 xPBS 5 % non-fat dry milk powder 0.1 % Tween 20
Blockingsolution (whole mount immunofluorescence staining):	0,1 M glycine 2 % powdered milk 5 % serum (goat, horse) in PBS-TD

Buffers and Media	
Cacodylatbuffer (0,1M):	0.2 M Cacodylat (Fuca/Sigma) 0.2 N HCl pH. 7,2
CoIP buffer:	50 mM Tris (pH 7.5) 150 mM NaCl 0.5 % NP-400
Danilchicks Medium for Amy (DFA)	53 mM NaCl 5 mM Na_2CO_3 4.5 mM Potassium Gluconate 32 mM Sodium Gluconate 1 mM $CaCl_2$ 1 mM $MgSo_4$ pH to 8.3 with 1 M Bicine Add 0.5 g/ml BSA Sterile filter into a 50 ml Falcon store at -20°C
Denhardts (100x):	2 % BSA 2 % Polyvinylpyrrolidon (Sigma) 2 % Ficoll 400 in ddH_2O
Dent's fixative:	80 % methanol 20 % dimethylsulfoxide (DMSO)
Gelatin/albumin embedding medium:	4.4 % gelatin 27 % bovine serum albumin (BSA) 18 % saccharose in 1x PBS
Glutaraldehyd:	6.25 % Glutaraldehyd (Roth) 0.1 M Cacodlyat pH 7.2
Hyaloronidase in sodium acetate:	1 µg/ml hyloronidase (Sigma) in 50 mM sodium acetate.

Buffers and Media	
Hybridization mix (Hybmix):	50 % (v/v) Formamid 5 x SSC 1 mg/ml Torula RNA (Sigma) 100 µg/ml Heparin (Roth) 1 x Denhardts 0.1 % (v/v) Tween-20 0.1 % (v/v) CHAPS (Sigma) 10 mM EDTA Store at -20°C
Injection buffer:	1 x MBS 2 % (w/v) Ficoll400 (Roth)
Laemmli loading buffer (6x):	350 mM Tris-HCl (pH 6.8) 9.3 % Dithiotreit 30 % (v/v) Glycerol 10 % SDS 0.02 % Bromphenolblue (Roth)
Laemmli running buffer (10x):	250 mM Tris-base 2.5 M Glycine 0.1 % SDS
LB-Agar:	1.5 % (w/v) agar-agar (Roth) in LB-medium
Loading Dye:	6 x Loading Dye Solution (Fermentas)
Luria-Bertani (LB)- Medium:	1 % (w/v) Bacto-Trypton (Roth) 0.5 % (w/v) yeast extract (Roth) 1 % (w/v) NaCl pH 7.5
MAB (5x):	0,5 M maleinacid (Roth) 0.75 M NaCl pH 7.5

Buffers and Media	
MBS (Ringersche Lösung, 1 x):	10 mM Hepes (Roth), pH 7.0 88 mM NaCl 1 mM KCl 2.4 mM $NaHCO_3$ 0.82 mM $MgSo_4$ 0.41 mM $CaCl_2$ 0.66 mM KNO_3
MEM (10 x):	1 M MOPS (Roth) 20 mM EGTA (Roth) 10 mM $MgSo_4$ heat and light sensitive
MEMFA:	1 x MEM 3.7 % (v/v) Formaldehyd (Roth/Merck)
Mowiol:	5 g Mowiol (Calbiochem) in 20 ml 1x PBS stirring 16 hours 10 ml Glyceros, stirring 16 hours Centrifuge at 20.000rpm for 30 min Store at -20°C
NBT/BCIP (Roche):	17.7 mg/ml NBT 50 mg/ml BCIP 67 % DMSO
PBS (10x):	1.37 M NaCl 27 mM KCl 100 mM Na_2HPO_4 18 mM KH_2PO_4 pH 7.4
PBS-TD (1 x):	1 % Triton X-100 1 % DMSO
Proteinase K-solution (Merck):	Stock solution 600U/ml; 0.25 µl/ml in PTw
PTw (1x) + FA:	4 % Formaldehyd in PTw

Buffers and Media	
PTw (1x):	1 xPBS, 0.1 % Tween20
SSC (20x):	0.3 M Sodium citrate 3 M NaCl pH 7.0
SSC (2x)/ RNase:	2 mg/ml RNase A, 5000 U/ml RNaseT1 (Thermos Scientific); 1:10000 in 2 x SSC
TAE (10x):	2 M Tris 100 mM EDTA (Roth) pH 7.7 with acetate
Transfer buffer (10x):	250 mM Tris 1.9 M glycine 20 % methanol
Triethanolamin (0,1 M):	1.86 % (w/v) Triethanolamin-Hydrochlorid pH 7.5
X-gal staining solution:	1 mg/ml X-Gal (Roth) 5 mM $K_3Fe(CN)_6$ (Roth) 5 mM $K_4Fe(CN)_6$ (Roth) 2 mM $MgCl_2$ 1 x PBS

2.3 Enzymes and Kit

Table 2: Enzymes and Kits

Enzymes and Kits	
Collagenase	Sigma Aldrich
DNase I (1 U/µl):	GE Healthcare
Dream Taq Polymerase (5 U/µl)	Thermo Fischer Scientific
Fast Digest Restriction Endonucleases,	Thermo Fischer Scientific
Hyaloronidase from bovine testes (400-1000 U/mg)	Sigma
IllustraTM RNA Mini Spin Kit	GE Healthcare

Enzymes and Kits	
Phusion DNA Polymerase (2 U/µl), Fynnzymes	Thermo Fischer Scientific
Proteinase K (20 mg/ml), Merck	Carl Roth
RNase A (2 mg/ml)	Thermo Fischer Scientific
RNase free water	Amresco
RNase Out (40 U/µl)	Invitrogen
RNase T1 1000 U/µl	Thermo Fischer Scientific
RNeasy Mini Kit	Quiagen
SP6 and T7 mMESSAGE mMACHINE Kit	Invitrogen
SP6, T3, T7 RNA Polymerases (20 U/µl)	Thermo Fischer Scientific
SuperSignal West Dura Extended Duration Substrate kit	Thermo Fischer Scientific
T4 DNA Ligase (1 U/µl)	Fermentas
Zymoclean Gel DNA Recovery Kit	Zymo Research

2.4 Additional Chemicals

Table 3: Chemicals and Reagens

Additional Chemicals and Reagens	
Benzocaine	Sigma Aldrich
DAKO	Deutschland GmbH
DAPI (1mg/ml)	Roth
DNA Ladder 1kb Plus	Thermo Fischer Scientific
Fibronectin	
Gel-Red (10.000x)	Biotium
Human Choriongonadotropin (hcG)	Sigma Aldrich
Laminin	Sigma Aldrich
Loading Dye (6x)	Thermo Fischer Scientific

Additional Chemicals and Reagens	
Phalloidin (TRITC, 0.5 mg/ml in DMSO)	Sigma Aldrich
Poly-D Lysine	Sigma Aldrich
X-gal (5-Bromo-4chloro-3indolyl α-D-galactopyranoside)	Roth
α-bungarotoxin (10 mg/ml, tetramethylrhodamine)	Sigma

2.5 Technical Hardware

Table 4: Technical Hardware

Technical Hardware	
Spinning Disc	Zeiss
Imaging System for Gel-Electrophoresis and Western blot	LI-COR ODDYSEY
Microsoft Office 2010	Microsoft
Prism8	GraphPad
Axio Observer Z1 inverted microscope	Zeiss
Confocal laser scan microscope (TCS-SP5)	Leica
Magnetic Glass Microelectrode Horizontal Needle Puller, PN-13)	Narishige AG
micromanipulation system (PV820 Pneumatic Pump, M3301 Micromanipulator	World Precision Instruments

2.6 Constructs

2.6.1 .. Expression constructs for *in situ* hybridization/overexpression

Table 5: Plasmids for *in situ* hybridization/ overexpression

Insert / Vector	Insert	Reference / clone strategy:
Caveolin 1α /pCS2+	Full length *Xenopus laevis* caveolin1α	cloned by Hanna Peradziryi, unpuplished data, *Xenopus laevis* full length Caveolin 1α was amplified using primers xcav1a F EcorI Xcav1a R xhoI RZPD, catalogue number IRBMp990B0725D
Caveolin 1α -HA /pCS2-HA	Full length *Xenopus laevis* caveolin 1α fused with HA-tag	cloned by Hanna Peradziryi, PhD thesis, full length caveolin 1a was amplified using primers Xcav1a F EcorI Xcav1a R XhoI . Reference lab book: HP III, p. 16
Caveolin 1α-rescue / pCS2-HA	*Xenopus laevis* caveolin 1α with deleted MO binding site	Cloned by Hanna Berger, PHD thesis (Berger, 2016, PhD). the caveolin 1α rescue construct was amplified from the Caveolin 1α-HA plasmid using following primers; Cav1a new ATG NheI for Cav1a new ATG NheI rev.
Caveolin 1α-rescue-S82A/ pCS2-HA	*Xenopus laevis* caveolin 1α with deleted MO binding site and a mutated serine residue 82 to alanine,	Amplified by two step mutagenesis PCR using the Caveolin 1α-rescue-HA as template. Following primers were used: Cav1a_S82A_fw2: Cav1a_S82A_rv2:
Caveolin 1α-rescue-S82E/ pCS2-HA	*Xenopus laevis* caveolin 1α with deleted MO binding site and a mutated serine residue 82 to glutamine, constitutive active	Amplified by two step mutagenesis PCR using the Caveolin 1α-rescue-HA as

Insert / Vector	Insert	Reference / clone strategy:
		template. Following primers were used: Cav1a_S82E_fw2: Cav1a_S82E_rv2:
Caveolin 1α-rescue-C135A/ pCS2-HA	*Xenopus laevis* caveolin 1α with deleted MO binding site	Amplified by two step mutagenesis PCR using the Caveolin 1α-rescue-HA as template. Following primers were used: Cav1a_S82A_fw2: Cav1a_S82A_rv2:
Caveolin 1α Y14A/ pCS2-HA	dominant negative mutant of caveolin 1a with a mutation in the thyrosin residue 14	Cloned by Hanna Peradziryi Amplified from pCS2 / cav 1a-HA by site-directed mutagenesis using following primers: cav1 Y14A F: cav1 Y14A R:
Sema3A	*Xenopus* full length semaphorin 3A	(Koestner et al., 2008)
Sema3F	*Xenopus* full length semaphorin 3F	(Koestner et al., 2008)
RFPRuby-N1-Lifeact; pcDNA 3.1	Lifeact tagged with RFP	unknown
lacZ/ pCS2+	Bacterial β-galactosidase	(Smith and Harland, 1991)
mGFP/pCS2+	GAP43-GFP, membrane localized GFP	(Moriyoshi et al., 1996)
Pax3	*Xenopus leavis*, Pax3	unknown
Sox2	*Xenopus leavis*, Sox2	unknown

Insert / Vector	Insert	Reference / clone strategy:
caCdc42 V12 / pCDNA3.1	Constitutive active cdc42 (Homo sapiens)	(Schambony and Wedlich, 2007)
dnCdc42 N17 / pCS2+	Dominant negative cdc42 (*Xenopus leavis*)	(Choi and Han, 2002)
caRac1 V12 / pCS2+	Constitutive active Rac1 (Homo sapiens)	Cloned from the pCDNA3.1 vector into the pCS2+ vector by Anita Grund Original plasmid: (Kashef et al., 2009; Schambony and Wedlich, 2007)
dnRac1 N17 / pCS2+	Dominant negative Rac1 (Homo sapiens)	Cloned from the pCDNA3.1 vector into the pCS2+ vectro by Anita Grund Original plasmid: (Kashef et al., 2009; Schambony and Wedlich, 2007)
caRhoA V12/V14 / pCS2+	Constitutive active RhoA (Homo sapiens)	Cloned from the pCDNA3.1 vector into the pCS2+ vectro by Anita Grund Original plasmid: (Kashef et al., 2009; Schambony and Wedlich, 2007)
dnRhoA N19 / pCS2+	Dominant negative RhoA (Homo sapiens)	Cloned from the pCDNA3.1 vector into the pCS2+ vectro by Anita Grund Original plasmid: (Kashef et al., 2009; Schambony and Wedlich, 2007)
n-tubulin	Beta II tubulin; Cytoskeletal protein/neural specific, plasmid backbone unknown	Oschwald R. et al Int J Dev Biol 1991,35,399-405, Chinis A et al 1995, Nature 375, 761-766

2.6.2 .... Linearization of DNA constructs for *in vitro* transcription

Table 6: Plasmids for *in vitro* transcription

Construct name	sense RNA		antisense RNA	
	enzyme	polymerase	enzyme	polymerase
Caveolin 1α	NotI	SP6	SalI	T7
Caveolin 1α-GFP	NotI	SP6		
Caveolin 1α-HA	NotI	SP6		
Caveolin 1α-rescue	NotI	SP6		
Caveolin 1α-rescue-S82E	NotI	SP6		
Caveolin 1α-rescue-C135A	NotI	SP6		
Caveolin 1α Y14A	NotI	SP6		
RFPRuby-N1-Lifeact	DraIII	T7		
lacZ	NotI	SP6		
xtwist			EcoRI	T7
mGFP	NotI	SP6		
Pax3			SalI	T7
Sox2			EcoRI	T3
N-tub			BamHI	T3

2.6.3 .... Oligonucleotides

DNA primers were purchased from Eurofins MWG Synthesis GmbH.

Table 7: Oligonucleotides

Name	Sequence 5`-3`
Cav1a_S82E_fw	5' GATGGGACACATGAGTTCGATGGCATCTGG 3'
Cav1a_S82E_rv2	5' CCAGATGCCATCGAACTCATGTGTCCCATC-3'

Name	Sequence 5`-3`
cav1 Y14A F:	5'-TGAAGAGGGTGTTCTCGCCACCACGCCGGTCATC-3'
cav1 Y14A R	5'-GATGACCGGCGTGGTGGCGAGAACACCCTCTTCA-3'
Cav1a_S82A_fw2	5' GATGGGACACATGCTTTCGATGGCATCTGG-3'
Cav1a_S82A_rv2	5' CCAGATGCCATCGAAAGCATGTGTCCCATC 3'
Cav1a new ATG NheI for	5'- ATGCTAGCATGGAAGAGGGTGTTCTCTACAC-3'
Cav1a new ATG NheI rev	5'- ATGCTAGCGAATCGATGGGATCCTGCAAA-3'
xcav1a F EcorI	5'-TTGAATTCAGCATGTCTGGTGGCAAATACATAG-3'
Xcav1a R xhoI	5'-TTCTCGAGCACTTCTTTGCGTAAGGAA-3'
CavBC07 intronFW	5'-CCAGCAACTGAAGGACAGC-3'
xCav1α-HA-fw-EcoRI	5'TTGAATTCCCAGCAACTGAAGGACAGCATGT-3'

2.7 DNA Methods and cloning procedure

2.7.1 .... Plasmid DNA preparation

For analytical purpose, Plasmid DNA from *E.coli* was isolated using the geneJET Plasmid Miniprep Kit (Thermo scientific). To yield larger, preparative amounts of DNA the NucleoBond® Xtra Midi Kit (Machery-Nagel) was used. Plasmid isolation was performed according to the manufracurer's instructions. The DNA was eluted in an appropriate colume of milliQ water and concentration was measured using the Nano Drop-2000 Spectrometer (Thermo Scientific.).

2.7.2 .... Polymerase chain reaction (PCR)

Amplification of DNA fragments was performed by Polymerase chain reaction. Therefore, an amount of 10-100 ng template DNA and a concentration of 10µM of Oligonucleotides was used. In the case of analytical purposes, DreamTaq™ DNA Polymerase, and for cloning procedures, Phusion™ High Fidelity DNA Polymerase was performed according to

maufracturer's instructions. PCR fragments were purified using the Gene Jet PCR purification or the Zymoclean Gel DNA Recovery Kit.

Table 8: PCR cycling instruction

Cycle step	Phusion™-polymerase	DreamTaq™-Polymerase
	Temperature/Time	Temperature/Time
Initial denaturation	98°C/ 30 sec	95°C/ 60 s
Denaturation	98°C/ 10 sec	95°C/ 30 s
Annealing	Specific annealing temperature according to used primers/ 30 sec	
Extension	72°C/ 20 sec/bp	72°C/ 1 min/bp
Final extension	72°C/ 10 min	72°C/ 10 min

2.7.2.1. Side directed mutagenesis PCR

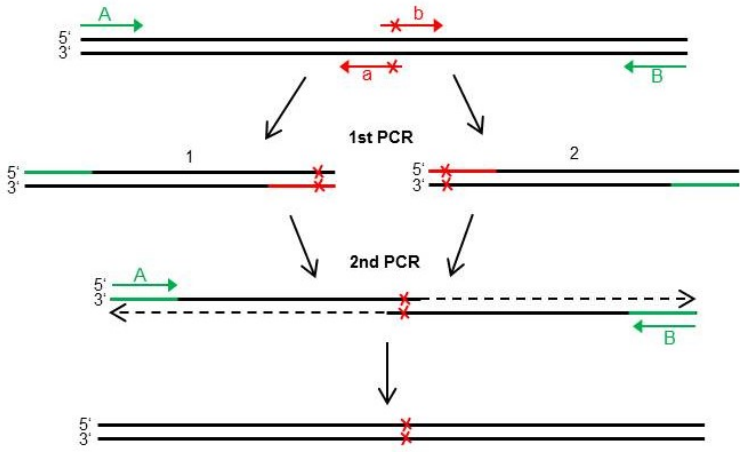

Side directed mutagenesis was performed to specifically mutate a desired amino acid residue within a protein. For this purpose two primer pairs were designed; a primer pair flanking the desired DNA fragment (A, B), and an internal primer pair, with complementary ends, containing the desired mutation (a,b). The mutagenesis was performed in two independent nested-PCR steps. In the first step, a PCR reaction with primer pair Aa and Bb, amplifying fragment 1 and 2, respectively, was performed to amplify the fragments containing the desired mutation. Subsequently the amplified fragments were purified by gel-extraction using the Zymoclean Gel DNA Recovery Kit (Zymo Research). In a second PCR, fragment 1 and 2 were mixed and amplified using primer pair A and B, to create the final construct containing the mutation. PCR fragments were purified using the the Zymoclean Gel DNA Recovery Kit

and were used for cloning. Phusion High-fidelity DNA-Polymerase and an amount of 10 ng template DNA and a concentration of 10 µM of Oligonucleotides were used.

Table 9: PCR cycling instruction

Cycle step	1th PCR	2nd PCR
	Temperature/Time	Temperature/Time
Initial denaturation	98°C/ 60 sec	98°C/ 60 s
Denaturation	98°C/ 10 sec	99°C/ 10 s
Annealing	Specific annealing temperature according to used primers/ 45 sec	
Extension	72°C/ 20 sec/bp	72°C/ 20 sec/bp
Final extension	72°C/ 10 min	72°C/ 10 min

2.7.3 ..DNA restriction digest

Restriction digests of DNA were performed with type II FastDigest® restriction endonucleases (Thermo Scientific) for 30 min at 37°C. Therefore 0.2-1 µg DNA was mixed with 1x FastDigest® buffer (10x) and 1 µl of FastDigest® restriction enzyme in a total volume of 20 µl. Nuclease free water was used to adjust the final volume.

2.7.4 ..Gel electrophoresis of nucleic acids

To qualify or purificate DNA or RNA, samples were separated by gel electrophoresis in a horizontal 1-2 % agarose gel according to standard protocol procedure. Nucleic acids were visualized by application of Gel Red (0.5 µl/ 10 ml) to the agarose gel.

2.7.5 ..Ligation of DNA fragments

Ligation of two DNA fragments was performed using an equimolar ratio of 1:3 of linearized vector and insert.

$$\text{insert mass [ng]} = 3 * \left(\frac{\text{insert bp}}{\text{vector bp}}\right) * \text{vector mass [ng]}$$

The purified DNA was incubated in a mixture of 1 µl T4-DNA ligase (Fermentas); 2 µl T4 Ligase buffer in a total volume of 20 µl for at least 4 h at room temperature. Reaction was terminated by incubation for 10 min at 65°C.

2.8 RNA Methods

2.8.1 .... *In vitro* transcription of sense RNA

For microinjection into *Xenopus* embryos, capped sense mRNA was *in vitro* synthezised using the SP6 or T7 mMassage mMachine kit (Ambion). Therefore, 1.2 µg of template RNA was used in a 20 µg reaction volume and incubated for 2 h at 37°C. Template DNA was removed by the addition of 1 µl of TurboDNaseI (Ambion) and the subsequent incubation for 15 min at 37°C. The newly synthesized mRNA was purified using the Illustra RNAspin Mini RNA Isolation Kit (GE Healthcare) according to the maufracturer's protocol. The mRNA-concentration was meassured using the Nano Drop-2000 Spectrometer (Thermo Scientific).

2.8.2 .. *In vitro* transcription of labeled antisense RNA

Expression analysis of mRNA was performed by whole mount *in situ* hybridization using Digoxigenin labelled antisense RNA probes. These were synthesized according to following protocol:

5x Transcription buffer (Fermentas)	5 µl
Digoxygenin-mix (Fermentas)	4 µl
0,75M DTT	1 µl
RNAse Out (Invitrogen)	1 µl
T3, T7 or SP6 polymerase (20 U/µl, Fermentas)	1 µl
linearized DNA template	1µg
add RNAse-free water to an end volume of:	25 µl

The synthesis of RNA was performed at 37°C for 2h, following a 15 min treatment at 37°C with 1 µl Turbo DnaseI (Ambion) to remove the residual DNA. Purification was performed using the he Illustra RNAspin Mini RNA Isolation Kit (GE Healthcare) according to the maufracturer's protocol. Quality and quantity of the synthetized RNA was estimated by gel electrophoresis in a 1% TAE agarose-gel. Dependent on the RNA quantity, RNA was diluted in Hybix and stored at -20°C.

2.8.3 ..cDNA synthesis / Reverse Transkriptase PCR

For verification of the Splice-blocking Morpholino as well as the time course analysis of endogenous Caveolin 1 mRNA, total RNA was isolated from *Xenopus* embryos at different developmental stages. RNA was isloated using the the GE Healthcare illustra RNAspin Mini Isolation Kit. cDNA was synthetized according to following protocol:

Following reaction was mixed and total volume was adjusted with nuclease free water:

Total RNA	1 ng- 5 µg
Random hexamer primer (Thermo Scientific)	0.2 µg
dNTP Mix (50 µM; Thermo Scientific)	1 mM
Total Volume	10 µl

Reaction mix was incubated for 5 min at 65°C and then put on ice. In a separate RNase-free microfuge tubes following reaction was mixed and adjusted to the total volume with nuclease free water.

MuLV Reverse transcriptase (Thermo Fischer Scientific)	20 units
5x RT Reaction Buffer (Thermo Scientific)	2 µl
RnaseOUt (Invitrogen)	20 units
Total volume	10 µl

The mixture was combined with the first reaction and incubated at 25°C for 5 min and subsequently for one hour at 42°C. The reaction was terminated in a brief incubation step for 20 min at 65°C. The cDNA was either used directly for following PCR analyzes or stored at -80°C.

2.9 Protein methods

2.9.1 ..Antibodies

Table 10: Antibodies

Name	Company, catalogue number	Description	Fixation	Dilution	
				WB	IF
actin	Merck, Millipore, MAB1501	Primary mouse monoclonal IgG, recognizes F- and G-actin		1:2000	

Name	Company, catalogue number	Description	Fixation	Dilution	
				WB	IF
Digoxigenin	Roche, 11093274910	Fab fragments from an anti-digoxigenin antibody from sheep, conjugated with alkaline phosphatase (AP)			1:5000
II-II6B3	Hybridoma Bank (DSHB)	Primary mouse monoclonal IgG recognizes chicken Collagen type II	Dents		1:10
NCAM (4d)	Hybridoma Bank (DSHB)	Primary mouse monoclonal IgG recognizes cytoplasmic region of chicken NCAM	Dents		1:30
Phalloidin-TRITC	Sigma-Aldrich (Merck)	SLBG6854V, 0.5 mg/ml, used for staining of F-actin	PFA		1:250
ZN-12	Developmental studies hybridoma bank	Primary mouse monoclonal IgG, neuronal cell surface marker (HNK-1)	PFA		1:50
α-Caveolin1	BD-Transduction Laboratories	610406, mouse primary monoclonal IgG, recognizes human Caveolin 1	Dents		1:100
α-Caveolin1	Abcam	Ab2910, primary rabbit Polyclonal IgG, recognizes the human Caveolin 1α isoform.		1:300	
α-GAPDH	Thermo Fisher Scientific	AM4300		1:4000	
α-GFP	Abcam/Biozol	Ab290 Primary rabbit polyclonal IgG	PFA		1:1000
α-GFP	Merck	11814460001 Primary mouse polyclonal IgG	PFA		1:1000
α-HA tag	Covance, MMS-101P-1000	Primary mouse monoclonal antibody against HA-tag	PFA	1:1000	

Name	Company, catalogue number	Description	Fixation	Dilution	
				WB	IF
α-mouse Alexa 594	Life Technologies	A21203 Goat secondary, polyclonal			1:400
α-mouse HRP	Santa Cruz, SC-2005	Secondary goat anti mouse IgG coupled with HRP		1:10000	
α-mouse-IRDye 680	Li-COR	926-68072 secondary mouse polyclonal IgG		1:5000	
α-mouse-IRDye 800	Li-COR	926-32212 secondary mouse polyclonal IgG		1:5000	
α-rabbit Alexa 488	Invitrogen	A-21206 Goat secondary, polyclonal			1:400
α-mouse Alexa 488	Invitrogen	A-11029 Goat secondary, polyclonal			1:400
α-rabbit HRP	Cell-Signaling	7074 Goat secundary Polyclonal IgG		1:1000	
α-rabbit-IRDye 680	Li-COR	956-68073, secondary rabbit polyclonal IgG		1:5000	
α-rabbit-IRDye 800	Li-COR	926-32213 secondary rabbit polyclonal IgG		1:5000	

2.9.2 ..Lysis of *Xenopus laevis* embryos for Western blotting

Protein extracts were prepared by the lysis of injected *Xenopus* embryos with insulin syringes in 10 µl/embryo Lysis buffer (CoIP buffer, 0.1% SDS, EDTA-free protease inhibitor cocktail tablet (Roche)). Lysates were centrifuged for 15 min by 16.000 g at 4°C and supernatant was transferred to a fresh Eppendorf tube. Protein lysates were diluted 1:6 with 6× Laemmli loading buffer and denatured for 5 min at 95°C before it was loaded to a 10 or 12 % SDS-PAGE gel.

2.9.3 ..Western Blotting

Proteins were separated by a 10-12 % SDS-PAGE in an electrical field. After separation, proteins were transferred to a nitrocellulose membrane (Whatman) by wet- or semi-dry blotting using either Bio-Rad wet blot cell (Bio-Rad), containing 1x transfer buffer/20% EtOH, at 100V for 1hour or semi dry Transfer system (Trans Blot-Turbo, Bio-Rad) at 25 V for 45 min.
Membrane was blocked in TBST-blocking buffer containing 5 % nonfat dried milk for at least 30 min. The antibody was removed by washing three times for 10 min each in blocking solution and the secondary antibody was applied for 1 h at room temperature. Proteins were detected using Pierce™ ECL Western Blotting Substrate (Thermo Scientific) and Odyssey® Fc Imaging System (LI-COR Bioscience).

*2.9.4 ..*Cultivation and Transformation of *E. coli Xl1-blue*

For bacterial transformation experiments, the chemo competent E. coli strain XL1-bue was cultivated in LB-medium supplemented with 100 mg/ml ampicillin (Roth) at 37°C and 200 rpm.
Transformation was performed by carefully mixing 5 µl plasmid DNA with 100 µl thawed chemo competent E. coli. The reaction was incubated for 30 min on ice. Afterwards, E. colis were heat shocked at 42°C for 30 seconds and immediately placed on ice for 1 -2 min. 800 µl prewarmed LB-medium was added to the tube following incubation for 1 hour at 37°C and 200 rpm. The culture was centrifuged for 1 min at 6000 rpm and 800 µl of the supernatant was removed by pipetting. The remaining pellet was carefully resuspended in the remaining medium and bacteria were plate out on LB agar containing 100 mg/ml Ampicillin. The plate was incubated over night at 37°C and colonies were picked for further analysis the following day.

Genotype: endA1 gyrA96(nal^{R}) thi-1 recA1 relA1 lac glnV44 F'[::Tn10 proAB^{+} lacI^{q} Δ(lacZ)M15] hsdR17(r_{K}^{-} m_{K}^{+})

2.10 *Xenopus* Methods

2.10.1 Statistical analysis

All experiments, if not indicated otherwise, were conducted at least three times. The total number of analyzed embryos (n) is indicated for each experiment. Normality of datasets was tested using D'Agostine & Pearson test, Shapiro-Wilk test and Kolmogorov-Smirnov test Significance was calculated by using either a two-tailed unpaired student's t-test or Mann-

Whitney test (Box blots) (* p-value ≤ 0.05; **p-value ≤0.01; ***p-value ≤ 0.001) using Microsoft excel (2013) or GraphPad Prism8. Standard errors of the mean (s.e.m) are shown for each graph.

2.10.2 .. *Xenopus laevis* testis macerates

Testis macerates were prepared by first euthanizing male *Xenopus* frogs in 0.05% benzocaine for 20-30 min at room temperature. To test if the frog was sufficiently euthanized, the male frog unresponsiveness was tested by pinching the skin between the toes with a tweezer. Additionally, as a second euthanasia method the spinal cord was severed by cervical section using a sharp knife. Both testes were dissected through opening the abdominal cavity and removal of the yellow body fat in the area of the genitourinary system with a sharp scissor and scalpel. The testes can be found directly attached to the kidney on both sites of the aorta. They were cut out and cleaned of residual fat and vascular tissue. Testes were stored up to two weeks in 1x MBS at 4°C. For fertilization of *Xenopus* oocytes, an appropriate amount of testes was macerated using a scalpel and stored in 1 ml of 1x MBS in a petri dish.

2.10.3 .. *In vitro* fertilization of *Xenopus laevis* eggs

Ovulation in female Xenopus frogs was stimulated by the subcutaneously injection of chorionic gonadrotropin (Ovogest, MSD, 500 units) into the dorsal lymph sac approximately 15 hours before the desired egg laying using insulin syringes.
Eggs from stimulated female frogs were collected in a petri dish by applying pressure at the pelvis region on both sites of the spinal-cord. The oocytes were fertilized with 100-200 µl testes macerate diluted 1:10 with H_2O bidest through gently mixing. After fertilization, eggs were covered with 0.1 x MBS and stored at 14-18 °C until the desired developmental stage for injection. Embryos were staged according to. (Nieuwkoop and Faber, 1994)

2.10.4 .. Removal of the jelly coat and microinjection

Xenopus eggs are covered with a thick layer of jelly coat. To dejelly the embryos, they were incubated for at least 5 min in 2% L-cysteine (pH 8.0) at 14-18°C in a petri dish by occasionally stirring the embryos with a pipette tip. After the complete removal of the jelly coat, embryos were carefully washed three times in 0.1x MBS and stored at 14-18 °C until the desired developmental stage for injection.
For microinjection, injection needles were prepared from glass capillaries via a Needle puller (Magnetic Glass Microelectrode Horizontal Needle Puller, Narishige PN-13) and a micromanipulation system (PV820 Pneumatic Pump, M3301 Micromanipulator, World Precision Instruments) was used. The needle was calibrated to the desired injection volume

corresponding to 5 -10 nl of injection volume. Therefore, the diameter of the droplet size was measured using a micrometer scale and adjusted by carefully pinching the tip of the glass needle with forceps. Embryos were kept prior and after the injection in injection buffer on a coolin plate at 14°C. For microinjection, embryos were transferred to small petri dishes containing injection buffer as well as a plastic mesh with a grid diameter of ~1mm to allow better orientation of embryo. Embryos were oriented according to the desired injection localization and the appropriate volume of injection solution was injected. In general, an injection volume of 10 nl for one- as well as two-cell stage embryos and 5 nl for 4- as well as 8-cell embryos was used. Embryos were kept in injection buffer for at least 1 hour at 14 °C and subsequently washed three times and cultivated at 14-18 °C in 0.1x MBS.

2.10.5 .. Morpholino Oligonucleotides

Antisense Morpholino oligonucleotides were used for knockdown studies and were generated by Gene Tools, LLC (Philomath, OR, USA). Morpholinos were diluted in RNase-free water to an end concentration of 80ng/10nl.

Table 11: **Morpholino Oligonucleotides**

Morpholino name	Target gene	Sequence 5'→3'	Working concentration	
			1-2 cell x ng/10nl	4-8 cell x ng/5nl
5miss Cav1α-MO	No target	CATATATCTATTTCCCACAA GAAAT	7-20 ng	-
5miss Cav1α-MO2	No target	CATGTATCTAATTCCCACCA CACAT	10-20ng	10 ng
Cav1α-MO	*Xenopus laevis* Caveolin1α	CATCTATGTATTTGCCACCA GACAT	7-20 ng	10 ng
Cav1α-Splice-MO	*Xenopus laevis* Caveolin1α, Exon/Intron2	CAGCGCCCAGATCATACAG CCTTAC	10-20ng	10 ng
Standard control MO	human β-globin intron mutation	CCTCTTACCTCAGTTACAAT TTATA	10-20 ng	10 ng

2.10.6 .. Neural tube explants

The protocol for neural tube explants was adapted from Lowery et al. (Lowery et al., 2012). Prior to explantation, plated coverslips have to be prepared. Therefore, 8 well chambered

coverslips (Sarstedt) were covered with 200 µl per chamber of 150-200 µg/ml poly-L-Lysine (P-1399 Sigma-Aldrich) and incubated for one hour at room temperature or overnight at 4°C. Solution was washed out by rinsing three times with 1x PBS. During preparation of the second coating, chambers were dried. The coverslips were then covered with 200 µl of 10µg/ml Laminin (L2020, Sigma-Aldrich) and incubated for one hour at 37°C. Solution was washed out by rinsing three time with 1x PBS and replaced with DFA medium. During this, it should be avoided to let the coated surface to be exposed to air. Spinal cords were explanted from stage 19-22 Embryos in 0.8x MBS and explants were cultivated in DFA medium. Embryos were sorted according to their fluorescence and the vitelline membrane was carefully removed using sharp forceps in agarose coated petri-dishes. Additionally, the ventral portion of the embryo was carefully removed, by making several incisions right beneath the head and the posterior end of the embryos. The remaining dorsal explants, which should consist of the head, somites, notochord and spinal cord, were placed in an Eppendorf tube containing 2mg/ml collagenase in 0.8 xMBS for 15-20 min depending on the developmental stage. Collagenase treatment loosens the tissue, which makes it easier to separate somitic tissue and epidermis from the spinal cord. The older the embryo, the stronger is the adhesion between the neural tube and the surrounding tissue. By using sharp forceps to stabilize the embryo and an eyebrow sword, the surrounding tissue was carefully dissected from the neural tube. Explanted neural tubes were then cut in small, evenly pieces and placed on the coated chamber slides for 12-24 h at 18 °C. Outgrowth of neurites were imaged using the Zeiss Axio Observer Z1 inverted microscope (63x oil objective). Outgrowth as well as morphology of spinal neurons was counted for each explant individually. Axon length, filopodia as well as lamellipodia area was determined using ImageJ. The area covered by lamellipodia was calculated by subtracting the area of the axon (Aa) from the total area including lamelipodia (Ta). Lamellipodia area was then normalized to the total area (Ta) per axon. Number of filopodia per axon was calculated by normalizing the number of counted filopodia (Fn) with the axon length (AL). The growth cone was excluded in both calculations. Filopodia number: (Fn/ AL)*100 µm; Lamellipodia area: (Ta- Aa)/ Ta

2.10.7 .. Fixation and X-gal staining of *Xenopus* embryos

To distinguish between injected and uninjected side, β-galactosidase (lacZ) mRNA was co-injected into the embryos as lineage tracer. Prior staining the embryos were fixed in MEMFA for 30-45 min and washed three times in 1x PBS for 10 min each. For the visualization of the β-galactosidase activity, embryos were incubated in X-gal solution in the dark until a blue staining was observed. Embryos were then immediately rinsed with 1-PBS until all of the yellow X-gal solution was removed and re-fixed overnight in MEMFA. For

long term storage or for following *in-situ* hybridization embryos were transferred to 100 % ethanol.

2.11 Histological analysis of *Xenopus laevis* tadpoles

2.11.1 Embedding for Electron microscopy

Embryos were fixed first for 30 min in MEMFA and afterwards in 6.25 % glutaraldehyde in 0.1 M acodylate buffer overnight. The fixative was washed out by washing three times in Cacodylate buffer for 30 min each. To contrast the samples for electron microscopy, embryos were incubated in 1 % OsO4 in 0.1 M Cocadylate (pH 7.2) for 60-90 min while gently shaking. To avoid contamination of the embedding medium, the Osmium had to completely removed by several washes as well as overnight incubation in 0.1 M Cacodylate. If the medium was completely depleted of Osmium, embryos were embedded in 2.5 % Agar-Agar in small cryo-mold forms or a small petri dish and trimmed to small square blocks to orientation of the embryos during embedding in Spurr's resin. For the embedding in Spurr, embryos were first dehydrated in an ascending alcohol series (50%, 70% ethanol) for 30 min each and finally incubated in Dioxan for 45 min until the embryos sank down in the solution. Afterwards, embryos were infiltrated twice in a mixture of Spurr's resin and Dioxan (1:1; 2:1) for 90 min each and then in pure Spurr overnight. The Spurr's resign was replaced with fresh Spurr and incubated 5-8 h under constant stirring. For embedding, the in Spurr infiltrated embryos were transferred into embedding molds and embedded in Spurr for 16 h at 70 C.
For histological analysis and electron microscopy, semi-thin as well as ultra-thin sections were prepared. For preparing 2 µm semi-thin sections, the embedded embryos were trimmed and sectioned using a LKB-Pyramitom and contrasted in a methylene blue solution at 70 °C for 2-3 minutes for following light microscopy. For electron microscopy, ultra-thin sections of 50-80 nm thickness were prepared Ultracut microtome (Reichert). Therefore, the previously trimmed Spurr blocks containing the samples, were sectioned with diamond knifes and collected on Cu/Rh nets (75 x 300 stiches). The sections were then contrasted by incubating them first in lead acetate for 15 min and subsequently briefly rinsed in H_2O bidest and incubated in uranyl acetate for 5 min. Afterwards, the nets were carefully washed two times in H_2O bidest to remove residual uranyl acetate.

2.11.2 Embedding for Vibratom sectioning

For vibratom sectioning and following immunofluorescence procedures, embryos were injected with GFP as lineage tracer. Before embedding, embryos were sorted according to

their fluorescence and fixed in MEMFA or 8 % Paraformaldehyde overnight. Embryos were then either embedded in 4 % low melting agarose or in a gelatin/albumin mixture. For embedding in agarose, embryos were washed three times in 1x PBS to remove the fixature and then placed in cryomolds. After the agarose was carefully poured in the cryomolds (Tissue-Tek®Cryomold® Biopsie, 10x10x5mm), embryos were quickly oriented in the desired position using forceps. For embedding with gelatin/albumin, embryos were transferred to 25 % glutaraldehyde and placed cryomolds. Residual fluids were removed by pipetting. In a separate pan placed on ice, a 1/10 mixture of the gelantin/albumin and 25 % glutaraldehyde was prepared and immediately poured in the cryomolds containing the embryos. The formation of small air bubbles should be avoided during the embedding. Embryos were again oriented into the right position using a small pipette tip. Embedded embryos stored in a humid atmosphere at 4°C. Embedded embryos were then trimmed to square blocks and sections of 40-50 µm of thickness were prepared using the Leica Vt1000S vibratom and caught on a coated microscope slides (Roth).

2.12 Immunofluorescence staining of *Xenopus* embryos

For immunostaining, the probes were permeabilized in PBS containing 0.2 % TritonX for 10 min and subsequently blocked in blocking buffer (1x PBS +1 % BSA) for one hour at room temperature. The first antibody was diluted in blocking solution and applied to the slides over night at 4°C. The following primary antibodies were used; GFP (Abcam, 278239, 1:1000). The antibodies were removed by washing three times in 1x PBS. Subsequently the probes were incubated with secondary antibodies diluted in blocking solution for 2 h at room temperature or overnight at 4°C. The following antibodies were used: anti-mouse Alexa 488 (Invitrogen, A11029, 1:400), anti-rabbit Alexa 488 (A-21206, 1:400), Phalloidin-TRITC (Sigma-Aldrich (Merck), SLBG6854V, 1:250). Antibodies were removed by washing three times with 1x PBS and probes were mounted with fluorescence mounting medium (Dako, Deutschland GmbH, Hamburg, Germany). Immuno-stained sections were imaged with the Leica TCS SP5 microscope (40x oil objective).

2.12.1 .. Immunostaining of Vibratome sections

All following steps were performed in a humid atmosphere. Samples were permeabilized in 1x PBS containing 0.2 % TritonX for 10 min, by submerging the sections in the solution on the coated microscope slide. For blocking, the solution was removed, the sections rinsed three times in 1x PBS and then blocked in 1x PBS containing 1 % BSA for 1 hour at room temperature. Meanwhile, first antibody was diluted in blocking solution and then applied to

the slices over night at 4 °C. The antibody was removed by washing three times with 1x PBS for 5 min each and then replaced with the secondary antibody, diluted in blocking solution. Incubation occurred for at least 2 h at room temperature or overnight at 4°C. Antibody was removed by three washing steps with 1x PBS and slices were mounted with fluorescence mounting medium (Dako, Deutschland GmbH, Hamburg, Germany). Immunostained sections were imaged with the Leica TCS SP5 microscope (40x oil objective).

2.12.2 .. Whole mount Immunofluorescence staining

For the following procedure embryos were fixed in in ice-cold Dents over-night at 4°C. Embryos were rehydrated in 1x PBS and photo-bleached in 2% H_2O_2 in 1x PBS for 4-5h under a light source. Afterwards, the bleaching solution was removed by rinsing with PBS-TD and washed twice in 50 mM sodium acetate buffer (pH 6) for 5 min each. Following, embryos were permeabilized with 1 mg/ml bovine testicular hyaluronidase (Sigma, SLBH0986V) in 50 mM sodium acetate buffer (pH 6,0) for 45 min at room temperature. Embryos were again washed twice in PBS-TD and then blocked in PBS-TD containing 0.1 M glycine, 2 % nonfat dried milk, and 5 % FBS at room temperature. Primary antibody was diluted in blocking solution and applied to the embryos overnight at 4 °C. Antibody was removed and embryos washed six times in PBS-TD for one hour each and then incubated in secondary antibody overnight at 4 °C. Embryos were washed six times for one hour each in PBS-TD at room temperature and then re-fixated in Dents overnight.

As Xenopus embryos are opaque, they have to be cleared for imaging. To this end embryos were thoroughly dehydrated two times in 100 % ethanol and cleared in Benzyl-alcohol/Benzyl-Benzoate (Sigma Aldrich) (BA/BB; 1:2) for 10 min in a glass bowl until all embryos sank down. For imaging BA/BB was replaced with fresh BA/BB.
Embryos were imaged using the Zeiss Spinning Disc system (Axio Observer Z1 with a 25x or 40x water objective) or a fluorescence stereo-microscope (Leica, M165-FC).

2.13 Whole mount *in situ* hybridization

The whole mount in situ hybridization protocol was adapted from standard protocols (Harland 1991). All embryos were fixed in MEMFA overnight and then stored in 100 % ethanol prior to the staining procedure.

Rehydration

Embryos were rehydrated in a descending ethanol series according to table 7

Table 12: Rehydration of embryos

Solution	Incubation time
100 % ethanol	5 min
75 % ethanol in H_2O	5 min
50 % ethanol in H_2O	5 min
25 % ethanol in H_2O	5 min
1x PTw	4 x 5 min

Proteinase K treatment

The accessibility of the RNA to the tissue was facilitated by the treatment of the embryos with proteinase K (0.5 µl proteinase K / 1 ml PTw). Thereby the incubation time and temperature have to be adjusted to the developmental stage of the embryos as indicated in table 13.

Table 13: Proteinase K treatment

Developmental stage	Incubation time (min)	Temperature
9 - 10.5	5	room temperature
14 - 16	7 - 8	room temperature
20 - 25	7 - 8	room temperature
36	7 - 8	room temperature
40	5	37°C

Acetylation

To avoid increased background of the staining, unspecific binding sites of the RNA probes has to be blocked. To this end embryos were treated with acetic anhydride (AA) and subsequently re-fixed in 4 % formaldehyde as described in table 14

Table 14: Aceltylation

Solution	Incubation time
4 ml 0,1 M TEA	2x; 5 min
4 ml 0,1 M TEA +12.5 µl AA	5 min
+ 12.5 µ AA	5 min

Solution	Incubation time
4 ml 1x PTw	2x; 5 min
2 ml 4 % formaldehyde in PTw	20 min
PTw	5x; 5 min

Hybridization

After the last washing step, 1 ml PTW as well as the same amount of HybMix was added to the embryos and incubated for 10 min at 65°C in a shaking water bath. The solution was replaced by 1 to 2 ml fresh HybMix and incubated for at least 4 h at 65°C. For the hybridization, the HybMix was completely removed and immediately replaced by the preheated RNA probe. The embryos were incubated overnight at 65 °C in the water bath.

Washing

The unbound RNA probe was removed, by several washing steps as well as RNase A/RNase T1 (1:10000) treatment as described in table 15.

Table 15: Washing and RNase treatment

Buffer	Incubation time	Temerpature
HybMix	1x 10 min	65°C
2x SSC	3x 15 min	65°C
2x SSC/RNase	1x; 60 min	37°C
2x SSC	1x; 5 min	room temperature
0.2x SSC	2x; 30 min	65°C
1 x MAB	2x; 15 min	room temperature

Antibody reaction

Unspecific binding sites were blocked by the incubation of the embryos in 2% BMB and 20 % horse serum. An alkaline phosphatase-coupled anti-Dig labelled antibody was used to detect the RNA probe as indicated in table 16.

Table 16: Blocking and antibody reaction

Solution	Incubation time	Temperature
MAB/ 2 % BMB	15 min	room temperature
MAB/ 2 % BMB/ 20 % horse serum	40 min	room temperature
MAB/ 2 % BMB/ 20 % horse serum/ 1:5000 α-DIG antibody	4 h	room temperature
MAB	3x 10 min	room temperature
MAB	overnight	4°C

Staining reaction

Unbound antibody was removed by several washing steps in MAB and then staining reaction was initiated by the incubation in the substrates BCIP (5-Bromo-4-chloro-3-indolyl phosphate) and NBT (Nitro blue tetrazolium chloride) as described in table 17. If a strong blue staining was visible, reaction was attenuated by rinsing the embryos in MAB and re-fixation in MEMFA overnight at 4°C.

In case of a strong background, embryos were incubated in a descending series of methanol prior fixation, as described in table 18.

Table 17: Washing and staining reaction

Solution	Incubation Time
MAB	5x 5 min
fresh APB	2x 5 min
APB/NBT/BCIP	Up to 3 days at 4°C

Table 18: Reduction of background /optional

Solution	Incubation time
100 % MeOH	1 min
75 % MeOH in 25 % H_2O	1 min
50 % MeOH in 50 % H_2O	1 min
25 % MeOH in 75 % H_2O	1 min
MEMFA	15 min
MEMFA	overnight at 4°C

Bleaching

If the pigmentation of the embryos interferes with the *in situ* signal, embryos were bleached in H_2O_2 as described in Table 19.

Table 19: Bleaching /optional

Solution	Incubation time
PTw	3x;10 min
0.5x SSC	2x; 5 min
bleaching solution	20 - 40 min on a light source
1x PBS	3x; 5 min
MEMFA	overnight at 4°C

3 Results

3.1 Knockdown of Cav1α results in morphological abnormalities

Although it has already been shown that the knockdown of Cav1α expression in *Xenopus* embryos leads to swimming defects (Berger, 2016), the underlaying mechanism causing this defect has not yet been analyzed. For this purpose, knockdown studies were carried out to assess the role of Cav1α during early development and its function in the locomotor system of *Xenopus* embryos.

In *Xenopus* the full length caveolin 1 gene is encoded on the L-(long) chromosome and is composed of three exons (E) (Figure 17A): E1. The first 30 bp exon containing the translation start site of the α-isoform. E2. The 171 bp second exon containing the tyrosine (Y14) phosphorylation site as well as the translation start site for the β-isoform. E3. The 342 bp third exon encoding the oligomerization, scaffolding and transmembrane domain and the serine (S80) phosphorylation site of the caveolin 1 protein (Figure 17A, B). For the loss-of-function experiments in this study, two different types of Morpholinos were used: a translation-blocking morpholino (Cav1α MO) that specifically binds the first 8 base pairs of the ATG region of the endogenous *cav1α* RNA (Figure 17B, red dashed box) and a Splice-blocking Morpholino (Cav1α-Splice MO), which specifically targets the second exon-intron boundary of the *cav1α* pre-mRNA (Figure 17B, blue dashed box). Injection of the Cav1α-Spl Morpholino ideally results in an aberrant spliced RNA and in the translation of a non-functional protein as shown in Figure 17B. Both Morpholinos were tested for their efficiency *in vivo* by Western blot analysis (Figure 17D-E) and by amplification of the cDNA from morphant embryos via reverse transcription-polymerase chain reaction (RT-PCR) (Figure 17C). To this end the Morpholinos were injected into one-cell stage embryos at a concentration of 20 ng in combination with *mGFP* RNA as a lineage tracer. Expression of cav1 was analyzed in stage 20 (RT-PCR) and stage 30 (Western blot) embryos, respectively. Embryos injected with 20 ng Co MO served as a control.

The amplification of cav1 from a cDNA prepared from Cav1α-Splice morphant embryos showed a shorter transcript variant (2) with an approximate size of 370 bp in addition to the full-length *cav1* RNA (1) (Figure 17C). Sequence analysis of this transcript variant by Sanger sequencing confirmed that the injection of the Cav1α-Spl MO leads to the exclusion of exon 2 as predicted in Figure 17B. Uninjected control embryos and embryos injected with Co MO served as controls and both showed the wild-type cav1 transcript of approximately 540 bp (Figure 17C). In all conditions an additional band of 300 pb was amplified, however the identity of this transcript is still unknown.

Western blot analysis verified that both Morpholinos (Cav1α MO and Cav1α-Spl MO) efficiently knocked down the endogenous Cav1 protein (Figure 17D-E). To detect the Cav1 protein (20-22 kDa), a monoclonal antibody was used that specifically recognizes the Cav1α isoform. The Cav1α expression level was determined in relation to GAPDH expression and normalized to Co MO-injected embryos. Convincingly, injection of either Cav1α MO or Cav1α-Spl MO significantly reduced endogenous Cav1 protein levels in *Xenopus* embryos (Figure 17D-E). In comparison to controls, the Cav1 protein level was reduced by approximately 50 % in the presence of the Cav1α MO and by 70 % in the presence of the Cav1α-Spl MO (Figure 17D-E).

To analyze the morphological consequence of the Cav1α knockdown, the Cav1α Morpholinos were injected unilaterally at a concentration of 20 ng into two-cell stage embryos. As control, a 5 mismatch Cav1α MO (Cav1α-5mis MO) was injected at the same concentration and co-injection of 80 pg *GFP* served as a lineage tracer. Embryos injected with either the splice-blocking Morpholino or the translation-blocking Morpholino are both referred to as Cav1α morphants. While control embryos showed a wild-type phenotype (Figure 17F), Cav1 morphant embryos displayed mild morphological abnormalities such as a shortening of the body axis, craniofacial malformations and edema formation in the heart region (Figure 17G-H). These phenotypes were more pronounced in embryos injected with the splice blocking Morpholino, which is consistent with the results obtained by western blotting (Figure 17D-E). Interestingly, although the loss-of-function of Cav1α causes morphological abnormalities in *Xenopus* embryos, no significant effects on the mortality of these embryos were observed, indicating that Cav1α expression is not essential for the viability of these embryos (data not shown).

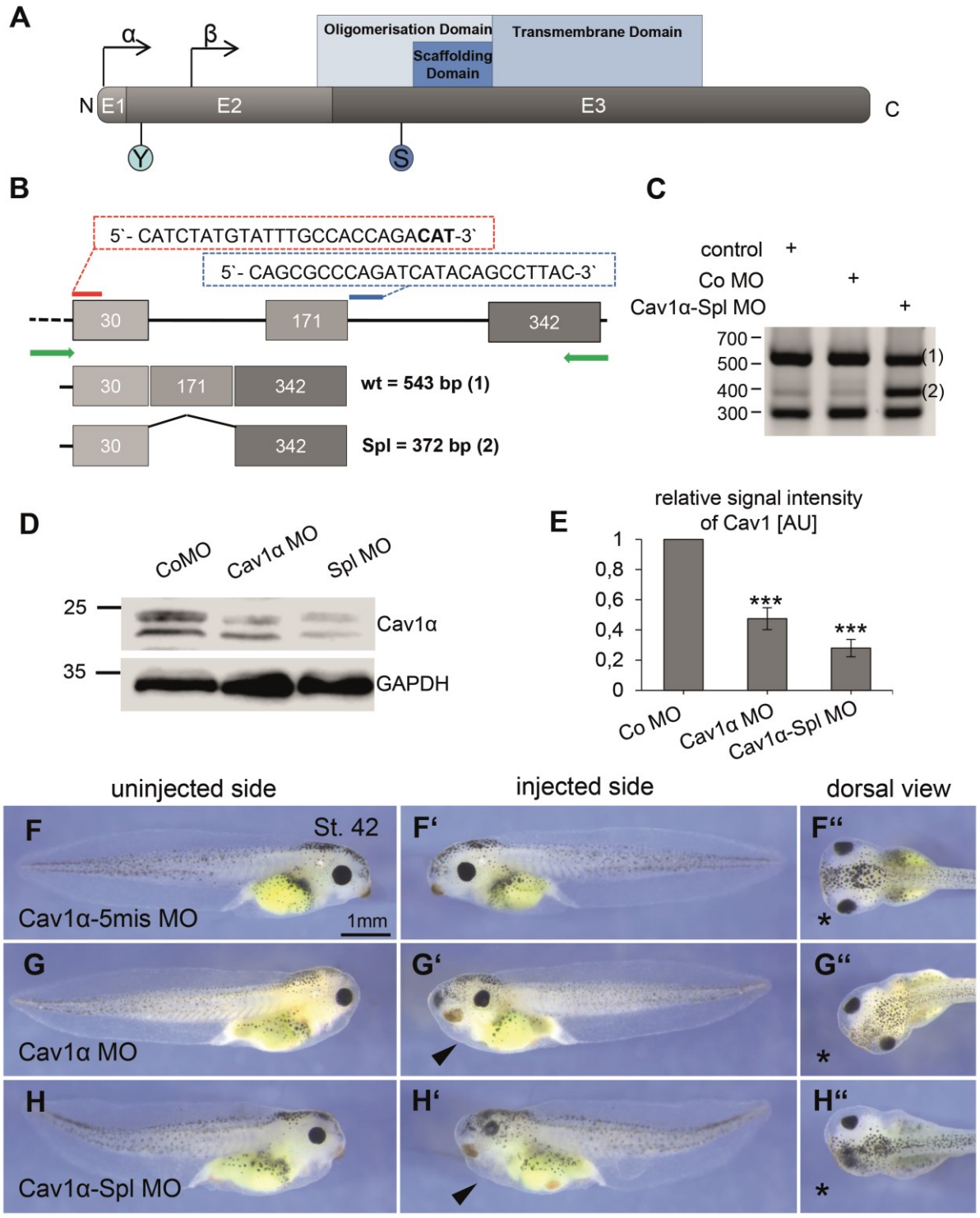

Figure 17: The knockdown of Cav1α leads to morphological abnormalities in *Xenopus*.
A Schematic of the Cav1α gene organization. *Xenopus* Cav1α consists of 3 coding Exons (E) encoding for the Cav1α translation start side, the tyrosine (Y14) phosphorylation site and Cav1β translation start site. **B** Schematic of the Morpholino design: The translation blocking MO (Cav1α MO, red dashed box) binds to the 5' end ATG region of the endogenous *cav1α* RNA and the splice blocking MO (Cav1α-Spl MO, blue dashed box) the non-coding region of the second intron, directly at the exon 2/ intron 2 boundary. Different splicing outcomes are shown: (1) A correctly spliced wild-type transcript of approx. 543 bp or (2) a deletion of the exon 2 resulting in a truncated transcript of approx. 372 bp in size. **C** The functionality of the Cav1α-Spl MO was tested on lysates of embryos injected with 20 ng of either the Spl-MO or a 5 base pair mismatch Morpholino by RT-PCR at stage 20. The primer combination indicated by green arrows in B was used. The gel electrophoresis shows the predicted results indicated

in A. **D, E** Cav1α MO and the Cav1α-Spl MO inhibit the expression of *Xenopus* Cav1α protein. **D** *Xenopus* embryos were injected with 20 ng MO at the one cell stage and Cav1α and GAPDH expression was analyzed by Western blotting at stage 27. **E** Graph summarizing the relative Cav1α expression determined in relation to GAPDH expression and normalized to Co MO injected embryos. Data from four experiments are presented as the ± S.E.M. ***p-value ≤ 0.001. **F-H** *Xenopus* embryos were injected with 20 ng MO and *mGFP* RNA in one blastomere at the two-cell stage and analyzed at stage 42: injected (F-G) and uninjected side (F'-H') as well as a dorsal view (* marks injected side) of each embryo are shown. Injection of the Cav1α or Cav1α-Spl MO leads to craniofacial malformations and edema formation (arrowhead).

3.2 Loss of Cav1α expression affects embryonic mobility and muscular integrity

Knockdown of Cav1α leads to relatively mild morphological abnormalities in the morphant embryos. The most noticeable phenotype observed in these embryos, however, was a striking swimming defect, as described in previous studies (Berger, 2016, PhD; Breuer, 2016, M.Sc.). Morphant embryos, injected with the translation blocking Morpholino (Cav1α MO) showed a characteristic circular swimming behavior, caused by the paralysis of the injected side (Supplementary Movie 2). In order to confirm that this defect is specially caused by Cav1α knockdown, the swimming behavior of embryos injected with 20 ng Cav1α-Spl MO was analyzed and compared to those of Cav1α morphant embryos. Injection of Co MO at the same concentration served as control. *mGFP* RNA was co-injected as a lineage tracer at the concentration of 80 pg. Similar to embryos injected with the Cav1α MO, the injection of the Cav1α-Spl MO caused severe swimming defects (Figure 18C, Supplementary Movie 3). While control embryos showed a normal swimming behavior (Supplementary Movie 1, 4), Cav1α morphant embryos moved in circles when injected unilaterally (Supplementary Movie 2-3), or were completely paralyzed when injected into both blastomeres at the two-cell stage (Supplementary Movie 5). For the quantification of the swimming defects, a distinction was made between mild and severe defects. The swimming behavior was counted as normal, if unilaterally injected embryos were able to move their tail in both directions. In contrast, the phenotype was considered mild, if the embryo could still move forward but showed a visible impairment of its swimming behavior. If the embryos were completely paralyzed on the injected side and were unable to move forward, this was considered a severe swimming defect. The percentage of embryos with swimming defects was significantly increased in embryos injected with the Cav1α MO (10 % ±4 % mild; 87% ±4 % severe) or Cav1α-Spl MO (13 % ±4 % mild; 76% ±7 % severe) in comparison to control embryos (1 % ±0 % mild) (Figure 18C). In addition, rescue experiments were carried out to verify that the swimming defects are specifically caused by Cav1α knockdown and not due to off-target effects. For the following rescue experiments 10 ng Morpholino was injected into one blastomere of two cell stage embryos in combination with the respective *cav1α* RNA and 80 pg *mGFP* RNA. The specificity of the translation blocking morpholino was previously verified by the partial rescue

of swimming defects by the dose-dependent co-injection of a *caveolin 1α-rescue* construct (Berger, 2016, PhD; Breuer, 2016, M.Sc.). In this construct, the morpholino binding site is deleted, thereby preventing the morpholino from binding to the *caveolin 1* rescue RNA (Berger, 2016, PhD; Breuer, 2016, M.Sc.) (Figure 18D). Co-Injection of 300 pg *Cav1α-res* RNA significantly improved the swimming behavior by 50 % (35% ±4%) in relation to injection of the Cav1α MO alone (70% ±7%) (Figure 18D). Similarly, the co-injection of 200 pg wild-type *cav1α* RNA could also significantly rescue the severity of the swimming defects in the Cav1α-Spl morphant embryos (Figure 18E). In this case the swimming defects per embryo were improved from 76% (36% ±4% mild; 40% ±5% severe) in the Cav1α splice morphants to 47% (34% ±4% mild; 13% ±4% severe) upon co-expression of *cav1α* RNA. This confirms that the swimming defects are specifically caused by Cav1α loss of function.

Impaired embryonic mobility can be caused by defects in muscular as well as neuromuscular development. It has been previously shown by phalloidin staining that the depletion of Cav1α expression leads to severe muscle defects (Berger, 2016, PhD; Breuer, 2016, M.Sc.). To verify, that the injection of the splice Morpholino causes similar muscular defects, muscular actin was stained in embryos that were injected unilaterally with 20 ng Cav1α MO or Cav1α-Spl MO, respectively. *mGFP* was co-injected as a lineage tracer and Phalloidin was used to stain the actin cytoskeleton of the embryos (Figure 18F-H). As previously shown, the knockdown of Cav1α expression in morphant embryos led to a drastic loss of muscular integrity (Figure 18G-H). While control embryos and the non-injected side of the Cav 1α morphants showed a highly organized muscular actin cytoskeleton, muscle cells of Cav1α morphant embryos contained highly disorganized and wavy actin fibers. Injection of the Cav1α MO or Cav1α-Spl MO likewise caused these defects (Figure 18G-H). In comparison to morphant embryos injected with the translation blocking Morpholino, the phenotype was more severe in the splice blocking morphant embryos. Here, the actin signal was severely reduced and the nuclei of the muscle cells were misaligned, indicating that injection of the splice blocking Morpholino also severely affected muscular integrity (Figure 18H).

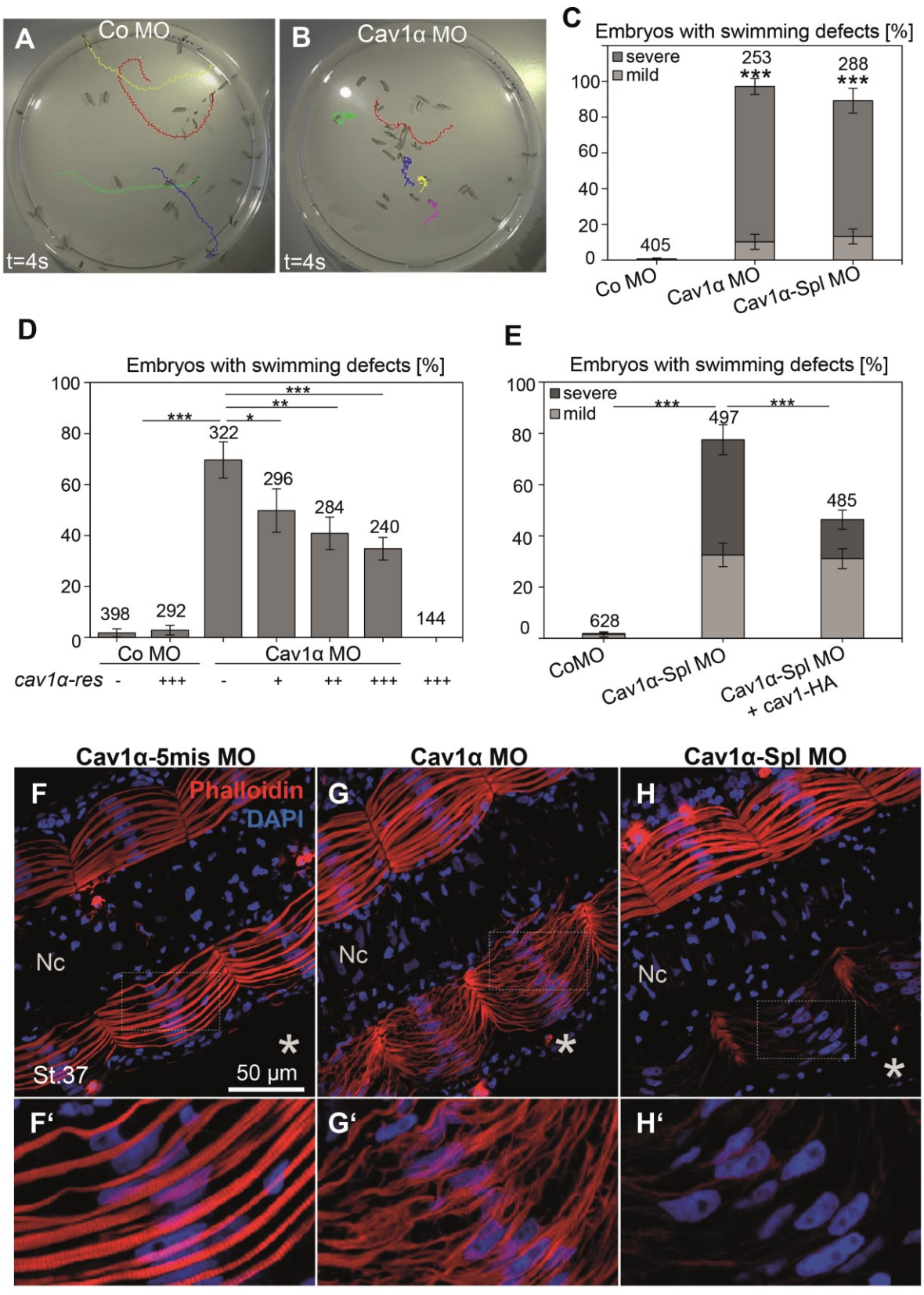

Figure 18: Cav1α loss-of-function causes swimming defects and severely affects sarcomeric organization of the muscles.

A-B Tracks of the swimming movement in a time frame of 4 sec are shown. Co MO embryos moved rapidly away after a tactile stimulus (A), while Cav1α morphants responded with a circling and tumbling behavior (B); (modified after Breuer, 2016, M.Sc.). **C** Graph summarizing the percentage of mild (light grey) or severe (dark grey) swimming defects of embryos unilaterally injected with 20 ng Co MO, Cav1α MO or Cav1α-Spl MO. Data from six independent experiments are presented as the mean ±

S.E.M. ***p-value ≤ 0.001. Number of analyzed embryos are shown above each column. **D** Graph summarizing the percentage of swimming defects of embryos unilaterally injected with Co MO or Cav1α MO (5 - 7.5ng) alone or in combination with *res-cav1α* RNA (+= 100 pg, ++= 200 pg, +++= 300 pg), a cav1 construct lacking the MO binding side; ± S.E.M. and number of injected embryos of five independent experiments are shown for each column (modified after Breuer, 2016, M.Sc.) **E** Graph summarizing the percentage of swimming defects of embryos injected with Co MO or Cav1α-Spl MO (10 ng) in combination with full-length c*av1α*-HA (200 pg) RNA of six independent experiments; ± S.E.M and number of injected embryos are shown for each column. Significance of the total number of swimming defects was calculated by using the Student's t-test and ordinary one-way ANOVA. * p-value < 0.05; **p-value < 0.01; ***p-value < 0.001. **F-H** Muscle morphology of Co MO, Cav1α MO or Cav1α-Spl MO (20ng) injected embryos analyzed at stage 37, injected side is marked by an asterisk. Phalloidin (red) staining visualizes sarcomeric actin; DAPI staining (blue) marks the nuclei. Higher magnification of the boxed areas is shown in F'-H'. Controls (F-F') show normal actin organization, while morphants (G-H') display wavy and disorganized actin fibers. Nc = notochord

3.3 Knockdown of Cav1α impairs convergent extension during gastrulation

Loss of Cav1α expression in *Xenopus* embryos leads to a shortening of the body axis. Impaired axis elongation can be caused either by defects during convergent extension (CE) movements or impaired notochord stability. It has recently been shown that Cav1 is involved in the convergent extension process by mediating the endocytosis of Wnt5a / RhoA during gastrulation (Puzik et al., 2019). On the other hand, the loss of caveolae formation in the zebrafish notochord leads to the mechanically induced collapse of notochord cells, which also results in a shortening of the body length (Lim et al., 2017). In order to investigate which of these two processes affects the Cav1α morphant body length, first the notochord was examined by histological analyzes (Figure 19A-B). In addition, *in situ* hybridization against the neural border specifier Pax3 was carried out to test for convergent extension defects (Figure 19C-F).

Histological and electron microscopic analyzes were carried out to assess whether Cav1 knockdown affects the notochord integrity and the formation of caveolae in this structure(Figure 19A-B). To this end, embryos were injected into both blastomeres with 10 ng Cav1α MO or Co MO in combination with GFP as a lineage tracer. Similar to control embryos (Figure 19A), the notochord of the Cav1α morphant embryos contained highly vacuolated cells with no apparent cellular damage (Figure 19A-B). However, the Cav1α morphant notochord appeared broarder in its diameter in comparison to control embryos. While the majority of the vacuolated cells are aligned in two rows within the notochord of control embryos (Figure 19A), notochord cells of the morphants failed to intercalate properly, which is likely due to impaired convergent extension (Figure 19B).

To verify that Cav1α knockdown results in impaired convergent extension in morphant embryos, *pax3* expression was analyzed in embryos injected unilaterally with 20 ng Cav1α MO or Co MO in combination with *LacZ* RNA as a lineage tracer (Figure 19-F). While *pax3*

expression was restricted to the neural plate border in control embryos (Figure 19C-D), it was significantly expanded on the injected side in 66% ±5 % of the Cav1α morphant embryos (Figure 19E-F) implying indeed a deficiency in convergent extension.

In summary, Cav1α functions in convergent extension movements during early development of *Xenopus* embryos, thereby likely affecting the notochord morphology. Caveolae could still be detected in the Cav1α morphant notochord, indicating that other caveolin proteins likely compensate for the loss of Cav1α expression in this tissue.

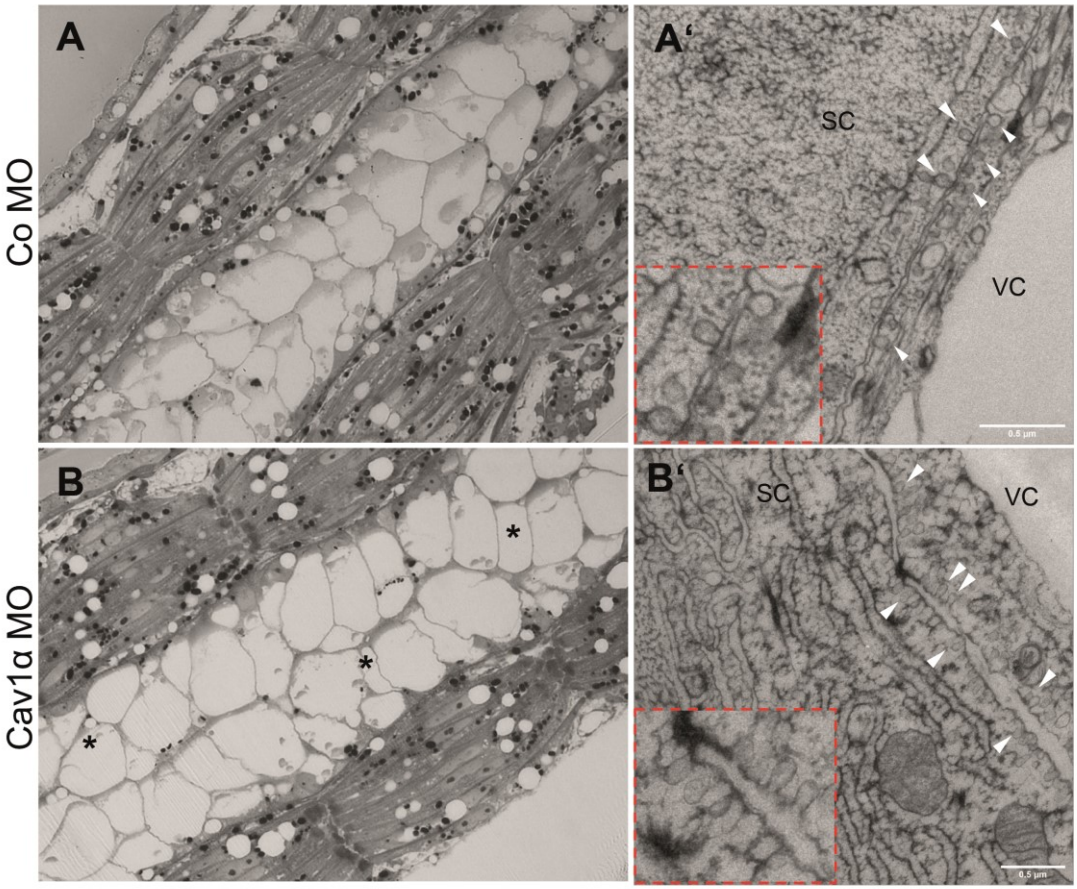

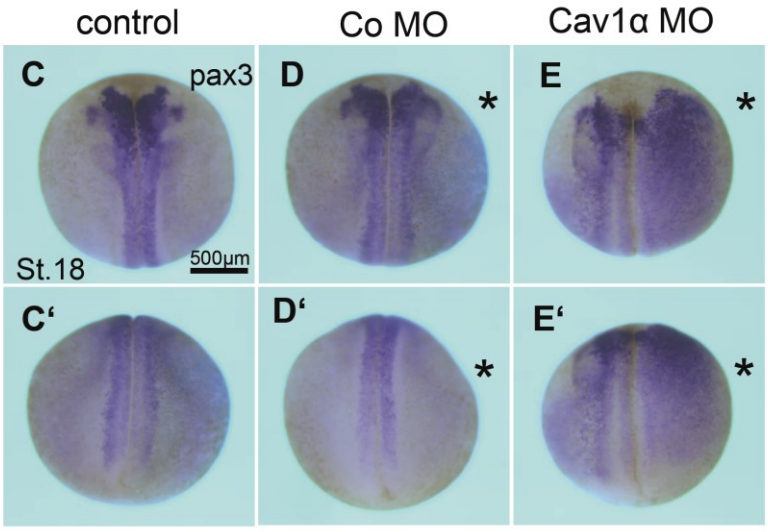

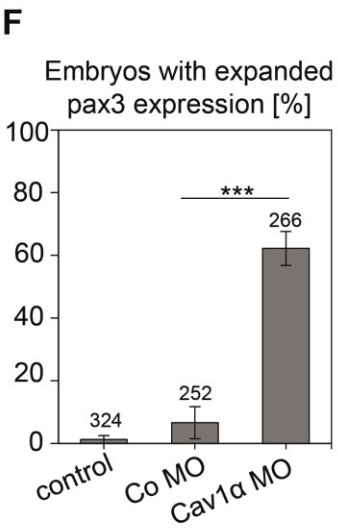

Figure 19: Convergent extension is disrupted by Cav1α loss-of-function.
A-B Histological (A-B) as well electron microscopic (A'-B') analysis of the notochord from embryos injected with 12 ng MO in each blastomere of two cell stage embryos. **A** Histological section of a Co MO embryo. **A'** Electron microscopic picture of a Co MO notochord. Caveolae are marked with white arrowheads. Red dashed box shows a magnified area from E. VC = vacuolated cell, SC= sheath cell. **B** Histological section of a Cav1α morphant notochord. Asterisk within the notochord mark incorrectly intercalated cells. **B'** Electron microscopic picture of a Cav1α morphant notochord. Caveolae are marked with white arrowheads. Red dashed box shows a magnified area from F. VC = vacuolated cell, SC= sheath cell. Scale bar = 0.5 µm **C-F** *pax3* expression was analyzed in stage 18 control embryos or embryos injected with 20 ng MO in combination with 75 pg *LacZ* RNA as lineage tracer. Dorsal (A-C) as well as posterior view (A'-C') is shown. Asterisk marks the injected site **C-D'** *pax3* is expressed in the anterior neural fold and neural plate border in control embryos (C-C') and embryos injected with Co MO (D-D'). **E-E'** Cav1α knockdown leads to an expansion of the *pax3* expression domain on the injected side. **F** Graph showing the percentage of embryos with expanded *pax 3* expression. Data from three experiments are presented as the mean ± S.E.M. ***p-value ≤ 0.001. Significance was calculated by using the student's t-test.

3.4 Knockdown of Cav1α results in morphological abnormalities

Knockdown of Cav1α causes morphological abnormalities, including craniofacial malformations and edema formation (Figure 17G-H). As craniofacial abnormalities are often caused by defective cartilage formation, stage 43 morphants embryos were stained for collagen to visualize the cartilage of these embryos. The cartilage in *Xenopus* embryos is subdivided into the neural crest derived Meckel's and Quadrate (Me), Ceratoyal (Ce) and Branchial/Gill (Br) cartilage as well as the mesodermal-derived Infrarostral (In) and Basihyal (Ba) cartilage (Figure 20D-E) (Gross and Hanken, 2008). In comparison to control embryos (Figure 20D-E), which showed normal craniofacial structures, 50% ±14% of the Cav1α MO and 87% ±0 % of the Cav1α-Splice MO injected embryos showed severely reduced cartilage structures on the injected side (Figure 20F-G). Interestingly, knockdown of Cav1α lead to a severe reduction of the neural crest-derived Meckel's and Quadrate (Me), Ceratoyal (Ce) as well as Branchial/Gill (Br) cartilage while the mesodermal-derived Infrarostral (In) as well as Basihyal (Ba) cartilages were unaffected (Figure 20F-G). These findings indicate that Cav1α may have a function in neural crest development as the knockdown of Cav1α expression leads to the loss of the neural crest-derived cartilage.

Edema in *Xenopus laevis* embryos are often caused by defects in pronephros development as the pronephros has an important function in osmoregulation (Nieuwkoop and Faber, 1994). In order to analyse whether the edema in the Cav1α morphants is caused by defective kidney development, the embryonic pronephros was stained by whole mount immunofluorescence staining. β-Dystroglycan is highly expressed in the developing pronephros and was therefore used as a marker (Figure 20K-M). The *Xenopus* pronephric

kidney can be subdivided into four tubular parts: the proximal tubule, the intermediate tubule, the distal tubule and the connecting tubule (Figure 20K). Embryos unilaterally injected with the Cav1α MO, which causes mild edema formation, showed a strong reduction of the proximal tubule size (Figure 20M') in comparison to the uninjected side (Figure 20M). In contrast, Cav1α-Spl morphant embryos displayed a severely malformed proximal, intermediate and distal tubule. The connecting tubule was not connected to the distal tubule in these embryos (Figure 20N'). The uninjected site as well as embryos injected with a Co MO showed a normal pronephric morphology (Figure 20L, N). These results suggest that Cav1α may act in kidney development in *Xenopus* embryos and that misexpression of Cav1α results in defects in pronephros formation. However, more experiments have to be conducted to verify this observation.

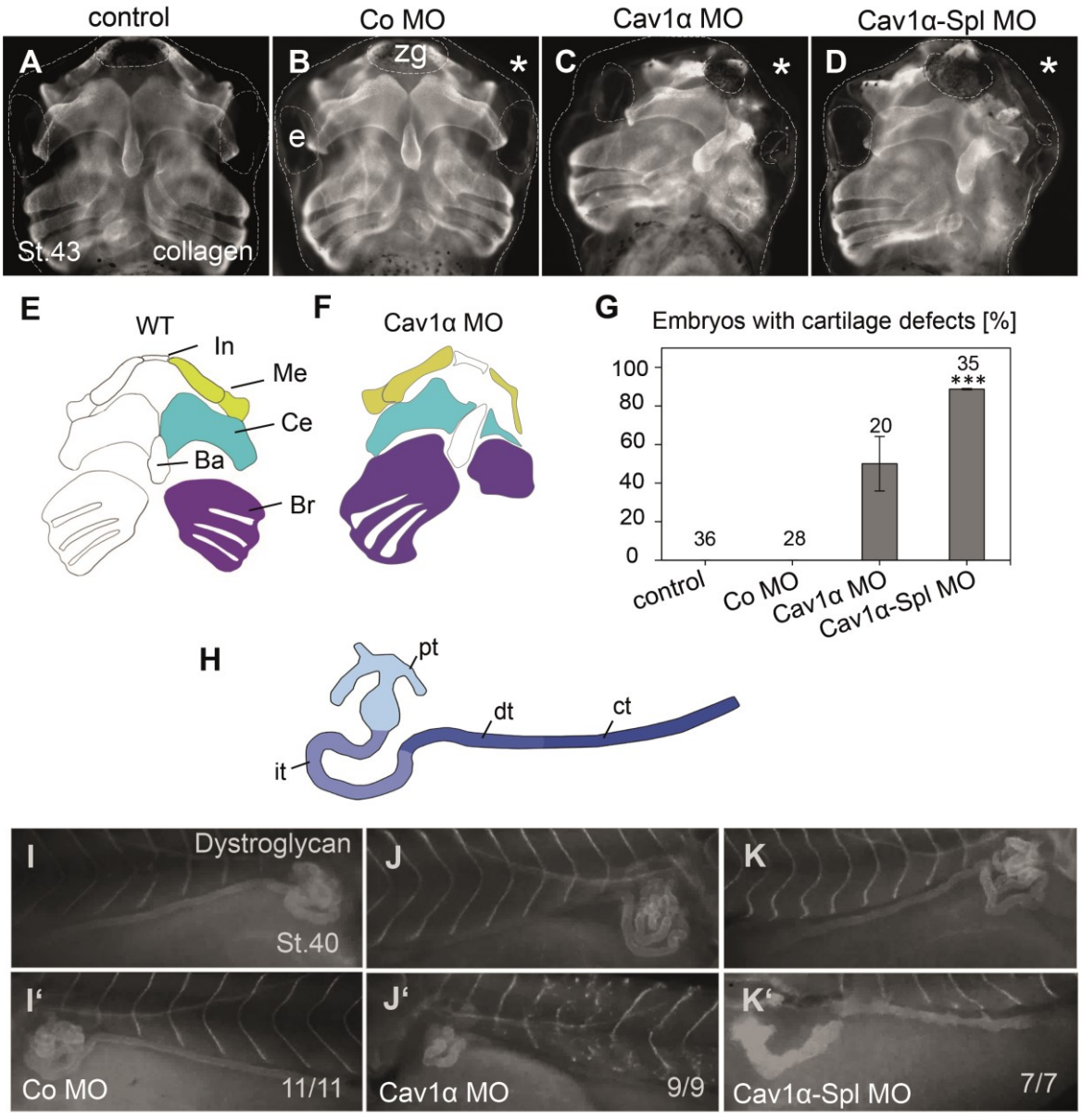

Figure 20: **Knockdown of Cav1α leads to mild morphological abnormalities.**
D-G Cartilage of stage 43 embryos injected unilateral with 20 ng MO was immuno-stained with anti-collagen. Asterisk marks the injected side. **D** control and **E** Co MO injected embryos are shown. E =

eye **F-G** Severely reduced cartilage in embryos injected with Cav1α MO (F) or Cav1α-Spl MO (G). **H** Schematic of the cartilage structures of control embryos. In= infrarostral, Me= meckel's and quadrate, Ce = ceratoyal, Ba = basihyal, Br = branchial/gill cartilage. **I** Schematic view of the cartilage structures of Cav1α morphants. **J** Graph summarizing the percentage of embryos with cartilage defects. Data from three experiments are presented as the mean ± S.E.M. ***p-value ≤ 0.001. Significance was calculated using a Student's t-test. For the Cav1α MO experiment only two experiments are shown as ± S.E. **K** Schematic view of a *Xenopus* pronephros, pt = proximal tubule, it = intermediate tubule, dt = distal tubule, ct = connecting tubule. **L-N** Pronephros of stage 40 control (L) and morphant embryos (M-N) was stained with anti-β-Dystroglycan. Embryos were unilaterally injected with 20 ng MO and 80 pg *mGFP* RNA. Uninjected (L-N) and injected (L'-N') site is shown. **L-L'** normal pronephros morphology Co MO injected embryos. **M-M'** reduced proximal tubule on the injected site of Cav1α MO injected embryos (M') in comparison to the uninjected site (M). **N-N'** severely malformed proximal, intermediate and distal tubule on the injected site of Cav1α-Spl MO injected embryos (N'). The number of embryos displaying a phenotype and the total number of analyzed embryos is shown.

3.5 Cav1 is predominantly expressed in the notochord and motoneurons

The data shown above indicate that Cav1α plays an important role in the maintenance of muscle integrity and, moreover, embryonic mobility during early *Xenopus* development. In order to understand how Cav1α functions in the locomotor system, the expression profile of cav1α during the embryogenesis of *Xenopus laevis* was analyzed by reverse transcriptase PCR, whole mount *in situ* hybridization as well as immunofluorescence staining (Figure 21; Figure 22; Figure 23). Reverse transcriptase PCR showed that *cav1* is maternally expressed in oocytes, in embryos of the early cleavage stages (2-4 cell) and also at low levels during gastrulation. Zygotic expression increased during neurulation, with the highest expression occurring in stage 28 and decreasing again from tadpole stage 30 (Figure 21A).

In situ hybridization revealed that *cav1* is highly expressed in the presumptive notochord and the epidermis from the early neurula stage 12.5 onwards (Figure 21B-K). Additionally, *cav1* expression could be found in the neuroectoderm as a thin stripe on both sites of the embryonic midline (Figure 21B-E). Transverse sections of these embryos demonstrated that *cav1* expression localizes in the sensory layer (sl) of the epidermis, the notochord (nc) as well as in the superficial/ epithelial layer of the neural plate (Figure 22A-D). Interestingly, at stage 18 *cav1* localizes at the most dorsal part of the neural folds, but no expression was detected once the neural tube is completely closed (Figure 22C, D). In contrast, *cav1* remains expressed in the notochord and the epidermis during older embryonic stages (Figure 21; Figure 22D). To analyze if this staining in the neural tube coincides with primary neurons, double *in situ* hybridization using the neuronal marker neuronal tubulin (n-tubulin, beta tubulin) was performed. *N-tubulin* is expressed in three distinct stripes within the deep or sensorial layer of the neural ectoderm. These represent the precursors of motoneurons (m), the interneurons (i) as well as the sensory neurons (s), located from medial to distal. *Cav1*,

which is expressed in the epithelial layer of the neuro-ectoderm, showed no co-expression with n-tubulin in primary neurons (Figure 21G).

At older developmental stages (37-43) *cav1* is also expressed in the heart as well as the vasculature of the branchial arches (aortic arches) and the tail. Specifically, staining was detected in the intersomitic veins (isv), the lymph heart (lh), the posterior cardinal vein (pcv) and the dorsal longitudinal anastomosing vessels (dlav) (Figure 21I-K; Figure 22-K). Moreover, a strong signal for *cav1* expression was also found in the developing lung (Figure 21J, J'). Longitudinal sectioning of stage 43 embryos showed a rather ubiquitous staining of *cav1* mRNA in the embryo, with a prominent expression in the epidermis (ep), the developing lung (lg) and the aortic arches (aa) and the heart (h) (Figure 22G-J). Transverse sections of a stage 43 embryo confirmed *cav1* staining in the developing lung (lg) (Figure 22K-M). *In situ* hybridization using a *cav1* sense probe showed no specific staining (Figure 21L-O).

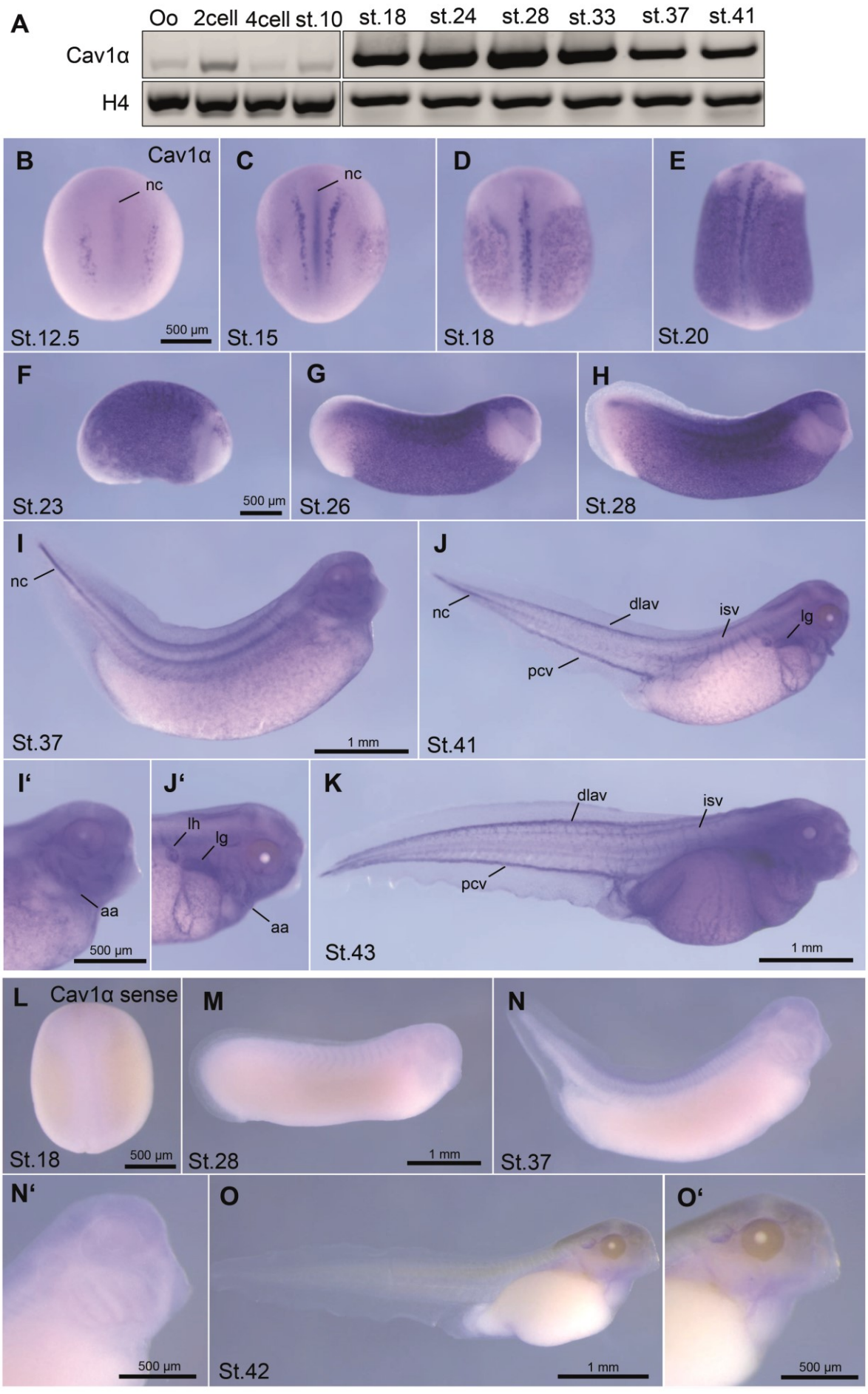
A
Oo
2cell
4cell
st.10
st.18
st.24
st.28
st.33
st.37
st.41
Cav1α
H4
B
Cav1α
nc
St.12.5
500 µm
C
nc
St.15
D
St.18
E
St.20
F
St.23
500 µm
G
St.26
H
St.28
I
nc
St.37
1 mm
J
nc
dlav
isv
lg
pcv
St.41
I‘
aa
500 µm
J‘
lh
lg
aa
K
dlav
isv
pcv
St.43
1 mm
L
Cav1α sense
St.18
500 µm
M
St.28
1 mm
N
St.37
N‘
500 µm
O
St.42
1 mm
O‘
500 µm

Figure 21: **Cav1α is expressed in the notochord during *Xenopus* development.**
A Temporal *cav1α* expression was analyzed by reverse transcriptase PCR at different developmental stages. H4 was used as a loading control. **B** Dorsal view of a stage 12.5 embryo. *cav1α* expression in the notochord (nc) and at two thin stripes on both sides at the dorsal midline is shown. **C** Dorsal view of an embryo at stage 15. *Cav1α* expression is visible in the notochord (nc) and in a punctuated pattern in the skin. **D** Stage 18 embryo showing the same expression pattern as described in C **E-H** *Cav1* expression is visible in the epidermis and around the eye of stage 20 (E), stage 23 (F), stage 26 (G) and stage 28 (H) embryos. **I** Stage 37 embryo. *Cav1* expression is visible in the notochord (nc), epidermis and aortic arches (aa). **J** Stage 41 embryo. *Cav1* expression in the notochord (nc), and the cardio-vasculature of the tail (dlav, pcv, isv). **I'** Magnification of the embryo shown in I. *Cav1* is expressed in the aortic arches (aa). **J'** Magnification of the embryo shown in J. *Cav1* is expressed in the lung (lg), lymph heart (lh) and aortic arches (aa). **K** Stage 43 embryo. *Cav1* expression is shown in the cardio-vasculature of the tail (dlav, pcv, isv) and epidermis. **L-O'** *Cav1* sense probe *in situ* hybridization. **L** Embryos at stage 18. **M** Embryo at stage 28. **N** Embryo at stage 37. **N'** Magnification of the embryo shown in N. **O** Embryo at stage 42. **O'** Magnification of the embryo shown in O.

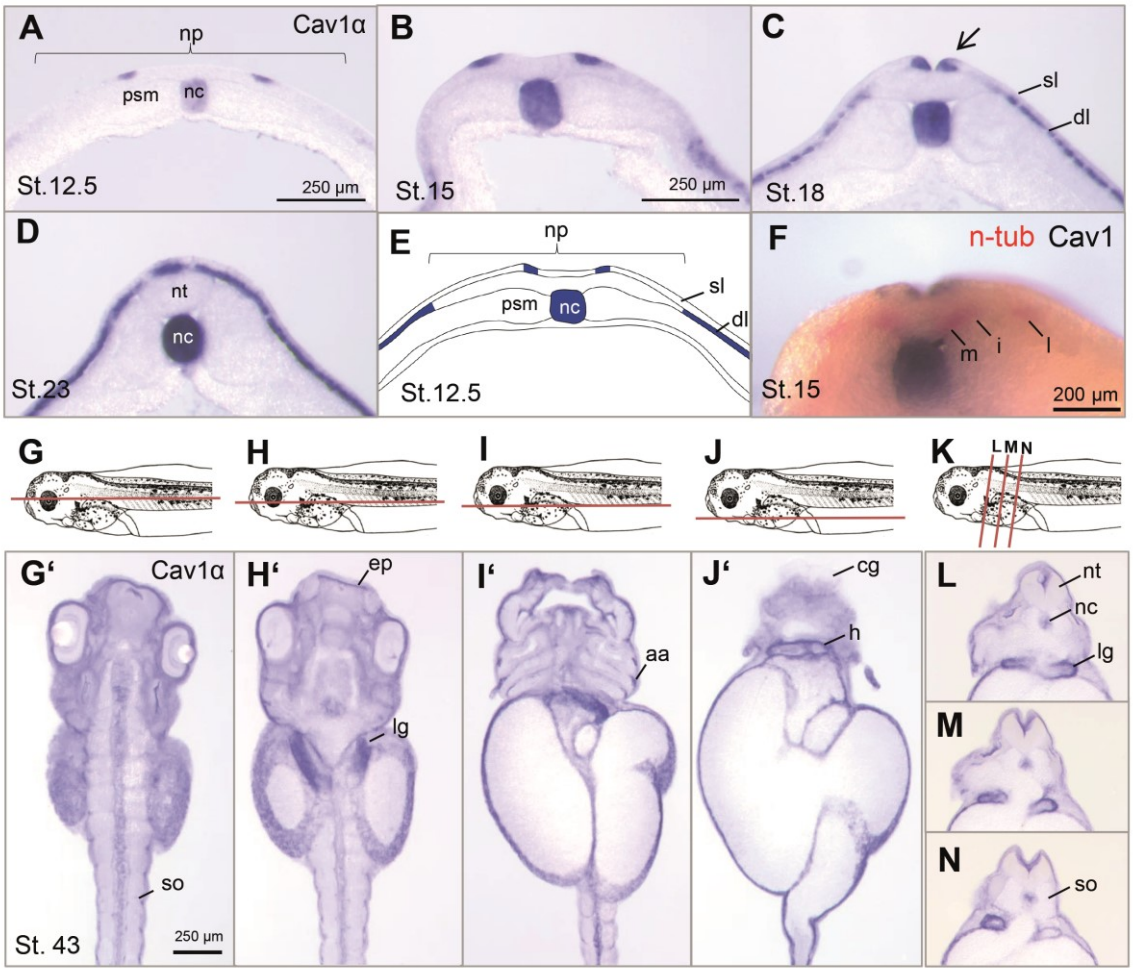

Figure 22: Cav1α is strongly expressed in the notochord, cardio-vasculature and lung during *Xenopus* development.
A-E Transverse sections of stage 12- 28 embryos shown in fig.5 **A-B** Stage 12.5 (A) and 15 (B) embryo: *cav1α* expression is located in the notochord (nc), and in the outer layer of the neural plate (np) at both sides of the midline. **C** Stage 18 embryo: *cav1α* expression is located in the notochord (nc), inner/deep layer (dl) of the epidermis and in the outer layer of the neural plate (np) at both sides of the midline (arrow). sl = sensory layer. **D** Stage 23 embryo: *cav1α* is expressed in the notochord (nc) and deep layer of the epidermis. **E** Schematic view of the expression profile of *cav1α* (violet) in a stage 12.5 embryo. *cav1α* (violet) can be found in the notochord, deep layer of the epidermis and

neural plate. Psm = paraxial mesoderm, np = neural plate, nc = notochord, sl= sensory layer, dl= deep layer. **F** Transverse section of a stage 15 embryo stained for *n-tubulin* (red) and *cav1α* (blue) expression. N-tubulin is expressed in three domains in the deep layer of the neural tube. m = medial domain, I = intermedial domain, l = lateral domain. **G-N** longitudinal (G-J) and transverse (K-N) sections of a stage 43 embryo stained for *cav1α* expression. **G-K** Schematic representation of the cutting position (red line). **G'-N'** *cav1α* is expressed in the epidermis (ep), lung (lg), aortic arches (aa) and the heart (h). Abbreviations: e= eye, nc= notochord, nt= neural tube, so= somite, cg= cement gland.

To validate the *in situ* expression pattern, Cav1 protein expression was analyzed by whole mount immunofluorescence using a polyclonal Cav1 antibody (Figure 23). In agreement with the results gained by *in situ* hybridization, Cav1 is expressed in the sensory layer of the epidermis as well as the notochord in *Xenopus* tadpoles (Figure 23K, D, J). Furthermore, Cav1 expression could also be detected in the developing lung (lg) (Figure 23D, F') and the vasculature in stage 42 embryos (Figure 23F, G, I). This includes the posterior cardinal vein (pcv), the dorsal longitudinal anastomosing vessels (dlav) of the tail and in the aortic arches (aa) of the branchial arches (Figure 23F, G, I). Interestingly, in contrast to the *in situ* hybridization, staining Cav1 protein was also detected in cranial nerves as well as spinal motoneurons (Figure 23A-H). Transverse sections of stage 35 embryos verified that Cav1 is expressed in the neuronal cells of the spinal cord, the notochord and the sensorial epidermal cells (Figure 23J-L). No expression of Cav1 could be detected in the musculature neither by *in situ* hybridization nor by immunofluorescence staining, indicating that Cav1 likely functions in the neuronal circuits controlling muscular function.

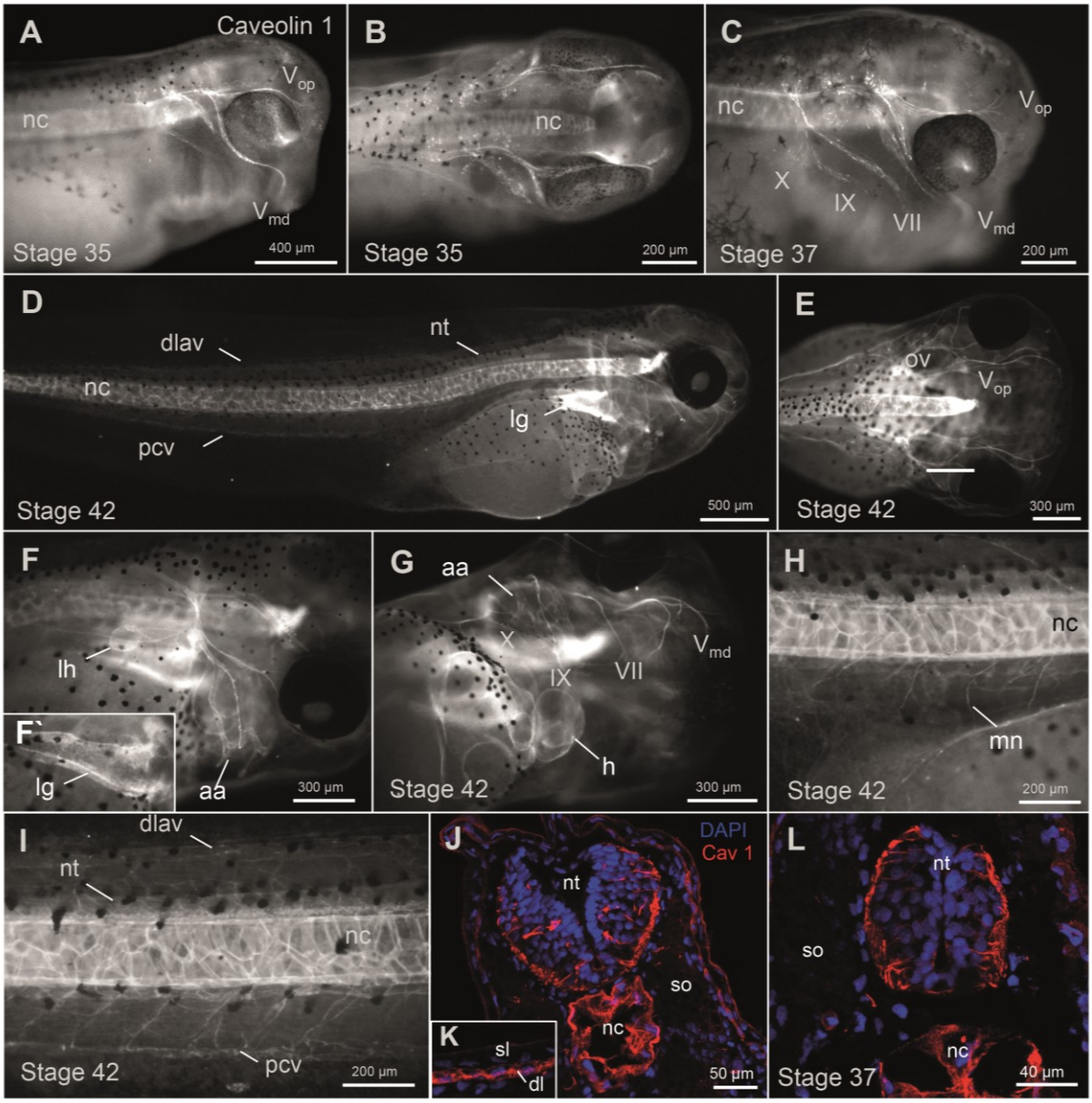

Figure 23: **Cav1 is strongly expressed in the notochord and the nervous system during *Xenopus* development.**
A Immunostaining of a stage 35 embryo showing Cav1 protein expression in the notochord and the cranial nerves (Vop= ophthalmic trigeminal ganglion, Vmd= mandibular trigeminal ganglion). **B** Dorsal view of a stage 35 embryo. Cav1 expression is visible in the cell bodies of the cranial nerve located in the brain **C** Stage 37 embryo. Cav1 is expressed in the notochord as well as the cranial nerves. **D** Stage 42 embryo showing Cav1 expression in the notochord neural tube, lung and cardio vasculature of the tail. **E** Dorsal view of the embryo shown in D. Cav1 is expressed in the cranial nerves. **F** Magnification of the embryo shown in D. Cav1 is expressed in the cranial nerves, aortic arches and the lymph heart. **F'** Magnification of embryo shown in F showing Cav1 expression in the lung **G** ventral view of the embryo shown in F. Cav1 staining is visible in the heart, aortic arches and cranial nerves. **H** Tail of a stage 42 embryos showing Cav1 expression in the notochord, neural tube as well as the axons of the motor neurons. **I** Tail of a stage 42 embryos showing Cav1 expression in the cardio vasculature of the tail. **J** Transverse section of the hindbrain of a stage 37 embryo showing Cav1 expression in red and DAPI staining in blue. Cav1 is expressed in neurons and the notochord. **K** Magnification of the epidermis of a stage 37 embryo. Cav1 is expressed in the inner layer of the epidermis. **L** Transverse section of the neural tube of a stage 37 embryo showing cav1 expression in the neural tube and notochord. Abbreviations: aa= aortic arches, Dlav = dorsal longitudinal

anastomosis vessel, ep = epidermis, h = heart, il = inner layer of the epidermis, Isv/Isa= intersomitic vessels/artery; lh = lymph heart, lg =lung, mn = motor neurons, nc = notochord, nt =notochord, Pcv = posterior cardinal vain, so= somites, sl= sensory layer of the epidermis, VII= facial nerve, IX= glossopharyngeal nerve, X= vagus nerve.

As the Cav1 antibody both recognize the Cav1α and the β-isoform, the specificity of the Cav1α expression was analyzed by whole mount immunofluorescence staining on embryos injected with either 12 ng Co MO or Cav1α MO in both blastomere of two-cell stage embryos (Figure 24). The relative signal intensity of the Cav1 staining was determined in relation to the DAPI signal and normalized against Co MO-injected embryos. Knockdown of Cav1α visibly reduced the Cav1 signal in the morphant embryos in comparison to control embryos (Figure 24A-B). Quantification of the signal intensity showed, that the Cav1 fluorescence signal in the Cav1α morphants was reduced by up to 30 % compared to control embryos (Figure 24C). These findings confirmed that the Cav1 staining is specific for Cav1α.

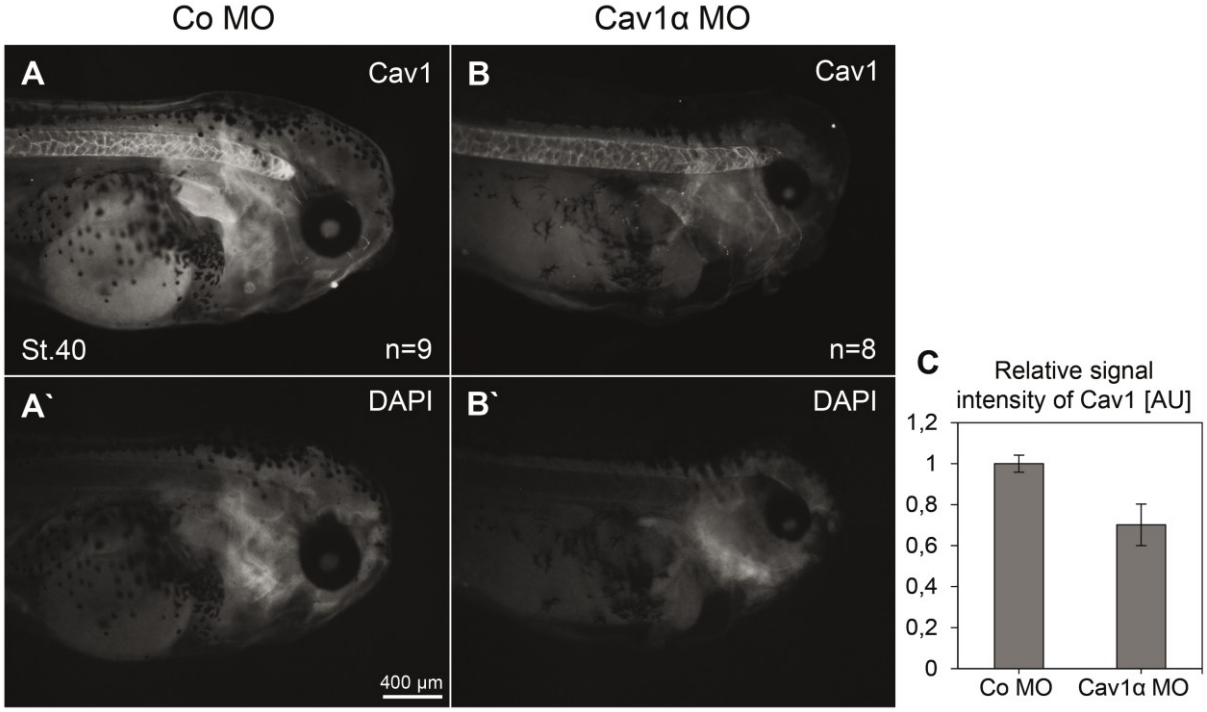

Figure 24: **Cav1α MO successfully reduces endogenous Cav1 protein levels**.
A-C Stage 40 embryos injected with 12 ng Co MO or Cav1α MO in both blastomeres of two-cell stage embryos were stained for endogenous Cav1 protein. **A-B** anti-Cav1 staining visible in the notochord, lung and cranial nerves. Injection of the Cav1α MO (B) reduced the Cav1 signal in all Cav1-expressing tissue. Number (n) of analyzed embryos is shown. **A'-B'** DAPI staining is shown. **C** Relative signal intensity of Cav1 signal in the Co MO and Cav1α MO injected embryos. The Cav1 signal was normalized to the DAPI signal. ± S.E. of two independent experiments is shown.

3.6 Loss-of-function of Cav1α in neural tissue, but not muscle tissue, causes severe swimming defects

Cav1α is expressed in nerve but not muscle tissue in *Xenopus* embryos, implying a function for Cav1α in neuronal tissue. To verify that Cav1α functions in neuronal but not muscular tissue, the swimming behavior and muscle phenotypes were analyzed in embryos specifically injected into mesodermal or neuronal tissue (Figure 25). For this purpose, 10 ng of the Cav1α Morpholinos were co-injected with *mGFP* RNA as a lineage tracer into the dorsal marginal zone of the vegetal blastomeres (the dorsal-vegetal blastomere) of 8-cell stage embryos to mainly target muscle cells. Alternatively, the Morpholinos were injected into the dorsal blastomere of the animal hemisphere to target neuronal cells in the brain and spinal cord. Interestingly, while the muscle-specific knockdown of Cav1α did not affect the swimming behavior (Figure 25A, C), the knockdown of Cav1α in neuronal tissue caused severe swimming defects in the in the morphant embryos (Figure 25B, D). In detail, 74 % of the neural-injected Cav1α morphants (36% ±3% severe, 38% ±4% mild) and 87% of the Cav1α-Spl morphants (56% ±5% severe; 31% ±5% mild) displayed an aberrant swimming behavior (Figure 25B, D). As previously shown, this swimming phenotype could be significantly improved by co-injection of the respective *cav1α* rescue constructs (Figure 25B, D). The total percentage of aberrant swimming behaviors could be significantly reduced by 23% (21% ±4% severe, 28% ±6% mild) upon co-expression of *cav1α-rescue RNA* in the Cav1α morphants (Figure 25D). Similarly, expression of the full-length *cav1α- RNA* was able to significantly improve the severe swimming defects by 21% (36% ±5% severe, 28% ±3% mild) in the Cav1α-Spl morphants (Figure 25B).

In order to examine if the rescue of the swimming defects is not due to unspecific rescue effects caused by RNA injection, 100 pg *LacZ* RNA was co-injected as neutral RNA together with the Cav1α-Spl MO and swimming defects were analyzed. In contrast to *Cav1α-HA, LacZ* did not improve the swimming behavior of the morphant embryos when co-injected with the Cav1α-Spl MO (Figure 25B). This suggests that the rescue by the co-expression of the *cav1α* constructs is indeed specific.

Injection of the Cav1α Morpholinos into one blastomere of two-cell stage embryos severely impaired the muscular integrity. In order to analyze if the neural-specific knockdown of Cav1α also affects the morphology of the musculature, muscular actin was stained by Phalloidin (Figure 25E-G). While control embryos show the characteristic striped muscular actin organization (Figure 25E-E'), the neural-injected Cav1α morphant embryos displayed a highly disrupted actin network in the muscle cells (Figure 25F-F'). This could again be restored by co-injection of the *res-cav1α* RNA (Figure 25G-G').

Collectively, these findings indicate that Cav1α is not directly required in the musculature but

functions in neuronal tissue affecting the neural muscular circuit that controls the embryonic swimming behavior.

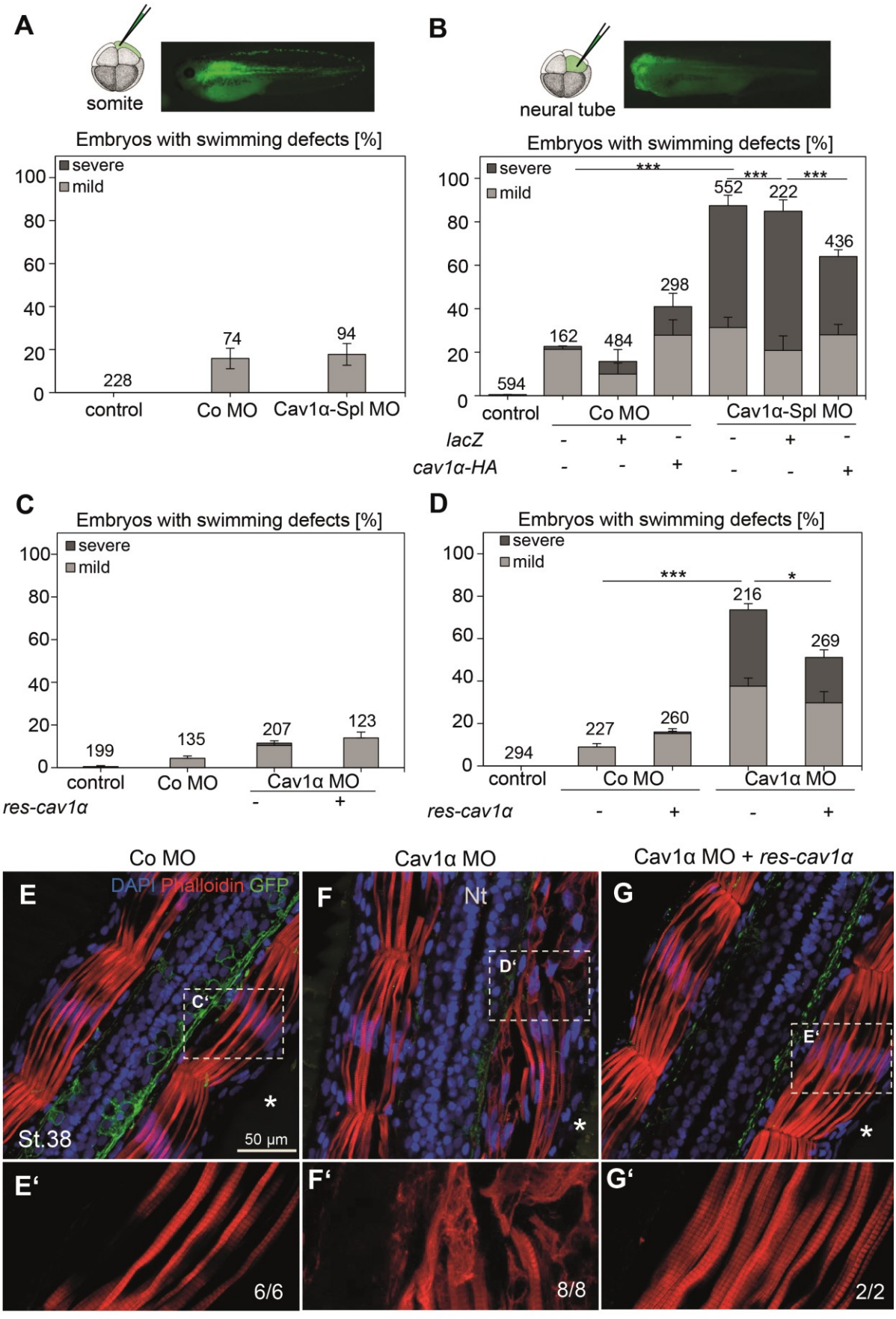

Figure 25: **Loss-of-function of Cav1α in neural tissue but not in the somites leads to swimming defects.**
Constructs were targeted to the mesodermal (A,C) or the neural tissue (B,D) and the percentage of swimming defects of at least three independent experiments was analyzed at stage 38. Morpholinos were injected at a concentration of 10 ng and *cav1α*- or *lacZ* RNA in a concentration of 100-200 pg. GFP (70 pg) was used as lineage tracer. **A,C** Targeted injection of the Cav1α-Spl MO (A) or Cav1α MO (C) in the somites only caused swimming defects in a low percentage of embryos. Data from at least three experiments are presented as the mean ± S.E.M. and number of injected embryos are indicated for each column. **B-D** Targeted injection of the Cav1α-Spl MO (B) or Cav1α MO (D) to neural tissue caused swimming defects. Graph summarizing the percentage of mild (light grey) or severe (dark grey) swimming defects of at least three independent experiments; ± S.E.M. and number of injected embryos are indicated for each column. Significance was calculated using the student's t-test and ordinary one-way ANOVA. * p-value ≤ 0.05; **p-value ≤0.01; ***p-value ≤ 0.001. **E-G** Muscle morphology of neural-injected embryos was analyzed by sectioning and Phalloidin staining. Asterisks indicate the injected side. **E'-G'** Higher magnification of the boxed areas shown in E, F, G. **E-E'** Normal actin organization in a control embryo. **F** Highly disrupted actin organization on the injected side of Cav1α morphant embryo. **G** Co-expression of *res-cav1α* RNA in neural tissue restored actin organization of Cav1α morphant muscle cells. Number of analyzed embryos are shown.

3.7 Swimming defects in the Cav1α morphants are not caused by defective notochord structure

It has been demonstrated in several studies, that caveolae protect the notochord against mechanically induced cell damage (Garcia et al., 2017; Lim et al., 2017; Nixon et al., 2007; Nixon et al., 2005). Knockout of cavin 1 expression in zebrafish is associated with the loss of caveolae formation even in the presence of caveolin proteins and results in locomotor-induced collapse of notochord cells (Garcia et al., 2017; Lim et al., 2017). As the notochord functions as an important axial-structural element in swimming larvae, it is not surprising that defects in this structure also correlate with an impaired swimming behaviour in these embryos (Lim et al., 2017). Similar to Cavin 1, Cav1 is also strongly expressed in the notochord. Injection of the Cav1α Morpholino into the animal blastomere caused severe swimming defects, which was not the case upon targeting the Morpholino into the dorsal/vegetal blastomere, suggesting a neural function for Cav1α. However, both blastomere also contribute equally to the presumptive notochord. To exclude the possibility, that the swimming phenotype in the Cav1α morphant embryos are due to defects in the notochord structure, Cavin1 knockdown studies were performed.

As Cavin 1 Morpholino concentrations above 1.5 ng result in a high lethality rate (data not shown), 8 cell stage embryos were injected with either 1 ng or 1.5 ng Cavin 1 MO into the neural/animal blastomere and swimming defects were analyzed (Figure 26). Injection of 1.5 ng Cavin 1 Morpholino significantly increased the number of embryos with convergent extension defects. Here, 56 % ±18% of the Cavin 1 morphant (1.5 ng) embryos displayed a significant shortened anterior/posterior axis, while embryos injected with either 1 ng Cavin 1 MO (13% ±6%) or 10 ng Cav1α MO (13% ±3%) showed these defects only in a low

percentage (Figure 26C-F). Similarly, embryos injected with 10 ng Co MO showed a normal morphology (Figure 26B, F).

As previously shown, the neural injection of the Cav1α Morpholino caused swimming abnormalities in the morphant embryos (Figure 26G). While knockdown of Cav1α led to mild swimming phenotype in 38% ±3% and severe swimming defects in 40% ±3% of the morphant embryos, the knockdown of Cavin 1 only resulted in a low percentage of swimming defects (Figure 26G). In comparison, injection of 1 ng Cavin 1 MO results in 8% ±5% mild and 5% ±3% severe swimming defects. Similarly, 17% ±4% of the embryos injected with 1.5 ng Morpholino developed a mild and 12% ±8% a severe swimming phenotype (Figure 26G). However, these swimming abnormalities were not significant in contrast to the effect of Cav1α Morpholino injection. It should be noted that, while Cav1α morphant embryos were still able to contract the uninjected side, Cavin 1 morphants with a strongly shortened anterior/posterior axis were unable to swim and displayed only uncoordinated twitching movements. Therefore, embryos with a severely reduced anterior/posterior body axis were excluded from the statistical evaluation and only embryos with the classical swimming defects were counted.

These data imply that the swimming defects in the Cav1α morphants are unlikely to be caused by defects in the notochord, since the loss-of-function of Cavin 1 does not causes swimming abnormalities to the same extent as the loss-of-function of Cav1α.

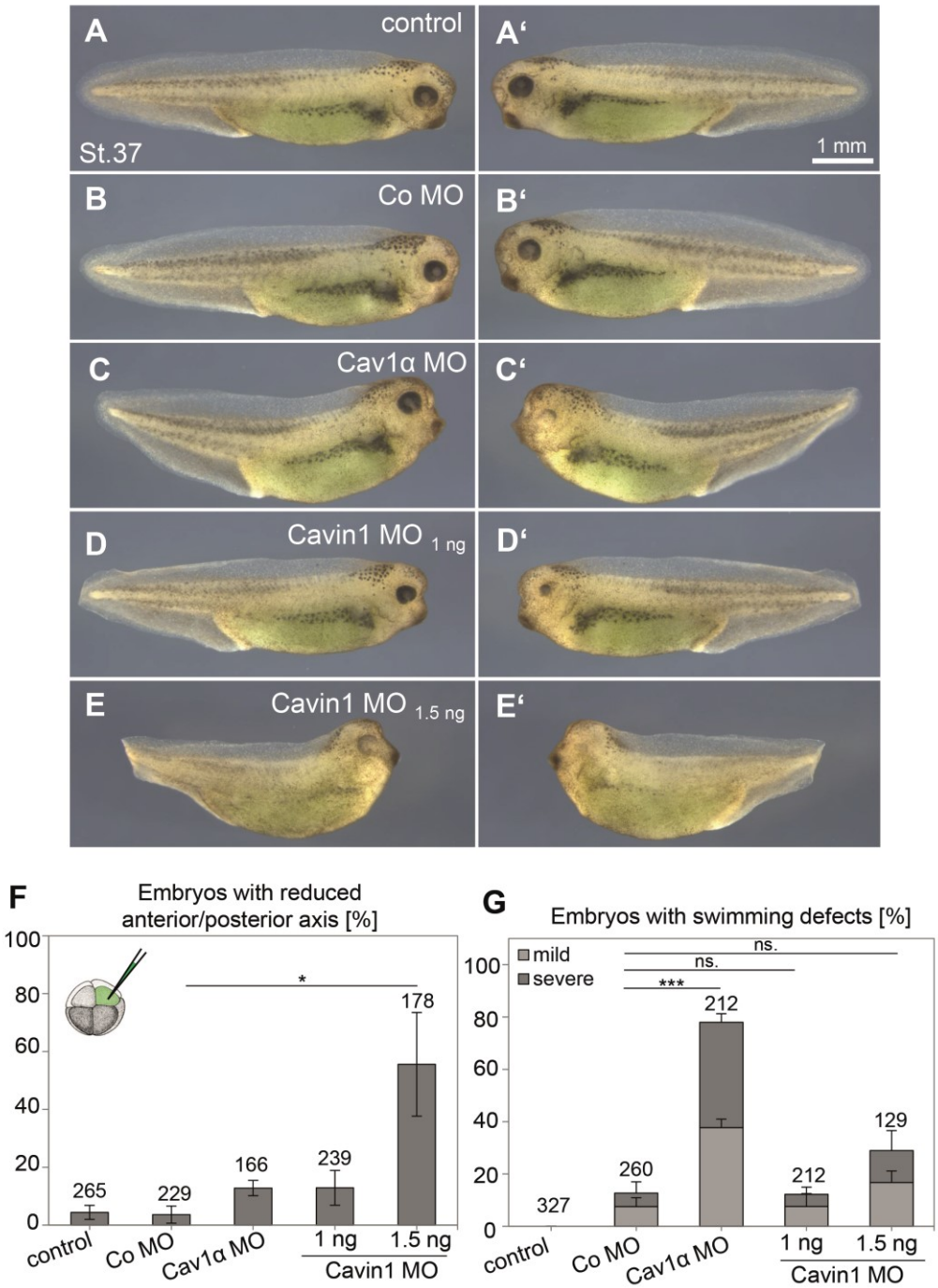

Figure 26: **Knockdown of cavin1 does not affects the swimming behavior.**
A-G Co MO (10 ng), Cav1α MO (10 ng) or Cavin 1 MO (1-1.5ng) were targeted to the neural tube. *GFP* RNA served as lineage tracer. Injected side (B-E) and uninjected side (B'-E') are shown. Embryos were analyzed at stage 37. **A-A'** Stage 37 control embryo. **B-B'** Wild-type morphology of a Co MO injected embryo. **C-C'** stage 37 embryo injected with 10 ng Cav1α MO **D-D'** stage 37 embryo injected with 1ng Cavin1 MO. **E-E'** Stage 37 embryo injected with 1.5 ng Cavin 1 MO. **F** Graph summarizing the percentage of embryos with shortened anterior/posterior axes. Injection of 1.5 ng Cavin 1 MO significantly increased the number of embryos with a shortened anterior/posterior axis. **G** Graph summarizing the percentage of mild (light grey) or severe (dark grey) swimming defects of three independent experiments. Embryos were analyzed at stage 38. Number of analyzed embryos are indicated for each column. Data from at least three experiments are presented as the mean ± S.E.M. * p-value ≤ 0.05; **p-value ≤0.01; ***p-value ≤ 0.001. Significance of the total number of swimming defects was calculated using the Student's t-test and ordinary one-way ANOVA. The total number of swimming defects was used for the statistical evaluation.

3.8 Inhibition of voltage- dependent sodium channels mimics the muscular defects of Cav1α morphants

The neural but not muscular specific knockdown of Cav1α causes swimming defects as well as impaired somitic integrity, which implies a neuromuscular function for Cav1α. A well-established connection between motoneurons and the musculature is fundamental for a healthy development and integrity of muscles (Gutmann, 1962; Sohal and Holt, 1980). Several animal models of neuromuscular diseases, including Huntington and spinal muscular atrophy (SMA), have shown that defects in the development of motoneurons and an impaired establishment of a neuro-muscular connection can cause severe muscular atrophy (Hsieh-Li et al., 2000; Monani et al., 2000).

To confirm that the muscular defects of the Cav1α morphants are due to defects in the neuro-muscular system, embryos were anesthetized with Benzocaine (Figure 27). Benzocaine is an inhibitor for voltage gated sodium channels, which blocks the transmission of an action potential from the nerve towards the muscle cell, thereby mimicking a denervated muscle. If the muscular defects of the morphant embryos are caused by impaired muscle innervation, benzocaine treatment should mimic these defects. To verify this hypothesis, Cav1α morphant embryos were incubated in 0.01 % benzocaine from the beginning of the swimming stage (stage 26 to 37). Muscular actin of treated as well as untreated embryos was stained using Phalloidin (Figure 27).

As previously shown, the knockdown of Cav1α leads to disorganized actin filaments in the musculature, while they were correctly aligned in control embryos (Figure 27B-C). Interestingly, Benzocaine-treated embryos – including the uninjected controls – displayed muscular defects, which are similar to those of the Cav1α morphant embryos. Independent of the side of MO injection, muscular actin filaments were disorganized and showed a wavy appearance in both the control and morphant embryos (Figure 27D-E). This observation indicates that a disruption in neuromuscular communication is sufficient to compromise muscle integrity.

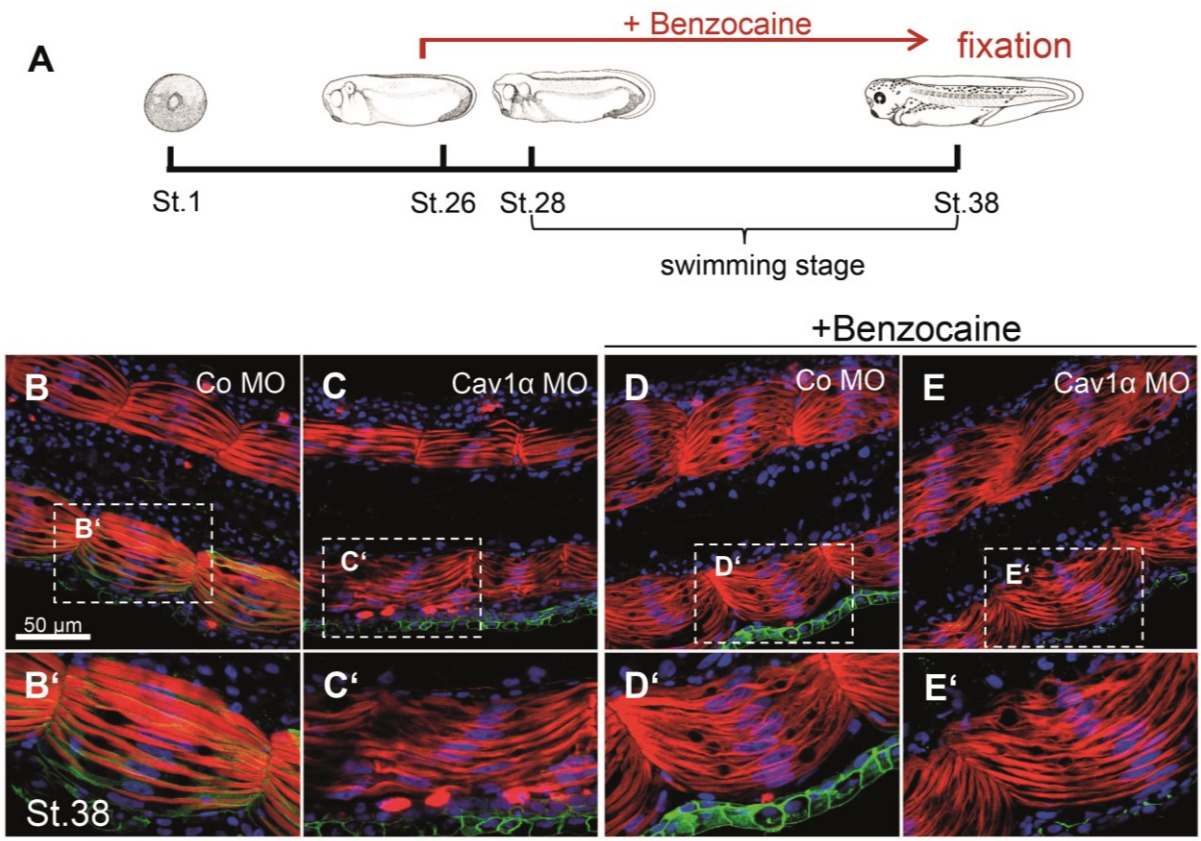

Figure 27: **Anesthetizing of *Xenopus* embryos mimics muscular actin disorganization observed in Cav1α morphants.**
A Schematic view of the experimental procedure. Embryos were injected with 20 ng MO in combination with *GFP* RNA into one blastomere at the two-cell stage and cultivated until stage 26 when Benzocaine was added to the medium. Embryos were fixed at stage 37/38, sectioned dorsally and stained with Phalloidin. **B** Normal muscle morphology in an untreated embryo injected with control MO. GFP signal indicates the injected side. The dashed line marks the magnified area shown in B'. **C** Loss-of-function of Cav1α disrupted somitic actin fiber organization. **C'** Magnification of the marked area shown in C (dashed line). **D-E** Benzocaine treated embryos. The absence of muscle activity caused by Benzocaine treatment results in disorganized actin fibers in controls (D) as well as Cav1α morphant embryos (E').

3.9 Cav1α loss-of-function affects axonal outgrowth of motoneurons

The data shown above indicate that Cav1α likely has a function in the neuromuscular system of *Xenopus* embryos and, thus, affects both muscular integrity and embryonic mobility. Furthermore, expression of Cav1 could be detected in neurons of the spinal cord, suggesting a function in the neuromuscular system. To examine how Cav1α loss-of-function affects the muscular integrity, the morphology of the motor nerves was analyzed by immunofluorescence staining in the morphant embryos (Figure 28). To this end, embryos were unilaterally injected with either 20 ng Cav1α MO or Cav1α-Spl MO. *mGFP* or *lacZ* were co-injected as a lineage tracer.

In control embryos axons of motoneurons protruded dorso-ventrally from the ventral neural tube to the somitic muscle, which led to a characteristic chevron-shaped pattern (Figure 28A-

A'). In contrast, motor nerve growth was severely impaired in 89% ±4% Cav1α MO and in 86% ±2% of the Cav1α-Spl MO-injected embryos (Figure 28E). Although the neurons of Cav1α MO-injected embryos were still able to extent axons, they randomly projected their axons in the periphery not following the boundaries of the somitic muscles (Figure 28B-B'). Motoneurons from embryos injected with the Cav1α-Spl MO, which is also more effective in blocking Cav1α expression compared to the translation blocking Cav1α MO, showed a similar pathfinding phenotype (Figure 28C-C') but also severe axonal outgrowth defects (Figure 28D-D'). In order to analyze if the neuronal phenotype is specific for Cav1α loss of function, rescue experiments were performed by the unilateral injection of 10 ng Cav1α-Spl MO in combination with 200 pg *cav1α-HA* RNA (Figure 29A-E). While the injection of the Cav1α-Spl MO caused motoneuron pathfinding (Figure 29B') as well as outgrowth defects (Figure 29C') in 64% ±3% of the morphant embryos, co-expression of *cav1α-HA* RNA significantly rescued these defects (31% ±4%; Figure 29D, E). These results indicate that the observed neuronal abnormalities are indeed specific to Cav1α loss-of-function.
Collectively, these data demonstrate that the muscular defects in the morphant embryos are likely caused by deficiencies in axonal outgrowth and pathfinding of motoneurons and consequently resulting in defective muscular innervation.

The injection of the Cav1α-Spl MO led to the formation of fewer axons that innervate the musculature, which could also be the result of a reduced number of motoneurons in the spinal cord. To investigate if loss-of-function of Cav1α affects early neuronal patterning, the expression of the neuronal marker *n-tubulin* (neuron specific class IIβ tubulin) was analyzed by *in situ* hybridization during early neurula stages (Figure 29F-J). *N-tubulin* is expressed in three longitudinal stripes on each site of the open neural plate: the medial domain, representing the future motoneurons; the intermediate stripe, which give rise to interneurons; and the lateral stripe, from which sensory neurons will derive. Additionally, it is also expressed in the trigeminal ganglion, a small domain located in the anterior part of the neural plate (Moody et al., 1996; Oschwald et al., 1991; Roberts, 2000a). Control embryos (Figure 29F-G,I) as well as the majority of the of the Cav1α morphant embryos (Figure 29H-I) showed normal n-tubulin expression in all four domains, indicating that loss-of-function of Cav1α has no impact on early neurogenesis and neuronal patterning in *Xenopus* embryos.

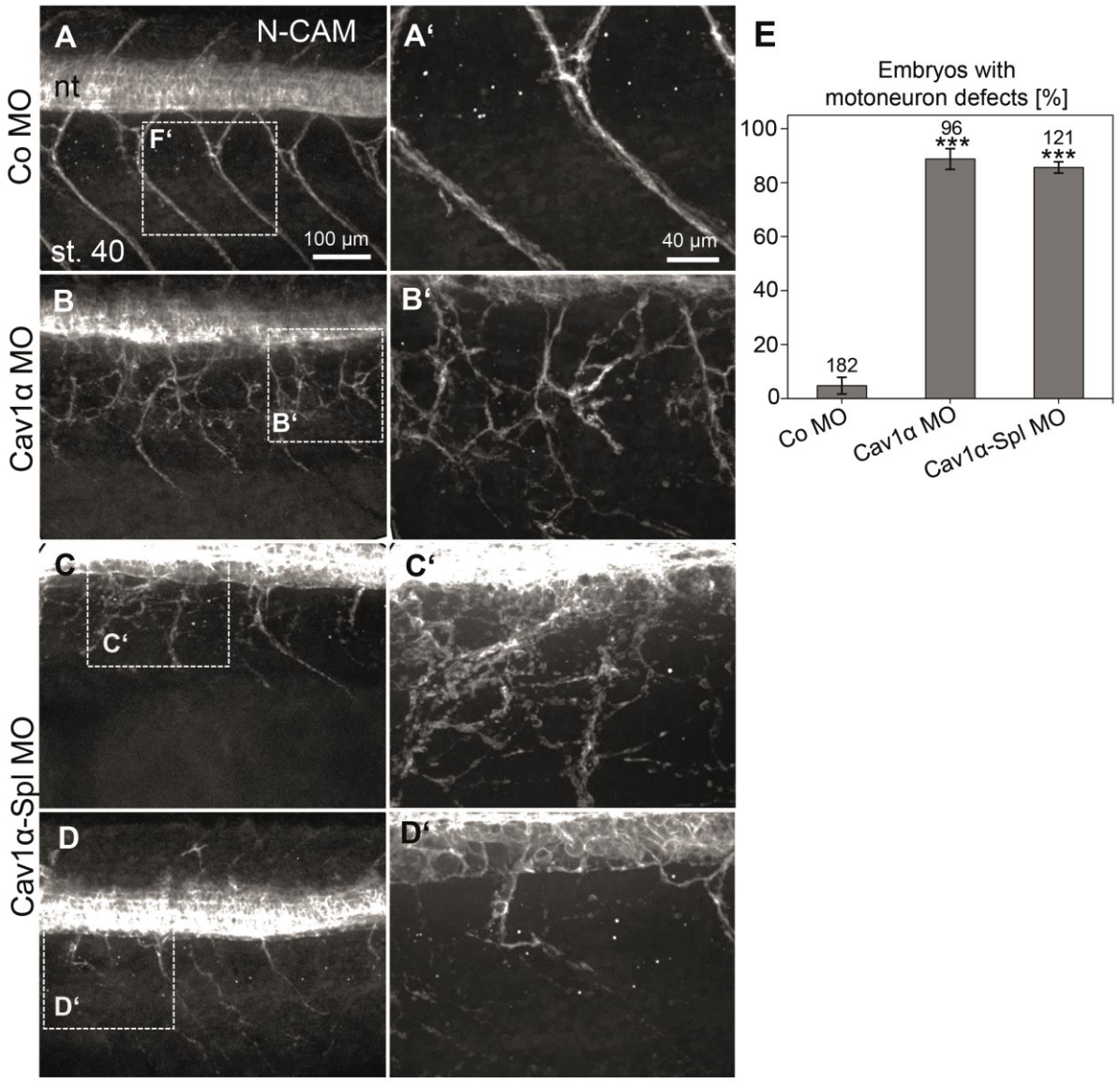

Figure 28: **Knockdown of Cav1α affects axonal morphology.**
A-D Embryos were injected with 20 ng MO in combination with *mGF*P RNA into one blastomere at the two-cell stage. The nervous system of stage 40 embryos was stained by whole mount immunostaining using the neuronal surface marker NCAM. **A** Motoneurons innervating the muscles of control embryos displaying the characteristic chevron-shaped pattern. **A**' Magnification of the dashed area shown in panel A. **B** Motoneuron pathfinding is severely impaired in Cav1α morphants. **C-D** Cav1α-Splice morphants showing severe motoneuron pathfinding (C) as well as outgrowth defects (D). Axons of motoneurons were highly disoriented and failed to innervate somitic muscles properly. **B-D'** Magnification of the dashed area shown in panel B and D. nt = neural tube **E** Graph summarizing the percentages of Co MO and Cav1α morphant embryos with motoneuron defects of at least four independent experiments; ± S.E.M. and number of analyzed embryos are indicated for each column. Significance was calculated using the Student's t-test and ordinary one-way ANOVA. ***p-value ≤ 0.001.

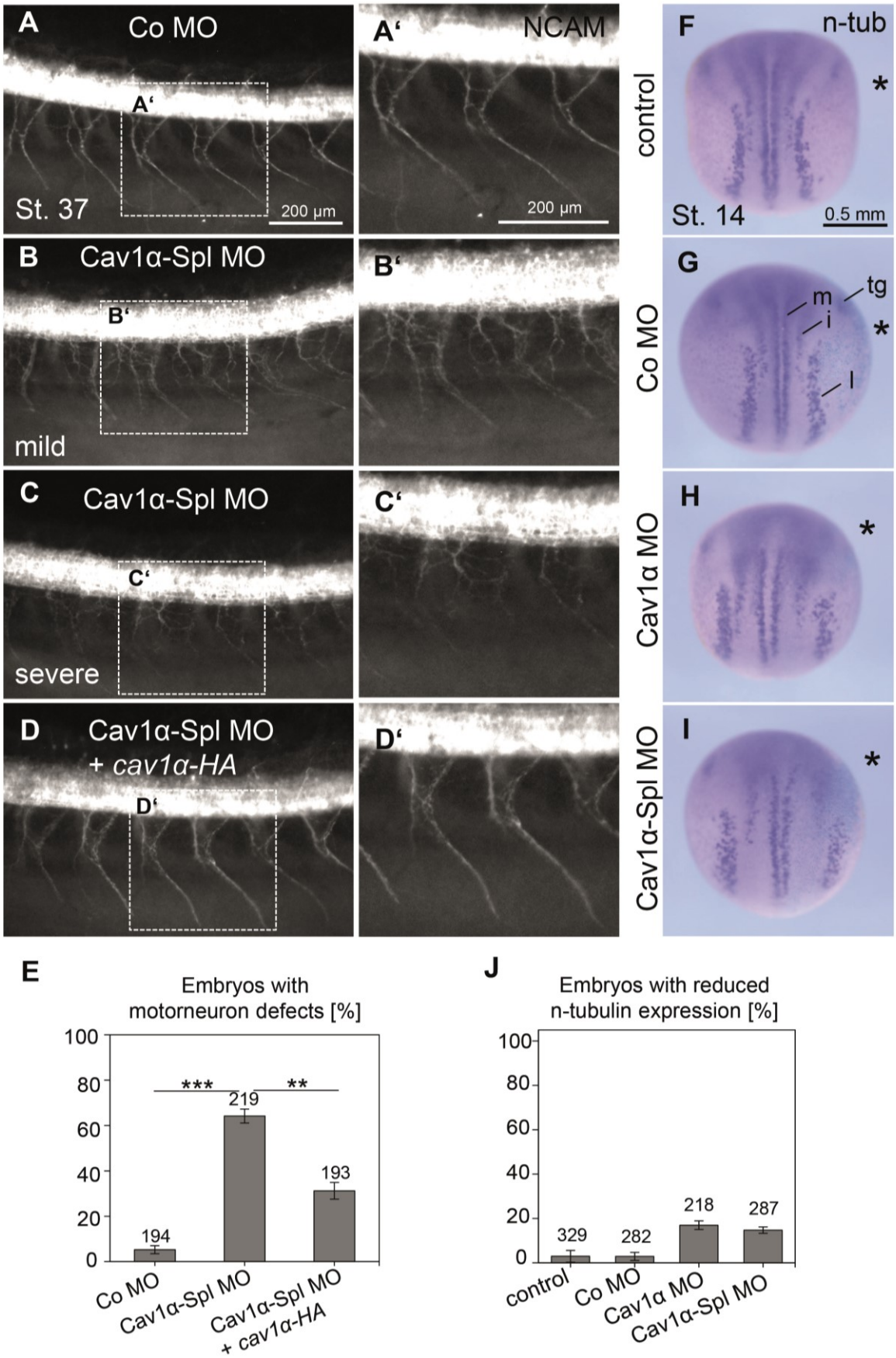

Figure 29: Cav1α-HA overexpression rescues motoneuron defects.
A-E Embryos were injected with 10 ng MO alone or in combination with 200 pg *cav1α-HA* RNA into one blastomere of two-cell stage embryos. *mGFP* RNA was co-injected as a lineage tracer. The nervous system of stage 37 embryos was stained by whole mount immunostaining using the neuronal

surface marker NCAM. Injected (A-D) and magnified area highlighted in A-D shown (A'-D'). **A-A'** Motoneurons of an embryo injected with Co MO. **B'-C'** Motoneuron outgrowth (B) as well as pathfinding (C') is severely affected by Cav1α knockdown. **D-D'** Co-expression of *cav1α-HA* RNA rescues motoneuron defects. **E** Graph summarizing the percentages of embryos with motoneuron defects of three independent experiments; ± S.E.M. and number of analyzed embryos are indicated for each column. Significance was calculated using the Student's t-test and ordinary one-way ANOVA. **p-value ≤ 0.01, ***p-value ≤ 0.001. **F-J** Control embryos (F) or embryos injected unilaterally with 20 ng Co MO (G), Cav1α MO (H) or Cav1α-Spl MO (I) were analyzed for *n-tubulin* expression by whole mount *in situ* hybridization. *LacZ* RNA was co-injected as a lineage tracer (blue staining). Asterisk indicates the injected side. **F-I** *n-tubulin* is expressed in the m= medial domain, l = intermedial domain and l = lateral domain as well as in the tg = trigeminal ganglion. **J** Percentage of reduced n-tubulin expression is shown from two independent experiments, ± S.E. and number of analyzed embryos is indicated for each column.

3.10 Cav1α loss-of-function affects axonal outgrowth and morphology *in vitro*

To understand how Cav1α loss-of-function affects axonal outgrowth, the morphological properties of spinal cord neurons were analyzed in cultured neural tube explants. Therefore, embryos were injected with 12 ng of the Cav1α Morpholinos and *mGFP* or *lifeact-RFP* RNA as a lineage tracer either into both blastomeres of the two-cell stage or into the two neural blastomeres of four-cell stage embryos. Neural tubes were isolated from stage 20-22 embryos and axonal outgrowth and morphology were analyzed by live-cell microscopy after approximately 24 h of incubation (Figure 30A). By whole mount immunofluorescence staining it could be shown that axonal outgrowth was severely affected in the Cav1α-Spl morphant embryos *in vivo* (Figure 30D). Similarly, injection of the Cav1α-Spl MO but not the translation blocking Morpholino Cav1α MO significantly reduced the outgrowth of axons in cultured spinal cord explants (Figure 30B). Interestingly, in addition to axonal outgrowth their morphology was affected by Cav1α knockdown. While control neurons extended long axons with a dynamic, actin-rich growth cone (Figure 30C, F, I-K), the axonal morphology in Cav1α morphant samples was severely affected. A significantly larger proportion of these neurons extended axons with an increased number of actin-rich filopodia-like structures on the axon shaft. This increased filopodia formation was observed in 55% ±5% of the Cav1α morphant and 52% ±5% of the Cav1α-Spl morphant axons (Figure 30D-J). Furthermore, also the number of axons with excessive lamellipodia formation was significantly increased both in Cav1α morphant (33% ±3%) and Cav1α-Spl morphant axons (48% ±5%) (Figure 30K). Quantification of this phenotype showed that these lamellipodia covered a significantly larger portion of the total axonal area in the axons of Cav1α morphant (50% ±2%) as well as Cav1α-Spl morphant (47% ±1%) explants in comparison to control axons (14% ±1%) (Figure 30L). Most axon shafts of control neurons showed only a low number of filopodia or lamellipodia protrusions (Figure 30, I, K).

To analyze if these morphological abnormalities are specific to the Cav1α knockdown, rescue experiments were performed (Figure 30M-O). To this end, 10 ng of the Cav1α-Spl MO was injected alone or in combination with 200 pg *cav1α-HA* RNA into both blastomeres of two-cell stage embryos followed by the isolation of neural tubes at stage 20-22. As described above, the Morpholino-mediated knockdown of Cav1α by Cav1α-Spl MO significantly impairs axonal outgrowth and led to an increased number of axons with excessive filopodia (50% ±3%) as well as lamellipodia (32%±8%) formation (Figure 30M-O). Co-expression of *cav1α-HA* RNA significantly rescued the axonal outgrowth defects as well as the increased filopodia (25% ±4%) and lamellipodia (9%±3%) formation observed in the Cav1α-Spl morphant explants (Figure 30M-O).

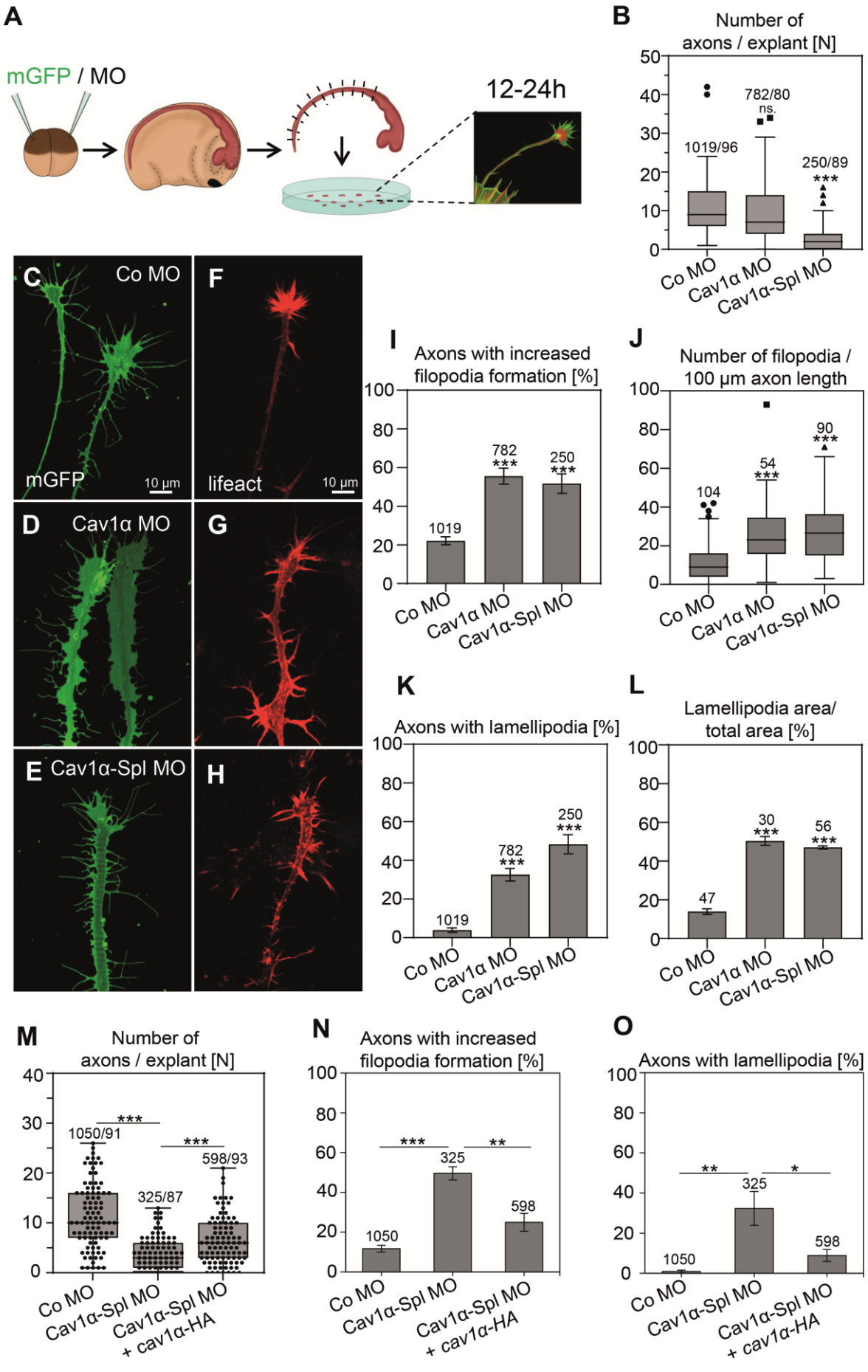
A
mGFP / MO
12-24h
B
Number of axons / explant [N]
1019/96
782/80
ns.
250/89
***
Co MO
Cav1α MO
Cav1α-Spl MO
C
Co MO
mGFP
10 µm
F
lifeact
10 µm
D
Cav1α MO
G
E
Cav1α-Spl MO
H
I
Axons with increased filopodia formation [%]
1019
782
***
250
***
J
Number of filopodia / 100 µm axon length
104
54
***
90
***
K
Axons with lamellipodia [%]
1019
782
***
250
***
L
Lamellipodia area/ total area [%]
47
30
***
56
***
M
Number of axons / explant [N]
1050/91
***
325/87
***
598/93
Co MO
Cav1α-Spl MO
Cav1α-Spl MO + cav1α-HA
N
Axons with increased filopodia formation [%]
***
325
**
1050
598
O
Axons with lamellipodia [%]
**
325
*
1050
598

Figure 30: Cav1α knockdown affects axonal growth and morphology *in vitro*.
A Schematic representation of the experimental procedure. Embryos were injected into both blastomeres with 12 ng Co MO, Cav1α Mo or Cav1α-Spl MO in combination with 70 pg *mGFP* or 200 pg *Lifeact-RFP* RNA. Neural tubes of stage 20-22 embryos were isolated, evenly dissected and cultured on poly-lysine and laminin-coated dishes. Axonal growth was monitored after 12-24h. **B** Graph showing the number of axons per explant for each condition. Injection of the Cav1α-Spl MO significantly decreases the outgrowth of axons per explant. ***p-value ≤ 0.001, ns = not significant. Significance was calculated using a Mann-Whitney test. Number of axons and explants is indicated for each column. **C-L** LOF of Caveolin increased filopodia and lamellipodia formation in cultured spinal cord neurons. **C, F** Control axons showed typical actin-positive growth cones. **D, G, E, H** Injection of either Cav1α Mo (D, G) or Cav1α-Spl MO (E, H) increased the formation of filopodia-like and lamellipodia-like actin-rich structures in cultured neurons. **I-L** Graphs summarizing percentages of axons with increased filopodia-like structures (I) or lamellipodia formation (K). **J** Graph summarizing the number of filopodia-like structures per 100 µm axon length. **L** Percentage of lamellipodia area in relation to total axon area. Data from at least three experiments are presented as ± S.E.M. ***p-value ≤ 0.001. Significance was calculated using a two-tailed unpaired Student's t-test, ordinary one-way ANOVA (Dunnett's multiple comparisons) or Mann-Whitney test (Box blots). Numbers of analyzed axons are indicated for each column. **M-O** Axonal outgrowth as well as filopodia and lamellipodia formation was analyzed in embryos injected with 10 ng Co MO, Cav1α Mo or Cav1α-Spl MO alone or in combination with 200 pg *cav1α-HA* RNA. Data of four independent experiments are shown. **M** Graph showing the number of axons per explant for each condition. Co-injection of *cav1α-HA* RNA significantly rescued the outgrowth of axons per explant. ***p-value ≤ 0.001. Significance was calculated using a Mann-Whitney test. **N-O** Graphs showing the numbers of axons with increased filopodia (N) or lamellipodia (O) formation. Co-injection of *cav1α-HA* RNA significantly rescued the excessive filopodia and lamellipodia formation. ± S.E.M. Significance was calculated using the Student's t-test and ordinary one-way ANOVA. * p-value ≤ 0.05; **p-value ≤0.01; ***p-value ≤ 0.001.

To investigate how these membrane protrusions are formed, the axonal outgrowth in control as well as Cav1α morphant neurons was analyzed by live-cell imaging (Figure 31). Growth cones from control axons dynamically extended and retracted the majority of the filopodia and lamellipodia protrusions over time (Figure 31A, B, Supplementary Movie 6, 7). Although axons from morphant explants showed similar dynamic growth cones as control axons, they fail to properly retract their lamellipodia and filopodia structures during growth (Figure 31C, D, Supplementary Movie 8, 9). It could be frequently observed that lamellipodia structures remained attached to the substrate as the growth cone continued to move (Figure 31D, Supplementary Movie 9).

Taken together, it could be demonstrated that Cav1α is not only expressed in the central nervous system, but also plays an important role during outgrowth and pathfinding of both cranial nerves and motoneurons *in vivo* as well as *in vitro*. These results provide strong evidence for an incorrect innervation as the main cause of the disrupted muscular integrity in the Cav1α morphant embryos.

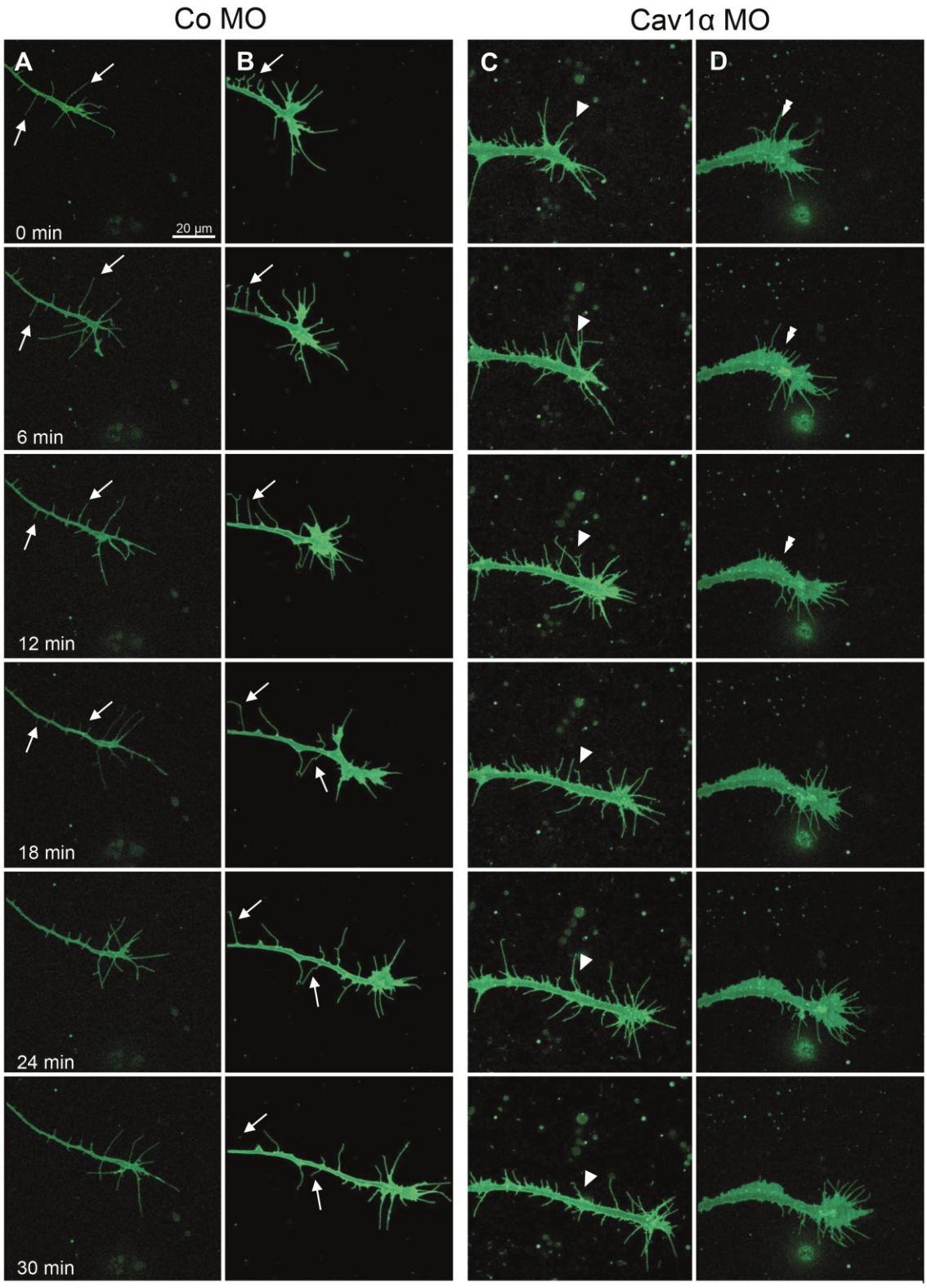

Figure 31: Cav1α morphant axons fail to retract filopodia and lamellipodia structures during axonal growth.
A-D Axonal outgrowth of control (A-B) as well as Cav1α morphant (C-D) neurons was analyzed by live-cell imaging over a time period of 30 min. **A-B** Growth cones of control axons dynamically extended and retracted the majority of their filopodia and lamellipodia protrusions during axonal growth over time. Arrows indicate retracting filopodia structures. **C-D** Cav1α morphant axons failed to retract filopodia (C, arrowhead) and lamellipodia (D, double arrowhead) structures during axonal growth.

3.11 Cav1α modulates Rho GTPase activity during axonal outgrowth

Rho GTPases are known regulators for lamellipodia and filopodia dynamics during axonal growth and guidance (Hall and Lalli, 2010; Heasman and Ridley, 2008). Further, it has already been shown, that knockdown of Cav1α in migrating mouse fibroblasts interferes with the activity of the small Rho GTPases RhoA and Rac1 (Grande-García et al., 2007).
Both filopodia and lamellipodia formation was significantly increased in axons upon Cav1α knockdown, suggesting that Cav1α also modulates the activity of the small Rho GTPases during axonal outgrowth. To understand how Cav1α functions in this process,
rescue experiments with either constitutively active (ca) or dominant negative (dn) mutants of the small Rho GTPases Cdc42, Rac1 or RhoA were performed. To this end, 10 ng of Co MO or Cav1α-Spl MO were co-injected with 10 pg DNA of the respective mutant construct into the dorsal blastomere of the animal hemisphere. The swimming behavior of embryos was analyzed at stage 37 (Figure 32). *mGFP* RNA was injected as a lineage tracer. As previously demonstrated, the neural-specific knockdown of Cav1α causes severe swimming defects in morphant embryos (Figure 32A-C). Interestingly, the total percentage of swimming defects of the Cav1α-Spl morphants (23% ±2% mild, 60% ±5% severe) was significantly improved by co-expression of dnRhoA (25 ±1% mild, 29% ±5% severe) but not caRhoA (19% ±1% mild, 61% ±4% severe) (Figure 32A). Similarly, dnRac1 (26% ±3% mild, 28% ±5% severe), but not the constitutive active mutant (37% ±6% mild, 44% ±5% severe) could partially rescued the swimming behavior of Cav1α-Spl morphants (21% ±2% mild, 60%±4% severe) by 27% (Figure 32B). Conversely, the swimming defects of the Cav1α-Spl morphant embryos (22% ±3% mild, 59% ±5% severe) could be significantly improved by 37% with simultaneous expression of ca (18% ±3% mild, 29% ±4% severe) but not dnCdc42 (13% ±4% mild, 71% ±5% severe) (Figure 32C). Co-injection of Co MO with the Rho GTPase mutants caused swimming defects only in a low percentage of embryos (Figure 32A-C). In summary, the swimming defects in the Cav1α morphant embryos could be improved by the co-expression of dnRac1, dnRhoA as well as caCdc42.
Consistently, co-expression of the dominant negative mutant of Rac1 and RhoA as well as the constitutive active mutant of Cdc42 also rescued the motoneuron defects caused by Cav1α knockdown (Figure 32D-I). While 79% ±2% of the Cav1α-Spl morphant motoneurons displayed shorter or missing axons, co-injection of these RhoGTPase mutants partially restored this phenotype. In detail, co-expression of dnRac1 could improve the motoneuron defects by 35% (44% ±2% motoneuron defects), dnRhoA by 36% (43% ±6% motoneuron defects) and caCdc42 by 36% (43% ±6%) (Figure 32D). These data demonstrate that Cav1α is likely required for the Rho GTPase-dependent axonal growth.

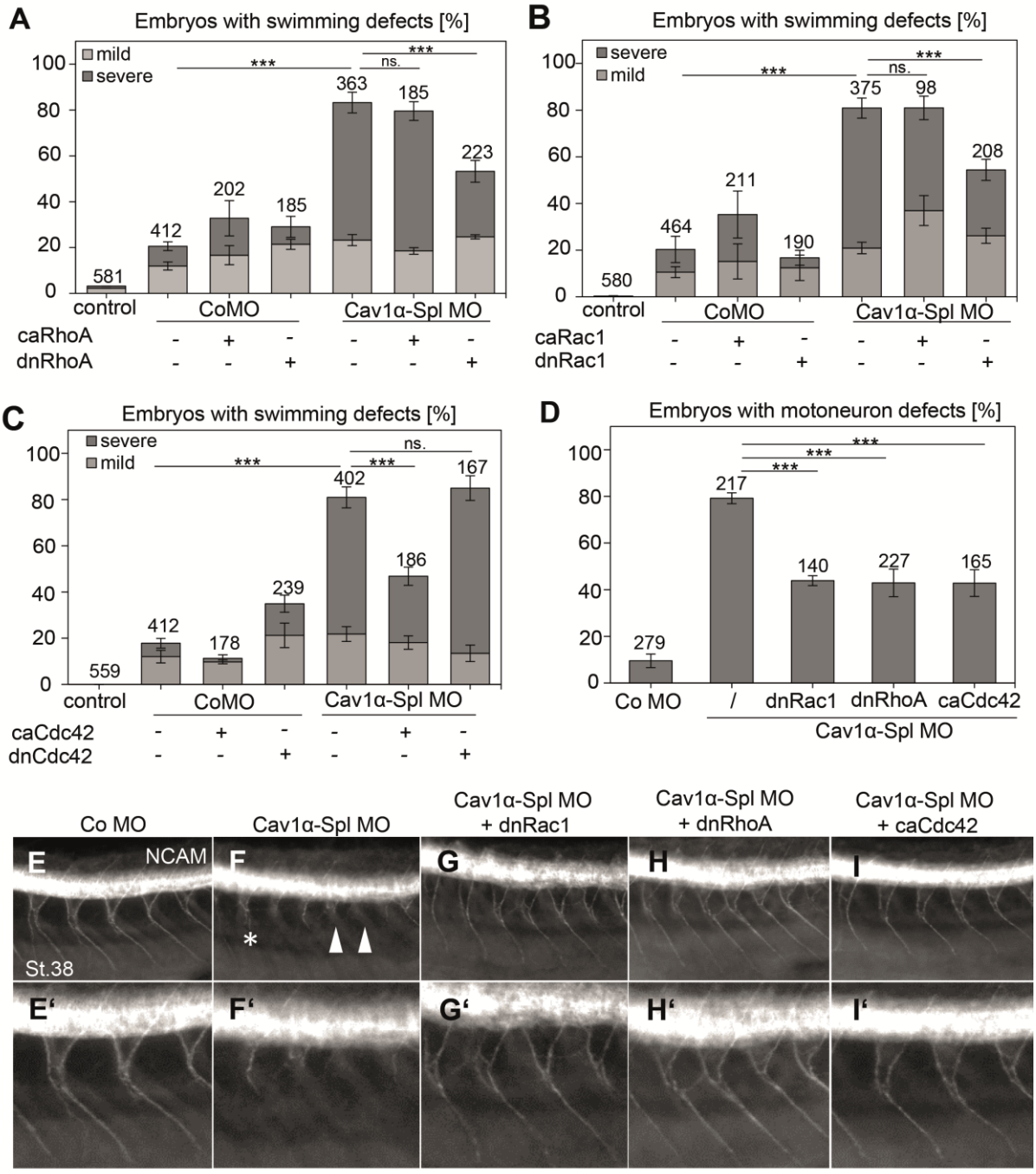

Figure 32: **Cav1α is required for Rho GTPase-dependent axonal outgrowth and pathfinding of motoneurons.**

A 10ng of Co MO or Cav1α-Spl MO alone or in combination with 10 pg of either dominant or constitutive active mutants of the Rho GTPases Rac1, RhoA and Cdc42 were injected into the dorsal blastomere of the animal hemisphere of 8-cell stage embryos. The swimming behavior (A-D) and neuronal phenotype (E-J) were analyzed **A-D** Graphs summarizing the percentage of embryos with mild (light grey) or severe (dark grey) swimming defects. Data from at least three experiments are presented as ± S.E.M. ***p-value ≤ 0.001. Significance was calculated using a two-tailed unpaired Student’s t-test, ordinary one-way ANOVA (Dunnett’s multiple comparisons). Numbers above each column indicate the number of analyzed embryos. **A** Co-injection of dnRhoA, but not caRhoA, into neural tissue in combination with Cav1α-Spl MO could significantly improve the swimming defect. **B** The swimming behavior could be significantly improved by neural expression of 10 pg dnRac1 but not 10 pg caRac1 in Cav1α-Spl morphant embryos. **C** Neural-injected caCdc42, but not dnCdc42, in combination with Cav1α-Spl MO partially rescued the aberrant swimming behavior of Cav1α-Spl

morphant embryos. **D-I** Motoneuron outgrowth was analyzed by NCAM immunostaining. The injected constructs are indicated. **D** Graph summarizing the percentage of embryos with motoneuron defects. Data from at least three experiments are presented as ± S.E.M. ***p-value ≤ 0.001. Significance was calculated using a two-tailed unpaired Student's t-test, ordinary one-way ANOVA (Dunnett's multiple comparisons). Numbers above each column indicate the number of analyzed embryos. **E-E'** Motoneurons of stage 38 embryos injected with Co MO. **F-F'** Motoneurons of stage 38 embryos injected with Cav1α-Spl MO. Asterisk marks motoneuron with pathfinding defects, arrowheads indicate motoneurons with outgrowth defects. **G-I** Co-expression of dnRac1 (G)**,** dnRhoA (H) and caCdc42 (I) rescued the motoneuron defects shown in Cav1α-Spl morphant embryos (F). **E'-I'** Magnified areas shown in E-I.

Src-dependent tyrosine (Y14) phosphorylation of Cav1α plays an important role in the regulation of RhoA and Rac/Cdc42 activity in mouse embryonic fibroblasts (Grande-García et al., 2007; Nethe et al., 2010; Núñez-Wehinger et al., 2014). To understand how Cav1α controls axonal outgrowth and subsequently muscular integrity, it was first analyzed whether this posttranslational modification is required for Cav1α function in the locomotor system of *Xenopus* embryos. To this end, rescue experiments were performed by co-injecting either 200 pg of the full length *caveolin 1α* mRNA (*cav1α-HA*) or a non-phosphorylatable *Cav1α* mutant (*cavY14A*) in combination with 10 pg MO into one animal blastomere of two-cell stage embryos (Figure 33). While co-injection of *cav1α-HA* could reduce the swimming defects in the morphant embryos significantly from 80% (28% ±5% mild, 52% ±7% severe) to 47% (34% ±4% mild, 13% ±4% severe), the phosphorylation mutant was not able to rescue this phenotype if co-expressed with the Cav1α-Spl Morpholino (9% ±0% mild, 80% ±1% severe) (Figure 33). In contrast, expression of *cav1Y14A* in the Cav1α-morpholino background increased the severity of swimming defects in the morphants. While injection of the Cav1α-Spl led to severe swimming defects in 52% ±7% of the injected embryos, co-injection of the CavY14A mutant increased the number of severe swimming defects to 80% ±1%, suggesting a dominant-negative function of this mutant (Figure 33B). Overall, these findings indicate that Y14 phosphorylation is indeed required for Cav1α function and possibly for the regulation of Rho GTPases in the locomotor system of *Xenopus laevis.*

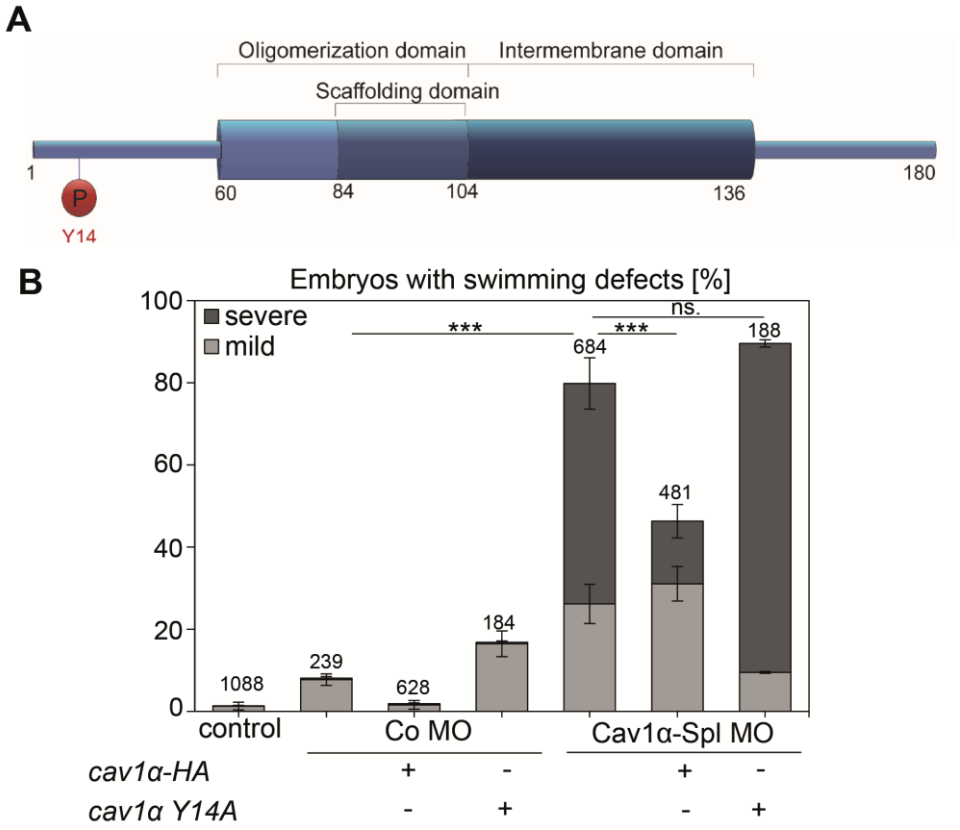

Figure 33: Y14 phosphorylation of Cav1α is necessary for Cav1α neural function.
A Schematic view of the caveolin 1α structure. Tyrosine (Y14) phosphorylation site is shown**. B** Two-cell stage embryos were injected unilaterally with 10 ng Co MO or Cav1α-Spl MO alone or in combination with 200 pg *Cav1α Y14A* or *Cav1α* RNA. Co-expression of *Cav1α* RNA but not *Cav1α Y14A* RNA in Cav1α morphant embryos rescued the swimming defect. Numbers above each column indicate the number of analyzed embryos. Data from at least three experiments are presented as ± S.E.M. ***p-value ≤ 0.001. Significance was calculated using a two-tailed unpaired Student's t-test.

3.12 Serine (S82) phosphorylation is required for Cav1α membrane localization but not for its neural function.

The biological function of the post-translational phosphorylation of Cav1α on tyrosine 14 is well understood. However, Cav1 contains a second conserved phosphorylation site, serine 80, the function of which is still largely unknown. It has been suggested that this phosphorylation site is required for the secretion of Cav1 in pancreas cells (Schlegel et al., 2001) as well as for sterol binding (Fielding et al., 2004).

In order to analyze the functional role of the serine phosphorylation, Cav1α localization studies were performed in *Xenopus* ectodermal explants with either a serine phosphorylation null (S82E) or a phospho-mimicking (S82A) mutant (Figure 34A). *Xenopus* ectodermal explants were isolated from stage 8 embryos injected with 500 pg of the respective Cav1α mutant (*cav1α-S80A-HA, cav1α-S80E-HA*) or a wild type *Cav1α* together with membrane-GFP as a lineage tracer.

In *Xenopus* ectodermal explants Cav1α-HA as well as Cav1α-S82A-HA co-localized with membrane GFP at the apical plasma membrane and in vesicle-like structures in the cytoplasm (Figure 34B-C). In contrast, the phosphorylation-mimicking mutant Cav1α-S82E-HA failed to localize at the plasma membrane and accumulated in large clusters in the cytoplasm with no visible polarization within these cells (Figure 34D).

Caveolin proteins accumulate as large oligomers at the plasma membrane to form the caveolae coat (Hayer et al., 2010). In order to analyze whether the mutation of the serine phosphorylation site affects the ability of Cav1α to form oligomers with other Caveolin proteins, the serine phosphorylation mutants were co-expressed with a GFP-tagged Cav1α in *Xenopus* ectodermal explants. Interestingly, while wild-type Cav1α as well as the phospho-mimicking mutant Cav1α-S82A-HA co-localized with Cav1α-GFP at the plasma membrane (Figure 35A-B), Cav1α-GFP showed no membrane localization when it was expressed together with the phospho-null mutant Cav1α-S82E-HA. However, Cav1α-GFP mainly co-localized together with Cav1α-S82E-HA in the cytoplasm and vesicular structures (Figure 35C). In summary, phosphorylation at serine residue 80 seems to be important for the membrane localization of Cav1α but has no effect on its ability to homo-oligomerize with Cav1α.

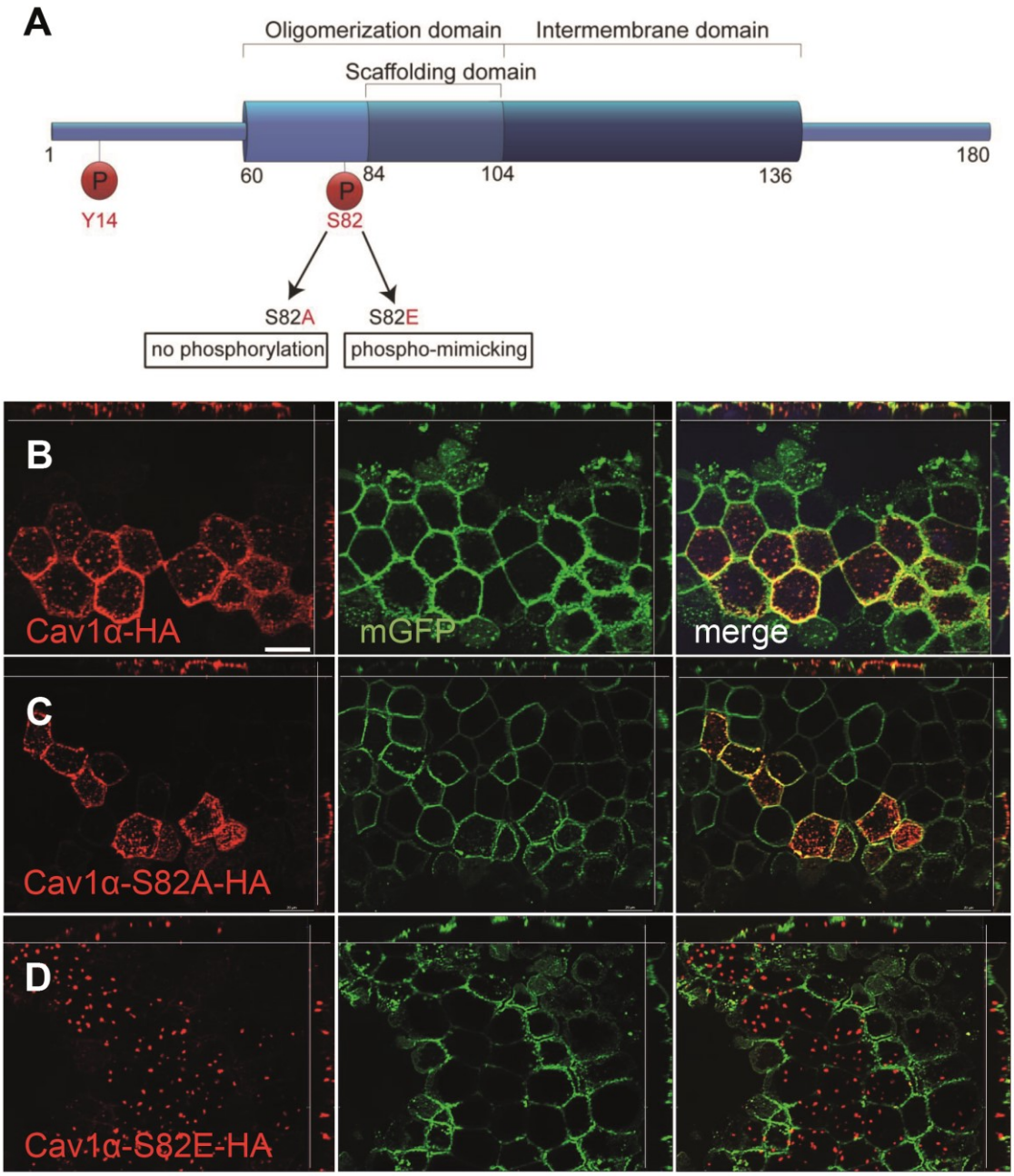

Figure 34: S82 phosphorylation is required for Cav1 membrane localization.
A Schematic of the caveolin 1α structure. Serine (S82) phosphorylation site is shown**.** Serine 82 was substituted with an alanine (S82A) or a glutamic acid. **B-C** One-cell stage embryos were injected with 500 pg of the indicated constructs in combination with *mGFP* as a lineage tracer. *Xenopus* ectodermal explants were isolated at stage 88. Explants were stained with anti-HA (red) and anti-GFP (green). **B-C** Cav1α-HA (B) and Cav1α-S82A-HA (C) co-localized with mGFP (B''-C'') at the plasma membrane of *Xenopus* ectodermal explants. **D** Cav1α-S82E-HA failed to co-localize with mGFP at the plasma membrane and showed cytoplasmic localization in vesicle-like structures.

Post-translational tyrosine (T14) phosphorylation of Cav1α has a potential function during axonal growth. Mutation of this phosphorylation site was not able to rescue the swimming defects of the Cav1α morphant embryos, indicating that this phosphorylation event is crucial for Cav1α function in this context. In order to analyze whether serine phosphorylation is also necessary for the neuronal function of Cav1α and subsequently for muscle innervation, rescue experiments with the serine phosphorylation mutants were carried out. To this end, 500 pg of the phospho-mimicking mutant (*S82A*) was co-injected with 10 ng Cav1α Morpholino into one blastomere of two cell stage embryos and swimming defects were analyzed (Figure 35D). Since injection of the phospho-null mutant (S82E) into two-cell stage embryos resulted in a high mortality rate during gastrulation, 100 pg of this mutant was co-injected with 10 pg Cav1α MO into the animal blastomere of 8-cell stage embryos (Figure 35E). Both the *cav1α-S82A* phospho-mimicking as well as the *cav1α-S82E* phospho-null mutant were able to partially rescue the swimming defect caused by Cav1α loss-of-function. In case of the *cav1α-S82A* mutant, the swimming defect could be restored by 21% (19% severe, 45% mild) in comparison to the Cav1α morphant embryos (35% severe, 49% mild) (Figure 35D). Co-expression of *cav1α-S82E* (17% severe, 42% mild) improved the swimming behavior by 30% in the morphant embryos (51% severe, 35% mild) (Figure 35E). These data suggest that the phosphorylation on serine 80 is not required for the neuronal function of Cav1α as demonstrated for the tyrosine (Y) phosphorylation. However, the rescue experiments using the serine phosphorylation mutants were carried out only once, thus, further repetitions must be carried out to validate these results.

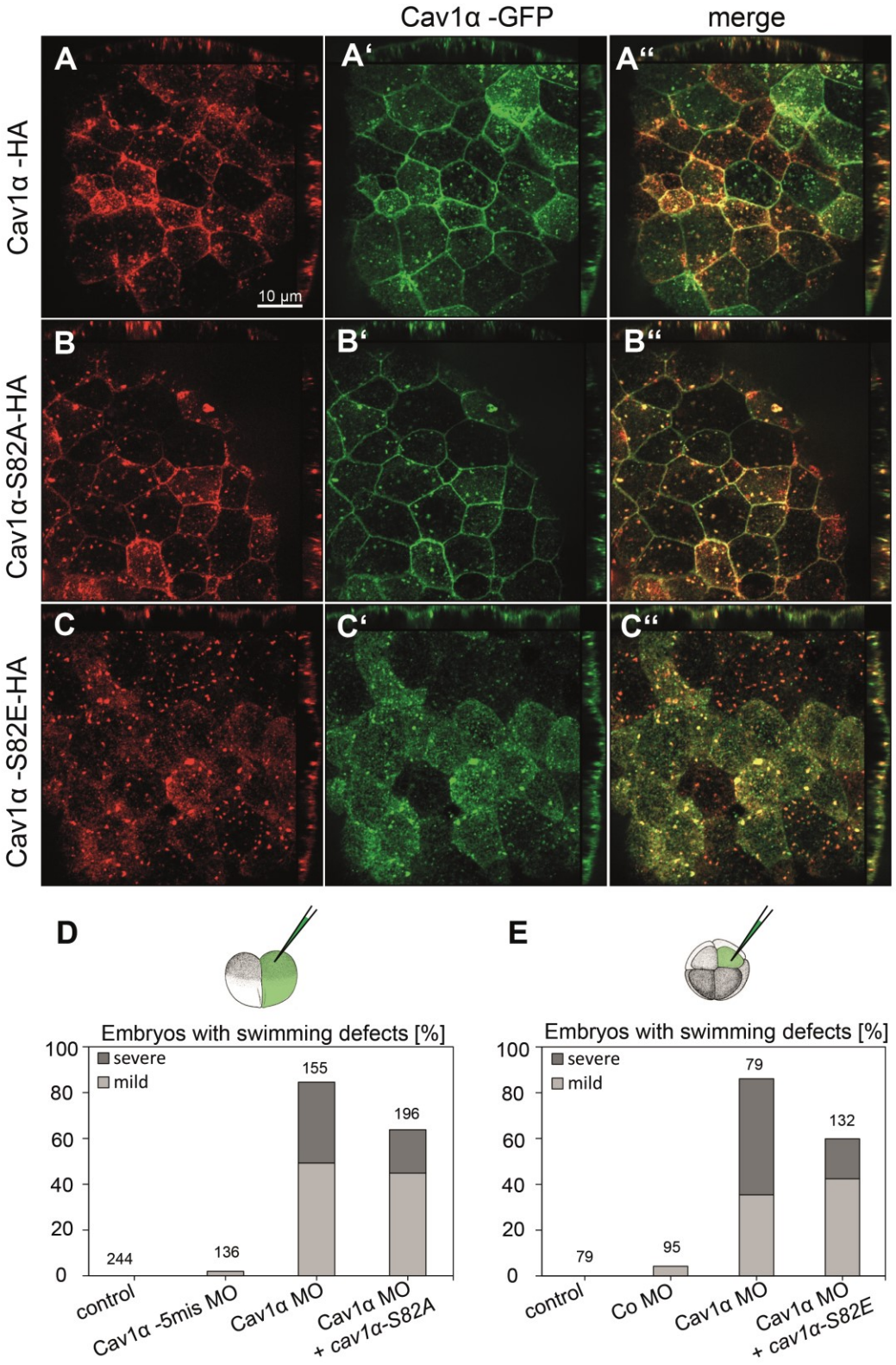

Figure 35: S82E mutant is required for membrane localization but not for Cav1 neural function.

B-C One-cell stage embryos were injected with 500 pg of the indicated constructs in combination with *Cav1α-GFP*. *Xenopus* ectodermal explants were isolated from stage 8 embryos. Explants were stained with anti-HA (red) and anti-GFP (green). **A-B** Cav1α-HA (A) and Cav1α-S82A-HA (B) co-localized with Cav1α-GFP (A''-B'') at the plasma membrane and in vesicle-like structures within the cytoplasm. **D** Cav1α-S82E-HA co-localized with Cav1α-GFP (C'') in vesicular-like structures within the cytoplasm

but failed to localize at the plasma membrane. **D** Two-cell stage embryos were unilaterally injected with 10 ng Co MO or Cav1α MO alone or in combination with 500 pg Cav1α-S82A-HA and swimming defects were analyzed in stage 37 embryos. Co-expression of Cav1α-S82A-HA improved the swimming behavior. Percentage of swimming defects are shown from one experiment. Number of analyzed embryos is indicated for each column. **E** 8-cell stage embryos were injected with 10 ng Co MO or Cav1α MO alone or in combination with 100 pg *cav1α-S82E-HA* into the animal/neural blastomere. Swimming defects were analyzed in stage 37 embryos. Co-expression of *cav1α-S82E-HA* improved the swimming behavior. Percentage of swimming defects is shown from one experiment. Number of analyzed embryos is indicated for each column.

4 Discussion

Cav1 is an essential structural protein driving the formation of caveolae in many cell types. The loss-of-function of this protein is associated with motor dysfunction and neurodegeneration in humans as well as in mice (Berger et al., 2002; Cao et al., 2008; Trushina et al., 2006a). However, so far, the underlying cellular mechanisms are not fully understood. For this purpose, detailed studies on the neuromuscular function of Cav1α in the model organism *Xenopus laevis* were carried out in the present study.

4.1 Cav1α loss-of-function impairs axonal growth during early development of *Xenopus laevis* embryos

Neuromotor activity plays an important role for the development and integrity of muscles (Midrio, 2006). It has been shown in several studies that loss of neural connectivity, for example due to denervation or spinal cord injuries, causes severe muscle atrophy. This is characterized by reduced muscle strength resulting from a loss of sarcomeric organization, reduced number of ribosomes and mitochondria and finally by myofiber apoptosis (Gutmann, 1962; Gutmann and Zelená, 1962; Heck and Davis, 1988; Hník, 1962; Tower, 1935).

Here, Cav1α was identified to function in the neuromuscular system during early development of *Xenopus laevis*. Morpholino-mediated knockdown of Cav1α leads to swimming defects as well as severely compromised muscle integrity (Figure 18). This was characterized by disorganized muscular actin (Figure 18) and a loss of sarcomeric organization within the somitic muscle cells (Breuer, 2016, M.Sc.). In previous studies, a potential defect on muscle differentiation and maturation has been excluded, as these processes were not affected by the loss of Cav1α expression (Breuer, 2016, M.Sc.). Interestingly, treatment with Benzocaine, which inhibits nerve to muscle communication by the inhibition of voltage-dependent sodium channels, mimics the muscle defects observed in the Cav1α morphant embryos (Figure 27). Further, Cav1α protein is expressed in *Xenopus* spinal cord neurons, including motoneurons, but not the musculature, suggesting that Cav1α functions in the neuro-muscular circuits controlling muscular integrity rather than in the musculature directly (Figure 21). This was confirmed by targeted knockdown studies of Cav1α in neural tissue as well as immunological analysis of the muscle innervation. Targeted loss-of-function of Cav1α in neural tissue, but not in muscle tissue, caused the characteristic swimming as well as muscular defects. Further, immunolabelling of the nervous system demonstrated that axonal growth of motoneurons was severely affected by Cav1α loss-of-function (Figure 28B-D). Here, the phenotypes ranged from aberrant axonal projections, which were mainly observed in the Cav1α morphants, to outgrowth defects in the Cav1α-Spl MO injected embryos.

A potential neuromuscular function of Cav1α in other model organisms has not been described so far. However, similar to the knockdown of Cav1α in *Xenopus*, the morpholino-mediated knockdown of Cav1α in zebrafish also leads to severe defects in the muscular actin organization (Fang et al., 2006). Although, the authors of this paper did not report any behavioral abnormalities in their zebrafish embryos, the depletion of Cav1α resulted in the loss of neuronal structures, as shown by the reduced expression of the neuronal markers pax 2.1 and otx2 (Fang et al., 2006). Interestingly, in *Xenopus*, the loss of Cav1α expression also leads to a temporal reduction of neuronal markers, such as NCAM, nrp1 as well as sox10 in early neurula stages (13-18) (Breuer, 2016, M.Sc. ; Maximillian Staps, 2016, B.Sc.). However, the expression of these markers recovered in older developmental stages (19 onwards, data not shown). This indicates that the reduced marker expressions in the morphant embryos are due to a developmental delay rather than a defect during early neuronal patterning. In agreement with this, no abnormalities of early neuronal patterning could be observed by n-tubulin staining, suggesting that Cav1α functions later during neuronal development and axogenesis (Figure 28). This could be confirmed by an *in vitro* spinal cord explantation assay, in which Cav1α morphant axons displayed both outgrowth defects, similar to the *in vivo* situation, and also an increased formation of lamellipodia as well as filopodia protrusions. This is likely due to the impaired activity of the small RhoGTPases Rac1, Cdc42 and RhoA, as both the aberrant swimming behavior and the motoneuron defect *in vivo* could be rescued by a constitutive active mutant of Cdc42 or a dominant negative mutant of Rac1 or RhoA, respectively. Thus, the findings of this thesis suggest a model whereby Cav1 regulates axonal growth by modulating the activity of the small RhoGTPases Rac1, Cdc42 and RhoA (Figure 36). In the wild-type situation this is mediated by supporting Cdc42 activity and suppressing RhoA and Rac1 activity. Further, this process likely requires the phosphorylation of Cav1α on tyrosine 14, as a phosphor-deficient mutant (Y14A) of Cav1 was not able to rescue the morphant swimming defects (Figure 33).

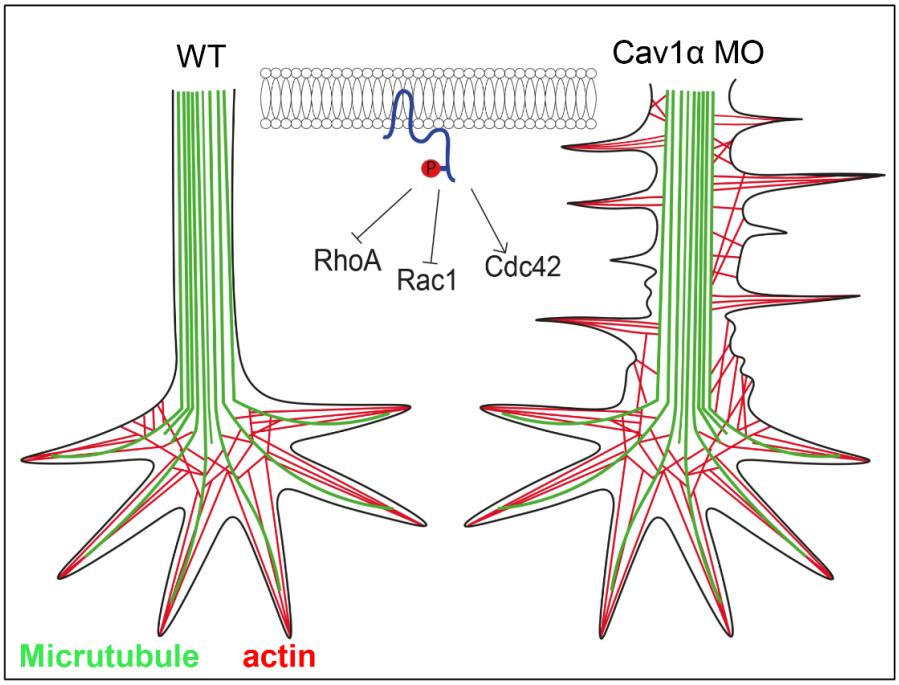

Figure 36: Model of Cav1α function in motor neuron outgrowth.
The morphology of a wild-type (WT) and Cav1α morphant motor neuron is shown; microtubules (green) and actin bundles (red) are shown. Tyrosine phosphorylated Cav1α (blue, with red Y14 phosphorylation) modulates the activity of the small RhoGTPases during axonal growth of *Xenopus* spinal cord neurons. In wild type neurons, Cav1α likely supports the activity of Cdc42 and suppresses the activity of Rac1 and RhoA.

4.2 Cav1α modulates the activity of small RhoGTPases during axonal growth

To reach their synaptic target and build new neural circuits, axons need to navigate long distances through the developing tissue. Thereby, the dynamic growth cones at the distal end of the migrating axons need to sense and adapt to the surrounding environment to enable a directional and targeted growth to the synaptic target (reviewed in Vitriol and Zheng, 2012). During this process, the small RhoGTPases Cdc42, Rac1 and RhoA act as molecular switches that translate extracellular cues, such as guidance as well as repellent cues, but also adhesiveness to the substratum, to directional responses by modulating actin cytoskeleton dynamics (reviewed in Luo, 2000). Thereby, RhoA regulates microtubule stabilization and stress fiber formation, while Rac1 promotes lamellipodia and Cdc42 filopodia formation by promoting actin polymerization (reviewed in da Silva and Dotti, 2002; Kozma et al., 1995; Ridley et al., 1992; Ridley and Hall, 1992).

Although, the function of Cav1 has been excessively studied in different cellular systems, so far, not much is known about the function of Cav1 in the regulation of small RhoGTPases in neuronal cells. Recently, Wang *et al.* proposed that tyrosine phosphorylated Cav1α regulates neuronal differentiation and axonal outgrowth downstream of Rac1/Cdc42 signaling in

cultured human neurons derived from iPSCs (Wang et al., 2019). The results obtained during this study, however, suggest a regulatory function of Cav1α upstream of these Rho GTPases by supporting the activity of Cdc42 and suppressing the activity of Rac1 and RhoA during axonal growth, as both the swimming as well as the motoneuron defects could be rescued by the co-injection of dnRac1, dnRhoA or caCdc42 (Figure 32). It has been shown that Cav1 modulates the spatial-temporal RhoGTPase activity during focal adhesion assembly and maturation and thereby regulating cell polarization and migration of mouse embryonic fobroblasts (Grande-García et al., 2007; Nethe et al., 2010; Nethe and Hordijk, 2011): Activated Rac1 at newly formed focal adhesion sites mediates the recruitment and the src-dependent phosphorylation of Cav1α (Nethe et al., 2010; Nethe and Hordijk, 2011). This initiates a negative feedback loop, involving the Cav1α-dependent ubiquitination and subsequent degradation of Rac1 as well as the activation of RhoA through Cav1α-mediated inactivation of the Src-p190RhoGAP pathway (Grande-García et al., 2007; Nethe et al., 2010): Src-dependent phosphorylation of Cav1 on Tyrosine 14 (Y14) induces the recruitment and activation of Csk at focal adhesion sites, which in turn phosphorylates and inactivates Src (Grande-García et al., 2007). In mouse embryonic fibroblasts, the Cav1α loss-of-function is associated with impaired cell polarity and directional migration due to the misregulation of the small RhoGTPases RhoA, Rac1 and Cdc42 at focal adhesion sites (Grande-García et al., 2007; Nethe et al., 2010; Nethe and Hordijk, 2011). Further, these cells also display an impaired maturation and increased turnover of focal adhesions, caused by elevated Rac1 activity and decreased RhoA activation (Grande-García et al., 2007; Nethe et al., 2010).

Focal adhesions (FA) are macromolecular complexes that functions as local anchor points of the cell to the extracellular matrix to stabilizes lamellipodia and filopodia structures (Myers and Gomez, 2011; Robles and Gomez, 2006). They are also domains for actin organization and remodeling during cell migration and growth cone steering in response to guidance cues during axonal growth (reviewed in DeMali and Burridge, 2003). The dynamics of focal adhesions are controlled by the cycling activation of the RhoGTPases Rac1 and RhoA (Hotchin and Hall, 1995; reviewed in Lawson and Burridge, 2014). Thereby, initial Rac1 activation and RhoA suppression is required for the formation of nascent FAs. In contrast, activated RhoA and repressed Rac1 results in the maturation and stabilization of FA sites (Lawson and Burridge, 2014). For example, the overexpression of either dominant negative or constitutive active Rac1 mutants in *Xenopus* spinal cord neurons led to impaired focal adhesion dynamics (Woo and Gomez, 2006). While expression of a dominant negative mutant of Rac1 reduced the number of focal adhesion sites but increased their stability, expression of a constitutively active mutant resulted in a decreased stability of these contact sites and consequently impaired axonal outgrowth (Woo and Gomez, 2006). By promoting actin polymerization as well as focal adhesion formation, Rac1 is a positive regulator for

lamellipodia formation (Ridley et al., 1992). Thus, constitutively active Rac1 activity is associated with an increased formation of this membrane structures (Ehrlich et al., 2002; Ridley et al., 1992). As Cav1 morphant axons also display increased lamellipodia-like structures as well as the inability to retract those during growth cone advance (Figure 31), it seems likely, that Cav1 negatively regulates the activity of Rac1 at focal adhesion sites during axonal outgrowth in *Xenopus* spinal cord neurons.

Interestingly, the data shown in this study also indicate that Cav1α suppresses RhoA and supports Cdc42 activity in neuronal cells (Figure 32). In contrast to that, loss-of-function studies in MEFs demonstrated, that Cav1α positively regulates the activity of RhoA by the inactivation of the Src-p190RhoGAP pathway (Grande-García et al., 2007). Consequently, loss-of-function of Cav1α in these cells leads to an elevated activity of Rac1/Cdc42 and decreased activity of RhoA in response to increased Src activity (Grande-García et al., 2007). How can these contractionary findings in the regulation of the RhoGTPases RhoA and Cdc42 in neuronal cells by Cav1α be explained? Although the role of these RhoGTPases has been extensively studied in fibroblasts, it has been shown that the functions of the RhoGTPases in neurons appear to be more complex. During axonal growth and navigation, axons are exposed to a variety of extracellular cues, such as guidance signals, differences in the ECM composition as well as receptor-ligand interactions that can elicit different regulatory mechanisms and crosstalk of these RhoGTPases during the various steps in neurogenesis and axonal outgrowth (Kim et al., 2002; Li et al., 2002; Matsuura et al., 2004; Myers et al., 2011; Woo and Gomez, 2006). In Drosophila, it has been demonstrated that Rac functions as a positive regulator for axonal growth by promoting this process in a Pak independent pathway, acting antagonistically to LIM kinase 1 (LIMK1) (Ng and Luo, 2004). Conversely, both Rho as well as Rac/Cdc42 GTPases also inhibit axonal growth via the Pak dependent activation of LIMK1 (Ng and Luo, 2004). Further, a growing body of evidence suggests that various levels of RhoGTPase activity can also target different downstream targets (Ng et al., 2002). Ng *et al*. were able to show that the progressive loss of Rac1 activity in the growth cone of *Drosophila* neurons leads first to impaired axonal branching, then guidance and finally to axonal growth defects (Ng et al., 2002). Likewise, while RhoA functions as negative regulator for axonal growth, its activity is also associated with axonal fasciculation and guidance (Brouns et al., 2001). The mis-regulation of RhoA, due to the loss of the p190RhoGAP, leads to axonal guidance as well as fasciculation defects of cortical neurons as well as cranial nerves in mice (Brouns et al., 2001). Further, the small RhoGTPases Rac1, Cdc42 and RhoA show a distinct spatial-temporal expression during neuronal development, suggesting that they regulate different aspects of neurogenesis. For example, while Cdc42 is mostly ubiquitously expressed in immature and mature neurons, Rac1 preferably localizes in putative axons, branching points and growth cone and RhoA is mostly expressed in

dendrites during neuronal maturation (Santos Da Silva et al., 2004). In line with this, Rac1 activity is mainly required for axonal plasticity and guidance, RhoA functions as negative regulator for axonal and dendritic growth and Cdc42 is required for neuronal polarity, but also for both axonal and dendritic growth (reviwed in Gonzalez-Billault et al., 2012). Interestingly, *in vivo* expression studies of Cav1 also revealed a spatial-temporal expression of this protein during neuronal development in the mouse hippocampus (Shikanai et al., 2018). Cav1 is highly expressed in the neurites of immature neurons located in the intermediate and marginal zone of the cortex. In contrast, while it is down-regulated in migrating neurons in the cortical plate, it is later up-regulated again in a subset of mature neurons (Shikanai et al., 2018). This suggests that Cav1 also regulates different aspects of neuronal development. And indeed, Shikanai and colleagues demonstrated that Cav1 functions in the early maturation of hippocampal mice neurons by regulating the recycling of N-cadherin and L-CAM during this process (Shikanai et al., 2018). Sh-RNA mediated knockdown of Cav1 in these neurons causes impaired pruning of the immature neurites as well as disrupted leading process elongation, leading to an delayed onset of neuronal maturation and migration (Shikanai et al., 2018). In view of this, it seems likely that Cav1 functions for the “fine-tuning” of the spatial-temporal regulation of the RhoGTPases Rac1, Cdc42 and RhoA during axonal development.

4.3 Cav1α expression is required for a healthy neuronal development

Evidence for a neuronal function of Cav1 in higher vertebrates has already been demonstrated by *in vivo* loss-of-function studies. For example, cav1 knockout (KO) mice displayed distinct traits associated with neurodegeneration, including deficits in motor coordination, gait abnormalities (shorter stride length), muscle weakness as well as a clasping and spinning phenotype (Trushina et al., 2006a). Further, cav1 KO mice show behavioral changes associated with cholinergic dysfunction, characterized by impaired spatial memory, increased anxiety and reduced exploratory behavior in a new environment (Gioiosa et al., 2008; Trushina et al., 2006a). Trushina *et al.* also reported an age-dependent decrease in both brain size as well as brain weight in the Cav1 KO mice, which is likely due to the progressive neuronal degeneration observed in these mice (Head et al., 2010; Trushina et al., 2006a). This indicates, that Cav1 is also required for the maintenance of neuronal integrity and normal brain aging. *In vivo* as well as overexpression studies in hippocampal cell cultures have shown that Cav1 positively regulates neuronal plasticity and neuronal intracellular signaling by recruiting neurotransmitters and neutrophil factors to synaptic membrane lipid rafts (MRLs) (Egawa et al., 2018; Stern and Mermelstein, 2010; Wang et al., 2019). Cav1 KO mice display a decreased membrane lipid raft (MRL) localization of synaptic

signaling components such as PSD-95 (postsynaptic density protein 95), NR2A (subunit of NMDA receptor), NR2B (subunit of NMDA receptor), and AMPAR (AMPA receptor) and show an increased vulnerability to ischemic stress (Head et al., 2010). Membrane lipid rafts are especially important for pro-survival and pro-growth receptor signaling in neuronal cells, as receptors and proteins required for synaptic communication and plasticity mainly localize in these membrane domains (Sebastião et al., 2013). These includes signaling molecules, such as RhoGTPases, integrins and N-cadherins, which are essential modulators for actin dynamics and adhesion (Causeret et al., 2005; Guirland et al., 2004; Guirland and Zheng, 2007; Kamiguchi, 2006; Michaely et al., 1999; Palazzo et al., 2004).

Cav1 has been shown to modulate the nanoscale organization of membrane lipid raft domains by regulating the expression of metabolic proteins, that are involved in glycosphingolipid, sphingolipid and ganglioside biosynthesis, including Ppap2A (Lpp1), B3GNT5 and Siat9 (GM3 synthase*)* (Ariotti et al., 2014). Misexpression of these proteins also correlate with the reduced content of GM3 (monosialodihexosylganglioside), the precursor for more complex gangliosides, observed in Cav1 KO mouse embryonic fibroblast (Ariotti et al., 2014; Sandhoff and Kolter, 2003). The expression of gangliosides is tightly regulated during the development of the brain and appears to be essential for the peripheral and central nervous system development and maintenance. Misexpression of gangliosides are associated with either severe early neurological defects and lethality or progressive neurodegenerative changes in mice, depending on which step the ganglioside biosynthesis is disrupted (Jennemann et al., 2005; Ohmi et al., 2009; Yu et al., 2009). Interestingly, mice lacking the GM3-synthase (Siat9) and thus the expression of complex gangliosides, display similar neurological abnormalities observed in Cav1 KO mice, including decreased balance, gait abnormalities (shorter stride length), reduced muscle strength and diminished exploration behavior (Chiavegatto et al., 2000; Niimi et al., 2011). So far, no detailed studies are available that analyze the possible regulatory function of Cav1 in the biosynthesis of neuronal gangliosides during brain development. However, there is evidence for a possible regulatory function between ganglioside biosynthesis and Cav1 expression in neurons. For example, the inhibition of glucosylceramide synthase and the subsequent reduction of gangliosides in the brain also leads to a reduced expression of Cav1 (Herzer et al., 2016). Conversely, overexpression of Cav1 increases gangliosides expression in hippocampal neurons, as shown by an increased membrane staining with cholera toxin B, which binds to glycosphingolipids in lipid raft domains (Head et al., 2011).

As MRLs are important signaling centers, it is likely that the observed neurological abnormalities in the Cav1α morphant embryos are due to impaired nanoscale organization of MRLs and consequently due to mis-localized signaling molecules regulating axonal growth and guidance. Interestingly, in comparison to the severe neuronal phenotypes obtained by

knockdown studies of Cav1 in *Xenopus*, the loss-of-function phenotype in mice is relatively mild in comparison. This suggests that compensatory mechanism might exist in mammals. A potential mechanism how mammalian cells could compensate for the loss of Cav1 expression, is through the Flotillin protein family consisting of Flotillin 1 and 2. Both Cav and Flotillin proteins are integral membrane proteins that organize signaling platforms in lipid raft regions by acting as scaffolds for a diverse number of signaling molecules (reviewed in Langhorst et al., 2005; and Razani et al., 2002c). Flotillin proteins are expressed in membrane lipid raft microdomains and, interestingly, have a membrane topology comparable to that of Cav proteins (Frick et al., 2007). In addition, like Cav proteins, they are able to induce membrane structures that are morphological similar to caveolae (Fra et al., 1994; Frick et al., 2007; Lang et al., 1998; Stuermer et al., 2001). Flotillin's have also been linked to the regulation of the actin cytoskeleton, as overexpression of either flotillin 1 or 2 induces actin-rich filopodia as well as lamellipodia formation in endothelial cells (Hazarika et al., 1999; Neumann-Giesen et al., 2004). In hippocampal neurons, the downregulation of Flotillin 1 results in impaired neurite growth and increased lamellipodia formation (Munderloh et al., 2009). Interestingly, however, the loss-of-function of Flotillin 1 in in mouse neuroblastoma cells (N2a) leads to elevated levels of activated RhoA and Rac1 as well as decreased levels of Cdc42 (Munderloh et al., 2009), similar to the knockdown of Cav1α in *Xenopus*. This in turn impairs downstream signaling pathways, such as decreased cofilin activation and impaired N-WASP, cortactin, and Arp2/3 complex formation that regulate actin cytoskeleton dynamics (Munderloh et al., 2009). The authors of this paper also found, that Flotillin proteins are involved in focal adhesion dynamics by regulating p38 and FAK signaling (Langhorst et al., 2008; Munderloh et al., 2009; Schrock et al., 2009). Due to the high similarity of the phenotypes between the Cav1α and Flotillin loss-of-function it seems likely that both proteins function in similar pathways controlling axonal growth. Thus, this suggests that the neuronal defects caused by Cav1α knockdown shown in this study are attributed to disrupted lipid raft integrity resulting in impaired signaling in these domains.

A potential candidate by which Cav1 could affect neuromuscular development is via the BDNF (Brain derived neurotrophic factor) signaling pathway. Head *et al*. reported that the loss-of-function of Cav1 leads to a reduced BDNF/TrkB-mediated signaling in neuronal cells (Head et al., 2011). Although the neurotrophin BDNF is not directly involved in axonal guidance, it controls processes such as axon growth and branching as well as targeted innervation by acting as a short range signal (Hellard et al., 2004; Huang et al., 2007; Marshak et al., 2007; Thanos et al., 1989). At nerve terminals, secreted BDNF binds its receptor TrkB and induces its translocation to membrane lipid rafts. This mediates the activation of downstream signaling cascades that regulate the activity of the small RhoGTPases Rac1, RhoA and Cdc42 and thereby affecting actin dynamics (Ravindran et al., 2019; Suzuki et al.,

2004; Yuan et al., 2003). The Morpholino-mediated loss-of-function of BDNF in *Xenopus* leads to paralysis and impaired end stage target innervation of peripheral sensory axons (Huang et al., 2007). Thus, it seems likely that Cav1 acts via BDNF to regulate the activity of the small RhoGTPases during axonal development of *Xenopus* motoneurons.

4.4 Serine phosphorylation of Cav1α is not required for its neuronal function

In this thesis, it could be shown that the tyrosine phosphorylation (pT14) is required for the neural function of Cav1α. The overexpression of a phosphorylation null mutant (Y14T) in the Cav1α morphant background was not able to rescue the swimming defects (Figure 33). As Cav1α contains a second phosphorylation site at serine residue 80 (Schlegel et al., 2001), the question arises whether this modification is also required for the neuronal function of Cav1α. To this end, localization studies as well as rescue experiments were performed with either a phosphorylation-mimicking mutant (S82A) or a phosphorylation-null mutant (S82E). In *Xenopus* ectodermal explants, both full-length Cav1α as well as Cav1αS82A localized at the apical plasma membrane and in vesicular-like structures within the cytoplasm (Figure 34A-B). In contrast, the phosphorylation-null mutant Cav1αS82E accumulated in large clusters and showed no membrane localization and visible polarization within these cells (Figure 34C). Interestingly, it has been shown that serine 80 phosphorylation of Cav1 seems to be required for its binding to cholesterol (Fielding et al., 2004): Substitution of the serine 80 with alanine (S80A) increases sterol binding and conversely mutation of the serine to glutamate (S80E) reduces the ability of Cav1 to bind to sterols (Fielding et al., 2004).

Cholesterol is essential for the trans-localization of Cav proteins from the Golgi apparatus to the membrane and ultimately for the formation of caveolae (Pol et al., 2005). Cholesterol depletion, by methyl-β-cyclodextrin treatment, decreases caveolae at the membrane and increases the mobility of Cav1 within the membrane (Rothberg et al., 1992; Thomsen et al., 2002; Westermann et al., 2005). Thus, it seems likely, that the lack of membrane localization of the serine phosphorylation-null mutant is due to impaired binding to cholesterol and consequently membrane transport.

In addition to that, while full-length Cav1α as well as the phosphorylation-mimicking mutant Cav1αS82A were able to co-localize with Cav1α-GFP at the plasma membrane, Cav1α-GFP remained at the cytoplasm when co-expressed with Cav1αS82E (Figure 35). Caveolin proteins can form large homo-and hetero-oligomeric complexes with themselves as well as other Cav proteins (Hayer et al., 2010). It seems likely, that the Cav1αS82E oligomerize with the co-expressed Cav1α-GFP and traps it in vesicular like structures in the cytoplasm. Interestingly, despite its impaired ability to localize to the plasma membrane, the expression of this mutant in the Cav1α Morpholino background was still able to rescue the swimming defects.

It is suggested, that Cav proteins also have caveolae-independent function (reviewed in Pol et al., 2020). For example, in MDCK cells (Madin-Darby canine kidney), caveolae have been found in the basolateral but not in the apical membrane by EM analysis (Scheiffele et al., 1998). However, Rangel *et al*. demonstrated that, while both Cav1α and Cav1β localizes to the basal membrane, only Cav1α shows localization at the apical membrane of MDCK cells (Rangel et al., 2019). There, phosphorylated Cav1α regulates the integrity of the actin meshwork by modulating the RhoGTPase activity (Rangel et al., 2019), indicating that Cav1 functions outside of caveolae at this membrane side. Interestingly, studies have shown that less than 1% of the total cellular Cav1 population is phosphorylated on Tyr14 (del Pozo et al., 2005). It is likely, that the function of tyrosine phosphorylated Cav1α in neuronal cells is also caveolae independent, as the serine phosphorylation deficient mutant Cav1S82E traps the majority of Cav1 in vesicular like structures, but is still able to rescue the morphant phenotype (Figure 35)

4.1 Caveolae are essential mechano-protectors in the notochord

Expression analysis showed that *cav1α* is highly expressed in the notochord, which serves as important structural element supporting locomotion in free-swimming larvae (Figure 21, Figure 22). Secreted signals derived from the notochord are essential for the patterning of adjacent tissues, including somites as well as the neural tube (Münsterberg and Lassar, 1995; Pourquié et al., 1993; Yamada et al., 1993; Yamada et al., 1991). It has been shown in zebrafish, that defects in notochord development can affect both the axial skeleton as well as the muscular innervation (Ferrari et al., 2014; Pagnon-Minot et al., 2008). Similarly, the knockdown of Cav1α in *Xenopus* leads both to impaired muscular integrity as well as defective motoneuron outgrowth. Cav1α is expressed in motoneurons and the notochord in the developing *Xenopus* embryo (Figure 22; Figure 21). Since both impairments of muscle innervation as well as defects in notochord development can affect muscle integrity (Midrio, 2006), the function of Cav1α in neuronal vs. notochord cells must be carefully evaluated.
The importance of caveolae for protecting the notochord from mechanical stress has already been emphasized in several studies (Garcia et al., 2017; Nixon et al., 2007; Nixon et al., 2005). Moreover, evolutionary analysis and loss-of-function studies have demonstrated a shared function of Cav proteins in the notochord among different species (Bhattachan et al., 2020; Garcia et al., 2017; Kirkham et al., 2008; Nixon et al., 2007). For instance, the ascidian Caveolin-a expression, which is closely related to the vertebrate Cav1 and 3, is required for the elongation as well as vacuolization of the ascidian notochord (Bhattachan et al., 2020). In the zebrafish, the depletion of caveolae, by either the double knockout of cav1 and 3 or a single KO of cavin 1, causes the mechanical induced collapse of notochord cells (Garcia et

al., 2017; Lim et al., 2017). Interestingly, Lim and colleagues reported an impaired swimming behavior in the cavin 1 knockout zebrafish embryos, although they did not further analyze the musculature or the nervous system (Lim et al., 2017). However, the swimming phenotype observed in these zebrafish embryos differs from the swimming defects caused by Cav1α loss-of-function in *Xenopus* embryos: While Cav1α morphant *Xenopus* embryos showed a clear paralysis of the injected site (Supplementary Movie 2, 3, 5), zebrafish depleted for caveolae only displayed a shorter swimming distance in comparison to wild type zebrafish, but were otherwise still able to swim normally (Lim et al., 2017). Thus, this indicates that the aberrant swimming behavior of the Cav1α morphant *Xenopus* embryos are likely not caused by impaired notochord integrity.

This is further supported by the results of the targeted injections performed in this study: Here, to distinguish between a muscular and neuronal function of Cav1α, the Cav1α Morpholinos were targeted into either the dorsal marginal zone (dorsal/ ventral blastomere; muscle) or the dorsal/ animal blastomere (neural tissue) at the 8-cell stage (Figure 25). Although this method allows a distinction between muscular versus neural function, it does not rule out a possible function of Cav1α in the notochord, as both blastomeres contribute equally to this structure (see also fate map on Xenbase). However, only the injection into the dorsal/animal blastomere, which also gives rise to neural tissue, but not injections into the dorsal/vegetal blastomere resulted in the characteristic swimming defects (Figure 25).

Moreover, to rule out a possible contribution of notochord defects to the aberrant swimming behavior, knockdown studies for cavin 1, which is known to impair caveolae formation even in the presence of caveolin proteins, were performed (Figure 26). The injection of higher cavin 1 Morpholino concentrations (1.5 ng or higher) caused severe convergent extension (CE) defects, which resulted in a shortening of the anterior-posterior axis of these embryos. This agrees with the findings obtained by Puzik *et al.*. They were able to show that Cavin 1 as well as Cav1 mediates convergent extension as well as gastrulation movements by regulating the endocytosis of Wnt5a/RhoA complexes during this process (Puzik et al., 2019). Interestingly, analysis of the swimming behavior of Cavin 1 morphant embryos (1.5 ng MO) revealed that only a minor, but insignificant percentage of these embryos displayed a swimming defect that was comparable to that of the Cav1α morphant embryos (Figure 26). In comparison, injection of the Cav1α MO into the neural blastomere caused a high percentage of swimming defects, but only a low number of embryos with a shortened anterior-posterior axis. These data imply that the swimming defect observed in the Cav1α morphant embryos is likely not due to defects in the notochord or impaired CE movements, but rather caused by impairments of the neuromuscular system in these embryos.

Electron microscopic analysis of Cav1 morphants showed that their notochord, similar to the notochord of wild type embryos, still contained a large number of the classical flask shaped invagination of approximately 50-100 nm in size (Figure 19), indicating that loss-of-function of Cav1α alone is not sufficient to completely abolish caveolae formation in the notochord. In support of these findings, studies in zebrafish demonstrated, that, in contrast to the double knockout, the single loss-of-function of either Cav1 or Cav 3, is not sufficient to cause the mechanical induced collapse of notochord cells (Garcia et al., 2017; Lim et al., 2017). This suggests, that other Cav proteins likely compensate for the loss of a single Caveolin isoform in the notochord.

While humans and mice only express three *cav* genes (*cav1, 2* and *3*), evolutionary analysis of Cav proteins showed that the *Xenopus (tropicalis* and *laevis)* genome encodes for six *cav* genes, namely *cav 1*, *2*, *cav2R*, *cav3-1*, *cav3-2* and *CavY* (Kirkham et al., 2008). In addition, due to gene duplications in the allotetraploid *Xenopus leavis,* most genes are expressed in two isoforms, the L and the S form, which are encoded on either the long (L) chromosome or the homologous short (S) chromosome, respectively (Lentini et al., 2008). For cav1, for example, there are two isoforms expressed: the full-length *cav1L* isoform as well as the shorter S-isoform, which misses the first N-terminal 32 amino acids of the L-isoform. Sequence analysis showed high homology between the two isoforms. It is striking, however, that the *cavL* isoform closely resembles the human cav1α isoform and the S isoform also shows homology to human and zebrafish cav1β isoform (Supplementary Figure 1). In contrast to *Xenopus,* in humans, mice as well as in zebrafish the cav1α an β isoforms are encoded by the same gene but are translated from distinct mRNA arising from alternative splice events (Fang et al., 2006; Kogo and Fujimoto, 2000; Scherer et al., 1995). However, similar to the human cav1α, the *Xenopus* cav1L isoform also has a putative alternative translation start site encoded on exon 2, which likely also leads to an expression of a Cav1L-α and Cav1L-β isoform. It is important to mention that both Cav1α Morpholinos used in this study, target the cav1-L but not the shorter cav1-S isoform, suggesting that the shorter cav1 isoform is still expressed in the cav1α morphants and possible compensates for the loss of Cav1L expression in the notochord. Supporting this, Morpholino mediated knockdown of Cav1β (Cav1S) causes swimming defects similar to Cav1α (Cav1L) knockdown in *Xenopus* embryos, suggesting that these two isoforms also have comparable functions in this model organism (Berger, 2016, PhD).

Although a growing body of evidence suggests that the swimming defects in the Cav1α morphant embryos are not caused by impaired notochord integrity, more refined experiments have to be carried out to further rule out a contribution of the notochord to the observed phenotypes and to what extent other caveolin proteins may compensate for the loss of Cav1 in this tissue.

4.1 Cav1 expression is highly conserved between different species

The similarity of *cav1* RNA and protein expression pattern in different organisms indicate a high degree of evolutionary conservation between amniotes and anamniotes species. In *Xenopus cav1* is already maternally expressed in the developing *Xenopus* embryo. Zygotic expression of *cav1* can be detected first around stage 12 by *in situ* hybridization in the presumptive notochord and epidermis. Additionally, expression was also found in a distinct domain on both sites of the embryonic midline in the superficial or epithelial layer of the neural plate (Figure 21, Figure 23). The identity of this expression region is yet not known. However, the superficial layer of the *Xenopus* neural tube gives rise to precursors of the secondary neurons. They differentiate with the onset of metamorphosis (st. 54) during a secondary neurogenic wave, to form the adult central nervous system (Hartenstein, 1989b; Thuret et al., 2015). It is likely that *cav1* may be expressed in secondary neuron precursor cells, as protein expression could also be detected in primary neurons. However, intriguingly, RNA expression of *cav1* in the neural tube is no longer detectable as soon as the superficial layer and deep layer are intercalated and the neural tube has closed (Figure 23). Therefore, further studies are required to identify the exact cell type of the neural tube that expresses *cav1*.

Cav1 expression in later developmental stages was analyzed by *in situ* hybridization, an also by whole mount immunofluorescence staining using an antibody that recognizes both Cav1 isoforms (Cav1α and β) (Figure 24). Morpholino-mediated knockdown of Cav1α successfully suppressed the Cav1 signal in all Cav1 expressing tissues, confirming that this staining is also specific for Cav1α expression (Figure 24). In zebrafish, it has already been shown that Cav1α and Cav1β share a similar but distinct expression pattern during development (Fang et al., 2006). The authors demonstrated that both isoforms are co-expresses in most tissues, except the intestinal epithelium, where only Cav1α expression was detected. Likewise, the respective loss-of-function of these two isoforms yielded similar phenotypes, which included neural, somitic, and vascular tissue defects. The loss-of-function of Cav1α resulted both in vascular as well as neural defects, while the knockdown of Cav1β only affected neural tissue (Fang et al., 2006). Further, the phenotypes caused by the loss-of-function of one Cav1 isoform could not be rescued with the other isoform, suggesting that Cav1α and Cav1β perform similar but non-overlapping roles during zebrafish development (Fang et al., 2006).

In situ hybridization as well as immunofluorescence assays suggest that *cav1* RNA and consequently also protein can be found in the cardiovascular system, the developing lungs and in the epithelium during later developmental stages (Figure 21, Figure 22). These findings are further corroborated by *in vivo* experiments in mice and zebrafish. In zebrafish, *cav1α* is expressed mainly in the epidermis, the heart, the vasculature of the pharyngeal arches, intestinal epithelium, the pronephric duct, neuromasts as well as the notochord. Likewise, in mice *cav1* RNA as well as protein expression can be found in the heart,

intersomitic vessels, the lung (lung epithelium, parenchyma and alveolar endothelial cells), kidney, gut as well as the brain (brain vasculature, neuronal cells) (Bullejos et al., 2002; Engelman et al., 1998b; Newman et al., 1999; Ramirez et al., 2002). Due to the high similarity of the expression pattern of Cav1 in *Xenopus* compared to higher vertebrates, *Xenopus* offers an ideal model to examine the tissue-specific function of Cav1 during development.

4.2 Cav1α is required for normal heart function

Both RNA as well as protein expression of Cav1α was detected in the cardio vasculature and the heart of *Xenopus* embryos, suggesting a function of Cav1α in heart development (Figure 21, Figure 22). And indeed, the knockdown of Cav1α in *Xenopus* resulted in the formation of severe pericardial edemas (Figure 20). A function of Cav1 in the cardiovascular system has already been demonstrated in other model organisms. Similar to *Xenopus*, the Morpholino-mediated knockdown of Cav1α in zebrafish also leads to edema, which is caused by defective cardiac development. The heart of these embryos shows an abnormal heart looping and an incorrect development of the heart chambers (Fang et al., 2006; Nixon et al., 2007). In addition, Cav1 plays a role in zebrafish heart regeneration: It has been shown, that the genetic ablation of Cav1 leads to decreased cardiomyocyte proliferation and regeneration after cardiac injury (Cao et al., 2016; Grivas et al., 2020). Similarly, the genetic ablation of Cav1 in mice leads to cardiac dysfunctions, such as pulmonary hypertension, cardiac hypertrophy with enlarged right ventricular cavity and thickening of the ventricular wall as well as systolic and diastolic dysfunctions (Cohen et al., 2003; Wunderlich et al., 2006; Zhao et al., 2002). Hyperactivation of ERK1/2 in the p42/44 MAP kinase cascade and increased levels in systemic NO (nitric oxide) leading to increased cardiac fibrosis are thought to be the cause of these cardiac defects in the cav1-KO mice (Cohen et al., 2003; Zhao et al., 2002). These findings point towards a conserved function of Cav1α in the development and integrity of the heart in amniotes as well as anamniotes species. Since a role of Cav1 has already been demonstrated in the heart of other model organisms, it is likely that the edema in the Cav1α morphants appear to be the result of defective heart development or morphology.

4.3 Cav1α function is required for pronephric morphology and convergent extension movements

Edema can develop not only due to malfunctions in the cardiovascular system, but also by disturbed osmoregulation of the pronephros (Nieuwkoop and Faber, 1994). Although expression of Cav1 could not be detected in the pronephros of *Xenopus* embryos, the knockdown of Cav1α leads to morphological abnormalities of the pronephric kidneys, such

as malformed proximal, intermediate as well as distal tubules (Figure 20Interestingly, other studies have already confirmed *cav1* expression in both the larval pronephros and in the adult *Xenopus laevis* kidney, which also suggest a function of Cav1 in the development of this organ (Cerqueira et al., 2014; Razani et al., 2002b). So far, relatively few studies are known that describe a function of Cav1 in the vertebrate kidney. It has been shown that Cav1 is expressed in the mice, rat as well as human kidney (Breton et al., 1998; Cao et al., 2003; McMahon et al., 2009). The loss-of-function of Cav1 in mice causes severe hypercalciuria and urolithiasis, which is due to impaired plasma membrane Ca^{2+} ATPase (PMCA) mediated Ca^{2+} absorption in the adult kidney (Breton et al., 1998; Cao et al., 2003; McMahon et al., 2009). However, a function of Cav1 in embryonic kidney development has yet not been described. A potential mechanism by which Cav1α could affect pronephric development, is its function in the lipid homeostasis of membrane lipid raft domains, since the integrity of these domains is crucial for the development of many organ systems (Ariotti et al., 2014; Fra et al., 1995; Murata et al., 1995; Ortegren et al., 2004; Thiele et al., 2000). Studies in *Xenopus* embryos have already illustrated the importance of a dynamic regulation of the lipid balance of membrane lipid rafts during pronephros development. For example, the knockdown of sterol carrier protein-2, a crucial regulator in sphingolipid metabolism, leads to a drastic reduction in the pronephric proximal tubule size (Cerqueira et al., 2014). These defects are directly related to the altered lipid composition of the membrane lipid raft domains and likely also due to the mis-localization of signaling molecules that could play a role in kidney development.

It has been shown, that Cav1 also functions in convergent extension movements during gastrulation in *Xenopus* embryos (Puzik et al., 2019). Convergent extension is a highly conserved process among different species, which is defined by the narrowing and extension of tissue that involve cell intercalation along an axis and the extension along a perpendicular axis through cell movements (Wallingford et al., 2002). In *Xenopus,* for example, both the notochord as well as the pronephros are formed by convergent extension movements (Keller et al., 1989; Lienkamp et al., 2012). Interestingly, Puzik and colleagues were able to show that the loss of Cav1α expression interferes with gastrulation and subsequently convergent extension in *Xenopus* embryos due to impaired Wnt5a/Ror2 signaling (Puzik et al., 2019). As mentioned above, the knockdown of Cav1α severely affects the morphology of the embryonic kidney; the proximal as well as intermediate tubule of the pronephros were significantly smaller in comparison to control kidneys (Figure 20J-K). Interestingly, this phenotype is highly similar to kidney defects induced by impaired CE movements, caused by either blebbistatin treatment or a dominant-negative form of Dishevelled-2 in *Xenopus* (Lienkamp et al., 2012).

Interfering with CE by disrupting planar cell polarity in the embryonic kidney, results in decreased nephron elongation and an increased tubule diameter (Lienkamp et al., 2012).
In summary, Cav1α likely affects the kidney development by either affecting the lipid composition of membrane lipid raft domains and thereby interfering with signaling pathways regulating kidney morphogenesis or by regulating convergent extension movements during pronephros development.

4.4 Loss of Cav1α expression affects neural crest-derived cartilage formation

In this study it was shown that Morpholino mediated knockdown of Cav1α significantly reduces cartilage structures. Interestingly only the neural crest, but not the mesodermal derived cartilage was affected by the loss-of-function of Cav1α, which implies a function of this protein in neural crest development (Figure 20C-D). Expression of Cav1α was not detected in *Xenopus* neural crest cells, neither by *in situ* hybridization nor by whole mount immunofluorescence staining. However, the expression pattern of Cav1 protein during embryonic development was only examined in stages where the neural crest cell migration is completed and neural crest cells start to differentiate (St. 35 onward) (Pauli et al., 2017). It is possible, that small amounts of *cav1*α mRNA are expressed in neural crest cells, but *in situ* hybridization may not be sensitive enough to detect this low level of expression. A function of Cav1α in neural crest development has not been reported in other model organisms so far. However, Berger *et al.* were able to demonstrate that the canonical Wnt dependent PTK7 (protein tyrosine kinase 7) internalization is mediated by Cav1 in *Xenopus* ectodermal explants (Berger et al., 2017). PTK7 is a versatile non-canonical Wnt co-receptor, which functions in diverse embryonic processes such as neural crest migration and the establishment of cell polarity (Paudyal et al., 2010; Shnitsar and Borchers, 2008). Morpholino-mediated knockdown of PTK7 severely affects neural crest migration in *Xenopus* embryos (Shnitsar and Borchers, 2008). It has been demonstrated that Cav1α expression contributes to the ability of PTK7 to inhibit canonical Wnt dependent secondary axis formation in *Xenopus* (Berger et al., 2017). Since PTK7 functions in neural crest migration and its Wnt-dependent endocytosis is mediated by Cav1α, a function of Cav1α during migration of neural crests seems likely (Berger, 2016, PhD; Shnitsar and Borchers, 2008).
In order to understand whether Cav1α has a function during neural crest migration, the migratory behavior of Cav1α morphant neural crest cells should be analyzed, for example, by performing explanation assays or whole mount *in situ* hybridization of the neural crest marker twist.

4.5 Future perspectives

In the present study Cav1α was identified to function in neuronal development by modulating the activity of small RhoGTPases during axonal development. However, there are still some open questions that should be addressed for further studies.

Studies performed in this laboratory have shown that nicotinic acetylcholine receptors (nAChR) clustering was perturbed in the Cav1α morphant embryos (Breuer, 2016, M.Sc.). Motoneuron and muscle cells communicate via chemical synapses called the neuromuscular junctions. During the establishment of the neuromuscular junction, nicotinic acetylcholine receptors (nAChR) become clustered at the postsynaptic membrane, which allows the muscle to respond to neurotransmitters secreted from motoneurons (Chow and Cohen, 1983). This process is initiated by the contact of the motoneuron synapse with the muscle cell, which induces an agrin/MuSK dependent clustering of nAChR at the postsynaptic contact site of the muscle cell (Bowe and Fallon, 1995; Cole and Halfter, 1996; DeChiara et al., 1996; Glass et al., 1996; Ruegg and Bixby, 1998). It is yet not known how Cav1α affects the clustering of the nicotinic acetylcholine receptors in the morphant embryos. Cav1 is expressed in motoneurons and the loss of Cav1α expression leads to severe pathfinding defects. It is likely that the diffuse nAChR staining observed in the morphant embryos is due to the fact, that the aberrant axonal branches of the motoneurons form synapses at several sites on the muscle cells. To visualize these contact sites, double immunostainings could be performed by using a presynaptic marker, such as synaptotagmin, and a postsynaptic marker like nAChR. This would also provide information on whether the morphant motoneurons are still able to form functional synapses or if the loss of Cav1α expression also interferes with synaptic transmission.

Further, albeit the present study primarily focused on the axonal growth of motoneurons, it is likely that other neurons of the spinal cord, such as GABAeric and glycerineric inhibitory as well as glutamateric excitatory interneurons and sensory Rohon-Beard neurons, are also affected by Cav1α loss-of-function (Roberts et al., 2010; Roberts, 2000b; Roberts and Clarke, 1982). This seems likely, as studies of this lab have already demonstrated, that Cav1α loss-of-function disrupts the outgrowth of cranial nerves in *Xenopus* embryos (Breuer, 2016, M.Sc.). Moreover, axonal growth but not dendritic morphology, which is also important for the establishment of synaptic connectivity and ultimately for locomotion, was analyzed (Heckman et al., 2003; Ryglewski et al., 2014; Scheibel and Scheibel, 1970). Furthermore, it is suggested that Cav1 is important for dendritic plasticity: Cav1 has been found to be expressed in the dendrites of hippocampal neurons and neuronal overexpression of this protein enhances dendritic growth and arborization (Bu et al., 2003; Head et al., 2011). To this end it would be interesting to analyze the effect of Cav1α knockdown on the dendritic

and synaptic physiology as well as axonal growth of both motoneurons, interneurons as well as sensory neurons of the *Xenopus* spinal cord.

The results of this thesis indicate that Cav1α regulates axonal growth by suppressing the activity of Rac1 and RhoA and supporting the activity of Cdc42. However, both the swimming as well as motoneuron defect were only rescued by the overexpression of either dominant negative or constitutive active mutants of this RhoGTPases, which means that it is not yet possible to make a precise assertion about the endogenous expression levels of the RhoGTPases in the morphant embryos. To this end, it would be important to analyze the endogenous spatial-temporal activity of these small RhoGTPases in the cultured morphant spinal cord neurons either by western blotting or by using activity assays. There are several reporters available for X*enopus*, which contain the fluorophore-tagged GTPase-binding domain of effector proteins specific for the respective RhoGTPase, such as Rhotekin binding active RhoA, N-WASP detecting active Cdc42 and Pak3 binding active Rac1 (reviewed in Stephenson and Miller, 2017). This would allow to assess the activity of Rac1, RhoA and Cdc42 at steady state as well as following Cav1α loss-of-function.

5 Conclusion

As an essential component of caveolae, Cav1 is a key regulator for membrane dynamics. Over the last decades, the role of Cav1 in a diverse number of signaling pathways was analyzed in various cellular systems. However, its function in neuronal cells has long been ignored. This study demonstrates that Cav1α is required for the neuromuscular integrity of *Xenopus* embryos. Morpholino mediated knockdown of Cav1α results in severe swimming defects and a drastic loss of muscular integrity. Expression analysis revealed that Cav1 is strongly expressed in the embryonic notochord, cardio vasculature, skin as well as cranial- and spinal cord neurons, but not in the musculature. Targeted injection demonstrated that Cav1α is required in the neuronal circuits controlling locomotion, as loss-of-function of Cav1α in neural tissue causes paralysis of the morphant embryos. Further, axonal outgrowth as well as pathfinding was severely affected by Cav1α knockdown and treatment with Benzocaine, an inhibitor for voltage gated sodium channels, showed that the muscle defects in the Cav1α morphant embryos are likely due to impaired muscle innervation. In spinal cord explantation assays, it could be shown that axonal growth as well as morphology was severely affected by Cav1α knockdown. Spinal cord neurons extended axons with an increased formation of filopodia- as well as lamellipodia-like structures. Axonal growth defects of the spinal motor neuron as well as the swimming defects could be rescued by the overexpression of a dominant negative Rac1 and RhoA as well as by constitutively active Cdc42, which suggests that Cav1α modulates the activity of these small RhoGTPases during axonal development in *Xenopus*. This process is likely mediated by the tyrosine phosphorylation (pY14) of Cav1α, as a phosphomutant of Cav1α was not able to rescue the morphant phenotype. Taken together, these finding suggest a novel and previously unrecognized function of Cav1α in the development of the neuromuscular system of *Xenopus* embryos.

6 Supplementary information:

Movie 1: Normal swimming behavior of embryos injected with 20 ng Co MO into one blastomere at the two-cell stage.

Movie 2: Embryos injected unilaterally with 20 ng Cav1α MO at the two-cell stage show circular swimming behavior due to the paralysis of the injected site.

Movie 3: Circular swimming movements of embryos unilaterally injected with 20 ng Cav1α Spl-MO at the two-cell stage.

Movie 4: Normal swimming behavior of embryos injected with 10 ng Co MO in both blastomeres of two-cell stage embryos.

Movie 5: Embryos injected with 10 ng Cav1α MO into both blastomeres of two-cell stage embryos. Embryos are completely paralyzed.

Movie 6: Axonal outgrowth of control neuron analyzed by live-cell imaging over a time period of 30 min. Growth cones of control axons dynamically extended and retracted the majority of their filopodia and lamellipodia protrusions during axonal growth

Movie 7: Axonal outgrowth of control neuron analyzed by live-cell imaging over a time period of 30 min.

Movie 8: Axonal outgrowth of Cav1α morphant neuron analyzed by live-cell imaging over a time period of 30 min. Cav1α morphant axon fail to retract their filopodia protrusions during axonal growth.

Movie 9: Axonal outgrowth of Cav1α morphant neuron analyzed by live-cell imaging over a time period of 30 min. Cav1α morphant axon fail to retract their lamellipodia protrusions during axonal growth.

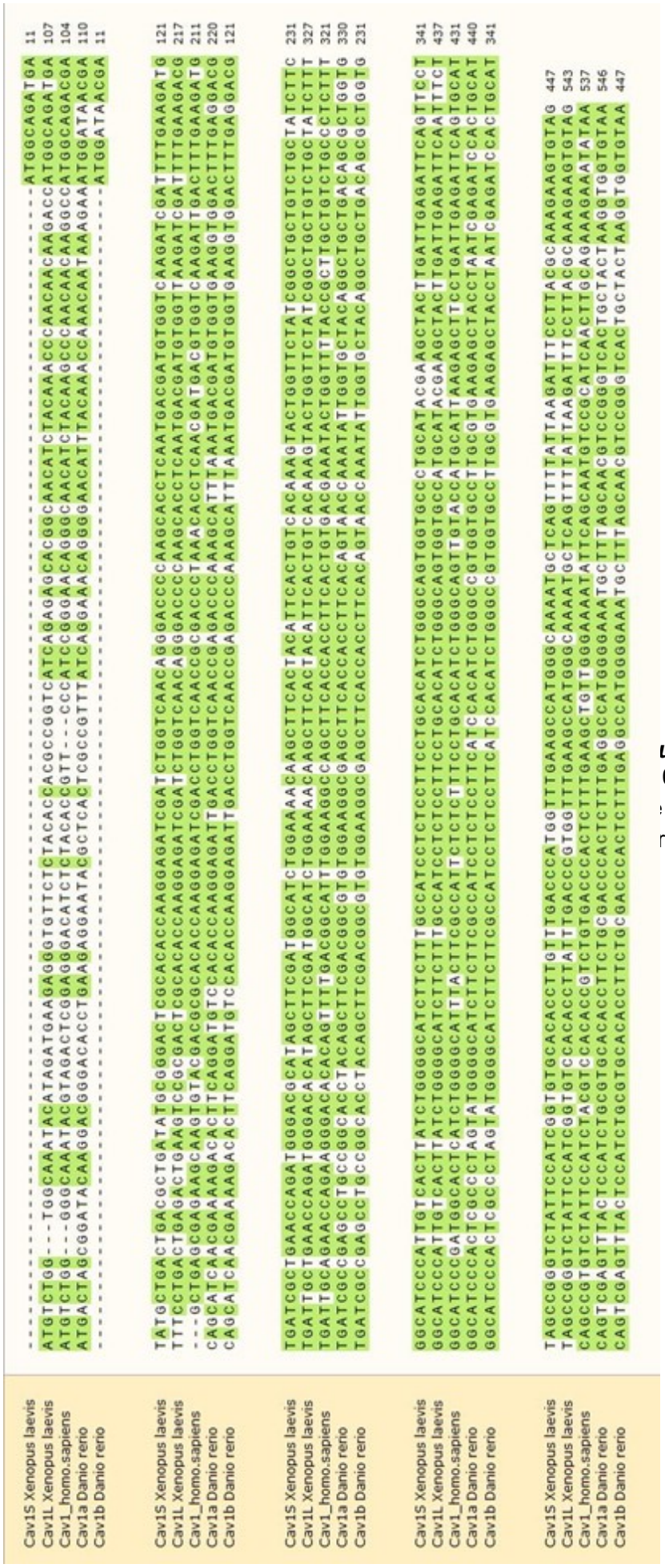

***us cav1 L* and S with human and zebraf**
090118.1), homo sapiens cav1 (GenBan
analysis was performed by using SnapGe
reen.

7 References

Allen, J.A., Yadav, P.N., Setola, V., Farrell, M., Roth, B.L., 2011. Schizophrenia risk gene CAV1 is both pro-psychotic and required for atypical antipsychotic drug actions in vivo. Translational psychiatry 1, e33. https://doi.org/10.1038/tp.2011.35.

Arbuzova, A., Wang, L., Wang, J., Hangyás-Mihályné, G., Murray, D., Honig, B., McLaughlin, S., 2000. Membrane binding of peptides containing both basic and aromatic residues. Experimental studies with peptides corresponding to the scaffolding region of caveolin and the effector region of MARCKS. Biochemistry 39 (33), 10330–10339. https://doi.org/10.1021/bi001039j.

Ariotti, N., Fernández-Rojo, M.A., Zhou, Y., Hill, M.M., Rodkey, T.L., Inder, K.L., Tanner, L.B., Wenk, M.R., Hancock, J.F., Parton, R.G., 2014. Caveolae regulate the nanoscale organization of the plasma membrane to remotely control Ras signaling. The Journal of cell biology 204 (5), 777–792. https://doi.org/10.1083/jcb.201307055.

Baker, J.C., Beddington, R.S., Harland, R.M., 1999. Wnt signaling in Xenopus embryos inhibits bmp4 expression and activates neural development. Genes & Development 13 (23), 3149–3159.

Barresi, V., Cerasoli, S., Paioli, G., Vitarelli, E., Giuffrè, G., Guiducci, G., Tuccari, G., Barresi, G., 2006. Caveolin-1 in meningiomas: expression and clinico-pathological correlations. Acta neuropathologica 112 (5), 617–626. https://doi.org/10.1007/s00401-006-0097-1.

Bastiani, M., Liu, L., Hill, M.M., Jedrychowski, M.P., Nixon, S.J., Lo, H.P., Abankwa, D., Luetterforst, R., Fernandez-Rojo, M., Breen, M.R., Gygi, S.P., Vinten, J., Walser, P.J., North, K.N., Hancock, J.F., Pilch, P.F., Parton, R.G., 2009. MURC/Cavin-4 and cavin family members form tissue-specific caveolar complexes. The Journal of cell biology 185 (7), 1259–1273. https://doi.org/10.1083/jcb.200903053.

Beardsley, A., Fang, K., Mertz, H., Castranova, V., Friend, S., Liu, J., 2005. Loss of caveolin-1 polarity impedes endothelial cell polarization and directional movement. Journal of Biological Chemistry 280 (5), 3541–3547. https://doi.org/10.1074/jbc.M409040200.

Bellefroid, E.J., 1998. Xiro3 encodes a Xenopus homolog of the Drosophila Iroquois genes and functions in neural specification. The EMBO journal 17 (1), 191–203. https://doi.org/10.1093/emboj/17.1.191.

Bellefroid, E.J., Bourguignon, C., Hollemann, T., Ma, Q., Anderson, D.J., Kintner, C., Pieler, T., 1996. X-MyT1, a Xenopus C2HC-Type Zinc Finger Protein with a Regulatory Function in Neuronal Differentiation. Cell 87 (7), 1191–1202. https://doi.org/10.1016/S0092-8674(00)81815-2.

Berger, H., 2016. PTK7 protein localization and stability is affected by canonical Wnt ligands (Dissertation). Dissertation.

Berger, H., Breuer, M., Peradziryi, H., Podleschny, M., Jacob, R., Borchers, A., 2017. PTK7 localization and protein stability is affected by canonical Wnt ligands. Journal of Cell Science 130 (11), 1890–1903. https://doi.org/10.1242/jcs.198580.

Berger, J.R., Oral, E.A., Taylor, S.I., 2002. Familial lipodystrophy associated with neurodegeneration and congenital cataracts. Neurology 58 (1), 43–47. https://doi.org/10.1212/wnl.58.1.43.

Bertrand, N., Castro, D.S., Guillemot, F., 2002. Proneural genes and the specification of neural cell types. Nat Rev Neurosci 3 (7), 517–530. https://doi.org/10.1038/nrn874.

Bhattachan, P., Rae, J., Yu, H., Jung, W., Wei, J., Parton, R.G., Dong, B., 2020. Ascidian caveolin induces membrane curvature and protects tissue integrity and morphology

during embryogenesis. FASEB journal : official publication of the Federation of American Societies for Experimental Biology 34 (1), 1345–1361. https://doi.org/10.1096/fj.201901281R.

Bist, A., Fielding, P.E., Fielding, C.J., 1997. Two sterol regulatory element-like sequences mediate up-regulation of caveolin gene transcription in response to low density lipoprotein free cholesterol. Proceedings of the National Academy of Sciences of the United States of America 94 (20), 10693–10698.

Blackshaw, S., Warner, A., 1976. Onset of acetylcholine sensitivity and endplate activity in developing myotome muscles of Xenopus. Nature 262 (5565), 217–218. https://doi.org/10.1038/262217a0.

Blumberg, B., Bolado, J., Moreno, T.A., Kintner, C., Evans, R.M., Papalopulu, N., 1997. An essential role for retinoid signaling in anteroposterior neural patterning. Development 124 (2), 373–379.

Borza, C.M., Chen, X., Mathew, S., Mont, S., Sanders, C.R., Zent, R., Pozzi, A., 2010. Integrin {alpha}1{beta}1 promotes caveolin-1 dephosphorylation by activating T cell protein-tyrosine phosphatase. The Journal of biological chemistry 285 (51), 40114–40124. https://doi.org/10.1074/jbc.M110.156729.

Bowe, M.A., Fallon, J.R., 1995. The role of agrin in synapse formation. Annu. Rev. Neurosci. 18, 443–462. https://doi.org/10.1146/annurev.ne.18.030195.002303.

Boyd, N.L., Park, H., Yi, H., Boo, Y.C., Sorescu, G.P., Sykes, M., Jo, H., 2003. Chronic shear induces caveolae formation and alters ERK and Akt responses in endothelial cells. American journal of physiology. Heart and circulatory physiology 285 (3), H1113-22. https://doi.org/10.1152/ajpheart.00302.2003.

Breen, M.R., Camps, M., Carvalho-Simoes, F., Zorzano, A., Pilch, P.F., 2012. Cholesterol depletion in adipocytes causes caveolae collapse concomitant with proteosomal degradation of cavin-2 in a switch-like fashion. PloS one 7 (4), e34516. https://doi.org/10.1371/journal.pone.0034516.

Breton, S., Lisanti, M.P., Tyszkowski, R., McLaughlin, M., Brown, D., 1998. Basolateral distribution of caveolin-1 in the kidney. Absence from H+-atpase-coated endocytic vesicles in intercalated cells. The journal of histochemistry and cytochemistry : official journal of the Histochemistry Society 46 (2), 205–214. https://doi.org/10.1177/002215549804600209.

Breuer, M., 2016. Functional analysis of caveolin 1 in Xenopus laevis (Msc). Master thesis. Marburg.

Brewster, R., Lee, J., Altaba, A.R.i., 1998. Gli/Zic factors pattern the neural plate by defining domains of cell differentiation. Nature 393 (6685), 579–583. https://doi.org/10.1038/31242.

Briand, N., Dugail, I., Le Lay, S., 2011. Cavin proteins: New players in the caveolae field. Biochimie 93 (1), 71–77. https://doi.org/10.1016/j.biochi.2010.03.022.

Briscoe, J., Ericson, J., 1999. The specification of neuronal identity by graded Sonic Hedgehog signalling. Seminars in cell & developmental biology 10 (3), 353–362. https://doi.org/10.1006/scdb.1999.0295.

Briscoe, J., Novitch, B.G., 2008. Regulatory pathways linking progenitor patterning, cell fates and neurogenesis in the ventral neural tube. Philosophical transactions of the Royal Society of London. Series B, Biological sciences 363 (1489), 57–70. https://doi.org/10.1098/rstb.2006.2012.

Briscoe, J., Pierani, A., Jessell, T.M., Ericson, J., 2000. A homeodomain protein code specifies progenitor cell identity and neuronal fate in the ventral neural tube. Cell 101 (4), 435–445.

Brou, C., Logeat, F., Gupta, N., Bessia, C., LeBail, O., Doedens, J.R., Cumano, A., Roux, P., Black, R.A., Israël, A., 2000. A novel proteolytic cleavage involved in Notch signaling: the role of the disintegrin-metalloprotease TACE. Molecular cell 5 (2), 207–216. https://doi.org/10.1016/s1097-2765(00)80417-7.

Brouns, M.R., Matheson, S.F., Settleman, J., 2001. p190 RhoGAP is the principal Src substrate in brain and regulates axon outgrowth, guidance and fasciculation. Nature cell biology 3 (4), 361–367. https://doi.org/10.1038/35070042.

Bryant, K.G., Camacho, J., Jasmin, J.-F., Wang, C., Addya, S., Casimiro, M.C., Fortina, P., Balasubramaniam, S., Knudsen, K.E., Schwarting, R., Lisanti, M.P., Mercier, I., 2011. Caveolin-1 overexpression enhances androgen-dependent growth and proliferation in the mouse prostate. The international journal of biochemistry & cell biology 43 (9), 1318–1329. https://doi.org/10.1016/j.biocel.2011.04.019.

Bu, J., Bruckner, S.R., Sengoku, T., Geddes, J.W., Estus, S., 2003. Glutamate regulates caveolin expression in rat hippocampal neurons. Journal of neuroscience research 72 (2), 185–190. https://doi.org/10.1002/jnr.10556.

Bullejos, M., Bowles, J., Koopman, P., 2002. Extensive vascularization of developing mouse ovaries revealed by caveolin-1 expression. Dev. Dyn. 225 (1), 95–99. https://doi.org/10.1002/dvdy.10128.

Burgener, R., Wolf, M., Ganz, T., Baggiolini, M., 1990. Purification and characterization of a major phosphatidylserine-binding phosphoprotein from human platelets. The Biochemical journal 269 (3), 729–734.

Cameron, P.L., Ruffin, J.W., Bollag, R., Rasmussen, H., Cameron, R.S., 1997. Identification of caveolin and caveolin-related proteins in the brain. The Journal of neuroscience : the official journal of the Society for Neuroscience 17 (24), 9520–9535.

Cao, G., Yang, G., Timme, T.L., Saika, T., Truong, L.D., Satoh, T., Goltsov, A., Park, S.H., Men, T., Kusaka, N., Tian, W., Ren, C., Wang, H., Kadmon, D., Cai, W.W., Chinault, A.C., Boone, T.B., Bradley, A., Thompson, T.C., 2003. Disruption of the Caveolin-1 Gene Impairs Renal Calcium Reabsorption and Leads to Hypercalciuria and Urolithiasis. The American journal of pathology 162 (4), 1241–1248. https://doi.org/10.1016/S0002-9440(10)63920-X.

Cao, H., Alston, L., Ruschman, J., Hegele, R.A., 2008. Heterozygous CAV1 frameshift mutations (MIM 601047) in patients with atypical partial lipodystrophy and hypertriglyceridemia. Lipids in health and disease 7, 3. https://doi.org/10.1186/1476-511X-7-3.

Cao, H., Sanguinetti, A.R., Mastick, C.C., 2004. Oxidative stress activates both Src-kinases and their negative regulator Csk and induces phosphorylation of two targeting proteins for Csk: caveolin-1 and paxillin. Experimental cell research 294 (1), 159–171. https://doi.org/10.1016/j.yexcr.2003.11.010.

Cao, J., Navis, A., Cox, B.D., Dickson, A.L., Gemberling, M., Karra, R., Bagnat, M., Poss, K.D., 2016. Single epicardial cell transcriptome sequencing identifies Caveolin 1 as an essential factor in zebrafish heart regeneration. Development (Cambridge, England) 143 (2), 232–243. https://doi.org/10.1242/dev.130534.

Capozza, F., Williams, T.M., Schubert, W., McClain, S., Bouzahzah, B., Sotgia, F., Lisanti, M.P., 2003. Absence of caveolin-1 sensitizes mouse skin to carcinogen-induced epidermal hyperplasia and tumor formation. The American journal of pathology 162 (6), 2029–2039. https://doi.org/10.1016/S0002-9440(10)64335-0.

Carozzi, A.J., Roy, S., Morrow, I.C., Pol, A., Wyse, B., Clyde-Smith, J., Prior, I.A., Nixon, S.J., Hancock, J.F., Parton, R.G., 2002. Inhibition of lipid raft-dependent signaling by a dystrophy-associated mutant of caveolin-3. Journal of Biological Chemistry 277 (20), 17944–17949. https://doi.org/10.1074/jbc.M110879200.

Carpentier, J., Perrelet, A., Orci, L., 1977. Morphological changes of the adipose cell plasma membrane during lipolysis. The Journal of cell biology 72 (1), 104–117.

Causeret, M., Taulet, N., Comunale, F., Favard, C., Gauthier-Rouvière, C., 2005. N-cadherin association with lipid rafts regulates its dynamic assembly at cell-cell junctions in C2C12 myoblasts. Molecular biology of the cell 16 (5), 2168–2180. https://doi.org/10.1091/mbc.E04-09-0829.

Cemal, C.K., Carroll, C.J., Lawrence, L., Lowrie, M.B., Ruddle, P., Al-Mahdawi, S., King, R.H.M., Pook, M.A., Huxley, C., Chamberlain, S., 2002. YAC transgenic mice carrying pathological alleles of the MJD1 locus exhibit a mild and slowly progressive cerebellar deficit. Human molecular genetics 11 (9), 1075–1094. https://doi.org/10.1093/hmg/11.9.1075.

Cerqueira, D.M., Tran, U., Romaker, D., Abreu, J.G., Wessely, O., 2014. Sterol carrier protein 2 regulates proximal tubule size in the Xenopus pronephric kidney by modulating lipid rafts. Developmental biology 394 (1), 54–64. https://doi.org/10.1016/j.ydbio.2014.07.025.

Chalmers, A.D., Welchman, D., Papalopulu, N., 2002. Intrinsic Differences between the Superficial and Deep Layers of the Xenopus Ectoderm Control Primary Neuronal Differentiation. Developmental cell 2 (2), 171–182. https://doi.org/10.1016/S1534-5807(02)00113-2.

Chanoine, C., Hardy, S., 2003. Xenopus muscle development: from primary to secondary myogenesis. Developmental dynamics : an official publication of the American Association of Anatomists 226 (1), 12–23. https://doi.org/10.1002/dvdy.10206.

Cheng, J.P.X., Nichols, B.J., 2016. Caveolae: One Function or Many? Trends in Cell Biology 26 (3), 177–189. https://doi.org/10.1016/j.tcb.2015.10.010.

Chiavegatto, S., Sun, J., Nelson, R.J., Schnaar, R.L., 2000. A functional role for complex gangliosides: motor deficits in GM2/GD2 synthase knockout mice. Experimental neurology 166 (2), 227–234. https://doi.org/10.1006/exnr.2000.7504.

Chitnis, A., Henrique, D., Lewis, J., Ish-Horowicz, D., Kintner, C., 1995. Primary neurogenesis in Xenopus embryos regulated by a homologue of the Drosophila neurogenic gene Delta. Nature 375 (6534), 761–766. https://doi.org/10.1038/375761a0.

Chitnis, A., Kintner, C., 1996. Sensitivity of proneural genes to lateral inhibition affects the pattern of primary neurons in Xenopus embryos. Development 122 (7), 2295–2301.

Choi, K.-H., Kim, H.-S., Park, M.-S., Kim, J.-T., Kim, J.-H., Cho, K.-A., Lee, M.-C., Lee, H.-J., Cho, K.-H., 2016. Regulation of Caveolin-1 Expression Determines Early Brain Edema After Experimental Focal Cerebral Ischemia. Stroke 47 (5), 1336–1343. https://doi.org/10.1161/STROKEAHA.116.013205.

Choi, S.-C., Han, J.-K., 2002. Xenopus Cdc42 regulates convergent extension movements during gastrulation through Wnt/Ca2+ signaling pathway. Developmental biology 244 (2), 342–357. https://doi.org/10.1006/dbio.2002.0602.

Chow, I., Cohen, M.W., 1983. Developmental changes in the distribution of acetylcholine receptors in the myotomes of Xenopus laevis. The Journal of physiology 339, 553–571. https://doi.org/10.1113/jphysiol.1983.sp014733.

Clarke, J.D., Hayes, B.P., Hunt, S.P., Roberts, A., 1984. Sensory physiology, anatomy and immunohistochemistry of Rohon-Beard neurones in embryos of Xenopus laevis. The Journal of physiology 348, 511–525. https://doi.org/10.1113/jphysiol.1984.sp015122.

Cohen, A.W., Hnasko, R., Schubert, W., Lisanti, M.P., 2004. Role of caveolae and caveolins in health and disease. Physiological reviews 84 (4), 1341–1379. https://doi.org/10.1152/physrev.00046.2003.

Cohen, A.W., Park, D.S., Woodman, S.E., Williams, T.M., Chandra, M., Shirani, J., Pereira de Souza, A., Kitsis, R.N., Russell, R.G., Weiss, L.M., Tang, B., Jelicks, L.A., Factor, S.M., Shtutin, V., Tanowitz, H.B., Lisanti, M.P., 2003. Caveolin-1 null mice develop cardiac hypertrophy with hyperactivation of p42/44 MAP kinase in cardiac fibroblasts. AJP: Cell Physiology 284 (2), C457-74. https://doi.org/10.1152/ajpcell.00380.2002.

Cole, G.J., Halfter, W., 1996. Agrin: an extracellular matrix heparan sulfate proteoglycan involved in cell interactions and synaptogenesis. Perspectives on developmental neurobiology 3 (4), 359–371.

Corral, R.D.d., Storey, K.G., 2001. Markers in vertebrate neurogenesis. Nat Rev Neurosci 2 (11), 835–839. https://doi.org/10.1038/35097587.

Couet, J., Li, S., Okamoto, T., Ikezu, T., Lisanti, M.P., 1997a. Identification of peptide and protein ligands for the caveolin-scaffolding domain. Implications for the interaction of caveolin with caveolae-associated proteins. The Journal of biological chemistry 272 (10), 6525–6533.

Couet, J., Sargiacomo, M., Lisanti, M.P., 1997b. Interaction of a Receptor Tyrosine Kinase, EGF-R, with Caveolins. Journal of Biological Chemistry 272 (48), 30429–30438. https://doi.org/10.1074/jbc.272.48.30429.

Couet, J., Sargiacomo, M., Lisanti, M.P., 1997c. Interaction of a receptor tyrosine kinase, EGF-R, with caveolins. Caveolin binding negatively regulates tyrosine and serine/threonine kinase activities. Journal of Biological Chemistry 272 (48), 30429–30438. https://doi.org/10.1074/jbc.272.48.30429.

da Silva, J.S., Dotti, C.G., 2002. Breaking the neuronal sphere: regulation of the actin cytoskeleton in neuritogenesis. Nat Rev Neurosci 3 (9), 694–704. https://doi.org/10.1038/nrn918.

Dale, N., Roberts, A., Ottersen, O.P., Storm-Mathisen, J., 1987. The morphology and distribution of 'Kolmer-Agduhr cells', a class of cerebrospinal-fluid-contacting neurons revealed in the frog embryo spinal cord by GABA immunocytochemistry. Proceedings of the Royal Society of London. Series B, Biological sciences 232 (1267), 193–203. https://doi.org/10.1098/rspb.1987.0068.

Davidson, L.A., Keller, R.E., 1999. Neural tube closure in Xenopus laevis involves medial migration, directed protrusive activity, cell intercalation and convergent extension. Development 126 (20), 4547–4556.

Dawson, S.R., Turner, D.L., Weintraub, H., Parkhurst, S.M., 1995. Specificity for the hairy/enhancer of split basic helix-loop-helix (bHLH) proteins maps outside the bHLH domain and suggests two separable modes of transcriptional repression. Molecular and Cellular Biology 15 (12), 6923–6931.

DeChiara, T.M., Bowen, D.C., Valenzuela, D.M., Simmons, M.V., Poueymirou, W.T., Thomas, S., Kinetz, E., Compton, D.L., Rojas, E., Park, J.S., Smith, C., DiStefano, P.S., Glass, D.J., Burden, S.J., Yancopoulos, G.D., 1996. The Receptor Tyrosine Kinase MuSK Is Required for Neuromuscular Junction Formation In Vivo. Cell 85 (4), 501–512. https://doi.org/10.1016/S0092-8674(00)81251-9.

del Pozo, M.A., Balasubramanian, N., Alderson, N.B., Kiosses, W.B., Grande-Garcia, A., Anderson, R.G.W., Schwartz, M.A., 2005. Phospho-caveolin-1 mediates integrin-regulated membrane domain internalization. Nature cell biology 7 (9), 901–908. https://doi.org/10.1038/ncb1293.

Delaune, E., Lemaire, P., Kodjabachian, L., 2005. Neural induction in Xenopus requires early FGF signalling in addition to BMP inhibition. Development 132 (2), 299–310. https://doi.org/10.1242/dev.01582.

DeMali, K.A., Burridge, K., 2003. Coupling membrane protrusion and cell adhesion. Journal of Cell Science 116 (Pt 12), 2389–2397. https://doi.org/10.1242/jcs.00605.

Dewulf, M., Köster, D.V., Sinha, B., Viaris de Lesegno, C., Chambon, V., Bigot, A., Bensalah, M., Negroni, E., Tardif, N., Podkalicka, J., Johannes, L., Nassoy, P., Butler-Browne, G., Lamaze, C., Blouin, C.M., 2019. Dystrophy-associated caveolin-3 mutations reveal that caveolae couple IL6/STAT3 signaling with mechanosensing in human muscle cells. Nat Comms 10 (1), 1974. https://doi.org/10.1038/s41467-019-09405-5.

Dietzen, D.J., Hastings, W.R., Lublin, D.M., 1995. Caveolin is palmitoylated on multiple cysteine residues. Palmitoylation is not necessary for localization of caveolin to caveolae. Journal of Biological Chemistry 270 (12), 6838–6842. https://doi.org/10.1074/jbc.270.12.6838.

Drab, M., Verkade, P., Elger, M., Kasper, M., Lohn, M., Lauterbach, B., Menne, J., Lindschau, C., Mende, F., Luft, F.C., Schedl, A., Haller, H., Kurzchalia, T.V., 2001. Loss of caveolae, vascular dysfunction, and pulmonary defects in caveolin-1 gene-disrupted mice. Science 293 (5539), 2449–2452. https://doi.org/10.1126/science.1062688.

Dulhunty, A.F., Franzini-Armstrong, C., 1975. The relative contributions of the folds and caveolae to the surface membrane of frog skeletal muscle fibres at different sarcomere lengths. The Journal of physiology 250 (3), 513–539. https://doi.org/10.1113/jphysiol.1975.sp011068.

Echarri, A., del Pozo, M.A., 2015. Caveolae - mechanosensitive membrane invaginations linked to actin filaments. Journal of Cell Science 128 (15), 2747–2758. https://doi.org/10.1242/jcs.153940.

Echarri, A., Muriel, O., Pavón, D.M., Azegrouz, H., Escolar, F., Terrón, M.C., Sanchez-Cabo, F., Martínez, F., Montoya, M.C., Llorca, O., del Pozo, M.A., 2012. Caveolar domain organization and trafficking is regulated by Abl kinases and mDia1. Journal of Cell Science 125 (Pt 13), 3097–3113. https://doi.org/10.1242/jcs.090134.

Edlund, A.F., Davidson, L.A., Keller, R.E., 2013. Cell segregation, mixing, and tissue pattern in the spinal cord of the Xenopus laevis neurula. Developmental dynamics : an official publication of the American Association of Anatomists 242 (10), 1134–1146. https://doi.org/10.1002/dvdy.24004.

Egawa, J., Zemljic-Harpf, A., Mandyam, C.D., Niesman, I.R., Lysenko, L.V., Kleschevnikov, A.M., Roth, D.M., Patel, H.H., Patel, P.M., Head, B.P., 2018. Neuron-Targeted Caveolin-1 Promotes Ultrastructural and Functional Hippocampal Synaptic Plasticity. Cerebral cortex (New York, N.Y. : 1991) 28 (9), 3255–3266. https://doi.org/10.1093/cercor/bhx196.

Ehrlich, J.S., Hansen, M.D.H., Nelson, W.J., 2002. Spatio-Temporal Regulation of Rac1 Localization and Lamellipodia Dynamics during Epithelial Cell-Cell Adhesion. Developmental cell 3 (2), 259–270. https://doi.org/10.1016/S1534-5807(02)00216-2.

Eisinger, K.R.T., Chapp, A.D., Swanson, S.P., Tam, D., Lopresti, N.M., Larson, E.B., Thomas, M.J., Lanier, L.M., Mermelstein, P.G., 2020. Caveolin-1 regulates medium spiny neuron structural and functional plasticity. Psychopharmacology. https://doi.org/10.1007/s00213-020-05564-2.

Engelman, J.A., Chu, C., Lin, A., Jo, H., Ikezu, T., Okamoto, T., Kohtz, D.S., Lisanti, M.P., 1998a. Caveolin-mediated regulation of signaling along the p42/44 MAP kinase cascade in vivo. A role for the caveolin-scaffolding domain. FEBS letters 428 (3), 205–211.

Engelman, J.A., Zhang, X.L., Galbiati, F., Lisanti, M.P., 1998b. Chromosomal localization, genomic organization, and developmental expression of the murine caveolin gene family (Cav-1, -2, and -3). FEBS letters 429 (3), 330–336. https://doi.org/10.1016/S0014-5793(98)00619-X.

Ericson, J., Briscoe, J., Rashbass, P., van Heyningen, V., Jessell, T.M., 1997. Graded sonic hedgehog signaling and the specification of cell fate in the ventral neural tube. Cold Spring Harbor symposia on quantitative biology 62, 451–466.

Ericson, J., Morton, S., Kawakami, A., Roelink, H., Jessell, T.M., 1996. Two critical periods of Sonic Hedgehog signaling required for the specification of motor neuron identity. Cell 87 (4), 661–673. https://doi.org/10.1016/s0092-8674(00)81386-0.

Eser Ocak, P., Ocak, U., Tang, J., Zhang, J.H., 2019. The role of caveolin-1 in tumors of the brain - functional and clinical implications. Cellular oncology (Dordrecht) 42 (4), 423–447. https://doi.org/10.1007/s13402-019-00447-x.

Etienne-Manneville, S., Hall, A., 2002. Rho GTPases in cell biology. Nature 420 (6916), 629–635. https://doi.org/10.1038/nature01148.

Faggi, F., Codenotti, S., Poliani, P.L., Cominelli, M., Chiarelli, N., Colombi, M., Vezzoli, M., Monti, E., Bono, F., Tulipano, G., Fiorentini, C., Zanola, A., Lo, H.P., Parton, R.G., Keller, C., Fanzani, A., 2015. MURC/cavin-4 Is Co-Expressed with Caveolin-3 in Rhabdomyosarcoma Tumors and Its Silencing Prevents Myogenic Differentiation in the Human Embryonal RD Cell Line. PloS one 10 (6), e0130287. https://doi.org/10.1371/journal.pone.0130287.

Fainsod, A., Deißler, K., Yelin, R., Marom, K., Epstein, M., Pillemer, G., Steinbeisser, H., Blum, M., 1997. The dorsalizing and neural inducing gene follistatin is an antagonist of BMP-4. Mechanisms of Development 63 (1), 39–50. https://doi.org/10.1016/S0925-4773(97)00673-4.

Fang, P.-K., Solomon, K.R., Zhuang, L., Qi, M., McKee, M., Freeman, M.R., Yelick, P.C., 2006. Caveolin-1alpha and -1beta perform nonredundant roles in early vertebrate development. The American journal of pathology 169 (6), 2209–2222.

Fernandez, I., Ying, Y., Albanesi, J., Anderson, R.G.W., 2002. Mechanism of caveolin filament assembly. Proceedings of the National Academy of Sciences 99 (17), 11193–11198. https://doi.org/10.1073/pnas.172196599.

Feron, O., Belhassen, L., Kobzik, L., Smith, T.W., Kelly, R.A., Michel, T., 1996. Endothelial nitric oxide synthase targeting to caveolae. Specific interactions with caveolin isoforms in cardiac myocytes and endothelial cells. Journal of Biological Chemistry 271 (37), 22810–22814. https://doi.org/10.1074/jbc.271.37.22810.

Ferrari, L., Pistocchi, A., Libera, L., Boari, N., Mortini, P., Bellipanni, G., Giordano, A., Cotelli, F., Riva, P., 2014. FAS/FASL are dysregulated in chordoma and their loss-of-function impairs zebrafish notochord formation. Oncotarget 5 (14), 5712–5724. https://doi.org/10.18632/oncotarget.2145.

Field, M.C., Gabernet-Castello, C., Dacks, J.B., 2007. Reconstructing the evolution of the endocytic system: insights from genomics and molecular cell biology. Advances in experimental medicine and biology 607, 84–96. https://doi.org/10.1007/978-0-387-74021-8_7.

Fielding, C.J., Bist, A., Fielding, P.E., 1997. Caveolin mRNA levels are up-regulated by free cholesterol and down-regulated by oxysterols in fibroblast monolayers. Proceedings of the National Academy of Sciences of the United States of America 94 (8), 3753–3758.

Fielding, P.E., Chau, P., Liu, D., Spencer, T.A., Fielding, C.J., 2004. Mechanism of platelet-derived growth factor-dependent caveolin-1 phosphorylation: relationship to sterol binding and the role of serine-80. Biochemistry 43 (9), 2578–2586. https://doi.org/10.1021/bi035442c.

Fra, A.M., Masserini, M., Palestini, P., Sonnino, S., Simons, K., 1995. A photo-reactive derivative of ganglioside GM1 specifically cross-links VIP21-caveolin on the cell surface. FEBS letters 375 (1-2), 11–14. https://doi.org/10.1016/0014-5793(95)95228-O.

Fra, A.M., Williamson, E., Simons, K., Parton, R.G., 1994. Detergent-insoluble glycolipid microdomains in lymphocytes in the absence of caveolae. Journal of Biological Chemistry 269 (49), 30745–30748.

Franco, P.G., Paganelli, A.R., López, S.L., Carrasco, A.E., 1999. Functional association of retinoic acid and hedgehog signaling in Xenopus primary neurogenesis. Development (Cambridge, England) 126 (19), 4257–4265.

Frick, M., Bright, N.A., Riento, K., Bray, A., Merrified, C., Nichols, B.J., 2007. Coassembly of flotillins induces formation of membrane microdomains, membrane curvature, and vesicle budding. Current Biology 17 (13), 1151–1156. https://doi.org/10.1016/j.cub.2007.05.078.

Fujimoto, T., Kogo, H., Nomura, R., Une, T., 2000. Isoforms of caveolin-1 and caveolar structure. Journal of Cell Science 113 Pt 19, 3509–3517.

Gabella, G., 1976. Quantitative morphological study of smooth muscle cells of the guinea-pig taenia coli. Cell and Tissue Research 170 (2), 161–186. https://doi.org/10.1007/BF00224297.

Galbiati, F., Engelman, J.A., Volonte, D., Zhang, X.L., Minetti, C., Li, M., Hou, H., Kneitz, B., Edelmann, W., Lisanti, M.P., 2001a. Caveolin-3 null mice show a loss of caveolae, changes in the microdomain distribution of the dystrophin-glycoprotein complex, and t-tubule abnormalities. Journal of Biological Chemistry 276 (24), 21425–21433. https://doi.org/10.1074/jbc.M100828200.

Galbiati, F., Volonte, D., Brown, A.M., Weinstein, D.E., Ben-Ze'ev, A., Pestell, R.G., Lisanti, M.P., 2000a. Caveolin-1 expression inhibits Wnt/beta-catenin/Lef-1 signaling by recruiting beta-catenin to caveolae membrane domains. Journal of Biological Chemistry 275 (30), 23368–23377. https://doi.org/10.1074/jbc.M002020200.

Galbiati, F., Volonte, D., Chu, J.B., Li, M., Fine, S.W., Fu, M., Bermudez, J., Pedemonte, M., Weidenheim, K.M., Pestell, R.G., Minetti, C., Lisanti, M.P., 2000b. Transgenic overexpression of caveolin-3 in skeletal muscle fibers induces a Duchenne-like muscular dystrophy phenotype. Proceedings of the National Academy of Sciences 97 (17), 9689–9694. https://doi.org/10.1073/pnas.160249097.

Galbiati, F., Volonte, D., Gil, O., Zanazzi, G., Salzer, J.L., Sargiacomo, M., Scherer, P.E., Engelman, J.A., Schlegel, A., Parenti, M., Okamoto, T., Lisanti, M.P., 1998. Expression of caveolin-1 and -2 in differentiating PC12 cells and dorsal root ganglion neurons: caveolin-2 is up-regulated in response to cell injury. Proceedings of the National Academy of Sciences 95 (17), 10257–10262.

Galbiati, F., Volonte', D., Liu, J., Capozza, F., Frank, P.G., Zhu, L., Pestell, R.G., Lisanti, M.P., 2001b. Caveolin-1 Expression Negatively Regulates Cell Cycle Progression by Inducing G0/G1 Arrest via a p53/p21WAF1/Cip1-dependent Mechanism. Molecular biology of the cell 12 (8), 2229–2244. https://doi.org/10.1091/mbc.12.8.2229.

Gambin, Y., Ariotti, N., McMahon, K.-A., Bastiani, M., Sierecki, E., Kovtun, O., Polinkovsky, M.E., Magenau, A., Jung, W., Okano, S., Zhou, Y., Leneva, N., Mureev, S., Johnston, W., Gaus, K., Hancock, J.F., Collins, B.M., Alexandrov, K., Parton, R.G., 2013. Single-molecule analysis reveals self assembly and nanoscale segregation of two distinct cavin subcomplexes on caveolae. eLife 3, e01434. https://doi.org/10.7554/eLife.01434.

Garcia, J., Bagwell, J., Njaine, B., Norman, J., Levic, D.S., Wopat, S., Miller, S.E., Liu, X., Locasale, J.W., Stainier, D.Y.R., Bagnat, M., 2017. Sheath Cell Invasion and Trans-differentiation Repair Mechanical Damage Caused by Loss of Caveolae in the Zebrafish Notochord. Current biology : CB 27 (13), 1982-1989.e3. https://doi.org/10.1016/j.cub.2017.05.035.

Gaudreault, S.B., Dea, D., Poirier, J., 2004. Increased caveolin-1 expression in Alzheimer's disease brain. Neurobiology of aging 25 (6), 753–759. https://doi.org/10.1016/j.neurobiolaging.2003.07.004.

Gaus, K., Le Lay, S., Balasubramanian, N., Schwartz, M.A., 2006. Integrin-mediated adhesion regulates membrane order. J Cell Biol 174 (5), 725–734. https://doi.org/10.1083/jcb.200603034.

Gil, J., 1983. Number and distribution of plasmalemmal vesicles in the lung. Federation proceedings 42 (8), 2414–2418.

Gingras, D., Gauthier, F., Lamy, S., Desrosiers, R.R., Béliveau, R., 1998. Localization of RhoA GTPase to endothelial caveolae-enriched membrane domains. Biochemical and biophysical research communications 247 (3), 888–893. https://doi.org/10.1006/bbrc.1998.8885.

Gioiosa, L., Raggi, C., Ricceri, L., Jasmin, J.-F., Frank, P.G., Capozza, F., Lisanti, M.P., Alleva, E., Sargiacomo, M., Laviola, G., 2008. Altered emotionality, spatial memory and cholinergic function in caveolin-1 knock-out mice. Behavioural brain research 188 (2), 255–262. https://doi.org/10.1016/j.bbr.2007.11.002.

Glass, D.J., Bowen, D.C., Stitt, T.N., Radziejewski, C., Bruno, J., Ryan, T.E., Gies, D.R., Shah, S., Mattsson, K., Burden, S.J., DiStefano, P.S., Valenzuela, D.M., DeChiara, T.M., Yancopoulos, G.D., 1996. Agrin Acts via a MuSK Receptor Complex. Cell 85 (4), 513–523. https://doi.org/10.1016/S0092-8674(00)81252-0.

Glenney, J.R., 1989. Tyrosine phosphorylation of a 22-kDa protein is correlated with transformation by Rous sarcoma virus. Journal of Biological Chemistry 264 (34), 20163–20166.

Glenney, J R Jr, 1989. Tyrosine phosphorylation of a 22-kDa protein is correlated with transformation by Rous sarcoma virus. The Journal of biological chemistry 264 (34), 20163–20166.

Gnedeva, K., Hudspeth, A.J., 2015. SoxC transcription factors are essential for the development of the inner ear. PNAS 112 (45), 14066–14071. https://doi.org/10.1073/pnas.1517371112.

Goetz, J.G., Joshi, B., Lajoie, P., Strugnell, S.S., Scudamore, T., Kojic, L.D., Nabi, I.R., 2008a. Concerted regulation of focal adhesion dynamics by galectin-3 and tyrosine-phosphorylated caveolin-1. The Journal of cell biology 180 (6), 1261–1275. https://doi.org/10.1083/jcb.200709019.

Goetz, J.G., Lajoie, P., Wiseman, S.M., Nabi, I.R., 2008b. Caveolin-1 in tumor progression: the good, the bad and the ugly. Cancer Metastasis Rev 27 (4), 715–735. https://doi.org/10.1007/s10555-008-9160-9.

Gomez-Skarmeta, J.L., 1998. Xiro, a Xenopus homolog of the Drosophila Iroquois complex genes, controls development at the neural plate. The EMBO journal 17 (1), 181–190. https://doi.org/10.1093/emboj/17.1.181.

Gómez-Skarmeta, J., de La Calle-Mustienes, E, Modolell, J., 2001. The Wnt-activated Xiro1 gene encodes a repressor that is essential for neural development and downregulates Bmp4. Development (Cambridge, England) 128 (4), 551–560.

Gonzalez-Billault, C., Muñoz-Llancao, P., Henriquez, D.R., Wojnacki, J., Conde, C., Caceres, A., 2012. The role of small GTPases in neuronal morphogenesis and polarity. Cytoskeleton (Hoboken, N.J.) 69 (7), 464–485. https://doi.org/10.1002/cm.21034.

GORRILL, R.H., 1956. Spinning disease of mice. The Journal of pathology and bacteriology 71 (2), 353–358. https://doi.org/10.1002/path.1700710209.

Grande-García, A., Echarri, A., Rooij, J. de, Alderson, N.B., Waterman-Storer, C.M., Valdivielso, J.M., del Pozo, Miguel A, 2007. Caveolin-1 regulates cell polarization and

directional migration through Src kinase and Rho GTPases. The Journal of cell biology 177 (4), 683–694. https://doi.org/10.1083/jcb.200701006.

Grivas, D., González-Rajal, Á., Rodríguez, C.G., Garcia, R., La Pompa, J.L. de, 2020. Loss of Caveolin-1 and caveolae leads to increased cardiac cell stiffness and functional decline of the adult zebrafish heart.

Gross, J.B., Hanken, J., 2008. Segmentation of the vertebrate skull: neural-crest derivation of adult cartilages in the clawed frog, Xenopus laevis. Integrative and comparative biology 48 (5), 681–696. https://doi.org/10.1093/icb/icn077.

Gu, Y., Zheng, G., Xu, M., Li, Y., Chen, X., Zhu, W., Tong, Y., Chung, S.K., Liu, K.J., Shen, J., 2012. Caveolin-1 regulates nitric oxide-mediated matrix metalloproteinases activity and blood-brain barrier permeability in focal cerebral ischemia and reperfusion injury. Journal of neurochemistry 120 (1), 147–156. https://doi.org/10.1111/j.1471-4159.2011.07542.x.

Guirland, C., Suzuki, S., Kojima, M., Lu, B., Zheng, J.Q., 2004. Lipid rafts mediate chemotropic guidance of nerve growth cones. Neuron 42 (1), 51–62. https://doi.org/10.1016/s0896-6273(04)00157-6.

Guirland, C., Zheng, J.Q., 2007. Membrane lipid rafts and their role in axon guidance. Advances in experimental medicine and biology 621, 144–155. https://doi.org/10.1007/978-0-387-76715-4_11.

Gupta, R., Toufaily, C., Annabi, B., 2014. Caveolin and cavin family members: Dual roles in cancer. Biochimie 107, 188–202. https://doi.org/10.1016/j.biochi.2014.09.010.

Gurdon, J.B., Lemaire, P., Mohun, T.J., 1997. Myogenesis in Xenopus embryos. Methods in cell biology 52, 53–66.

Gustincich, S., Schneider, C., 1993. Serum deprivation response gene is induced by serum starvation but not by contact inhibition. Cell growth & differentiation : the molecular biology journal of the American Association for Cancer Research 4 (9), 753–760.

Gutmann, E. (Ed.), 1962. The Denervated Muscle. Springer US; Imprint; Springer, Boston, MA, 1 online resource.

Gutmann, E., Zelená, J., 1962. Morphological Changes in the Denervated Muscle, in: Gutmann, E. (Ed.), The Denervated Muscle, vol. 34. Springer US; Imprint; Springer, Boston, MA, pp. 57–102.

Haenlin, M., Kunisch, M., Kramatschek, B., Campos-Ortega, J., 1994. Genomic regions regulating early embryonic expression of the Drosophila neurogenic gene Delta. Mechanisms of Development 47 (1), 99–110. https://doi.org/10.1016/0925-4773(94)90099-X.

Hagiwara, Y., Sasaoka, T., Araishi, K., Imamura, M., Yorifuji, H., Nonaka, I., Ozawa, E., Kikuchi, T., 2000. Caveolin-3 deficiency causes muscle degeneration in mice. Human molecular genetics 9 (20), 3047–3054. https://doi.org/10.1093/hmg/9.20.3047.

Hailstones, D., Sleer, L.S., Parton, R.G., Stanley, K.K., 1998. Regulation of caveolin and caveolae by cholesterol in MDCK cells. Journal of lipid research 39 (2), 369–379.

Hall, A., Lalli, G., 2010. Rho and Ras GTPases in axon growth, guidance, and branching. Cold Spring Harbor perspectives in biology 2 (2), a001818. https://doi.org/10.1101/cshperspect.a001818.

Hansen, C.G., Bright, N.A., Howard, G., Nichols, B.J., 2009. SDPR induces membrane curvature and functions in the formation of caveolae. Nature cell biology 11 (7), 807–814. https://doi.org/10.1038/ncb1887.

Hansen, C.G., Howard, G., Nichols, B.J., 2011. Pacsin 2 is recruited to caveolae and functions in caveolar biogenesis. Journal of Cell Science 124 (Pt 16), 2777–2785. https://doi.org/10.1242/jcs.084319.

Hansen, C.G., Shvets, E., Howard, G., Riento, K., Nichols, B.J., 2013. Deletion of cavin genes reveals tissue-specific mechanisms for morphogenesis of endothelial caveolae. Nat Comms 4, 1831. https://doi.org/10.1038/ncomms2808.

Harland, R., 2000. Neural induction. Current opinion in genetics & development 10 (4), 357–362.

Hartenstein, V., 1989a. Early neurogenesis in xenopus: The spatio-temporal pattern of proliferation and cell lineages in the embryonic spinal cord. Neuron 3 (4), 399–411. https://doi.org/10.1016/0896-6273(89)90200-6.

Hartenstein, V., 1989b. Early neurogenesis in Xenopus: the spatio-temporal pattern of proliferation and cell lineages in the embryonic spinal cord. Neuron 3 (4), 399–411.

Hartenstein, V., 1993. Early pattern of neuronal differentiation in the Xenopus embryonic brainstem and spinal cord. J. Comp. Neurol. 328 (2), 213–231. https://doi.org/10.1002/cne.903280205.

Harvey, R.D., Calaghan, S.C., 2012. Caveolae create local signalling domains through their distinct protein content, lipid profile and morphology. Journal of molecular and cellular cardiology 52 (2), 366–375. https://doi.org/10.1016/j.yjmcc.2011.07.007.

Hayer, A., Stoeber, M., Bissig, C., Helenius, A., 2010. Biogenesis of Caveolae: Stepwise Assembly of Large Caveolin and Cavin Complexes. Traffic 11 (3), 361–382. https://doi.org/10.1111/j.1600-0854.2009.01023.x.

Hazarika, P., Dham, N., Patel, P., Cho, M., Weidner, D., Goldsmith, L., Duvic, M., 1999. Flotillin 2 is distinct from epidermal surface antigen (ESA) and is associated with filopodia formation. J. Cell. Biochem. 75 (1), 147–159. https://doi.org/10.1002/(SICI)1097-4644(19991001)75:1<147:AID-JCB15>3.0.CO;2-D.

Head, B.P., Hu, Y., Finley, J.C., Saldana, M.D., Bonds, J.A., Miyanohara, A., Niesman, I.R., Ali, S.S., Murray, F., Insel, P.A., Roth, D.M., Patel, H.H., Patel, P.M., 2011. Neuron-targeted caveolin-1 protein enhances signaling and promotes arborization of primary neurons. The Journal of biological chemistry 286 (38), 33310–33321. https://doi.org/10.1074/jbc.M111.255976.

Head, B.P., Peart, J.N., Panneerselvam, M., Yokoyama, T., Pearn, M.L., Niesman, I.R., Bonds, J.A., Schilling, J.M., Miyanohara, A., Headrick, J., Ali, S.S., Roth, D.M., Patel, P.M., Patel, H.H., Ferreira, S.T., 2010. Loss of Caveolin-1 Accelerates Neurodegeneration and Aging. PloS one 5 (12), e15697. https://doi.org/10.1371/journal.pone.0015697.

Heasman, S.J., Ridley, A.J., 2008. Mammalian Rho GTPases: new insights into their functions from in vivo studies. Nature reviews. Molecular cell biology 9 (9), 690–701. https://doi.org/10.1038/nrm2476.

Heck, C.S., Davis, H.L., 1988. Effect of denervation and nerve extract on ultrastructure of muscle. Experimental neurology 100 (1), 139–153. https://doi.org/10.1016/0014-4886(88)90207-5.

Heckman, C.J., Lee, R.H., Brownstone, R.M., 2003. Hyperexcitable dendrites in motoneurons and their neuromodulatory control during motor behavior. Trends in Neurosciences 26 (12), 688–695. https://doi.org/10.1016/j.tins.2003.10.002.

Hellard, D., Brosenitsch, T., Fritzsch, B., Katz, D.M., 2004. Cranial sensory neuron development in the absence of brain-derived neurotrophic factor in BDNF/Bax double null mice. Developmental biology 275 (1), 34–43. https://doi.org/10.1016/j.ydbio.2004.07.021.

Henley, J.R., Krueger, E.W., Oswald, B.J., McNiven, M.A., 1998. Dynamin-mediated internalization of caveolae. J Cell Biol 141 (1), 85–99. https://doi.org/10.1083/jcb.141.1.85.

Herzer, S., Meldner, S., Rehder, K., Gröne, H.-J., Nordström, V., 2016. Lipid microdomain modification sustains neuronal viability in models of Alzheimer's disease. Acta neuropathologica communications 4 (1), 103. https://doi.org/10.1186/s40478-016-0354-z.

Hill, M.M., Bastiani, M., Luetterforst, R., Kirkham, M., Kirkham, A., Nixon, S.J., Walser, P., Abankwa, D., Oorschot, V.M.J., Martin, S., Hancock, J.F., Parton, R.G., 2008. PTRF-Cavin, a Conserved Cytoplasmic Protein Required for Caveola Formation and Function. Cell 132 (1), 113–124. https://doi.org/10.1016/j.cell.2007.11.042.

Hník, P., 1962. Rate of Denervation Muscle Atrophy, in: Gutmann, E. (Ed.), The Denervated Muscle, vol. 139. Springer US; Imprint; Springer, Boston, MA, pp. 341–375.

Ho, C.-C., Huang, P.-H., Huang, H.-Y., Chen, Y.-H., Yang, P.-C., Hsu, S.-M., 2002. Up-regulated caveolin-1 accentuates the metastasis capability of lung adenocarcinoma by inducing filopodia formation. The American journal of pathology 161 (5), 1647–1656. https://doi.org/10.1016/S0002-9440(10)64442-2.

Hommelgaard, A.M., Roepstorff, K., Vilhardt, F., Torgersen, M.L., Sandvig, K., van Deurs, B., 2005. Caveolae: stable membrane domains with a potential for internalization. Traffic 6 (9), 720–724. https://doi.org/10.1111/j.1600-0854.2005.00314.x.

Hotchin, N.A., Hall, A., 1995. The assembly of integrin adhesion complexes requires both extracellular matrix and intracellular rho/rac GTPases. J Cell Biol 131 (6 Pt 2), 1857–1865. https://doi.org/10.1083/jcb.131.6.1857.

Huang, J.K., Dorey, K., Ishibashi, S., Amaya, E., 2007. BDNF promotes target innervation of Xenopus mandibular trigeminal axons in vivo. BMC developmental biology 7, 59. https://doi.org/10.1186/1471-213X-7-59.

Izumi, Y., Hirai, S.-i., Tamai, Y., Fujise-Matsuoka, A., Nishimura, Y., Ohno, S., 1997. A Protein Kinase C -binding Protein SRBC Whose Expression Is Induced by Serum Starvation. Journal of Biological Chemistry 272 (11), 7381–7389. https://doi.org/10.1074/jbc.272.11.7381.

Jaalouk, D.E., Lammerding, J., 2009. Mechanotransduction gone awry. Nature reviews. Molecular cell biology 10 (1), 63–73. https://doi.org/10.1038/nrm2597.

Jansa, P., 1998. Cloning and functional characterization of PTRF, a novel protein which induces dissociation of paused ternary transcription complexes. The EMBO journal 17 (10), 2855–2864. https://doi.org/10.1093/emboj/17.10.2855.

Jasmin, J.-F., Yang, M., Iacovitti, L., Lisanti, M.P., 2009. Genetic ablation of caveolin-1 increases neural stem cell proliferation in the subventricular zone (SVZ) of the adult mouse brain. Cell cycle (Georgetown, Tex.) 8 (23), 3978–3983. https://doi.org/10.4161/cc.8.23.10206.

Jennemann, R., Sandhoff, R., Wang, S., Kiss, E., Gretz, N., Zuliani, C., Martin-Villalba, A., Jäger, R., Schorle, H., Kenzelmann, M., Bonrouhi, M., Wiegandt, H., Gröne, H.-J., 2005. Cell-specific deletion of glucosylceramide synthase in brain leads to severe neural defects after birth. Proceedings of the National Academy of Sciences 102 (35), 12459–12464. https://doi.org/10.1073/pnas.0500893102.

Jennings, B., Preiss, A., Delidakis, C., Bray, S., 1994. The Notch signalling pathway is required for Enhancer of split bHLH protein expression during neurogenesis in the Drosophila embryo. Development 120 (12), 3537–3548.

Joshi, B., Bastiani, M., Strugnell, S.S., Boscher, C., Parton, R.G., Nabi, I.R., 2012. Phosphocaveolin-1 is a mechanotransducer that induces caveola biogenesis via Egr1

transcriptional regulation. J Cell Biol 199 (3), 425–435. https://doi.org/10.1083/jcb.201207089.

Joshi, B., Strugnell, S.S., Goetz, J.G., Kojic, L.D., Cox, M.E., Griffith, O.L., Chan, S.K., Jones, S.J., Leung, S.-P., Masoudi, H., Leung, S., Wiseman, S.M., Nabi, I.R., 2008. Phosphorylated Caveolin-1 Regulates Rho/ROCK-Dependent Focal Adhesion Dynamics and Tumor Cell Migration and Invasion. Cancer Research 68 (20), 8210–8220. https://doi.org/10.1158/0008-5472.CAN-08-0343.

Ju, H., Zou, R., Venema, V.J., Venema, R.C., 1997. Direct interaction of endothelial nitric-oxide synthase and caveolin-1 inhibits synthase activity. Journal of Biological Chemistry 272 (30), 18522–18525. https://doi.org/10.1074/jbc.272.30.18522.

Kamiguchi, H., 2006. The region-specific activities of lipid rafts during axon growth and guidance. Journal of neurochemistry 98 (2), 330–335. https://doi.org/10.1111/j.1471-4159.2006.03888.x.

Kang, M.J., Chung, Y.H., Hwang, C.I., Murata, M., Fujimoto, T., Mook-Jung, I.H., Cha, C.I., Park, W.Y., 2006. Caveolin-1 upregulation in senescent neurons alters amyloid precursor protein processing. Experimental & molecular medicine 38 (2), 126–133. https://doi.org/10.1038/emm.2006.16.

Kashef, J., Köhler, A., Kuriyama, S., Alfandari, D., Mayor, R., Wedlich, D., 2009. Cadherin-11 regulates protrusive activity in Xenopus cranial neural crest cells upstream of Trio and the small GTPases. Genes & Development 23 (12), 1393–1398. https://doi.org/10.1101/gad.519409.

Kassan, A., Egawa, J., Zhang, Z., Almenar-Queralt, A., Nguyen, Q.M., Lajevardi, Y., Kim, K., Posadas, E., Jeste, D.V., Roth, D.M., Patel, P.M., Patel, H.H., Head, B.P., 2017. Caveolin-1 regulation of disrupted-in-schizophrenia-1 as a potential therapeutic target for schizophrenia. Journal of neurophysiology 117 (1), 436–444. https://doi.org/10.1152/jn.00481.2016.

Keller, R., Cooper, M.S., Danilchik, M., Tibbetts, P., Wilson, P.A., 1989. Cell intercalation during notochord development in Xenopus laevis. The Journal of experimental zoology 251 (2), 134–154. https://doi.org/10.1002/jez.1402510204.

Kim, M.D., Kolodziej, P., Chiba, A., 2002. Growth Cone Pathfinding and Filopodial Dynamics Are Mediated Separately by Cdc42 Activation. The Journal of neuroscience : the official journal of the Society for Neuroscience 22 (5), 1794–1806. https://doi.org/10.1523/JNEUROSCI.22-05-01794.2002.

Kirkham, M., Nixon, S.J., Howes, M.T., Abi-Rached, L., Wakeham, D.E., Hanzal-Bayer, M., Ferguson, C., Hill, M.M., Fernandez-Rojo, M., Brown, D.A., Hancock, J.F., Brodsky, F.M., Parton, R.G., 2008. Evolutionary analysis and molecular dissection of caveola biogenesis. Journal of Cell Science 121 (Pt 12), 2075–2086. https://doi.org/10.1242/jcs.024588.

Kishi, M., Mizuseki, K., Sasai, N., Yamazaki, H., Shiota, K., Nakanishi, S., Sasai, Y., 2000. Requirement of Sox2-mediated signaling for differentiation of early Xenopus neuroectoderm. Development (Cambridge, England) 127 (4), 791–800.

Knowles, R.B., Wyart, C., Buldyrev, S.V., Cruz, L., Urbanc, B., Hasselmo, M.E., Stanley, H.E., Hyman, B.T., 1999. Plaque-induced neurite abnormalities: implications for disruption of neural networks in Alzheimer's disease. Proceedings of the National Academy of Sciences 96 (9), 5274–5279. https://doi.org/10.1073/pnas.96.9.5274.

Koestner, U., Shnitsar, I., Linnemannstöns, K., Hufton, A.L., Borchers, A., 2008. Semaphorin and neuropilin expression during early morphogenesis of Xenopus laevis. Dev. Dyn. 237 (12), 3853–3863. https://doi.org/10.1002/dvdy.21785.

Kogo, H., Fujimoto, T., 2000. Caveolin-1 isoforms are encoded by distinct mRNAs. Identification Of mouse caveolin-1 mRNA variants caused by alternative transcription initiation and splicing. FEBS letters 465 (2-3), 119–123.

Kovtun, O., Tillu, V.A., Ariotti, N., Parton, R.G., Collins, B.M., 2015. Cavin family proteins and the assembly of caveolae. Journal of Cell Science 128 (7), 1269–1278. https://doi.org/10.1242/jcs.167866.

Kovtun, O., Tillu, V.A., Jung, W., Leneva, N., Ariotti, N., Chaudhary, N., Mandyam, R.A., Ferguson, C., Morgan, G.P., Johnston, W.A., Harrop, S.J., Alexandrov, K., Parton, R.G., Collins, B.M., 2014. Structural insights into the organization of the cavin membrane coat complex. Developmental cell 31 (4), 405–419. https://doi.org/10.1016/j.devcel.2014.10.002.

Kozma, R., Ahmed, S., Best, A., Lim, L., 1995. The Ras-related protein Cdc42Hs and bradykinin promote formation of peripheral actin microspikes and filopodia in Swiss 3T3 fibroblasts. Molecular and Cellular Biology 15 (4), 1942–1952. https://doi.org/10.1128/mcb.15.4.1942.

Kunisch, M., Haenlin, M., Campos-Ortega, J.A., 1994. Lateral inhibition mediated by the Drosophila neurogenic gene delta is enhanced by proneural proteins. Proceedings of the National Academy of Sciences 91 (21), 10139–10143. https://doi.org/10.1073/pnas.91.21.10139.

Kuo, J.S., Patel, M., Gamse, J., Merzdorf, C., Liu, X., Apekin, V., Sive, H., 1998. Opl: a zinc finger protein that regulates neural determination and patterning in Xenopus. Development 125 (15), 2867–2882.

Kuroda, H., Wessely, O., Robertis, E.M.D., Christof Niehrs, 2004. Neural Induction in Xenopus: Requirement for Ectodermal and Endomesodermal Signals via Chordin, Noggin, β-Catenin, and Cerberus. PLoS Biol 2 (5), e92. https://doi.org/10.1371/journal.pbio.0020092.

Kurzchalia, T.V., Dupree, P., Parton, R.G., Kellner, R., Virta, H., Lehnert, M., Simons, K., 1992. VIP21, a 21-kD membrane protein is an integral component of trans-Golgi-network-derived transport vesicles. The Journal of cell biology 118 (5), 1003–1014.

Kwon, H., Jeong, K., Pak, Y., 2009. Identification of pY19-caveolin-2 as a positive regulator of insulin-stimulated actin cytoskeleton-dependent mitogenesis. Journal of cellular and molecular medicine 13 (8A), 1549–1564. https://doi.org/10.1111/j.1582-4934.2009.00391.x.

Lalonde, R., Strazielle, C., 2011. Brain regions and genes affecting limb-clasping responses. Brain research reviews 67 (1-2), 252–259. https://doi.org/10.1016/j.brainresrev.2011.02.005.

Lang, D.M., Lommel, S., Jung, M., Ankerhold, R., Petrausch, B., Laessing, U., Wiechers, M.F., Plattner, H., Stuermer, C.A., 1998. Identification of reggie-1 and reggie-2 as plasmamembrane-associated proteins which cocluster with activated GPI-anchored cell adhesion molecules in non-caveolar micropatches in neurons. Journal of neurobiology 37 (4), 502–523. https://doi.org/10.1002/(sici)1097-4695(199812)37:4<502:aid-neu2>3.0.co;2-s.

Langhorst, M.F., Jaeger, F.A., Mueller, S., Sven Hartmann, L., Luxenhofer, G., Stuermer, C.A.O., 2008. Reggies/flotillins regulate cytoskeletal remodeling during neuronal differentiation via CAP/ponsin and Rho GTPases. European journal of cell biology 87 (12), 921–931. https://doi.org/10.1016/j.ejcb.2008.07.001.

Langhorst, M.F., Reuter, A., Stuermer, C.A.O., 2005. Scaffolding microdomains and beyond: the function of reggie/flotillin proteins. Cellular and molecular life sciences : CMLS 62 (19-20), 2228–2240. https://doi.org/10.1007/s00018-005-5166-4.

Lawson, C.D., Burridge, K., 2014. The on-off relationship of Rho and Rac during integrin-mediated adhesion and cell migration. Small GTPases 5, e27958. https://doi.org/10.4161/sgtp.27958.

Le Lay, S., Hajduch, E., Lindsay, M.R., Le Liepvre, X., Thiele, C., Ferre, P., Parton, R.G., Kurzchalia, T., Simons, K., Dugail, I., 2006. Cholesterol-induced caveolin targeting to lipid droplets in adipocytes: a role for caveolar endocytosis. Traffic (Copenhagen, Denmark) 7 (5), 549–561. https://doi.org/10.1111/j.1600-0854.2006.00406.x.

Le Lay, S., Kurzchalia, T.V., 2005. Getting rid of caveolins: phenotypes of caveolin-deficient animals. Biochimica et biophysica acta 1746 (3), 322–333. https://doi.org/10.1016/j.bbamcr.2005.06.001.

Lebbink, M.N., Jiménez, N., Vocking, K., Hekking, L.H., Verkleij, A.J., Post, J.A., 2010. Spiral coating of the endothelial caveolar membranes as revealed by electron tomography and template matching. Traffic (Copenhagen, Denmark) 11 (1), 138–150. https://doi.org/10.1111/j.1600-0854.2009.01008.x.

Lecourtois, M., Schweisguth, F., 1995. The neurogenic suppressor of hairless DNA-binding protein mediates the transcriptional activation of the enhancer of split complex genes triggered by Notch signaling. Genes & Development 9 (21), 2598–2608. https://doi.org/10.1101/gad.9.21.2598.

Lee, H., Xie, L., Luo, Y., Lee, S.-Y., Lawrence, D.S., Wang, X.B., Sotgia, F., Lisanti, M.P., Zhang, Z.-Y., 2006. Identification of phosphocaveolin-1 as a novel protein tyrosine phosphatase 1B substrate. Biochemistry 45 (1), 234–240. https://doi.org/10.1021/bi051560j.

Lee, J.E., Hollenberg, S.M., Snider, L., Turner, D.L., Lipnick, N., Weintraub, H., 1995. Conversion of Xenopus ectoderm into neurons by NeuroD, a basic helix-loop-helix protein. Science 268 (5212), 836–844. https://doi.org/10.1126/science.7754368.

Lentini, D., Guzzi, F., Pimpinelli, F., Zaninetti, R., Cassetti, A., Coco, S., Maggi, R., Parenti, M., 2008. Polarization of caveolins and caveolae during migration of immortalized neurons. Journal of neurochemistry 104 (2), 514–523. https://doi.org/10.1111/j.1471-4159.2007.05005.x.

Li, S., Couet, J., Lisanti, M.P., 1996a. Src tyrosine kinases, Galpha subunits, and H-Ras share a common membrane-anchored scaffolding protein, caveolin. Caveolin binding negatively regulates the auto-activation of Src tyrosine kinases. The Journal of biological chemistry 271 (46), 29182–29190.

Li, S., Galbiati, F., Volonte', D., Sargiacomo, M., Engelman, J.A., Das, K., Scherer, P.E., Lisanti, M.P., 1998. Mutational analysis of caveolin-induced vesicle formation. FEBS letters 434 (1-2), 127–134. https://doi.org/10.1016/S0014-5793(98)00945-4.

Li, S., Seitz, R., Lisanti, M.P., 1996b. Phosphorylation of Caveolin by Src Tyrosine Kinases. Journal of Biological Chemistry 271 (7), 3863–3868. https://doi.org/10.1074/jbc.271.7.3863.

Li, S., Song, K.S., Koh, S.S., Kikuchi, A., Lisanti, M.P., 1996c. Baculovirus-based expression of mammalian caveolin in Sf21 insect cells. A model system for the biochemical and morphological study of caveolae biogenesis. Journal of Biological Chemistry 271 (45), 28647–28654. https://doi.org/10.1074/jbc.271.45.28647.

Li, W.C., Perrins, R., Soffe, S.R., Yoshida, M., Walford, A., Roberts, A., 2001. Defining classes of spinal interneuron and their axonal projections in hatchling Xenopus laevis tadpoles. J. Comp. Neurol. 441 (3), 248–265. https://doi.org/10.1002/cne.1410.

Li, W.-C., Soffe, S.R., Roberts, A., 2003. The Spinal Interneurons and Properties of Glutamatergic Synapses in a Primitive Vertebrate Cutaneous Flexion Reflex. The Journal of neuroscience : the official journal of the Society for Neuroscience 23 (27), 9068–9077. https://doi.org/10.1523/JNEUROSCI.23-27-09068.2003.

Li, Y., Liu, L.-B., Ma, T., Wang, P., Xue, Y.-X., 2015. Effect of caveolin-1 on the expression of tight junction-associated proteins in rat glioma-derived microvascular endothelial cells. International Journal of Clinical and Experimental Pathology 8 (10), 13067–13074.

Li, Y., Luo, J., Lau, W.-M., Zheng, G., Fu, S., Wang, T.-T., Zeng, H.-P., So, K.-F., Chung, S.K., Tong, Y., Liu, K., Shen, J., 2011. Caveolin-1 plays a crucial role in inhibiting neuronal differentiation of neural stem/progenitor cells via VEGF signaling-dependent pathway. PloS one 6 (8), e22901. https://doi.org/10.1371/journal.pone.0022901.

Li, Z., Aizenman, C.D., Cline, H.T., 2002. Regulation of Rho GTPases by Crosstalk and Neuronal Activity In Vivo. Neuron 33 (5), 741–750. https://doi.org/10.1016/S0896-6273(02)00621-9.

Lienkamp, S.S., Liu, K., Karner, C.M., Carroll, T.J., Ronneberger, O., Wallingford, J.B., Walz, G., 2012. Vertebrate kidney tubules elongate using a planar cell polarity-dependent, rosette-based mechanism of convergent extension. Nat Genet 44 (12), 1382–1387. https://doi.org/10.1038/ng.2452.

Lim, Y.-W., Lo, H.P., Ferguson, C., Martel, N., Giacomotto, J., Gomez, G.A., Yap, A.S., Hall, T.E., Parton, R.G., 2017. Caveolae Protect Notochord Cells against Catastrophic Mechanical Failure during Development. Current biology : CB 27 (13), 1968-1981.e7. https://doi.org/10.1016/j.cub.2017.05.067.

Lipardi, C., Mora, R., Colomer, V., Paladino, S., Nitsch, L., Rodriguez-Boulan, E., Zurzolo, C., 1998. Caveolin transfection results in caveolae formation but not apical sorting of glycosylphosphatidylinositol (GPI)-anchored proteins in epithelial cells. J Cell Biol 140 (3), 617–626. https://doi.org/10.1083/jcb.140.3.617.

Liu, J., Oh, P., Horner, T., Rogers, R.A., Schnitzer, J.E., 1997. Organized endothelial cell surface signal transduction in caveolae distinct from glycosylphosphatidylinositol-anchored protein microdomains. Journal of Biological Chemistry 272 (11), 7211–7222. https://doi.org/10.1074/jbc.272.11.7211.

Liu, J., Weaver, J., Jin, X., Zhang, Y., Xu, J., Liu, K.J., Li, W., Liu, W., 2016. Nitric Oxide Interacts with Caveolin-1 to Facilitate Autophagy-Lysosome-Mediated Claudin-5 Degradation in Oxygen-Glucose Deprivation-Treated Endothelial Cells. Molecular neurobiology 53 (9), 5935–5947. https://doi.org/10.1007/s12035-015-9504-8.

Liu, L., Brown, D., McKee, M., LeBrasseur, N.K., Yang, D., Albrecht, K.H., Ravid, K., Pilch, P.F., 2008. Deletion of Cavin/PTRF Causes Global Loss of Caveolae, Dyslipidemia, and Glucose Intolerance. Cell Metabolism 8 (4), 310–317. https://doi.org/10.1016/j.cmet.2008.07.008.

Liu, L., Pilch, P.F., 2008. A critical role of cavin (polymerase I and transcript release factor) in caveolae formation and organization. Journal of Biological Chemistry 283 (7), 4314–4322. https://doi.org/10.1074/jbc.M707890200.

Liu, P., Li, W.P., Machleidt, T., Anderson, R.G., 1999. Identification of caveolin-1 in lipoprotein particles secreted by exocrine cells. Nature cell biology 1 (6), 369–375. https://doi.org/10.1038/14067.

Liu, Y., Liang, Z., Liu, J., Zou, W., Li, X., Wang, Y., An, L., 2013. Downregulation of caveolin-1 contributes to the synaptic plasticity deficit in the hippocampus of aged rats. Neural regeneration research 8 (29), 2725–2733. https://doi.org/10.3969/j.issn.1673-5374.2013.29.004.

Lo, H.P., Hall, T.E., Parton, R.G., 2016. Mechanoprotection by skeletal muscle caveolae. Bioarchitecture 6 (1), 22–27. https://doi.org/10.1080/19490992.2015.1131891.

Lo, H.P., Nixon, S.J., Hall, T.E., Cowling, B.S., Ferguson, C., Morgan, G.P., Schieber, N.L., Fernandez-Rojo, M.A., Bastiani, M., Floetenmeyer, M., Martel, N., Laporte, J., Pilch, P.F., Parton, R.G., 2015. The caveolin-cavin system plays a conserved and critical role

in mechanoprotection of skeletal muscle. J Cell Biol 210 (5), 833–849. https://doi.org/10.1083/jcb.201501046.

Lowery, L.A., Faris, A.E.R., Stout, A., van Vactor, D., 2012. Neural Explant Cultures from Xenopus laevis. Journal of visualized experiments : JoVE (68), e4232. https://doi.org/10.3791/4232.

Ludwig, A., Howard, G., Mendoza-Topaz, C., Deerinck, T., Mackey, M., Sandin, S., Ellisman, M.H., Nichols, B.J., Hughson, F., 2013. Molecular Composition and Ultrastructure of the Caveolar Coat Complex. PLoS Biol 11 (8), e1001640. https://doi.org/10.1371/journal.pbio.1001640.

Luo, L., 2000. Rho GTPases in neuronal morphogenesis. Nat Rev Neurosci 1 (3), 173–180. https://doi.org/10.1038/35044547.

MacDonald, J.L., Fame, R.M., Gillis-Buck, E.M., Macklis, J.D., 2018. Caveolin1 Identifies a Specific Subpopulation of Cerebral Cortex Callosal Projection Neurons (CPN) Including Dual Projecting Cortical Callosal/Frontal Projection Neurons (CPN/FPN). eNeuro 5 (1). https://doi.org/10.1523/ENEURO.0234-17.2017.

Machleidt, T., Li, W.P., Liu, P., Anderson, R.G., 2000. Multiple domains in caveolin-1 control its intracellular traffic. J Cell Biol 148 (1), 17–28. https://doi.org/10.1083/jcb.148.1.17.

Malek-Ahmadi, M., Perez, S.E., Chen, K., Mufson, E.J., 2016. Neuritic and Diffuse Plaque Associations with Memory in Non-Cognitively Impaired Elderly. Journal of Alzheimer's disease : JAD 53 (4), 1641–1652. https://doi.org/10.3233/JAD-160365.

Mandyam, C.D., Schilling, J.M., Cui, W., Egawa, J., Niesman, I.R., Kellerhals, S.E., Staples, M.C., Busija, A.R., Risbrough, V.B., Posadas, E., Grogman, G.C., Chang, J.W., Roth, D.M., Patel, P.M., Patel, H.H., Head, B.P., 2017. Neuron-Targeted Caveolin-1 Improves Molecular Signaling, Plasticity, and Behavior Dependent on the Hippocampus in Adult and Aged Mice. Biological psychiatry 81 (2), 101–110. https://doi.org/10.1016/j.biopsych.2015.09.020.

Marshak, S., Nikolakopoulou, A.M., Dirks, R., Martens, G.J., Cohen-Cory, S., 2007. Cell-autonomous TrkB signaling in presynaptic retinal ganglion cells mediates axon arbor growth and synapse maturation during the establishment of retinotectal synaptic connectivity. The Journal of neuroscience : the official journal of the Society for Neuroscience 27 (10), 2444–2456. https://doi.org/10.1523/JNEUROSCI.4434-06.2007.

Mason, S.W., Sander, E.E., Grummt, I., 1997. Identification of a transcript release activity acting on ternary transcription complexes containing murine RNA polymerase I. EMBO J 16 (1), 163–172. https://doi.org/10.1093/emboj/16.1.163.

Matsuura, R., Tanaka, H., Go, M.J., 2004. Distinct functions of Rac1 and Cdc42 during axon guidance and growth cone morphogenesis in Drosophila. European Journal of Neuroscience 19 (1), 21–31. https://doi.org/10.1046/j.1460-9568.2003.03084.x.

Maximillian Staps, 2016. Functional analysis of Caveolin 1α in Xenopus development. Bachelor thesis. Marburg.

Mayor, S., Parton, R.G., Donaldson, J.G., 2014. Clathrin-independent pathways of endocytosis. Cold Spring Harbor perspectives in biology 6 (6). https://doi.org/10.1101/cshperspect.a016758.

McGrew, L.L., Hoppler, S., Moon, R.T., 1997. Wnt and FGF pathways cooperatively pattern anteroposterior neural ectoderm in Xenopus. Mechanisms of Development 69 (1-2), 105–114. https://doi.org/10.1016/S0925-4773(97)00160-3.

McMahon, K.-A., Zajicek, H., Li, W.-P., Peyton, M.J., Minna, J.D., Hernandez, V.J., Luby-Phelps, K., Anderson, R.G.W., 2009. SRBC/cavin-3 is a caveolin adapter protein that

regulates caveolae function. EMBO J 28 (8), 1001–1015. https://doi.org/10.1038/emboj.2009.46.

Megason, S.G., McMahon, A.P., 2002. A mitogen gradient of dorsal midline Wnts organizes growth in the CNS. Development 129 (9), 2087–2098.

Michaely, P.A., Mineo, C., Ying, Y.s., Anderson, R.G., 1999. Polarized distribution of endogenous Rac1 and RhoA at the cell surface. Journal of Biological Chemistry 274 (30), 21430–21436. https://doi.org/10.1074/jbc.274.30.21430.

Midrio, M., 2006. The denervated muscle: facts and hypotheses. A historical review. European journal of applied physiology 98 (1), 1–21. https://doi.org/10.1007/s00421-006-0256-z.

Mikol, D.D., Hong, H.L., Cheng, H.L., Feldman, E.L., 1999. Caveolin-1 expression in Schwann cells. Glia 27 (1), 39–52.

Mizuseki, K., Kishi, M., Matsui, M., Nakanishi, S., Sasai, Y., 1998a. Xenopus Zic-related-1 and Sox-2, two factors induced by chordin, have distinct activities in the initiation of neural induction. Development (Cambridge, England) 125 (4), 579–587.

Mizuseki, K., Kishi, M., Shiota, K., Nakanishi, S., Sasai, Y., 1998b. SoxD: an essential mediator of induction of anterior neural tissues in Xenopus embryos. Neuron 21 (1), 77–85.

Mobley, B.A., Eisenberg, B.R., 1975. Sizes of components in frog skeletal muscle measured by methods of stereology. The Journal of general physiology 66 (1), 31–45. https://doi.org/10.1085/jgp.66.1.31.

Monier, S., Parton, R.G., Vogel, F., Behlke, J., Henske, A., Kurzchalia, T.V., 1995. VIP21-caveolin, a membrane protein constituent of the caveolar coat, oligomerizes in vivo and in vitro. Molecular biology of the cell 6 (7), 911–927.

Moody, S.A., Je, H.-S., 2002. Neural induction, neural fate stabilization, and neural stem cells. TheScientificWorldJournal 2, 1147–1166. https://doi.org/10.1100/tsw.2002.217.

Moody, S.A., Miller, V., Spanos, A., Frankfurter, A., 1996. Developmental expression of a neuron-specific ?: -tubulin in frog (Xenopus laevis): A marker for growing axons during the embryonic period. J. Comp. Neurol. 364 (2), 219–230. https://doi.org/10.1002/(SICI)1096-9861(19960108)364:2<219:AID-CNE3>3.0.CO;2-8.

Morén, B., Shah, C., Howes, M.T., Schieber, N.L., McMahon, H.T., Parton, R.G., Daumke, O., Lundmark, R., 2012. EHD2 regulates caveolar dynamics via ATP-driven targeting and oligomerization. Molecular biology of the cell 23 (7), 1316–1329. https://doi.org/10.1091/mbc.E11-09-0787.

Mumm, J.S., Schroeter, E.H., Saxena, M.T., Griesemer, A., Tian, X., Pan, D.J., Ray, W.J., Kopan, R., 2000. A ligand-induced extracellular cleavage regulates gamma-secretase-like proteolytic activation of Notch1. Molecular cell 5 (2), 197–206. https://doi.org/10.1016/s1097-2765(00)80416-5.

Munderloh, C., Solis, G.P., Bodrikov, V., Jaeger, F.A., Wiechers, M., Málaga-Trillo, E., Stuermer, C.A.O., 2009. Reggies/flotillins regulate retinal axon regeneration in the zebrafish optic nerve and differentiation of hippocampal and N2a neurons. The Journal of neuroscience : the official journal of the Society for Neuroscience 29 (20), 6607–6615. https://doi.org/10.1523/JNEUROSCI.0870-09.2009.

Münsterberg, A.E., Lassar, A.B., 1995. Combinatorial signals from the neural tube, floor plate and notochord induce myogenic bHLH gene expression in the somite. Development 121 (3), 651–660.

Murata, M., Peränen, J., Schreiner, R., Wieland, F., Kurzchalia, T.V., Simons, K., 1995. VIP21/caveolin is a cholesterol-binding protein. Proceedings of the National Academy of Sciences 92 (22), 10339–10343. https://doi.org/10.1073/pnas.92.22.10339.

Muriel, O., Echarri, A., Hellriegel, C., Pavón, D.M., Beccari, L., del Pozo, M.A., 2011. Phosphorylated filamin A regulates actin-linked caveolae dynamics. Journal of Cell Science 124 (Pt 16), 2763–2776. https://doi.org/10.1242/jcs.080804.

Myers, J.P., Gomez, T.M., 2011. Focal adhesion kinase promotes integrin adhesion dynamics necessary for chemotropic turning of nerve growth cones. The Journal of neuroscience : the official journal of the Society for Neuroscience 31 (38), 13585–13595. https://doi.org/10.1523/JNEUROSCI.2381-11.2011.

Myers, J.P., Santiago-Medina, M., Gomez, T.M., 2011. Regulation of axonal outgrowth and pathfinding by integrin-ECM interactions. Developmental neurobiology 71 (11), 901–923. https://doi.org/10.1002/dneu.20931.

Naito, D., Ogata, T., Hamaoka, T., Nakanishi, N., Miyagawa, K., Maruyama, N., Kasahara, T., Taniguchi, T., Nishi, M., Matoba, S., Ueyama, T., 2015. The coiled-coil domain of MURC/cavin-4 is involved in membrane trafficking of caveolin-3 in cardiomyocytes. American journal of physiology. Heart and circulatory physiology 309 (12), H2127-36. https://doi.org/10.1152/ajpheart.00446.2015.

Nakata, K., Nagai, T., Aruga, J., Mikoshiba, K., 1997. Xenopus Zic3, a primary regulator both in neural and neural crest development. Proceedings of the National Academy of Sciences of the United States of America 94 (22), 11980–11985.

Navarro, A., Anand-Apte, B., Parat, M.-O., 2004. A role for caveolae in cell migration. FASEB journal : official publication of the Federation of American Societies for Experimental Biology 18 (15), 1801–1811. https://doi.org/10.1096/fj.04-2516rev.

Nethe, M., Anthony, E.C., Fernandez-Borja, M., Dee, R., Geerts, D., Hensbergen, P.J., Deelder, A.M., Schmidt, G., Hordijk, P.L., 2010. Focal-adhesion targeting links caveolin-1 to a Rac1-degradation pathway. Journal of Cell Science 123 (Pt 11), 1948–1958. https://doi.org/10.1242/jcs.062919.

Nethe, M., Hordijk, P.L., 2011. A model for phospho-caveolin-1-driven turnover of focal adhesions. Cell adhesion & migration 5 (1), 59–64. https://doi.org/10.4161/cam.5.1.13702.

Neumann-Giesen, C., Falkenbach, B., Beicht, P., Claasen, S., Lüers, G., Stuermer, C.A.O., Herzog, V., Tikkanen, R., 2004. Membrane and raft association of reggie-1/flotillin-2: role of myristoylation, palmitoylation and oligomerization and induction of filopodia by overexpression. The Biochemical journal 378 (Pt 2), 509–518. https://doi.org/10.1042/BJ20031100.

Newman, G.R., Campbell, L., Ruhland, C. von, Jasani, B., Gumbleton, M., 1999. Caveolin and its cellular and subcellular immunolocalisation in lung alveolar epithelium: implications for alveolar epithelial type I cell function. Cell and Tissue Research 295 (1), 111–120. https://doi.org/10.1007/s004410051217.

Ng, J., Luo, L., 2004. Rho GTPases regulate axon growth through convergent and divergent signaling pathways. Neuron 44 (5), 779–793. https://doi.org/10.1016/j.neuron.2004.11.014.

Ng, J., Nardine, T., Harms, M., Tzu, J., Goldstein, A., Sun, Y., Dietzl, G., Dickson, B.J., Luo, L., 2002. Rac GTPases control axon growth, guidance and branching. Nature 416 (6879), 442–447. https://doi.org/10.1038/416442a.

Nieuwkoop, P.D., Faber, J. (Eds.), 1994. Normal table of Xenopus laevis (Daudin): A systematical and chronological survey of the development from the fertilized egg till the end of metamorphosis. Garland Pub, New York, 252 pp.

Niimi, K., Nishioka, C., Miyamoto, T., Takahashi, E., Miyoshi, I., Itakura, C., Yamashita, T., 2011. Impairment of neuropsychological behaviors in ganglioside GM3-knockout mice. Biochemical and biophysical research communications 406 (4), 524–528. https://doi.org/10.1016/j.bbrc.2011.02.071.

Nixon, S.J., Carter, A., Wegner, J., Ferguson, C., Floetenmeyer, M., Riches, J., Key, B., Westerfield, M., Parton, R.G., 2007. Caveolin-1 is required for lateral line neuromast and notochord development. Journal of Cell Science 120 (Pt 13), 2151–2161. https://doi.org/10.1242/jcs.003830.

Nixon, S.J., Wegner, J., Ferguson, C., Méry, P.-F., Hancock, J.F., Currie, P.D., Key, B., Westerfield, M., Parton, R.G., 2005. Zebrafish as a model for caveolin-associated muscle disease; caveolin-3 is required for myofibril organization and muscle cell patterning. Human molecular genetics 14 (13), 1727–1743. https://doi.org/10.1093/hmg/ddi179.

Nobes, C.D., Hall, A., 1995. Rho, rac, and cdc42 GTPases regulate the assembly of multimolecular focal complexes associated with actin stress fibers, lamellipodia, and filopodia. Cell 81 (1), 53–62. https://doi.org/10.1016/0092-8674(95)90370-4.

Núñez-Wehinger, S., Ortiz, R.J., Díaz, N., Díaz, J., Lobos-González, L., Quest, A.F.G., 2014. Caveolin-1 in cell migration and metastasis. Current molecular medicine 14 (2), 255–274. https://doi.org/10.2174/1566524014666140128112827.

Oellers, N., Dehio, M., Knust, E., 1994. bHLH proteins encoded by the Enhancer of split complex of Drosophila negatively interfere with transcriptional activation mediated by proneural genes. Molecular & general genetics : MGG 244 (5), 465–473. https://doi.org/10.1007/BF00583897.

Ogata, T., Ueyama, T., Isodono, K., Tagawa, M., Takehara, N., Kawashima, T., Harada, K., Takahashi, T., Shioi, T., Matsubara, H., Oh, H., 2008. MURC, a Muscle-Restricted Coiled-Coil Protein That Modulates the Rho/ROCK Pathway, Induces Cardiac Dysfunction and Conduction Disturbance. Molecular and Cellular Biology 28 (10), 3424–3436. https://doi.org/10.1128/MCB.02186-07.

Oh, P., McIntosh, D.P., Schnitzer, J.E., 1998. Dynamin at the neck of caveolae mediates their budding to form transport vesicles by GTP-driven fission from the plasma membrane of endothelium. J Cell Biol 141 (1), 101–114. https://doi.org/10.1083/jcb.141.1.101.

Ohashi, K., Fujiwara, S., Mizuno, K., 2017. Roles of the cytoskeleton, cell adhesion and rho signalling in mechanosensing and mechanotransduction. Journal of biochemistry 161 (3), 245–254. https://doi.org/10.1093/jb/mvw082.

Ohmi, Y., Tajima, O., Ohkawa, Y., Mori, A., Sugiura, Y., Furukawa, K., Furukawa, K., 2009. Gangliosides play pivotal roles in the regulation of complement systems and in the maintenance of integrity in nerve tissues. PNAS 106 (52), 22405–22410. https://doi.org/10.1073/pnas.0912336106.

Oka, N., Yamamoto, M., Schwencke, C., Kawabe, J., Ebina, T., Ohno, S., Couet, J., Lisanti, M.P., Ishikawa, Y., 1997. Caveolin interaction with protein kinase C. Isoenzyme-dependent regulation of kinase activity by the caveolin scaffolding domain peptide. Journal of Biological Chemistry 272 (52), 33416–33421. https://doi.org/10.1074/jbc.272.52.33416.

Orr, A.W., Helmke, B.P., Blackman, B.R., Schwartz, M.A., 2006. Mechanisms of mechanotransduction. Developmental cell 10 (1), 11–20. https://doi.org/10.1016/j.devcel.2005.12.006.

Ortegren, U., Karlsson, M., Blazic, N., Blomqvist, M., Nystrom, F.H., Gustavsson, J., Fredman, P., Strålfors, P., 2004. Lipids and glycosphingolipids in caveolae and surrounding plasma membrane of primary rat adipocytes. European journal of biochemistry 271 (10), 2028–2036. https://doi.org/10.1111/j.1432-1033.2004.04117.x.

Oschwald, R., Richter, K., Grunz, H., 1991. Localization of a nervous system-specific class II beta-tubulin gene in Xenopus laevis embryos by whole-mount in situ hybridization. The International journal of developmental biology 35 (4), 399–405.

Ostrom, R.S., Insel, P.A., 2004. The evolving role of lipid rafts and caveolae in G protein-coupled receptor signaling: implications for molecular pharmacology. British Journal of Pharmacology 143 (2), 235–245. https://doi.org/10.1038/sj.bjp.0705930.

Pagnon-Minot, A., Malbouyres, M., Haftek-Terreau, Z., Kim, H.R., Sasaki, T., Thisse, C., Thisse, B., Ingham, P.W., Ruggiero, F., Le Guellec, D., 2008. Collagen XV, a novel factor in zebrafish notochord differentiation and muscle development. Developmental biology 316 (1), 21–35. https://doi.org/10.1016/j.ydbio.2007.12.033.

Palade, G.E., 1953. Fine Structure of Blood Capillaries. J Appl Phys. 24.

Palazzo, A.F., Eng, C.H., Schlaepfer, D.D., Marcantonio, E.E., Gundersen, G.G., 2004. Localized stabilization of microtubules by integrin- and FAK-facilitated Rho signaling. Science (New York, N.Y.) 303 (5659), 836–839. https://doi.org/10.1126/science.1091325.

Park, D.S., Cohen, A.W., Frank, P.G., Razani, B., Lee, H., Williams, T.M., Chandra, M., Shirani, J., De Souza, Andrea P, Tang, B., Jelicks, L.A., Factor, S.M., Weiss, L.M., Tanowitz, H.B., Lisanti, M.P., 2003. Caveolin-1 null (-/-) mice show dramatic reductions in life span. Biochemistry 42 (51), 15124–15131. https://doi.org/10.1021/bi0356348.

Park, J.-S., Kim, H.-Y., Kim, H.-W., Chae, G.-N., Oh, H.-T., Park, J.-Y., Shim, H., Seo, M., Shin, E.-Y., Kim, E.-G., Park, S.C., Kwak, S.-J., 2005. Increased caveolin-1, a cause for the declined adipogenic potential of senescent human mesenchymal stem cells. Mechanisms of ageing and development 126 (5), 551–559. https://doi.org/10.1016/j.mad.2004.11.014.

Park, W.Y., Park, J.S., Cho, K.A., Kim, D.I., Ko, Y.G., Seo, J.S., Park, S.C., 2000. Up-regulation of caveolin attenuates epidermal growth factor signaling in senescent cells. Journal of Biological Chemistry 275 (27), 20847–20852. https://doi.org/10.1074/jbc.M908162199.

Parton, R.G., 2018. Caveolae: Structure, Function, and Relationship to Disease. Annual review of cell and developmental biology 34, 111–136. https://doi.org/10.1146/annurev-cellbio-100617-062737.

Parton, R.G., del Pozo, M.A., 2013. Caveolae as plasma membrane sensors, protectors and organizers. Nat Rev Mol Cell Biol 14 (2), 98–112. https://doi.org/10.1038/nrm3512.

Parton, R.G., Joggerst, B., Simons, K., 1994. Regulated internalization of caveolae. The Journal of cell biology 127 (5), 1199–1215.

Parton, R.G., Simons, K., 2007. The multiple faces of caveolae. Nature reviews. Molecular cell biology 8 (3), 185–194. https://doi.org/10.1038/nrm2122.

Parton, R.G., Way, M., Zorzi, N., Stang, E., 1997. Caveolin-3 Associates with Developing T-tubules during Muscle Differentiation. J Cell Biol 136 (1), 137–154. https://doi.org/10.1083/jcb.136.1.137.

Paudyal, A., Damrau, C., Patterson, V.L., Ermakov, A., Formstone, C., Lalanne, Z., Wells, S., Lu, X., Norris, D.P., Dean, C.H., Henderson, D.J., Murdoch, J.N., 2010. The novel mouse mutant, chuzhoi, has disruption of Ptk7 protein and exhibits defects in neural tube, heart and lung development and abnormal planar cell polarity in the ear. BMC developmental biology 10, 87. https://doi.org/10.1186/1471-213X-10-87.

Pauli, S., Bajpai, R., Borchers, A., 2017. CHARGEd with neural crest defects. American journal of medical genetics. Part C, Seminars in medical genetics 175 (4), 478–486. https://doi.org/10.1002/ajmg.c.31584.

Pelkmans, L., Burli, T., Zerial, M., Helenius, A., 2004. Caveolin-stabilized membrane domains as multifunctional transport and sorting devices in endocytic membrane traffic. Cell 118 (6), 767–780. https://doi.org/10.1016/j.cell.2004.09.003.

Pera, E.M., Ikeda, A., Eivers, E., De Robertis, Eddy M, 2003. Integration of IGF, FGF, and anti-BMP signals via Smad1 phosphorylation in neural induction. Genes & Development 17 (24), 3023–3028. https://doi.org/10.1101/gad.1153603.

Peters, K.R., Carley, W.W., Palade, G.E., 1985. Endothelial plasmalemmal vesicles have a characteristic striped bipolar surface structure. J Cell Biol 101 (6), 2233–2238. https://doi.org/10.1083/jcb.101.6.2233.

Piccolo, S., Sasai, Y., Lu, B., Robertis, E.M. de, 1996. Dorsoventral Patterning in Xenopus: Inhibition of Ventral Signals by Direct Binding of Chordin to BMP-4. Cell 86 (4), 589–598. https://doi.org/10.1016/S0092-8674(00)80132-4.

Pol, A., Martin, S., Fernández, M.A., Ingelmo-Torres, M., Ferguson, C., Enrich, C., Parton, R.G., 2005. Cholesterol and fatty acids regulate dynamic caveolin trafficking through the Golgi complex and between the cell surface and lipid bodies. Molecular biology of the cell 16 (4), 2091–2105. https://doi.org/10.1091/mbc.e04-08-0737.

Pol, A., Morales-Paytuví, F., Bosch, M., Parton, R.G., 2020. Non-caveolar caveolins - duties outside the caves. Journal of Cell Science 133 (9). https://doi.org/10.1242/jcs.241562.

Pourquié, O., Coltey, M., Teillet, M.A., Ordahl, C., Le Douarin, N.M., 1993. Control of dorsoventral patterning of somitic derivatives by notochord and floor plate. Proceedings of the National Academy of Sciences 90 (11), 5242–5246. https://doi.org/10.1073/pnas.90.11.5242.

Pozzoli, O., Bosetti, A., Croci, L., Consalez, G.G., Vetter, M.L., 2001. Xebf3 is a regulator of neuronal differentiation during primary neurogenesis in Xenopus. Developmental biology 233 (2), 495–512. https://doi.org/10.1006/dbio.2001.0230.

Puzik, K., Tonnier, V., Opper, I., Eckert, A., Zhou, L., Kratzer, M.-C., Le Noble, F., Nienhaus, G.U., Gradl, D., 2019. Lef1 regulates caveolin expression and caveolin dependent endocytosis, a process necessary for Wnt5a/Ror2 signaling during Xenopus gastrulation. Scientific reports 9 (1), 15645. https://doi.org/10.1038/s41598-019-52218-1.

Radel, C., Rizzo, V., 2005. Integrin mechanotransduction stimulates caveolin-1 phosphorylation and recruitment of Csk to mediate actin reorganization. American journal of physiology. Heart and circulatory physiology 288 (2), H936-45. https://doi.org/10.1152/ajpheart.00519.2004.

Rajendran, L., Simons, K., 2005. Lipid rafts and membrane dynamics. Journal of Cell Science 118 (Pt 6), 1099–1102. https://doi.org/10.1242/jcs.01681.

Ramirez, M.I., Pollack, L., Millien, G., Cao, Y.X., Hinds, A., Williams, M.C., 2002. The alpha-isoform of caveolin-1 is a marker of vasculogenesis in early lung development. The journal of histochemistry and cytochemistry : official journal of the Histochemistry Society 50 (1), 33–42. https://doi.org/10.1177/002215540205000104.

Rangel, L., Bernabé-Rubio, M., Fernández-Barrera, J., Casares-Arias, J., Millán, J., Alonso, M.A., Correas, I., 2019. Caveolin-1α regulates primary cilium length by controlling RhoA GTPase activity. Scientific reports 9 (1), 1116. https://doi.org/10.1038/s41598-018-38020-5.

Ravindran, S., Nalavadi, V.C., Muddashetty, R.S., 2019. BDNF Induced Translation of Limk1 in Developing Neurons Regulates Dendrite Growth by Fine-Tuning Cofilin1 Activity. Frontiers in molecular neuroscience 12, 64. https://doi.org/10.3389/fnmol.2019.00064.

Razani, B., Combs, T.P., Wang, X.B., Frank, P.G., Park, D.S., Russell, R.G., Li, M., Tang, B., Jelicks, L.A., Scherer, P.E., Lisanti, M.P., 2002a. Caveolin-1-deficient mice are lean, resistant to diet-induced obesity, and show hypertriglyceridemia with adipocyte abnormalities. Journal of Biological Chemistry 277 (10), 8635–8647. https://doi.org/10.1074/jbc.M110970200.

Razani, B., Engelman, J.A., Wang, X.B., Schubert, W., Zhang, X.L., Marks, C.B., Macaluso, F., Russell, R.G., Li, M., Pestell, R.G., Di Vizio, D., Hou, H., Kneitz, B., Lagaud, G., Christ, G.J., Edelmann, W., Lisanti, M.P., 2001. Caveolin-1 null mice are viable but show evidence of hyperproliferative and vascular abnormalities. The Journal of biological chemistry 276 (41), 38121–38138. https://doi.org/10.1074/jbc.M105408200.

Razani, B., Lisanti, M.P., 2001. Two distinct caveolin-1 domains mediate the functional interaction of caveolin-1 with protein kinase A. AJP: Cell Physiology 281 (4), C1241-50. https://doi.org/10.1152/ajpcell.2001.281.4.C1241.

Razani, B., Park, D.S., Miyanaga, Y., Ghatpande, A., Cohen, J., Wang, X.B., Scherer, P.E., Evans, T., Lisanti, M.P., 2002b. Molecular cloning and developmental expression of the caveolin gene family in the amphibian Xenopus laevis. Biochemistry 41 (25), 7914–7924.

Razani, B., Woodman, S.E., Lisanti, M.P., 2002c. Caveolae: from cell biology to animal physiology. Pharmacological reviews 54 (3), 431–467.

Rhim, J.H., Kim, J.H., Yeo, E.-J., Kim, J.C., Park, S.C., 2010. Caveolin-1 as a novel indicator of wound-healing capacity in aged human corneal epithelium. Molecular medicine (Cambridge, Mass.) 16 (11-12), 527–534. https://doi.org/10.2119/molmed.2010.00046.

Richter, T., Floetenmeyer, M., Ferguson, C., Galea, J., Goh, J., Lindsay, M.R., Morgan, G.P., Marsh, B.J., Parton, R.G., 2008. High-resolution 3D quantitative analysis of caveolar ultrastructure and caveola-cytoskeleton interactions. Traffic (Copenhagen, Denmark) 9 (6), 893–909. https://doi.org/10.1111/j.1600-0854.2008.00733.x.

Ridley, A.J., Hall, A., 1992. The small GTP-binding protein rho regulates the assembly of focal adhesions and actin stress fibers in response to growth factors. Cell 70 (3), 389–399. https://doi.org/10.1016/0092-8674(92)90163-7.

Ridley, A.J., Paterson, H.F., Johnston, C.L., Diekmann, D., Hall, A., 1992. The small GTP-binding protein rac regulates growth factor-induced membrane ruffling. Cell 70 (3), 401–410. https://doi.org/10.1016/0092-8674(92)90164-8.

Roberts, A., 2000a. Early functional organization of spinal neurons in developing lower vertebrates. Brain research bulletin 53 (5), 585–593.

Roberts, A., 2000b. Early functional organization of spinal neurons in developing lower vertebrates. Brain research bulletin 53 (5), 585–593. https://doi.org/10.1016/S0361-9230(00)00392-0.

Roberts, A., Clarke, J.D., 1982. The neuroanatomy of an amphibian embryo spinal cord. Philosophical transactions of the Royal Society of London. Series B, Biological sciences 296 (1081), 195–212. https://doi.org/10.1098/rstb.1982.0002.

Roberts, A., Kahn, J.A., Soffe, S.R., Clarke, J.D., 1981. Neural control of swimming in a vertebrate. Science 213 (4511), 1032–1034. https://doi.org/10.1126/science.7196599.

Roberts, A., Li, W.-C., Soffe, S.R., 2010. How neurons generate behavior in a hatchling amphibian tadpole: an outline. Frontiers in behavioral neuroscience 4, 16. https://doi.org/10.3389/fnbeh.2010.00016.

Roberts, A., Walford, A., Soffe, S.R., Yoshida, M., 1999. Motoneurons of the axial swimming muscles in hatchlingXenopus tadpoles: Features, distribution, and central synapses. J. Comp. Neurol. 411 (3), 472–486. https://doi.org/10.1002/(SICI)1096-9861(19990830)411:3<472:AID-CNE9>3.0.CO;2-B.

Robles, E., Gomez, T.M., 2006. Focal adhesion kinase signaling at sites of integrin-mediated adhesion controls axon pathfinding. Nature neuroscience 9 (10), 1274–1283. https://doi.org/10.1038/nn1762.

Rogers, C.D., Archer, T.C., Cunningham, D.D., Grammer, T.C., Casey, E.M.S., 2008. Sox3 expression is maintained by FGF signaling and restricted to the neural plate by Vent proteins in the Xenopus embryo. Developmental biology 313 (1), 307–319. https://doi.org/10.1016/j.ydbio.2007.10.023.

Root, K.T., Julien, J.A., Glover, K.J., 2019. Secondary structure of caveolins: a mini review. Biochemical Society transactions 47 (5), 1489–1498. https://doi.org/10.1042/BST20190375.

Rothberg, K.G., Heuser, J.E., Donzell, W.C., Ying, Y.-S., Glenney, J.R., Anderson, R.G.W., 1992. Caveolin, a protein component of caveolae membrane coats. Cell 68 (4), 673–682. https://doi.org/10.1016/0092-8674(92)90143-Z.

Ruegg, M.A., Bixby, J.L., 1998. Agrin orchestrates synaptic differentiation at the vertebrate neuromuscular junction. Trends in Neurosciences 21 (1), 22–27. https://doi.org/10.1016/S0166-2236(97)01154-5.

Ryglewski, S., Kadas, D., Hutchinson, K., Schuetzler, N., Vonhoff, F., Duch, C., 2014. Dendrites are dispensable for basic motoneuron function but essential for fine tuning of behavior. PNAS 111 (50), 18049–18054. https://doi.org/10.1073/pnas.1416247111.

Sandhoff, K., Kolter, T., 2003. Biosynthesis and degradation of mammalian glycosphingolipids. Philosophical transactions of the Royal Society of London. Series B, Biological sciences 358 (1433), 847–861. https://doi.org/10.1098/rstb.2003.1265.

Sanguinetti, A.R., Cao, H., Corley Mastick, C., 2003. Fyn is required for oxidative- and hyperosmotic-stress-induced tyrosine phosphorylation of caveolin-1. The Biochemical journal 376 (Pt 1), 159–168. https://doi.org/10.1042/BJ20030336.

Sanguinetti, A.R., Mastick, C.C., 2003. c-Abl is required for oxidative stress-induced phosphorylation of caveolin-1 on tyrosine 14. Cellular signalling 15 (3), 289–298.

Sanna, E., Miotti, S., Mazzi, M., Santis, G. de, Canevari, S., Tomassetti, A., 2007. Binding of nuclear caveolin-1 to promoter elements of growth-associated genes in ovarian carcinoma cells. Experimental cell research 313 (7), 1307–1317. https://doi.org/10.1016/j.yexcr.2007.02.005.

Santos Da Silva, J., Schubert, V., Dotti, C.G., 2004. RhoA, Rac1, and cdc42 intracellular distribution shift during hippocampal neuron development. Molecular and cellular neurosciences 27 (1), 1–7. https://doi.org/10.1016/j.mcn.2004.03.008.

Sargiacomo, M., Scherer, P.E., Tang, Z., Kübler, E., Song, K.S., Sanders, M.C., Lisanti, M.P., 1995. Oligomeric structure of caveolin: implications for caveolae membrane organization. Proceedings of the National Academy of Sciences 92 (20), 9407–9411.

Sawada, A., Wang, S., Jian, M., Leem, J., Wackerbarth, J., Egawa, J., Schilling, J.M., Platoshyn, O., Zemljic-Harpf, A., Roth, D.M., Patel, H.H., Patel, P.M., Marsala, M., Head, B.P., 2019. Neuron-targeted caveolin-1 improves neuromuscular function and extends survival in SOD1G93A mice. FASEB journal : official publication of the Federation of American Societies for Experimental Biology 33 (6), 7545–7554. https://doi.org/10.1096/fj.201802652RR.

Schambony, A., Wedlich, D., 2007. Wnt-5A/Ror2 regulate expression of XPAPC through an alternative noncanonical signaling pathway. Developmental cell 12 (5), 779–792. https://doi.org/10.1016/j.devcel.2007.02.016.

Scheibel, M.E., Scheibel, A.B., 1970. Developmental relationship between spinal motoneuron dendrite bundles and patterned activity in the hind limb of cats. Experimental neurology 29 (2), 328–335. https://doi.org/10.1016/0014-4886(70)90062-2.

Scheiffele, P., Verkade, P., Fra, A.M., Virta, H., Simons, K., Ikonen, E., 1998. Caveolin-1 and -2 in the exocytic pathway of MDCK cells. J Cell Biol 140 (4), 795–806. https://doi.org/10.1083/jcb.140.4.795.

Scherer, P.E., 1996a. Expression of Caveolin-3 in Skeletal, Cardiac, and Smooth Muscle Cells. CAVEOLIN-3 IS A COMPONENT OF THE SARCOLEMMA AND CO-FRACTIONATES WITH DYSTROPHIN AND DYSTROPHIN-ASSOCIATED GLYCOPROTEINS. Journal of Biological Chemistry 271 (25), 15160–15165. https://doi.org/10.1074/jbc.271.25.15160.

Scherer, P.E., Lewis, R.Y., Volonte, D., Engelman, J.A., Galbiati, F., Couet, J., Kohtz, D.S., van Donselaar, E., Peters, P., Lisanti, M.P., 1997. Cell-type and tissue-specific expression of caveolin-2. Caveolins 1 and 2 co-localize and form a stable hetero-oligomeric complex in vivo. Journal of Biological Chemistry 272 (46), 29337–29346. https://doi.org/10.1074/jbc.272.46.29337.

Scherer, P.E., Lisanti, M.P., Baldini, G., Sargiacomo, M., Mastick, C.C., Lodish, H.F., 1994. Induction of caveolin during adipogenesis and association of GLUT4 with caveolin-rich vesicles. J Cell Biol 127 (5), 1233–1243. https://doi.org/10.1083/jcb.127.5.1233.

Scherer, P.E., Okamoto, T., Chun, M., Nishimoto, I., Lodish, H.F., Lisanti, M.P., 1996b. Identification, sequence, and expression of caveolin-2 defines a caveolin gene family. Proceedings of the National Academy of Sciences of the United States of America 93 (1), 131–135.

Scherer, P.E., Tang, Z., Chun, M., Sargiacomo, M., Lodish, H.F., Lisanti, M.P., 1995. Caveolin isoforms differ in their N-terminal protein sequence and subcellular distribution. Identification and epitope mapping of an isoform-specific monoclonal antibody probe. The Journal of biological chemistry 270 (27), 16395–16401.

Schlegel, A., Arvan, P., Lisanti, M.P., 2001. Caveolin-1 binding to endoplasmic reticulum membranes and entry into the regulated secretory pathway are regulated by serine phosphorylation. Protein sorting at the level of the endoplasmic reticulum. The Journal of biological chemistry 276 (6), 4398–4408. https://doi.org/10.1074/jbc.M005448200.

Schlegel, A., Lisanti, M.P., 2000. A molecular dissection of caveolin-1 membrane attachment and oligomerization. Two separate regions of the caveolin-1 C-terminal domain mediate membrane binding and oligomer/oligomer interactions in vivo. Journal of Biological Chemistry 275 (28), 21605–21617. https://doi.org/10.1074/jbc.M002558200.

Schrock, Y., Solis, G.P., Stuermer, C.A.O., 2009. Regulation of focal adhesion formation and filopodia extension by the cellular prion protein (PrPC). FEBS letters 583 (2), 389–393. https://doi.org/10.1016/j.febslet.2008.12.038.

Schroeter, E.H., Kisslinger, J.A., Kopan, R., 1998. Notch-1 signalling requires ligand-induced proteolytic release of intracellular domain. Nature 393 (6683), 382–386. https://doi.org/10.1038/30756.

Sebastião, A.M., Colino-Oliveira, M., Assaife-Lopes, N., Dias, R.B., Ribeiro, J.A., 2013. Lipid rafts, synaptic transmission and plasticity: impact in age-related neurodegenerative diseases. Neuropharmacology 64, 97–107. https://doi.org/10.1016/j.neuropharm.2012.06.053.

Seemann, E., Sun, M., Krueger, S., Tröger, J., Hou, W., Haag, N., Schüler, S., Westermann, M., Huebner, C.A., Romeike, B., Kessels, M.M., Qualmann, B., 2017. Deciphering caveolar functions by syndapin III KO-mediated impairment of caveolar invagination. eLife 6. https://doi.org/10.7554/eLife.29854.

Senju, Y., Itoh, Y., Takano, K., Hamada, S., Suetsugu, S., 2011. Essential role of PACSIN2/syndapin-II in caveolae membrane sculpting. Journal of Cell Science 124 (Pt 12), 2032–2040. https://doi.org/10.1242/jcs.086264.

Seo, S., Herr, A., Lim, J.-W., Richardson, G.A., Richardson, H., Kroll, K.L., 2005. Geminin regulates neuronal differentiation by antagonizing Brg1 activity. Genes & Development 19 (14), 1723–1734. https://doi.org/10.1101/gad.1319105.

Seo, S., Kroll, K.L., 2006. Geminin's double life: chromatin connections that regulate transcription at the transition from proliferation to differentiation. Cell cycle (Georgetown, Tex.) 5 (4), 374–379. https://doi.org/10.4161/cc.5.4.2438.

Shikanai, M., Nishimura, Y.V., Sakurai, M., Nabeshima, Y.-I., Yuzaki, M., Kawauchi, T., 2018. Caveolin-1 Promotes Early Neuronal Maturation via Caveolae-Independent Trafficking of N-Cadherin and L1. iScience 7, 53–67. https://doi.org/10.1016/j.isci.2018.08.014.

Shnitsar, I., Borchers, A., 2008. PTK7 recruits dsh to regulate neural crest migration. Development (Cambridge, England) 135 (24), 4015–4024. https://doi.org/10.1242/dev.023556.

Simionescu, N., Siminoescu, M., Palade, G.E., 1975. Permeability of muscle capillaries to small heme-peptides. Evidence for the existence of patent transendothelial channels. J Cell Biol 64 (3), 586–607. https://doi.org/10.1083/jcb.64.3.586.

Simone, L.C., Caplan, S., Naslavsky, N., 2013. Role of phosphatidylinositol 4,5-bisphosphate in regulating EHD2 plasma membrane localization. PloS one 8 (9), e74519. https://doi.org/10.1371/journal.pone.0074519.

Simons, K., Toomre, D., 2000. Lipid rafts and signal transduction. Nat Rev Mol Cell Biol 1 (1), 31–39. https://doi.org/10.1038/35036052.

Singh, R.D., Marks, D.L., Holicky, E.L., Wheatley, C.L., Kaptzan, T., Sato, S.B., Kobayashi, T., Ling, K., Pagano, R.E., 2010. Gangliosides and beta1-integrin are required for caveolae and membrane domains. Traffic (Copenhagen, Denmark) 11 (3), 348–360. https://doi.org/10.1111/j.1600-0854.2009.01022.x.

Sinha, B., Köster, D., Ruez, R., Gonnord, P., Bastiani, M., Abankwa, D., Stan, R.V., Butler-Browne, G., Vedie, B., Johannes, L., Morone, N., Parton, R.G., Raposo, G., Sens, P., Lamaze, C., Nassoy, P., 2011. Cells respond to mechanical stress by rapid disassembly of caveolae. Cell 144 (3), 402–413. https://doi.org/10.1016/j.cell.2010.12.031.

Smith, W.C., Harland, R.M., 1991. Injected Xwnt-8 RNA acts early in Xenopus embryos to promote formation of a vegetal dorsalizing center. Cell 67 (4), 753–765.

Smith, W.C., McKendry, R., Ribisi, S., Harland, R.M., 1995. A nodal-related gene defines a physical and functional domain within the Spemann organizer. Cell 82 (1), 37–46. https://doi.org/10.1016/0092-8674(95)90050-0.

Soffe, S.R., Roberts, A., 1982. Activity of myotomal motoneurons during fictive swimming in frog embryos. Journal of neurophysiology 48 (6), 1274–1278. https://doi.org/10.1152/jn.1982.48.6.1274.

Sohn, J., Brick, R.M., Tuan, R.S., 2016. From embryonic development to human diseases: The functional role of caveolae/caveolin. Birth defects research. Part C, Embryo today : reviews 108 (1), 45–64. https://doi.org/10.1002/bdrc.21121.

Sokol, S.Y., 2016. Mechanotransduction During Vertebrate Neurulation. Current topics in developmental biology 117, 359–376. https://doi.org/10.1016/bs.ctdb.2015.11.036.

Song, K.S., Tang, Z., Li, S., Lisanti, M.P., 1997. Mutational analysis of the properties of caveolin-1. A novel role for the C-terminal domain in mediating homo-typic caveolin-caveolin interactions. Journal of Biological Chemistry 272 (7), 4398–4403. https://doi.org/10.1074/jbc.272.7.4398.

Sonnino, S., Prinetti, A., 2009. Sphingolipids and membrane environments for caveolin. FEBS letters 583 (4), 597–606. https://doi.org/10.1016/j.febslet.2009.01.007.

Sowa, G., Xie, L., Xu, L., Sessa, W.C., 2008. Serine 23 and 36 phosphorylation of caveolin-2 is differentially regulated by targeting to lipid raft/caveolae and in mitotic endothelial cells. Biochemistry 47 (1), 101–111. https://doi.org/10.1021/bi701709s.

Stahlhut, M., van Deurs, B., 2000. Identification of filamin as a novel ligand for caveolin-1: evidence for the organization of caveolin-1-associated membrane domains by the actin cytoskeleton. Molecular biology of the cell 11 (1), 325–337.

Stamatovic, S.M., Keep, R.F., Wang, M.M., Jankovic, I., Andjelkovic, A.V., 2009. Caveolae-mediated internalization of occludin and claudin-5 during CCL2-induced tight junction remodeling in brain endothelial cells. Journal of Biological Chemistry 284 (28), 19053–19066. https://doi.org/10.1074/jbc.M109.000521.

Stephenson, R.E., Miller, A.L., 2017. Tools for live imaging of active Rho GTPases in Xenopus. Genesis (New York, N.Y. : 2000) 55 (1-2). https://doi.org/10.1002/dvg.22998.

Stern, C.M., Mermelstein, P.G., 2010. Caveolin regulation of neuronal intracellular signaling. Cellular and molecular life sciences : CMLS 67 (22), 3785–3795. https://doi.org/10.1007/s00018-010-0447-y.

Stoeber, M., Stoeck, I.K., Hänni, C., Bleck, C.K.E., Balistreri, G., Helenius, A., 2012. Oligomers of the ATPase EHD2 confine caveolae to the plasma membrane through association with actin. EMBO J 31 (10), 2350–2364. https://doi.org/10.1038/emboj.2012.98.

Strooper, B. de, Annaert, W., Cupers, P., Saftig, P., Craessaerts, K., Mumm, J.S., Schroeter, E.H., Schrijvers, V., Wolfe, M.S., Ray, W.J., Goate, A., Kopan, R., 1999. A presenilin-1-dependent gamma-secretase-like protease mediates release of Notch intracellular domain. Nature 398 (6727), 518–522. https://doi.org/10.1038/19083.

Stuermer, C.A., Lang, D.M., Kirsch, F., Wiechers, M., Deininger, S.O., Plattner, H., 2001. Glycosylphosphatidyl inositol-anchored proteins and fyn kinase assemble in noncaveolar plasma membrane microdomains defined by reggie-1 and -2. Molecular biology of the cell 12 (10), 3031–3045. https://doi.org/10.1091/mbc.12.10.3031.

Sullivan, S.A., Akers, L., Moody, S.A., 2001. foxD5a, a Xenopus winged helix gene, maintains an immature neural ectoderm via transcriptional repression that is dependent on the C-terminal domain. Developmental biology 232 (2), 439–457. https://doi.org/10.1006/dbio.2001.0191.

Suzuki, S., Numakawa, T., Shimazu, K., Koshimizu, H., Hara, T., Hatanaka, H., Mei, L., Lu, B., Kojima, M., 2004. BDNF-induced recruitment of TrkB receptor into neuronal lipid rafts: roles in synaptic modulation. J Cell Biol 167 (6), 1205–1215. https://doi.org/10.1083/jcb.200404106.

Sverdlov, M., Shinin, V., Place, A.T., Castellon, M., Minshall, R.D., 2009. Filamin A regulates caveolae internalization and trafficking in endothelial cells. Molecular biology of the cell 20 (21), 4531–4540. https://doi.org/10.1091/mbc.e08-10-0997.

Tang, Z., Scherer, P.E., Okamoto, T., Song, K., Chu, C., Kohtz, D.S., Nishimoto, I., Lodish, H.F., Lisanti, M.P., 1996. Molecular cloning of caveolin-3, a novel member of the caveolin gene family expressed predominantly in muscle. The Journal of biological chemistry 271 (4), 2255–2261.

Thanos, S., Bähr, M., Barde, Y.-A., Vanselow, J., 1989. Survival and Axonal Elongation of Adult Rat Retinal Ganglion Cells. The European journal of neuroscience 1 (1), 19–26. https://doi.org/10.1111/j.1460-9568.1989.tb00770.x.

Thiele, C., Hannah, M.J., Fahrenholz, F., Huttner, W.B., 2000. Cholesterol binds to synaptophysin and is required for biogenesis of synaptic vesicles. Nature cell biology 2 (1), 42–49. https://doi.org/10.1038/71366.

Thomsen, P., Roepstorff, K., Stahlhut, M., van Deurs, B., 2002. Caveolae are highly immobile plasma membrane microdomains, which are not involved in constitutive endocytic trafficking. Molecular biology of the cell 13 (1), 238–250. https://doi.org/10.1091/mbc.01-06-0317.

Thuret, R., Auger, H., Papalopulu, N., 2015. Analysis of neural progenitors from embryogenesis to juvenile adult in Xenopus laevis reveals biphasic neurogenesis and continuous lengthening of the cell cycle. Biology open 4 (12), 1772–1781. https://doi.org/10.1242/bio.013391.

Tillu, V.A., Rae, J., Ya, G., Ariotti, N., Floetenmeyer, M., Kovtun, O., McMahon, K.-A., Chaudhary, N., Parton, R.G., Collins, B.M., 2019. Cavin1 intrinsically disordered domains are essential for fuzzy electrostatic interactions and caveola formation.

Timmer, J.R., Wang, C., Niswander, L., 2002. BMP signaling patterns the dorsal and intermediate neural tube via regulation of homeobox and helix-loop-helix transcription factors. Development 129 (10), 2459–2472.

Tower, S.S., 1935. Atrophy and degeneration in skeletal muscle. Am. J. Anat. 56 (1), 1–43. https://doi.org/10.1002/aja.1000560102.

Trushina, E., Canaria, C.A., Lee, D.-Y., McMurray, C.T., 2014. Loss of caveolin-1 expression in knock-in mouse model of Huntington's disease suppresses pathophysiology in vivo. Human molecular genetics 23 (1), 129–144. https://doi.org/10.1093/hmg/ddt406.

Trushina, E., Du Charme, J., Parisi, J., McMurray, C.T., 2006a. Neurological abnormalities in caveolin-1 knock out mice. Behavioural brain research 172 (1), 24–32. https://doi.org/10.1016/j.bbr.2006.04.024.

Trushina, E., Singh, R.D., Dyer, R.B., Cao, S., Shah, V.H., Parton, R.G., Pagano, R.E., McMurray, C.T., 2006b. Mutant huntingtin inhibits clathrin-independent endocytosis and causes accumulation of cholesterol in vitro and in vivo. Human molecular genetics 15 (24), 3578–3591. https://doi.org/10.1093/hmg/ddl434.

Uittenbogaard, A., Smart, E.J., 2000. Palmitoylation of caveolin-1 is required for cholesterol binding, chaperone complex formation, and rapid transport of cholesterol to caveolae. The Journal of biological chemistry 275 (33), 25595–25599. https://doi.org/10.1074/jbc.M003401200.

Ulloa, F., Martí, E., 2010. Wnt won the war: antagonistic role of Wnt over Shh controls dorso-ventral patterning of the vertebrate neural tube. Developmental dynamics : an official publication of the American Association of Anatomists 239 (1), 69–76. https://doi.org/10.1002/dvdy.22058.

van Deurs, B., Roepstorff, K., Hommelgaard, A.M., Sandvig, K., 2003. Caveolae: Anchored, multifunctional platforms in the lipid ocean. Trends in Cell Biology 13 (2), 92–100. https://doi.org/10.1016/S0962-8924(02)00039-9.

van Mier, P., Armstrong, J., Roberts, A., 1989. Development of early swimming in Xenopus laevis embryos: myotomal musculature, its innervation and activation. Neuroscience 32 (1), 113–126.

Virgintino, D., Robertson, D., Errede, M., Benagiano, V., Tauer, U., Roncali, L., Bertossi, M., 2002. Expression of caveolin-1 in human brain microvessels. Neuroscience 115 (1), 145–152. https://doi.org/10.1016/S0306-4522(02)00374-3.

Vitriol, E.A., Zheng, J.Q., 2012. Growth cone travel in space and time: the cellular ensemble of cytoskeleton, adhesion, and membrane. Neuron 73 (6), 1068–1081. https://doi.org/10.1016/j.neuron.2012.03.005.

Vogel, V., Sheetz, M., 2006. Local force and geometry sensing regulate cell functions. Nat Rev Mol Cell Biol 7 (4), 265–275. https://doi.org/10.1038/nrm1890.

Volonte, D., Kahkonen, B., Shapiro, S., Di, Y., Galbiati, F., 2009. Caveolin-1 expression is required for the development of pulmonary emphysema through activation of the ATM-p53-p21 pathway. Journal of Biological Chemistry 284 (9), 5462–5466. https://doi.org/10.1074/jbc.C800225200.

Wallingford, J.B., Fraser, S.E., Harland, R.M., 2002. Convergent Extension. Developmental cell 2 (6), 695–706. https://doi.org/10.1016/s1534-5807(02)00197-1.

Walser, P.J., Ariotti, N., Howes, M., Ferguson, C., Webb, R., Schwudke, D., Leneva, N., Cho, K.-J., Cooper, L., Rae, J., Floetenmeyer, M., Oorschot, V.M.J., Skoglund, U., Simons, K., Hancock, J.F., Parton, R.G., 2012. Constitutive formation of caveolae in a bacterium. Cell 150 (4), 752–763. https://doi.org/10.1016/j.cell.2012.06.042.

Wanaski, S.P., Ng, B.K., Glaser, M., 2003. Caveolin scaffolding region and the membrane binding region of SRC form lateral membrane domains. Biochemistry 42 (1), 42–56. https://doi.org/10.1021/bi012097n.

Wang, S., Zhang, Z., Almenar-Queralt, A., Leem, J., DerMardirossian, C., Roth, D.M., Patel, P.M., Patel, H.H., Head, B.P., 2019. Caveolin-1 Phosphorylation Is Essential for Axonal Growth of Human Neurons Derived From iPSCs. Front. Cell. Neurosci. 13, 324, 123. https://doi.org/10.3389/fncel.2019.00324.

Wang, X.B., Lee, H., Capozza, F., Marmon, S., Sotgia, F., Brooks, J.W., Campos-Gonzalez, R., Lisanti, M.P., 2004. Tyrosine phosphorylation of caveolin-2 at residue 27: differences in the spatial and temporal behavior of phospho-Cav-2 (pY19 and pY27). Biochemistry 43 (43), 13694–13706. https://doi.org/10.1021/bi049295.

Wary, K.K., Mariotti, A., Zurzolo, C., Giancotti, F.G., 1998. A Requirement for Caveolin-1 and Associated Kinase Fyn in Integrin Signaling and Anchorage-Dependent Cell Growth. Cell 94 (5), 625–634. https://doi.org/10.1016/S0092-8674(00)81604-9.

Way, M., Parton, R.G., 1996. M-caveolin, a muscle-specific caveolin-related protein. FEBS letters 378 (1), 108–112.

Wei, Y., Yang, X., Liu, Q., Wilkins, J.A., Chapman, H.A., 1999. A role for caveolin and the urokinase receptor in integrin-mediated adhesion and signaling. J Cell Biol 144 (6), 1285–1294. https://doi.org/10.1083/jcb.144.6.1285.

Werner, J.M., Negesse, M.Y., Brooks, D.L., Caldwell, A.R., Johnson, J.M., Brewster, R.M., 2019. Hingepoints and neural folds reveal conserved features of primary neurulation in the zebrafish forebrain.

Westermann, M., Steiniger, F., Richter, W., 2005. Belt-like localisation of caveolin in deep caveolae and its re-distribution after cholesterol depletion. Histochemistry and cell biology 123 (6), 613–620. https://doi.org/10.1007/s00418-004-0750-5.

Wettstein, D.A., Turner, D.L., Kintner, C., 1997. The Xenopus homolog of Drosophila Suppressor of Hairless mediates Notch signaling during primary neurogenesis. Development 124 (3), 693–702.

Wickström, S.A., Lange, A., Hess, M.W., Polleux, J., Spatz, J.P., Krüger, M., Pfaller, K., Lambacher, A., Bloch, W., Mann, M., Huber, L.A., Fässler, R., 2010. Integrin-linked kinase controls microtubule dynamics required for plasma membrane targeting of caveolae. Developmental cell 19 (4), 574–588. https://doi.org/10.1016/j.devcel.2010.09.007.

Williams, T.M., Lisanti, M.P., 2004. The caveolin proteins. Genome Biology 5 (3), 214. https://doi.org/10.1186/gb-2004-5-3-214.

Williams, T.M., Lisanti, M.P., 2005. Caveolin-1 in oncogenic transformation, cancer, and metastasis. American journal of physiology. Cell physiology 288 (3), C494-506. https://doi.org/10.1152/ajpcell.00458.2004.

Wilson, S.I., Graziano, E., Harland, R., Jessell, T.M., Edlund, T., 2000. An early requirement for FGF signalling in the acquisition of neural cell fate in the chick embryo. Current Biology 10 (8), 421–429. https://doi.org/10.1016/S0960-9822(00)00431-0.

Woo, S., Gomez, T.M., 2006. Rac1 and RhoA promote neurite outgrowth through formation and stabilization of growth cone point contacts. The Journal of neuroscience : the official journal of the Society for Neuroscience 26 (5), 1418–1428. https://doi.org/10.1523/JNEUROSCI.4209-05.2006.

Wullimann, M.F., Rink, E., Vernier, P., Schlosser, G., 2005. Secondary neurogenesis in the brain of the African clawed frog, Xenopus laevis, as revealed by PCNA, Delta-1, Neurogenin-related-1, and NeuroD expression. The Journal of comparative neurology 489 (3), 387–402. https://doi.org/10.1002/cne.20634.

Wunderlich, C., Schober, K., Lange, S.A., Drab, M., Braun-Dullaeus, R.C., Kasper, M., Schwencke, C., Schmeisser, A., Strasser, R.H., 2006. Disruption of caveolin-1 leads to enhanced nitrosative stress and severe systolic and diastolic heart failure. Biochemical and biophysical research communications 340 (2), 702–708. https://doi.org/10.1016/j.bbrc.2005.12.058.

Yamada, E., 1955. The fine structure of the renal glomerulus of the mouse. The journal of histochemistry and cytochemistry : official journal of the Histochemistry Society 3 (4), 309.

Yamada, T., Pfaff, S.L., Edlund, T., Jessell, T.M., 1993. Control of cell pattern in the neural tube: Motor neuron induction by diffusible factors from notochord and floor plate. Cell 73 (4), 673–686. https://doi.org/10.1016/0092-8674(93)90248-O.

Yamada, T., Placzek, M., Tanaka, H., Dodd, J., Jessell, T.M., 1991. Control of cell pattern in the developing nervous system: Polarizing activity of the floor plate and notochord. Cell 64 (3), 635–647. https://doi.org/10.1016/0092-8674(91)90247-V.

Yang, B., Radel, C., Hughes, D., Kelemen, S., Rizzo, V., 2011. p190 RhoGTPase-activating protein links the β1 integrin/caveolin-1 mechanosignaling complex to RhoA and actin remodeling. Arteriosclerosis, Thrombosis, and Vascular Biology 31 (2), 376–383. https://doi.org/10.1161/ATVBAHA.110.217794.

Yao, Q., Chen, J., Cao, H., Orth, J.D., McCaffery, J.M., Stan, R.-V., McNiven, M.A., 2005. Caveolin-1 interacts directly with dynamin-2. Journal of molecular biology 348 (2), 491–501. https://doi.org/10.1016/j.jmb.2005.02.003.

Yu, R.K., Nakatani, Y., Yanagisawa, M., 2009. The role of glycosphingolipid metabolism in the developing brain. Journal of lipid research 50 Suppl, S440-5. https://doi.org/10.1194/jlr.R800028-JLR200.

Yu, W., McDonnell, K., Taketo, M.M., Bai, C.B., 2008. Wnt signaling determines ventral spinal cord cell fates in a time-dependent manner. Development 135 (22), 3687–3696. https://doi.org/10.1242/dev.021899.

Yuan, X.-b., Jin, M., Xu, X., Song, Y.-q., Wu, C.-p., Poo, M.-m., Duan, S., 2003. Signalling and crosstalk of Rho GTPases in mediating axon guidance. Nature cell biology 5 (1), 38–45. https://doi.org/10.1038/ncb895.

Zhang, B., Peng, F., Wu, D., Ingram, A.J., Gao, B., Krepinsky, J.C., 2007. Caveolin-1 phosphorylation is required for stretch-induced EGFR and Akt activation in mesangial cells. Cellular signalling 19 (8), 1690–1700. https://doi.org/10.1016/j.cellsig.2007.03.005.

Zhao, Y.-Y., Liu, Y., Stan, R.-V., Fan, L., Gu, Y., Dalton, N., Chu, P.-H., Peterson, K., Ross, J., Chien, K.R., 2002. Defects in caveolin-1 cause dilated cardiomyopathy and pulmonary hypertension in knockout mice. Proceedings of the National Academy of Sciences 99 (17), 11375–11380. https://doi.org/10.1073/pnas.172360799.

Zimmerman, L.B., Jesús-Escobar, J.M. de, Harland, R.M., 1996. The Spemann Organizer Signal noggin Binds and Inactivates Bone Morphogenetic Protein 4. Cell 86 (4), 599–606. https://doi.org/10.1016/S0092-8674(00)80133-6.

Zimnicka, A.M., Husain, Y.S., Shajahan, A.N., Sverdlov, M., Chaga, O., Chen, Z., Toth, P.T., Klomp, J., Karginov, A.V., Tiruppathi, C., Malik, A.B., Minshall, R.D., 2016. Src-dependent phosphorylation of caveolin-1 Tyr-14 promotes swelling and release of caveolae. Molecular biology of the cell 27 (13), 2090–2106. https://doi.org/10.1091/mbc.E15-11-0756.

8 Danksagung

Ein großes Dankeschön möchte ich meiner Betreuerin Prof. Dr. Annette Borchers aussprechen, die es mir erst möglich gemacht hat meine Promotion in Ihrer Arbeitsgruppe anfertigen zu können. Danke, dass du mich während meiner Zeit bei dir immer mit deiner wissenschaftlichen Expertise unterstützt, mich motiviert und mich dazu ermutigt hast neue Wege zu gehen. Mit deiner Hilfe habe ich mich zu der selbstbewussten und selbständigen Wissenschaftlerin entwickelt die ich jetzt bin.

Ein weiteres Dankeschön möchte ich meinem „Thesis Advisory Committee“ Prof. Dr. Ralf Jacob sowie Prof. Dr. Thomas Worzfeld aussprechen, die mir während meiner Zeit im Graduiertenkolleg GRK2213 immer mit ihrem wissenschaftlichen Rat zur Seite gestanden und zum Erfolg meiner Promotion beigetragen haben. Auch möchte ich Prof. Dr. Helker sowie Prof. Dr. Uwe Homberg meinen Dank aussprechen, dass sie sich dazu bereit erklärt haben Teil meiner Prüfungskommission zu sein.
Ich danke auch allen Mitgliedern des GRK2213 für die hilfreichen Beiträge und interessanten Diskussionen sowie der tollen Zeit miteinander. Hier gilt auch vor allem Prof. Dr. Marco Rust sowie Felix Schneider mein Dank, da sie mir bei neuronalen Fragestellungen immer zur Seite standen.

Des Weiteren möchte ich allen ehemaligen und derzeitigen Mitgliedern der AG Borchers danken. Ein besonderes Dankeschön hierbei gilt vor allem Janina, Hanna, Anita, Elisabeth, Barbara, Ingrid und Melanie. Danke für die super tolle Zeit mit euch, für das tolle Arbeitsklima und eure stetige Unterstützung während meiner Promotion. Es war eine unvergessliche Zeit mit euch und ich werde euch alle sehr vermissen.
Ich möchte auch meinen Bachelor- sowie Masterstudenten, Max, Nils und Hannah für die tolle Zusammenarbeit danken. Ohne euch wäre mein Projekt nicht dort wo es jetzt ist.

Abschließend möchte ich all meinen Freunden, vor allem Katharina, Elisabeth und Saskia, sowie meiner Familie danken, die mir all die Jahre zur Seite standen, mir viel Liebe und Freude geschenkt haben und mit deren Unterstützung ich auch schwierige Zeiten überstanden habe. Danke!

9 Erklärung

Hiermit versichere ich, dass ich die vorliegende Dissertation mit dem Titel „The analysis of Cav1α function in *Xenopus* motoneuron outgrowth and neuromuscular integrity“ unter der Leitung von Prof. Dr. Annette Borchers selbstständig und ohne fremde Hilfe verfasst und mich keiner anderen als die im Text angegebenen Quellen oder Hilfsmittel bedient habe.
Alle wörtlichen oder sinngemäß entnommenen Zitate aus anderen Werken wurden als solche kenntlich gemacht.

Die Dissertation wurde in der vorliegenden oder einer ähnlichen Form noch bei keiner anderen in- oder ausländischen Hochschule eingereicht und hat noch keinen sonstigen Prüfungszwecken gedient.

Abgrenzung der Eigenleistung

Die in dieser Arbeit gezeigten Experimente wurden von mir selbst und ohne andere als die hier aufgeführte Hilfe durchgeführt.

Das in Abbildung 18D gezeigte Rettungsexperiment wurde in Teilen von Dr. Hanna Berger im Rahmen ihrer Doktorarbeit, sowie während meiner Masterarbeit durchgeführt. Von Ihr stammen 3 von den jeweils 5 durchgeführten Experimenten.

Abbildung 18A-B wurde während meiner Masterarbeit erstellt und aus dieser übernommen.

Die *pax3 in situ* Hybridisierung, präsentiert in Abbildung 19C-F, wurde in Teilen während meiner Masterarbeit durchgeführt (1 Experiment) und während meiner Doktorarbeit vervollständigt (2 Experimente).

Marburg, den

(Marlen Breuer)